This is to certify that the
dissertation entitled

PROTON MOVEMENT IN CYTOCHROME *C* OXIDASE OF
RHODOBACTER SPHAEROIDES

presented by

NAMJOON KIM

has been accepted towards fulfillment
of the requirements for the

Ph.D. degree in Biochemistry and Molecular Biology

S. Ferguson-Miller
Major Professor's Signature

May 15, 2009
Date

PROTON MOVEMENT IN CYTOCHROME *C* OXIDASE OF *RHODOBACTER SPHAEROIDES*

VOLUME I

By

NAMJOON KIM

A DISSERTATION

Submitted to
Michigan State University
in partial fulfillment of the requirements
for the degree of

DOCTOR OF PHILOSOPHY

Biochemistry & Molecular Biology

2009

ABSTRACT

PROTON MOVEMENT IN CYTOCHROME *C* OXIDASE OF *RHODOBACTER SPHAEROIDES*

By

Namjoon Kim

Membrane bound cytochrome *c* oxidase couples the movement of electrons and protons in order to achieve both oxygen reduction and proton translocation across the membrane, resulting in the generation of an electrochemical gradient to support ATP synthesis. Proton movement from the inner surface of cytochrome *c* oxidase to the active site through the "D" and "K" proton uptake pathways has been identified. However, the proton release pathway to the exterior of the protein is not well established. A hydrogen bonded network involving a number of water molecules above the hemes has been postulated to be involved in proton release and to possibly have reversibility for the backflow of protons. It is also proposed that proton backflow may be an important process in physiological regulation of energy efficiency.

To observe and quantify proton pumping and proton backflow in reconstituted vesicles containing cytochrome c oxidase (COV), conditions were established for the use of pH sensitive dyes, phenol red on the outside and fluorescent pyranine trapped on the inside, to allow measurement of proton movement on both sides of the membrane under the same conditions. Stopped-flow techniques were used to follow the catalytic reaction in the millisecond time scale, by fluorescence or rapid scanning visible spectroscopy. The conditions for preparing COVs were optimized by using Biobeads for detergent removal rather than dialysis and by purifying COVs that contained his-tagged oxidase purified by Ni-NTA resin. These procedures increased the size and homogeneity of COVs resulting in improved signal/noise for the internal pH measurements. The size of the vesicles was measured by transmission electron microscopy after fixation with osmium tetroxide by a

negative staining method. Several mutants involved in the proton uptake pathway and the postulated proton release/backflow pathways were examined to quantify the rate and extent of proton movement and clarify the role of each proton pathway in cytochrome oxidase activity. Micromolar levels of zinc, an oxidase inhibitor, caused strong inhibition of proton backflow, supporting the idea that proton backflow is important for oxidase activity when uptake of protons from the inside is inhibited, as in the presence of a high membrane potential or by site-directed mutations. Issues still remain concerning the quantitative contributions of protons from the inside and the outside to supporting oxidase activity under various conditions.

The region of H93 has been suggested to be involved in proton pumping in the bovine oxidase and is also a candidate for the inhibitory zinc site. Various mutant forms were produced and tested in order to determine whether H93 has a role in proton pumping or backflow in the bacterial oxidase and whether H93 its alteration diminished zinc inhibition. Various H93 mutants show close to normal proton pumping suggesting H93 is not important in the proton pumping of *R. sphaeroides* oxidase. Zinc inhibition was also observed in these mutants, ruling out the possibility that H93 plays a role in zinc binding. A decreased activity in the controlled state, particularly at high pH, caused an increased RCR for all the H93 mutants. Since the proton supply from the outside is important in the controlled state, the data suggests that H93 may be involved in proton backflow.

Preliminary results from global fitting and kinetic modeling of the complete spectra from the rapid-scanning data, obtained from the stopped-flow kinetic analysis of proton movements, suggests that this method will provide a more powerful approach to quantitative modeling of proton pumping kinetics. This approach may provide a more definitive answer to the role of proton backflow in oxidase activity and a better understanding of the physiological control of cytochrome *c* oxidase.

Dedicated to my wife

Hyunjoo Jun

ACKNOWLEDGEMENTS

I would like to express my sincere appreciation to Dr. Shelagh M Ferguson-Miller, a truly inspiring teacher and counselor; for her guidance, teaching and friendship during the course of this investigation. Grateful appreciation is also extended to Dr. J.Gregory Zeikus, Dr. Honggao Yan, Dr. Lee R.Kroos and Dr. Robert I.Cukier for serving on my guidance committee.

Special thanks go to our research team members that I have had great opportunity to work with during my graduate training. Thanks to Dr. Denise Mills for the training of the kinetic and mechanism study and to Dr. Carrie Hiser for her help of making oxidase mutants. I also greatly appreciate to Dr. Ling Qin for his crystal structures. I also thank to my fellow graduate student Jian Liu and former graduates of the lab. I am grateful to academic specialist, Alicia Pastor, for the help of TEM technique. I also appreciate my friends and fellow Korean graduate students in MSU who always encouraged in the past and present.

Finally, I am especially grateful to my family for their prayer and support. Most of all I would like to thank to my mother for being a constant support and friend. Very special thanks go to my loving wife for her patience and love while I worked on this thesis. Especially, I would like to thank to brothers and sisters of the church (New Hope Baptist church and TMS). I sincerely thank God for His loving-kindness and grace for every moment in my life.

TABLE OF CONTENTS

LIST OF TABLES

LIST OF FIGURES

"Images in this dissertation are presented in color"

LIST OFABBREVIATIONS

Aa	Arachidonic acid
BSA	bovine serum albumin
CCCP	Carbonyl cyanide 3-chlorophenylhydrazone
C*c*O	Cytochrome *c* Oxidase
CMC	critical micelle concentration
COVs	Cytochrome Oxidase Vesicles
DPX	p-Xylene-bis(N-pyridinium bromide)
FPLC	fast protein liquid chromatography
$DiSC_3(5)$	3',3'-diprophlthiadicarbocyanine
DEAE	diethylaminoehtyl
EPR	electron paramagnetic resonance
FCCP	Carbonyl cyanide 4-(trifluoromethoxy)-phenylhydrazone
FTIR	Fourier transform infrared spectroscopy
H^+/e^-	ratio of protons pumped per electron transferred from cytochrome *c* into cytochrome oxidase
HEPES	4-(2-hydroxyethyl)-1-piperazine-ethanesulfonic acid
His-tag	histidines that are genetically attached to an enzyme to allow purification by a nickel affinity column
K_D	equilibrium dissociation constant
LUV	large unilamellar vesicles
MD	molecular dynamics

Phenol Red	**phenolsulfophthalein**
Pyranine	**8-Hydroxypyrene-1,3,6-trifulfonic acid**
RCR	**respiratory control ratio**
***R.sp* (*or Rs*)**	***Rhodobacter sphaeroides***
ROS	**reactive oxygen species**
SDS	**sodium dodecyl sulfate**
SUV	**small unilamellar vesicles**
SVD	**singlular value decomposition**
TEM	**transmission electron microscopy**
Tris	**Tris(hydroxymethyl)aminomethane**
TMPD	**N,N,N',N'-tetramethyl-p-phenylenediamine**
ΔpH	**transmembrane pH gradient**
$\Delta\Psi$	**transmembrane electrical gradient**

Chapter 1 Background on cytochrome *c* oxidase (Literature Review)

1.1. Energy Transduction and Cytochrome *c* Oxidase

Aerobic organisms obtain energy from their environment by extracting electrons derived from many food sources by the oxidation of protein, carbohydrate and fat. Reduced substrates, such as NADH or succinate, donate electrons to the respiratory chain complexes which are metalloproteins embedded in a mitochondrial or bacterial membrane. In most aerobic systems, the final acceptor of electrons in the respiratory chain is an oxygen molecule, which is reduced to water by the addition of four electrons and four protons, providing a large redox potential drop and maximizing the free energy. Much of the free energy released in the reduction of O_2 to water is converted into an electrochemical proton gradient across the membrane which is used for ATP synthesis by the ATP synthase (Hosler *et al.*, 2006)(Figure1.1).

Cytochrome *c* oxidase (C*c*O) is the terminal enzyme of the respiratory chain, which catalyzes the reduction of oxygen to water and pumps protons across the membrane, contributing to the electrochemical potential gradient. The respiratory system can be "uncoupled"; that is, the electron transfer process can proceed without resulting in net proton pumping or ATP synthesis, either because the pumped protons are leaked back across the membrane by protonophores or by uncoupling proteins that dissipate $\Delta\mu H^+$, leading to the production of heat. Cytochrome *c* oxidase itself also appears to have an intrinsic uncoupling mechanism that may contribute to the control of the efficiency of its energy coupling in response to the build up a membrane potential (Mills *et al.*, 2002).

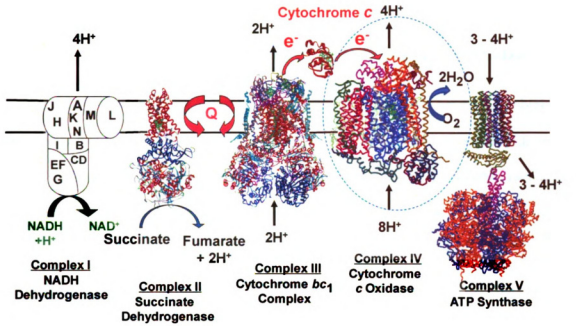

Figure 1.1 The respiratory chain complex.
Complex I or NADH dehydrogenase, (PDB:1PP9); complex II or succinate dehydrogenase (1NEN); complex III, cytochrome bc_1 (1PP9) and complex IV, cytochrome *c* oxidase (1V54). Succinate dehydrogenase mediates electron transfer through coenzyme Q to the cytochrome bc_1 complex. An electron is transferred to cytochrome *c* (1HRC) and moves to the final electron acceptor, cytochrome *c* oxidase to reduce O_2 to water. Most of the free energy in this process is converted to produce a proton gradient which is used by ATP synthase, complex V (1QO1) for the synthesis of ATP. There is no available crystal structure as yet for complex I (NADH dehydrogenase), although the Fe/S centers have been defined. The figure is from Dr. Hosler *et al.* (Hosler *et al.*, 2006).

1.1.1. Overall Stucture of the Cytochrome *c* Oxidase

1.1.1.1. X-ray Crystal Structure of Cytochrome *c* Oxidase

High resolution X-ray crystallographic structures of C*c*O have been obtained. They reveal distinct proton conducting pathways (Iwata *et al.*, 1995; Svensson-Ek *et al.*, 2002; Tsukihara *et al.*, 1996). The D- and K-pathways were named after two well-conserved key residues, D132 and K362 (*Rhodobacter sphaeroides* numbering), respectively, in the proton uptake pathways. Even with the crystal structures, there are still unsolved questions about the roles of the channels in terms of the number and destination of protons and how the proton uptake events are coupled to electron transfer.

The structure determination of a mechanistically complex enzyme like C*c*O is important for understanding its function. However, only the combined investigation of the structural data and mechanistic studies, using time-resolved techniques, can solve the proton pumping mechanism (Svensson-Ek *et al.*, 2002).

1.1.1.2. Catalytic Core Subunits and Function

The mitochondrial C*c*O has 13 subunits, whereas the bacterial C*c*O has four subunits (Figure 1.2). The 3 largest core subunits (I, II, and III) are encoded by the mitochondrial genome and are highly homologous to the core subunits of the bacterial C*c*O which have high amino acid sequence and structural similarity to the mammalian

oxidase. The structure of C*c*O has been well characterized spectroscopically and crystallographically including its four redox-active cofactors, which are located in subunit I and II: heme a and a_3, and a type II copper (Cu_B) are placed in subunit I, whereas a dinuclear copper center (Cu_A) is found in subunit II. Along with these redox active cofactors, non-redox active metals, Mg^{2+} and Ca^{2+}/Na^{2+}, are also found in the structure (Ferguson-Miller and Babcock, 1996; Gennis and Ferguson-Miller, 1995; Hosler *et al.*, 1995; Tsukihara *et al.*, 1996).

Subunit III is a highly hydrophobic membrane protein with 7 helices. Unlike the two other core subunits (I &II), it does not contain any redox centers. The function of subunit III is not entirely certain; however, there is evidence that subunit III may have an important role in the proton pumping of C*c*O (Prochaska and Fink, 1987). Even without subunit III, the two-subunit oxidase is as active as wild type, but with a generally lower H^+/e^- stoichiometry (Haltia *et al.*, 1991) and with spontaneous and irreversible suicide inactivation after multiple catalytic turnovers during O_2 reduction (Mills and Hosler, 2005). This suicide inactivation has been attributed to oxygen radical damage leading to loss of a ligand of Cu_B that normally helps to maintain the structural integrity of the active site (Bratton *et al.*, 1999).

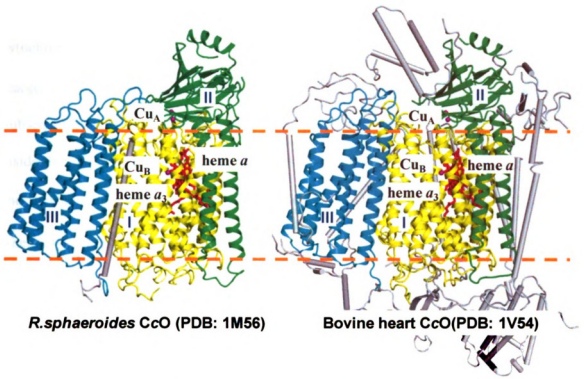

Figure 1.2 Comparison between bovine heart C*c*O and *R.sphaeroides* (*Rs*) C*c*O based on the X-ray crystal structures.

Bovine heart C*c*O contains a total of 13 subunits, including the mitochondrial encoded catalytic core subunits (I,II, and III). Bacterial C*c*O from *R.sphaeroides* only contains 4 subunits. Both structures have the same redox active metal centers (dinuclear Cu_A in subunit II, and heme *a* Fe, a_3 Fe and Cu_B in subunit I), as well as the non-redox active centers of Mg^{2+}, Na^+ (bovine) or Ca^{2+} (*R.sp*). The three catalytic core subunits are highly conserved between the bacterial and mammalian oxidases. (The figure is from Dr. Ling Qin, unpublished)

Time resolved spectroscopic studies have shown that electrons from soluble cytochrome *c* are delivered first to the electron acceptor, Cu_A in subunit II, which is placed at the interface between the external aqueous P-side and the membrane. Subsequently, electrons move to the six-coordinate heme *a* iron in subunit I, which lies inside the membrane, at a distance corresponding to 1/3 of the total membrane dielectric, and then the electrons move laterally to the heme a_3/Cu_B active site, also in subunit I, where O_2 is reduced to water.

Rhodobacter (R.) sphaeroides C*c*O is a good model for functional and mechanistic studies of the mammalian C*c*O. The bacterial C*c*O is experimentally more amenable because it can be easily grown and genetically altered. Removal of subunits and the use of site-directed mutagenesis of protein residues have been powerful in studying the mechanism of proton pumping and sites of inhibition. Using substitution of the core metals, Mg^{2+} to Mn^{2+}, has allowed EPR analysis of the subunit I/II interface. Several mutations in the core subunits in the D and K-pathways have been made in order to clarify the role of these channels and to probe the proton movement and how it is coupled to electron transfer.

1.1.1.3. Structure of the Heme a_3-Cu_B Site

The binuclear center heme a_3/Cu_B is where the oxygen reduction takes place in C*c*O. The O-O bond cleavage in cytochrome oxidase is a very complicated reaction, which is coupled to electron and proton movement. The mechanism of this reaction, O-O bond cleavage, is not completely understood.

The electron density at the binuclear center indicates the presence of a covalent bond between a histidine imidazole group and a tyrosine phenol group in the fully reduced bovine C*c*O crystal structure at 1.8 Å resolution *(Tsukihara et al.*, 2003). The covalent linkage has also been observed in the fully oxidized *Paracoccus* C*c*O at 2.7 Å resolution (Ostermeier *et al.*, 1997) and the *R.sphaeroides* (*R.sp*) C*c*O (Qin *et al.*, 2006) and confirmed by mass spectrometric analyses (Buse *et al.*, 1999). It has been suggested that this unique linkage between His-Tyr lowers the pKa of the tyrosine phenol group below that of free TyrOH allowing the deprotonated form of tyrosine OH even at physiological pH. This makes the tyrosine a potential electron and proton donor which has the possibility of becoming a radical during catalysis. The involvement of tyrosine in the oxygen reduction chemistry is supported by a number of findings (Ostermeier *et al.*, 1997; Proshlyakov *et al.*, 2000) but is not yet established.

Cu_B has a distorted tetrahedral coordination with three histidine residues and electron density that has been interpreted as a hydroxyl ion (OH^-) (Svensson-Ek *et al.*, 2002). In the bovine oxidase, peroxide was modeled as a bridge between the Cu_B and the Fe atom (Yoshikawa *et al.*, 1998) in the fully oxidized form. The possibility of one

hydroxyl ion and one water, as the Cu_B ligand, has been proposed for the ligands of the heme a_3-Cu_B site in the fully oxidized *P.denitrificans* C*c*O at 2.7Å resolution (Ostermeier *et al.*, 1997) and for the oxidized *R.sphaeroides* C*c*O (Qin *et al.*, 2006). However, the exact nature of the bridging atoms in the crystal structure of the heme a_3-Cu_B site remains controversial as does the immediate source of electrons and protons during catalysis.

1.1.1.4. Non-Redox Metal Binding Sites

In addition to five redox active metal ions (Cu_A binuclear center, Cu_B, heme *a* and a_3), mammalian C*c*O contains tightly bound non-redox metal ions including Ca^{2+}/Na^+, Mg^{2+} and Zn^{2+} (Ferguson-Miller and Babcock, 1996). There are structural differences between the bovine and the bacterial enzymes in this respect (Kirichenko *et al.*, 1998). For example, the optical spectrum of reduced heme *a* is red-shifted by Ca^{2+} in bovine heart mitochondrial C*c*O (Nicholls, 1975; Wikstrom and Saari, 1975). However, the Ca^{2+} induced shift is specific for the mammalian enzyme and is not observed with the highly homologous oxidase from bacteria, where Ca^{2+} is tightly bound unlike the mammalian Ca^{2+} which can be removed with EGTA and substituted with Na^+. It has been shown that Na^+ and H^+ compete with Ca^{2+} for binding in bovine C*c*O (Kirichenko *et al.*, 1998; Saari *et al.*, 1980). The Na^+ ions have been reported to inhibit proton pumping by C*c*O in mitochondria (Lam and Tu, 1980). These results suggest that the Ca^{2+} binding site may be functionally associated with the proton movement in subunit I of the

mammalian C*c*O , especially in the proton exit pathway (Kirichenko *et al.*, 1998). Reversible binding of Ca^{2+} to the bovine oxidase may be involved in physiological regulation of respiration and energy transduction. However, neither the ligand binding nor changes in the oxidation states induced any detectable conformational change in the Na^{+}/Ca^{2+} in bovine C*c*O (Yoshikawa *et al.*, 1998). It is also unlikely that C*c*O undergoes large scale conformational changes due to Ca^{2+} binding in bacterial C*c*O (Lee *et al.*, 2002).

A non-redox active Mg^{2+} ion lies at the bottom of a proposed water channel, 12 Å from the surface, bridging subunit I and II of C*c*O. The natural Mg^{2+} site can be substituted for Mn^{2+} for EPR studies and is situated above the hemes where there is a hydrogen-bonded network of water. Time-resolved water movement was monitored by the introduction of D_2O, or an oxygen isotope ^{17}O, with the Mn^{2+} substituted enzyme in stopped-flow, freeze quench, and EPR experiments (Schmidt *et al.*, 2003). Using $^{17}O_2$ for formation of $H_2{}^{17}O$ at the active site, it was seen bound to the Mg/Mn site during the brief turnover before freezing, suggesting a specific exit pathway for product water close to Mg. Using D_2O, added externally, the maximal proton/deuterium exchange at the Mn^{2+} site occured in less than 11.4 ms at room temperature suggesting rapid equilibrium between the Mn site and the bulk solvent (Florens *et al.*, 2001). The results suggest that the Mn^{2+}/Mg^{2+} site is involved in proton and/or water movement during turnover.

Because of the complex hydrogen-bonding network of waters around Mn^{2+}, it is unclear where exactly water or protons are moving.

The binding of metals, such as Zn^2, to C*c*O is interesting because they inhibit proton movement in many proton-dependent systems (Cherny and DeCoursey, 1999). Metal inhibition was rigorously studied in voltage-gated proton channels (Cherny and DeCoursey, 1999; DeCoursey, 2003). In C*c*O, proton uptake is inhibited by micromolar concentrations of Zn^{2+} or Cd^{2+} (Aagaard *et al.*, 2002; Mills *et al.*, 2002). Histidine and carboxylate residues or waters act as metal coordinating groups in most cases, where sites have been defined from Zn^{2+} inhibition. The specific metal binding site is not easily determined unless multi-wavelength anomalous diffraction (MAD) is used in X-ray crystallography. Heavier atoms such as Cd^{2+} can give significant anomalous scattering from incoming X-rays at the particular wavelength used for the diffraction. Since Zn^{2+} or Cd^{2+} inhibits C*c*O activity both in the purified detergent solubilized state and in reconstituted vesicles under steady state turnover (Mills *et al.*, 2002), three possible inhibitory metal binding sites in *R. sphaeroides* C*c*O need to be considered: two sites are on the inner surface for proton uptake (D and K paths) as well as one on the outer surface (the exit/backflow path) (Hosler *et al.*, 2006). Zinc binding at the entrance to the D-pathway has been suggested, based on a kinetic study (Aagaard *et al.*, 2002) as well as EXAFS (Extended X-ray absorption fine structure) analysis (Francia *et al.*, 2007). A cadmium binding site was clearly identified at the entrance of the K-pathway involving side chain atoms of $E101_{II}$ and $H96_{II}$ in subunit II, which was observed in two subunit

isotropic crystals (2.0 Å) of *R.spharoides* C*c*O (Qin *et al.*, 2006). This position at the bottom of subunit II has been previously suggested as the entry point for the K-pathway (Branden *et al.*, 2002). Other structures of the bovine C*c*O (Francia *et al.*, 2007) show Zn^{2+} binding at the entrance of the D-pathway, as predicted. However, so far there has not been a site defined on the outside surface that is a likely candidate for the exit/backflow pathway.

1.1.2. The Role of the Cytochrome *c* Oxidase

Cytochrome *c* oxidase (C*c*O) is the terminal enzyme of the respiratory chain in mitochondrial and many bacterial cell membranes. It uses the energy from the exergonic reduction of oxygen to pump protons across the cytoplasmic or mitochondrial membrane. Electrons are delivered from the P-side (periplasmic or positive) of the membrane via the cytochrome *c,* with coupled proton uptake from the N-side (cytoplasmic or negative side) of the membrane, producing a charge separation across the membrane (Figure 1.3). The additional translocation of protons across the membrane, against the electrochemical gradient, augments the transmembrane proton gradient, which is used for the synthesis of ATP by the membrane protein ATP synthase (García-Horsman *et al.*, 1994).

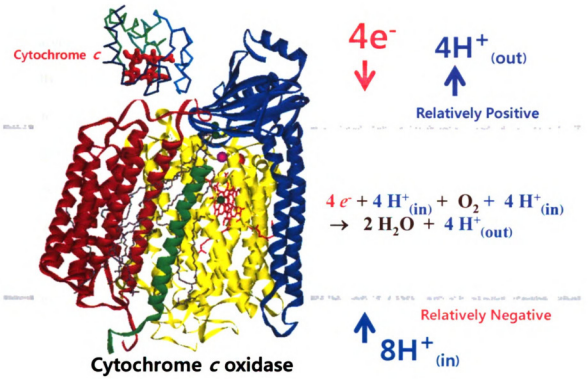

Figure 1.3 Building-up a potential gradient across the membrane in Cytochrome *c* Oxidase

A potential gradient will be made in three ways during the oxygen chemistry. Electrons are consumed from the outside (P-side) of the membrane via cytochrome *c*, with proton consumption from the inside (N-side) of the membrane. The additional prroton pumping across the membrane increases the transmembrane electrochemical gradient. These reactions result in a relatively positive outside and negative inside during turnovers.

The incorporation of C*c*O into small unilamellar phospholipid vesicles has proven to be a very useful tool in quantitative investigations of respiration (Hinkle *et al.*, 1972; Nicholls, 1974). The cytochrome oxidase vesicles (COVs) represent the simplest biological model system, and they show an increase in oxygen consumption induced by the addition of ionophores such as valinomycin and FCCP, which are classic uncouplers of mitochondrial respiration (Brunori *et al.*, 1985), exhibiting "respiratory control"; that is, the slow rate of oxygen consumption in the presence of a membrane potential that can be stimulated when the potential is broken down. A measure of this respiratory control is the Respiratory Control Ratio, RCR. The RCR of COVs is obtained from the uncontrolled rate, in the presence of ionophores, divided by the controlled rate in the absence of ionophores. Measurement of the RCR is often used as an indication of how well C*c*O is reconstituted into vesicles. The RCR can be as high as 10 or more for COVs prepared using the bovine or *Rhodobacter* enzymes.

COVs have also been shown to pump protons from the interior to the exterior medium during turnover, as in mitochondria (Sigel and Carafoli, 1978). However, in the small artificial vesicles proton availability may be one of the rate limiting factors to observation of proton extrusion. The presence of the membrane potential, $\Delta\Psi$, and pH gradient are also limiting factors in the controlled state. The addition of ionophores such as valinomycin, a potassium ionophore, increases the rate of the reaction by dissipating the $\Delta\Psi$ and allowing the pumping of protons to be observed with about 1 H^+/e^- stoichiometry. When FCCP is added, a proton conducting ionophore, the protons are

leaked back as fast as they are pumped, so that only net consumption is observed (Figure 1.4).

Electrons are taken up from the opposite side of the membrane (P-side). The proximity of heme *a* to heme a_3, shown in the crystal structures, suggest that the six-coordinated heme *a* serves as an effective electron donor to heme a_3, consistent with resonance Raman results (Han *et al.*, 1990) and confirmed by the absorption spectral change (Verkhovsky *et al.*, 1994). Heme *a* lies close to heme a_3, at almost *van der Waals* contact, donating one electron at a time to the heme a_3/Cu_B active site (Ferguson-Miller and Babcock, 1996).

The directionality of proton uptake from the inside and electron movement from the outside contributes to the generation of electro-chemical gradient across the membrane during the O_2 reduction to water (Babcock and Wikstrom, 1992; Ferguson-Miller and Babcock, 1996). Even though there is no consensus regarding the details of the proton pumping process, it has been suggested that the introduction of negative charge (electrons) into the buried heme *a*/ heme a_3/ Cu_B centers is the driving force for all of the protons taken up by cytochrome *c* oxidase. Pump protons are directed to a site (pump site) separate from the intermediates of the O_2 chemistry. Subsequent substrate proton uptake supplies the protons needed for oxygen reduction and provides the charge repulsion that expels the pump protons to the outside. Because of the complexity of the mechanism of C*c*O, structural determinations are essential for understanding the function.

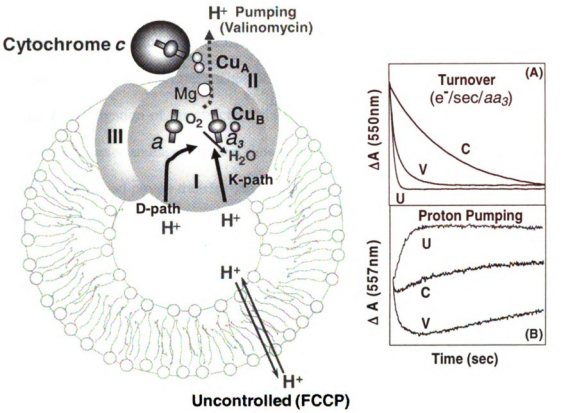

Figure 1.4 Cytochrome *c* oxidation and proton pumping with *Cc*O vesicles.
A stopped-flow instrument (OLIS-rsm—rapid scanning spectrophotometer) is used to monitor kinetic rates of the oxidation of cytochrome *c*, the electron donor to *Cc*O, at 550 nm (top panel, A). In order to monitor proton movement, specific pH-sensitive dyes are placed on the outside (phenol red) or inside (pyranine) of COVs. During turnover a membrane potential ($\Delta\Psi$) is formed from the movement of protons and electrons. This inhibits activity (controlled state) but the addition of the ionophore, valinomycin, dissipates the $\Delta\Psi$, which increases the rate of the reaction and results in proton pumping to the outside of the COVs. In the presence of FCCP, together with valinomycin, COVs are not limited by $\Delta\Psi/\Delta$pH and give the fastest turnover, as FCCP freely transports protons across the membrane allowing protons to leak back as fast as they are pumped. C: controlled state. V: with valinomycin addition, proton pumping is observed. U: uncontrolled condition.

Various biochemical methods, as well as spectroscopic, X-ray crystallographic, and biomimetic modeling studies, have been used to understand the functional and structural characteristics of this enzyme. The full understanding of proton pumping needs a combined investigation of the structural data and mechanistic studies, using techniques such as site directed mutagenesis and time resolved spectroscopy to define the specific steps of electron and proton transfer and how they are coupled (Brzezinski and Adelroth, 1998).

1.1.3. Intrinsic Uncoupling of Oxidase and Energy Efficiency

During oxidative phosphorylation by mitochondria, part of the free energy is stored as chemical energy, ATP, or is dissipated as heat. The mechanism of the physiological control of efficiency in energy transduction still remains elusive. While energy transduction by substrate level phosphorylation results in a defined stoichiometry, oxidative phosphorylation by the respiratory enzymes exhibits variable efficiencies of proton pumping. It has been proposed that there are two types of partial coupling, which result in a low yield of oxidative phosphorylation: slip and leak (Murphy, 1989).

Some protons under the control of a proton gradient may bypass the ATP synthase and go directly through the mitochondrial inner membrane without synthesizing ATP. This $\Delta\mu H^+$ dependent proton movement is called "leak" (Brown and Brand, 1991; Nicholls, 1974) and will result in the dissipation of some of the free energy stored during the respiratory reaction. This leak is highly specific for protons relative to other ions. The mitochondrial membrane permeability to protons, although very low, was 6 to 8 orders of magnitude higher than other cations (Brown and Brand, 1991). The

relationship between the respiration rate and the proton-electrochemcial gradient (in rat liver mitochondria respiring on succinate) was nonlinear when the respiration rate was gradually decreased by the inhibitor, malonate (Nicholls, 1974). This suggests that the non-linear relationship may be caused by an increase in the proton conductance of the mitochondrial inner membrane at a high value of the proton gradient or membrane potential ($\Delta\Psi$), causing leak through the membrane (Krishnamoorthy and Hinkle, 1984). The inner membrane would allow protons pumped out to leak back through the membrane when a high proton gradient is created. It has been proposed that the mitochondrial leak is through the phospholipid bilayers rather than the respiratory proteins. Anologous nonlinear relationships have been reported in related systems such as thylakoid chloroplast membranes (Schonfeld and Neumann, 1977) and membrane vesicles prepared from *Paracoccus (P.) denitrificans* (Kell *et al.*, 1978).

If the number of protons translocated across the membrane compared to the number of electrons consumed is decreased during respiration, then a lesser buildup of the membrane potential occurs due to a decreased $\Delta\mu H^+$ (proton-electrochemical gradient). This is called "slip" (Steverding *et al.*, 1993) and will result in the dissipation of the stored free energy as heat. It has been proposed that the stoichiometry of H^+/e^- in mitochondria is intrinsically decreased due to the slippage in the pump (Murphy and Brand, 1987) as the membrane potential ($\Delta\Psi$) is raised. However, the evidence for a change in the stoichiometry of proton pumping by slippage is not conclusive. Slip seems to occur in cytochrome oxidase, but not in the cytochrome *bc*1 complex (Murphy, 1989). The stoichiometry (H^+/e^-) changes can be caused by various conditions, including

modification of C*c*O by removing subunit III (Casey *et al.*, 1984; Sarti *et al.*, 1985). Another way of considering slip in cytochrome oxidase has been proposed (Blair *et al.*, 1986), where electrons pass through the complex without pumping protons by a "redox slip" process. There are technical difficulties to distinguishing between any of these "slip" and "leak" processes.

An alternative explanation for an intrinsic uncoupling mechanism has been proposed with recent COVs measurements by stopped flow techniques. There is evidence that C*c*O has the ability to control its own pumping efficiency via proton backflow through the protein itself under a high membrane potential, providing protons from the outside of the membrane instead of only from the inside to support oxygen reduction. It suggests that the efficiency of energy transduction could be regulated by physiological effectors of proton backflow, including a membrane potential (Mills et al., 2002) or by regulatory signals such as adenine nucleotides and phosphorylation (Kadenbach, 2003).

Proton backflow may be one of the mechanisms used to prevent the buildup of a high membrane potential, which can inhibit electron transfer and allow reduced intermediates to persist upstream of cytochrome oxidase. The prolonged lifetime of some of these reduced intermediates leads to the production of reactive oxygen species (ROS) (Brand *et al.*, 2004) such as superoxide or a hydroxyl radical, both of which are highly reactive toxic chemicals to the cell (Hosler *et al.*, 2006). Even though the mitochondria have sophisticated systems to annihilate ROS, including proteins such as superoxide dismutase, low levels of ROS can seriously damage the cell. The extra nuclear-encode

subunits in the mitochondrial oxidase may provide some protection and stability under toxic conditions, but the bacterial forms have fewer subunits, which may cause more deleterious conditions. It is unclear whether backflow may also be regulated by the nuclear encoded extra subunits which are absent in bacterial C*c*O.

Some bacterial cytochrome oxidases including that from *Thermus thermophilus*, have a H^+/e^- ratio that is close to 0.5 instead of 1.0 under standard conditions (Kannt *et al.*, 1998b). Mammalian cytochrome *c* oxidase shows decreased H^+/e^- ratio when subunit III is removed or chemically modified (Prochaska and Fink, 1987). However, the regulation of energy metabolism is not fully understood.

Heme-copper (a_3/Cu_B) oxidase catalyzes 90% of the molecular oxygen reduction in the biosphere without being directly involved in the formation of measurable reactive oxygen species (ROS), which are known to accelerate aging and to cause degenerative diseases. However, heme copper oxidase deficiencies, or naturally occurring mutations that inhibit oxidase activity can contribute to reactive oxygen species as well as strong inhibition of ATP production. Such defects have been linked to Alzheimer's disease (Davis *et al.*, 1997), Leigh syndrome (Zhu *et al.*, 1998), and aging (Paradies *et al.*, 1997). Therefore, cytochrome *c* oxidase exerts a major control of energy metabolism and ROS formation (Ludwig *et al.*, 2001).

1.2. Structure and Function of Cytochrome *c* Oxidase

1.2.1. Comparison of Mitochondrial and Prokaryotic Enzymes

There are significant differences in structure (number of subunits and metal binding sites), catalytic function and specifically bound lipids in mitochondrial and prokaryotic oxidases. However, there are many common features such as the redox active metal centers and the strong coupling between protons and electrons during the respiratory reaction. X-ray crystal data is now available for 4 of the 5 energy-transducing electron transfer complexes of oxidative phosphorylation, succinate dehydrogenase, the *bc*1 complex, cytochrome *c* oxidase and ATP synthase. Structural information, mutational and kinetic information is also available concerning proton transfer coupled to electron transfer in these proteins. Since evidence is accumulating that these respiratory complexes in both eukaryotes and prokaryotes may act as supramolecular structures, the function of oxidase may turn out to be modified and regulated by interactions with its respiratory chain neighbors.

1.2.1.1. Bovine Heart Cytochrome *c* Oxidase

Bovine heart C*c*O exists as a dimer when it is in detergent or in the crystalline state. The whole structure of the 13-subunit C*c*O was first revealed by X-ray crystallography in its oxidized form at 2.8 Å resolution (Tsukihara *et al.*, 1996) (Figure 1.2). It is composed of the mitochondrial-encoded three core subunits which are essential for the catalytic cycle, and ten nuclear-encoded subunits (Kadenbach *et al.*, 1987). Subsequently, crystal structures of bovine heart C*c*O in the fully oxidized, fully reduced,

azide-bound, and carbon monoxide-bound states were determined at 2.30, 2.35, 2.9, and 2.8 Å resolution, respectively (Yoshikawa *et al.*, 1998). Comparison of the crystal structures in various oxidation and ligand-binding states, at high resolution, has illuminated some aspects of the mechanism of C*c*O. With the help of a higher resolution crystal (1.8Å), a considerable amount of water was defined within the protein, which could be involved in the proton pumping mechanism, particularly in the D-pathway (Tsukihara *et al.*, 2003). A conformational change of Asp-51 (Bovine numbering) in subunit I, between the fully reduced and oxidized states, is suggested to be an important factor in the pumping mechanism. A significant rearrangement of the hydrogen-bonding network above heme *a* is proposed to drive the proton uptake and release. The pKa of the carboxyl group is strongly influenced by its redox environment. In the oxidized state, Asp-51 is most likely protonated and oriented into the protein, whereas in the reduced state it seems to be oriented to the outside. The H-pathway, including Asp-51, and a number of residues and water cavities, is defined as the proton pump pathway in the bovine enzyme. However, in the bacterial enzyme these residues are not conserved and mutations of residues within this pathway have little or no effect on the activity of the C*c*O from *R. sphaeroides* (Lee *et al.*, 2000).

The X-ray structure of bovine heart C*c*O shows that the lipids contribute to the stabilization of the dimer state and the interaction between the three core subunits and the 10 nuclear-encoded subunits. Thirteen lipids, including two cardiolipins, one phosphatidylcholine, three phosphatidylethanolamines, four phosphatidylglycerols and three triglycerides, are identified in a crystalline bovine heart C*c*O preparation

(Shinzawa-Itoh *et al.*, 2007). Mass spectrometry (MS) and tandem mass spectrometry (MS-MS) techniques were applied to determine the identity of the lipid structures, especially the unsaturated bond position and chain length of the hydrophobic tails, which are well resolved in the X-ray crystal structure. The *cis*-vaccinate (*cis*-Δ^{11}-octadecenoate) of the phosphatidylglycerol found both in C*c*O of bovine and *P. denitrificans*, were determined by mass spectrometry and X-ray structural analysis, and are suggested to be a key structural feature, important in O_2 transfer to the active site.

1.2.1.2. Prokaryotic Cytochrome *c* Oxidase

The prokaryotic enzyme is a good model system for mechanistic studies because the catalytic core is highly homologous to that of the mammalian oxidase (Figure 1.2). Moreover, it is easily amenable to site-directed mutagenesis, allowing the production of numerous mutants based on well-studied genome sequences. Since the first crystal structure of *P. denitrificans* oxidase at 2.8Å resolution (Iwata *et al.*, 1995), a lot more structural information, based on crystals with improved resolution, has enriched the understanding of the proton pumping mechanism of C*c*O. As in the bovine oxidase, the covalent bond between the histidine imidazole group that is one of the Cu_B ligands (H284) and the tyrosine phenol group (Y288) has been observed in a oxidized *Paracoccus* cytochrome *c* oxidase at 2.7 Å resolution (Ostermeier *et al.*, 1997) and *R.sphaeroides* at 2.0 Å resolution (Qin *et al.*, 2006). The His-Tyr crosslink has been suggested to have a role in the catalytic mechanism of the bacterial form of C*c*O

(Ostermeier *et al.*, 1997; Qin *et al.*, 2006) as observed in the bovine forms. The heme a_3-Cu_B bridging ligands at the active site are still controversial. A hydroxide ion and a water molecule are proposed (Ostermeier *et al.*, 1997; Qin *et al.*, 2006) as ligands of the heme a_3-Cu_B site in the oxidized bacterial C*c*O, instead of the bridging peroxide proposed for the bovine C*c*O (Yoshikawa *et al.*, 1998; Yoshikawa *et al.*, 2000). It is however difficult to assign the position and identity of the ligands at the active site because of the density of the metals and the questions about the actual redox state of the protein when it has been exposed to the X-ray beam.

The overall structure of subunits (I, II, III, and IV) of *R. sphaeroides* C*c*O are very similar to those of the *P. denitrificans*, and the core subunits (I, II, and III) are similar to the corresponding subunits of the bovine heart enzyme. There is a high sequence identity between the *P.denitrificans* and *R.sphaeroides* C*c*O (81% in subunit I, 49% in subunit II, 69% in subunit III, and 48% in subunit IV). Subunit IV, whose role is not yet known, has no direct interactions with the other subunits in the regions where it is resolved. It maintains its position mainly by indirect contacts via lipid molecules. A total of six phosphatidylethanolamines were identified in the four subunit C*c*O crystal structure from *R.sphaeroides* (Svensson-Ek *et al.*, 2002), with four positioned on the interface between subunit IV and I/III, and two associated with subunit III and subunit I. Subunit IV is not completely resolved and can be incompletely proteolyzed which may be a problem in making good resolution crystals for X-ray crystallography. Two- subunit crystals of *R.sphaeroides* C*c*O at 2.0 Å resolution revealed that the positions of lipid and detergent substitutes are also highly conserved, compared with bovine, with amino acid

residues in their vicinity, suggesting a specific role of lipid in membrane proteins (Qin *et al.*, 2006) (Figure 1.5).

As many as 178 water molecules form a hydrogen bonded network inside the *Rs*C*c*O protein. There is a high degree of conservation of ordered hydrogen- bonded waters in the proton pathways, suggesting a critical role of water in proton transfer (Sharpe *et al.*, 2005).

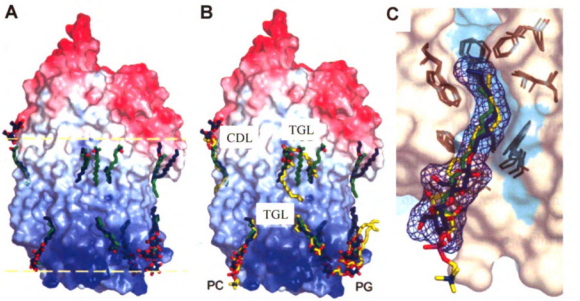

Figure 1. 5 Superposition of crystal structure showing conserved detergent/lipid binding site found in oxidase.

Conserved detergent/lipid sites were found in *R.sphaeroides (Rs), P.denitrificans (Pd)*, and bovine cytochrome *c* oxidase crystal structures (Qin *et al*., 2006). (A) Molecular surface colored by relative electrostatic potential (blue, positive; red, negative) and the detergent molecules. The alkyl chains resolved in the *Rs* C*c*O (C,dark blue; O,red), *Pd* C*c*O (C,green; O,red; N,blue) superimposed together. (B) Lipid molecules in the bovine C*c*O occupy the same sites as in Rs/Pd C*c*O structure. PC, phosphatidyl choline; PG, phosphatidyl glycerol; CDL, cardiolipin; TGL, triacylglycerol. (C) Detailed view of one of the conserved lipid-binding sites, where an alkyl chain of phosphatidyl choline resolved in bovine C*c*O occupies the same site as detergents resolved in *Rs* C*c*O and *Pd* CcO (Qin *et al*., 2006).

No conformational change is observed in the protein structure including Cu_B and heme *a* as well as other metal centers (Cu_A,heme *a*, Mg^{2+}/Mn^{2+} binding site), upon reduction in the *Paracoccus* C*c*O (Harrenga and Michel, 1999) whereas a small conformational change has been described for the bovine heart C*c*O, affecting a loop in subunit I around the residue Asp51 (bovine numbering) and the tail of heme *a* (Yoshikawa *et al.*, 1998). Recently, a high resolution structure of the fully reduced form of *R.sphaeroides* C*c*O shows a significant change in the orientation of heme a_3, which suggests an opening of the K-pathway.

1.2.2. Electron Transfer in Cytochrome *c* Oxidase

The reduction of dioxygen to two molecules of water is a complicated process that involves coupling between electron and proton transfer. An electron transfer pathway has been suggested that allows the rapid transfer of electrons from Cu_A to heme *a*, 19 Å into the membrane, but the need for a specific pathway has been challenged (Moser *et al.*, 2006). The next step, to heme a_3/Cu_B, involves a shorter (~ 4Å) transfer. Both these steps appear to be coupled to specific proton movements (Figure 1.6).

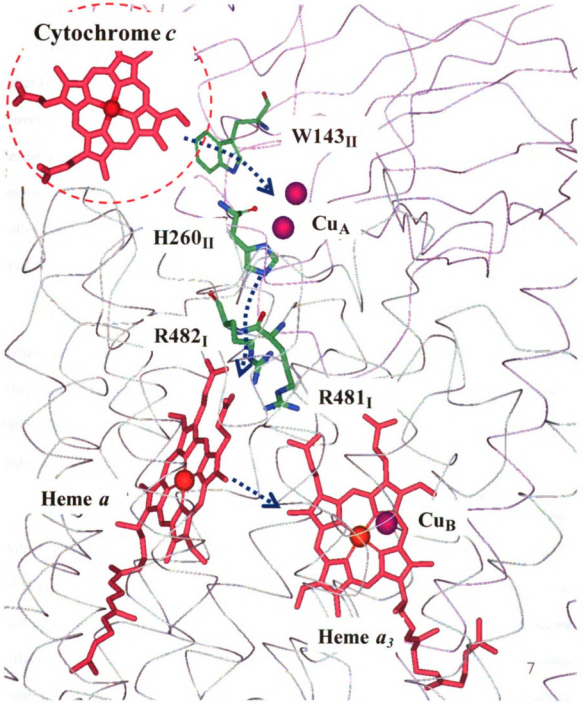

Figure 1. 6 The electron transfer pathway within Cytochrome *c* Oxidase.
Each molecule of cytochrome *c* delivers one electron at a time (Cu_A → heme *a* → heme a_3). Each electron transfer appears to be coupled to uptake of one proton from the interior. (The figure is from Dr. Frank Millett, unpublished)

1.2.3. Proton Movement in Cytochrome *c* Oxidase

Biochemical studies and analysis of crystallographic waters have led to the proposal that certain amino acids, along with resolved waters, are involved in the movement of protons into and through the interior of the C*c*O. These residues and waters define at least two distinct proton uptake pathways called the D- and K-pathways for key residues D132 and K362 (*R.sphaeroides* numbering), respectively. Both proton uptake pathways were identified with the help of site-directed mutagenesis experiments (Fetter *et al.*, 1995; Gennis, 1998; Hosler *et al.*, 1993) in bacterial forms of the enzyme.

Protons move rapidly through hydrogen bonded chains of water and amino acid residues, presumably via a Grotthus proton hopping mechanism (de Grotthuss, 1806), which allows proton transfer between hydrogen-bonded waters and amino acids (Agmon, 1995; Xu and Voth, 2005). Thus, one proton is added to one end of a chain of waters, while another proton is released from the other end.

Proton transfer through proteins may be rapid because the proton mobility along a hydrogen-bonded water chain exceeds that of proton transfer in bulk water by a factor of 40 (Dellago *et al.*, 2003). In this proton pathway, residues with exchangeable protons such as carboxylate, histidine and arginine, start or terminate the pathway at the protein surface (Hosler *et al.*, 2006). The flow of protons can be interrupted by a protonatable group in the middle of a pathway that can store a proton and then release it, as needed to satisfy the demands of the next proton acceptor.

Defining the site of water molecules in C*c*O is important for understanding long-range proton movement though proteins. Water molecules are generally coordinated with polar side chains of proteins, but are expected to be found in hydrophobic regions as well (Wu and Voth, 2003). Both waters that are resolved in the crystal structures of C*c*O, and added waters, which can be simulated by molecular dynamic calculations, are used to predict channels in the C*c*O structure, based on x-ray crystal information (Cukier, 2005). Because not all of the waters that play a role in proton transfer are resolved in the crystal structure, even at high resolution, the modeling effort is very crucial.

For example, waters that could mediate substrate proton flow from E286 to Cu_B (10-12 Å distance) are not revealed in the crystal structure, but can be modeled through a hydrophobic cavity between E286 and the active site via water molecules (Cukier, 2004; Sharpe *et al.*, 2005; Tashiro and Stuchebrukhov, 2005; Wikstrom *et al.*, 2003).

Neither the proton exit pathway nor the proton backflow pathway is obvious from either the crystal structures, or biochemical mutational studies. This may relate to the ability of proton pathways to form and dissipate during the catalytic cycle. In bacteriorhodopsin, the energy dependent conformational changes enable the access of protons on one membrane side while the other side is closed (Lanyi, 1997), and then the outer side is opened for water access, allowing the transfer of a proton across the membrane. Transient proton transfer pathways may be used by proteins to "gate" the flow of protons, in order to provide directionality or to control the timing of proton delivery.

1.2.4. The Catalytic Reaction Cycle for Oxygen Reduction

The catalytic cycle of C*c*O can be divided into three types of reactions. Oxygen binds to the reduced catalytic site first, then its O-O bond is split by a four electron transfer event and concomittant proton transfer (Gorbikova *et al.*, 2008). The cross-linked tyrosine (Y288 in *R.sphaeroides* numbering) has been suggested to be an electron and proton donor required for O-O bond cleavage. Four separate one-electron transfer reactions must occur for the complete reaction of C*c*O. Each electron transfer reaction is coupled to the uptake of two protons, a substrate proton into the active site and another proton destined to move across the membrane (Bloch *et al.*, 2004). The overall driving force for these reactions is obtained from the redox potential difference between the electron donor (cyt *c*, Em 270mV) and the acceptor(O_2/H_2O; Em 815mV) (Wikstrom and Verkhovsky, 2007). The reaction catalyzed by C*c*O is:

$$4e^- + 8H_{in}^+ + O_2 \rightarrow 4H_{out}^+ + 2H_2O$$

where the subscripts in and out refer to the inside and outside of the membrane, respectively.

1.2.4.1. Oxygen Pathway

A possible oxygen pathway has been suggested in a crystal structure of bovine C*c*O (Tsukihara *et al.*, 1996) and in *R. sphaeroides* C*c*O where they used an O_2 analog, xenon, to detect likely oxygen binding sites (Svensson-Ek *et al.*, 2002). Oxygen is very

soluble in the membrane and can easily diffuse into the transmembrane portion of C*c*O, giving access to the active site. The xenon molecule can be more easily identified in the electron density map because xenon has more electrons than oxygen (Svensson-Ek *et al.*, 2002). Two xenon molecules are resolved in the hydrophobic cavity suggesting a possible oxygen channel leading to the binuclear center. The proposed entrance of the oxygen into the protein is in the membrane spanning region, about 30 Å from the top surface of the protein, between helices II and III in subunit III.

Oxygen pathways have been identified in other oxidase structures (Soulimane *et al.*, 2000) and by computational methods (Hofacker and Schulten, 1998), and also tested by mutagenesis (Riistama *et al.*, 2000).

1.2.4.2. Catalytic Cycle of Cytochrome *c* Oxidase

At the present resolution (1.8 Å bovine heart C*c*O), C*c*O appears as a fairly rigid protein, showing only subtle conformational changes upon reduction suggesting that the mechanism of oxygen reduction and energy coupling is not dependent on conformational change. Extensive studies using spectroscopic and kinetic methods such as FTIR and fast electron transfer techniques (Millett and Durham, 2002; Namslauer *et al.*, 2002; Verkhovsky *et al.*, 1992), which measure the absorption spectral changes, have revealed a number of chemical intermediates that likely important in the catalytic mechanism and are spectrally and functionally distinct upon reduction or upon ligand binding.

During one turnover of C*c*O, several intermediates are formed that represent different redox states of metal centers such as Cu_A, heme a/a_3, and Cu_B. Various forms of intermediates have been proposed with different catalytic cycles, in which the

mechanism is coupled to electron and proton transfer (Antonini *et al.*, 1977; Brunori *et al.*, 2005). Site directed mutagenesis and time-resolved spectroscopic studies have been used to study the catalytic reaction at the active site at specific reaction steps.

During C*c*O turnover (Figure 1.7), cytochrome *c* binds to C*c*O at the electrically positive side of the membrane (P-side) and donates one electron at a time to the primary electron acceptor, Cu_A. Consecutively, an electron is transfered to heme *a* and to the catalytic site, heme a_3/Cu_B (Faxen *et al.*, 2005). The transfer of two electrons to the oxidized C*c*O results in reduction of Cu_B (state E), and also to heme a_3 (state R). The O_2 binds to heme a_3 when C*c*O has two electrons delivered to the active site, forming the intermediate A. C*c*O is more likely in a "mixed valence" form under physiological conditions, in which heme a_3 and Cu_B are reduced and heme *a* and Cu_A are oxidized. C*c*O is less likely to be fully reduced under *in vivo* conditions because electron delivery by cytochrome *c* is slower than the rate at which internal electrons are delivered to oxygen bound at the active site, unless oxygen availability is limited. Binding of O_2 to heme a_3 of mixed valence C*c*O is followed by the cleavage of the O-O bond and the formation of a state called P_M with a time constant of ~300 μs (Karpefors *et al.*, 2000b).

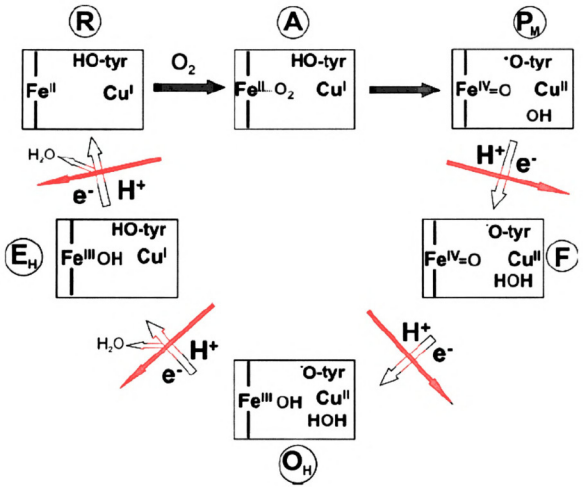

Figure 1.7 The catalytic cycle of cytochrome *c* oxidase during turnover.
The proposed model was obtained from Wikstrom *et al.* (Wikstrom and Verkhovsky, 2007). Red arrows indicate translocation of one proton across the membrane. The green arrow indicates binding of O_2 into the reduced binuclear site. The blue arrow indicates the reduction of bound oxygen in the site. The O_2 binds to a two-electron reduced R intermediate where heme a_3 and Cu_B are reduced while heme *a* and Cu_A are oxidized. Binding of O_2 to heme a_3 of mixed valence C*c*O is followed by the cleavage of the O-O bond, resulting in an intermediate, P_M. As the electron moves from Cu_A to heme *a*, a proton is taken up through D-pathway resulting in formation of the F state. Another proton and electron are transferred, forming the oxidized C*c*O (O_H). Transfer of two electrons to O_H completes the catalytic cycle through E_H.

This is a four-electron requiring reaction, and Cu_B and heme a_3 can only provide three. The cross-linked histidine-tyrosine may provide the fourth electron in O_2 reduction, and could also be a proton donor for O-O bond cleavage, when heme *a* is oxidized (Gorbikova *et al.*, 2008; Proshlyakov *et al.*, 2000). The initial assignments of P_M postulated that it contained an intact bond, a_3^{3+}-O-O^{2-} species, hence its designation as P for "peroxy" (Babcock and Wikstrom, 1992; Wikstrom, 1989) but this form was undetectable by time-resolved Raman measurements. Recent data suggests that the O-O bond is already broken in the P_M state (Fabian *et al.*, 1999) and forms a ferryl state, Fe a_3^{4+}=O^{2-}, and Cu_A^{2+}-OH^- instead of the previously proposed peroxy form (Kitagawa and Ogura, 1998). In the next step, as an electron moves from Cu_A to heme *a*, a proton is taken up from the solution through the D-pathway to the catalytic site, resulting in formation of the ferryl intermediate, F. Finally, another proton and electron are transferred to the catalytic site, resulting in formation of the oxidized C*c*O (O intermediate), which completes the catalytic cycle.

In the parallel reaction of the fully reduced C*c*O, a peroxy intermediate (P_R) is formed that also has a split oxygen bond, but the fourth electron can be donated more rapidly from the reduced heme *a*. The structures of P_M and P_R are presumably the same (Gorbikova *et al.*, 2008; Morgan *et al.*, 2001). Each of the electron transfers during the O →E, E→R, P→F and F→O transitions is coupled to proton uptake from the membrane negative side, and has been suggested to be associated with proton pumping (Wikstrom and Verkhovsky, 2007).

1.2.4.3. Missing Electron during O_2 Cleavage

As indicated above, during the reductive cleavage of the dioxygen at the active site of C*c*O, the intermediate (P) is formed, with the O-O bond broken ($Fe^{4+}=O^{2-}$, Cu_B^{2+}-OH^-). In order to break the O-O bond, four electrons and one proton are required. But only three of the four electrons that are required for this process can be provided by the metal centers (two from heme a_3 and one from Cu_B). The missing electron is likely to be donated by an amino acid residue close to the binuclear center (Svensson-Ek *et al.*, 2002). It has been suggested that the fourth electron comes from the cross-linked tyrosine (Y288-H284) that is oxidized to a neutral tyrosyl radical when the P_M is formed (Proshlyakov *et al.*, 2000) (Figure 1.8).

A tyrosine radical has been found in the P_M and F intermediates of *Paraccocus* C*c*O using EPR spectroscopy by addition of H_2O_2 (MacMillan et al., 2006). From the mutant study of conserved residues, the origin of the radical found in C*c*O has been assigned to tyrosine 175 (*Rhodobacter* numbering) first. However, this residue is not essential for the function of the enzyme, because an equivalent mutation in *P. denitrificans* C*c*O (Y167F) was still able to form the P_M intermediate and maintain a high turnover rate while retaining full proton pumping activity. Recent pre-steady state reaction kinetics of C*c*O suggests that W280 (*R.sphaeroides* numbering) could be the actual donor of the missing electron in the oxygen bond cleavage reaction (Wiertz *et al.*, 2004). The results measured with C*c*O from *P. denitrificans* suggest that a tryptophan residue (W272 in *Paracoccus* numbering, W280 in *R.sp* numbering) might form an

intermediate radical state between the original donor Y167 (Y175 in *R.sp*), and the cross-linked Y280 (Y288 in *R.sp*). Mutations of the tryptophan, W272M (W280 in *R.sp*), W272F, lead to the complete loss of catalytic activity and the ability to form the oxoferryl intermediates (P_M, F) in the reaction with hydrogen peroxide, indicating that the cleavage of the oxygen bond might not be possible in either of the W272 mutants. Moreover, the EPR signal did not show the presence of radical species in these mutants. The W272 may be the original donor of the missing electron, which is then replenished by a nearby tyrosine residue, either tyrosine 167 (3 Å away) or the cross linked tyrosine 280 (MacMillan *et al.*, 2006).

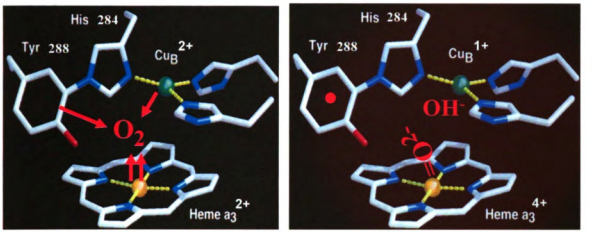

Figure 1.8 The active binuclear site structure of cytochrome *c* oxidase.
The rapid, concerted supply of 4 electrons from cytochrome *c* is required for the reduction of O_2 to H_2O. The mechanism is designed to prevent the production of harmful intermediates such as radical species. When the active site is reduced with two electrons, oxygen is bound. The other electrons come from heme a_3 iron ($Fe^{2+} \rightarrow Fe^{4+}$) and Cu_B. The last electron is obtained from a CcO tyrosine cross-linked to a histidine, producing a neutral tyrosine radical.

1.2.5. Control of Activity in Cytochrome *c* Oxidase

1.2.5.1. Effect of Membrane Potential and pH Gradient

The mechanism of energy coupling in C*c*O can be studied by measuring the effect of an electrochemical proton gradient on the steady state spectra with tightly coupled C*c*O vesicles using either cytochrome *c* (Gregory and Ferguson-Miller, 1989) or hexaammineruthenium (II) as a reductant to rapidly reduce cytochrome *c*. It was observed that the electron transfer between heme *a* and heme a_3 was inhibited by the build up of an electrochemical gradient (Moroney *et al.*, 1984). Heme *a* was reduced up to 80% in the steady state in the coupled vesicles, as measured by the absorbance at 446nm. With the addition of nigericin, an ionophore that allows the overall neutral exchange of K^+ for H^+, which causes a decreases in the ΔpH while increasing the ΔΨ, heme *a* became more oxidized, without a change in the rate of respiration, in the steady state condition. On the other hand, uncouplers, such as CCCP, transport H^+ across the membrane and lower both the □ □ and□ pH, which causes a 2- to 8-fold stimulation of the respiration, and lowers the steady state level of the reduction of heme *a*. Solubilized C*c*O also showed a pH dependency on the reduction kinetics of heme *a*. This result indicates that the electron transfer between heme *a* and a_3 is sensitive to the pH gradient. This is consistent with analysis of the steady-state by Gregory *et al.* (Gregory and Ferguson-Miller, 1989), which showed that the membrane potential had greater control of the Cu_A to heme *a* rate, while the pH gradient affected the heme *a* →a_3 electron transfer more strongly. It is also proposed that the pH on the inside of the membrane fully determines the kinetics of

internal electron transfers that are linked to proton pumping (Faxen and Brzezinski, 2007). In the mitochondria, the midpoint potential of C*c*O heme *a* was sensitive to the pH inside (Wilson *et al.*, 1976) indicating that the matrix side of the membrane controls the steady-state level of reduction of heme *a*.

Time resolved optical absorption spectroscopy, using redox dependent absorption changes of the two hemes and Cu_A in the visible-near infrared, was used to study electron transfer through C*c*O during the catalytic cycle. Both the steady-state turnover rate of C*c*O, and the rate of the specific reaction steps which are associated with proton uptake and pumping displayed pH-dependent kinetics when studied in detergent solution (Oliveberg *et al.*, 1989; Thornstrom *et al.*, 1988). The effect of pH gradients on the reaction catalyzed by C*c*O, showed that the catalytic site is in proton equilibrium with the inside of the vesicles (Sharpe *et al.*, 1995). The rates of the individual reaction steps depend on pH. The measured kinetics of an internal electron transfer suggested that the pH on the inside of the vesicles fully determines the rates of the reaction steps that are linked to proton pumping (Faxen and Brzezinski, 2007). The transition kinetics were insensitive to the pH on the outside of the vesicles.

The stopped-flow kinetics of the cytochrome *c* oxidation rates suggested that the electrochemical potential controlled the activity of C*c*O (Brunori *et al.*, 1985). The time course of the oxidation of reduced cytochrome *c* binding to COVs was measured by a rapid mixing stopped-flow experiment in the presence of various ionophores. In the presence of valinomycin and CCCP, where the electrochemical potential and pH gradients are totally collapsed, the time course of the reaction is very close to being

exponential. The ionophore, valinomycin alone, collapses the electrochemical gradient and also allows increased activity. These results lead to a proposal that the activity of C*c*O is controlled by the electrochemical potential gradient. As the reduced cytochrome *c* is oxidized, there is a buildup in the membrane potential due to the translocation of protons and consumption of electrons. The complexity of the electron and proton transfer reactions in C*c*O, and the difference in size and buffering in artificial reconstituted systems may account for the conflicting data obtained by various investigations. Studies reported in this thesis were aimed at clarifying some of these issues.

1.2.5.2. Cytochrome *c* Binding to the Complex

The electron transfer reaction between cytochrome *c* and *R. sphaeroides* C*c*O was studied using a cytochrome *c* derivative labeled with ruthenium trisbipyridine at lysine 55 (Ru-55-C*c*) (Wang *et al.*, 1999). Flash photolysis of a 1:1 complex between Ru-55-C*c* and C*c*O at low ionic strength results in rapid electron transfer from the photo-reduced heme *c* to Cu_A followed by electron transfer from Cu_A to heme *a*. A highly conserved tryptophan was mutated to an alanine (W143A) which decreased the intracomplex electron transfer, suggesting an important role of W143, to mediate electron transfer from the heme group of C*c* to Cu_A (Figure 1.9).

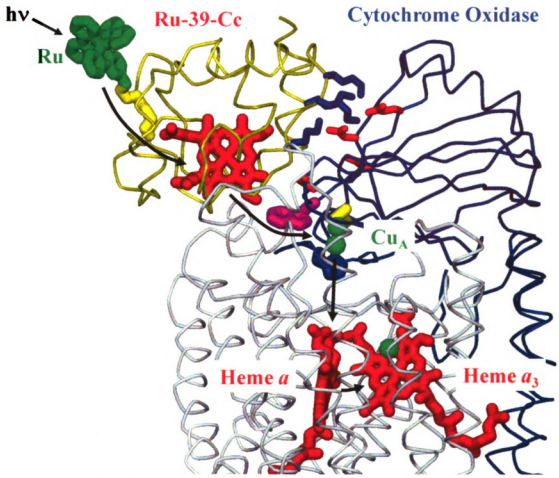

Figure 1.9 Intracomplex electron transfer in C*c*O using a Ru-39 derivative of cytochrome *c*.
Laser induced electron transfer occurs from an activated Ru(II*) to the heme of C*c* and then to Cu_A and heme *a*. Each individual reaction rate is measured by monitoring absorbance changes at 580nm (F intermediate), 605nm (heme *a*), and 830nm (Cu_A). Tryptophan 143 is shown in purple. The figure is from Dr. Frank Millett, unpublished.

The electron transfer may be controlled by the rate of cytochrome *c* dissociation from the C*c*O (Errede and Kamen, 1978). The kinetic constants obtained support the idea that the binding of cytochrome *c* is the dominant parameter in reactivity. Efficient electron transfer between cytochrome *c* (C*c*) and cytochrome *c* oxidase (C*c*O) depends on the binding interaction between them (Wang *et al.*, 1999). Facilitation of the rapid formation of a complex and an optimal orientation of the complex is required for rapid electron transfer to the electron acceptor, Cu_A. Rapid dissociation, to release ferricytochrome *c*, as well as rapid binding, is also important in maintaining activity. Steady state kinetics showed that the reaction rate was limited by cytochrome *c* dissociation at low ionic strength, and by cytochrome *c* association at high ionic strength, indicating a significant electrostatic interaction between the cytochrome *c* and C*c*O. Chemical modification studies have shown that the highly conserved lysine amino groups in cytochrome *c* are involved in the electrostatic complex with cytochrome oxidase (Ferguson-Miller *et al.*, 1978). There is evidence that at least four carboxylate groups on subunit II of C*c*O might be involved in the electrostatic interaction with cytochrome *c* (Ferguson-Miller *et al.*, 1978; Millett *et al.*, 1983). Stopped-flow spectroscopy has been used to measure the rate of complex formation, but this method has insufficient time resolution to measure the intracomplex electron transfer.

A photoreduction technique using ruthenium derivatives has allowed the study of individual steps in the mechanism, during intracomplex electron transfer from C*c* to the initial acceptor in C*c*O (Siletsky *et al.*, 2006). For example, time-resolved electron transfer and vectorial charge translocation in the F →O transition has been studied with

the N139D mutant using the ruthenium (II)-tris-bipyridyl complex as a photoactive single electron donor (Siletsky *et al.*, 2004).

1.2.5.3. Role of Subunit III

While mammalian oxidase is composed of 13 different subunits, only three of the largest subunits form the catalytic core of the enzyme. Subunit III of C*c*O is a highly conserved hydrophobic protein that contains no metal redox centers. Subunit III is part of the catalytic core of C*c*O along with subunit I and II and is encoded by the mitochondrial genome. Subunit III is closely associated with subunit I but is easily removed from C*c*O by using high pH and a detergent such as Triton X-100. Subunit III-depleted oxidase generally exhibits a decreased proton pumping efficiency without inhibiting the initial activity of the enzyme (Bratton *et al.*, 1999; Gilderson *et al.*, 2003; Gregory and Ferguson-Miller, 1988). Subunit III has been suggested to play a role in the proton pumping efficiency of C*c*O (Wilson and Prochaska, 1990), proton channeling (Thompson *et al.*, 1985), oxidase assembly (Haltia *et al.*, 1989), and O_2 channeling (Riistama *et al.*, 1996). Recent work shows that subunit III has an effect on the transfer of protons through subunit I (Hosler, 2004). The D and K-pathways lead protons from the inner surface into the heme region of C*c*O, but only the D-pathway is close to subunit III. In fact, the crystal structures of C*c*O show that D132 is located at a junction of subunit I and III, such that half of the residues surrounding D132 come from subunit III. When subunit III is depleted, D132 is more likely to be exposed to the bulk solvent. Single turnover experiments show large differences in the rate of D-pathway proton uptake in the presence and absence of subunit III, from >1000 to ~350 s^{-1}, respectively, at

pH 8 (Gilderson *et al.*, 2003). However, rapid proton uptake is restored at low pH (<6) to subunit III–depleted C*c*O. In the steady state turnover, the overall activity of subunit III-depleted C*c*O is limited by the rate of proton uptake through the D-pathway at pH 7 and above.

Slow proton uptake in the absence of subunit III is attributed to changes in the pKa of D132 or the loss of proton-collecting groups on the inner surface (Marantz *et al.*, 2001; Marantz *et al.*, 1998). A proton antenna has been proposed to aid proton uptake in bacteriorhodopsin (Checover *et al.*, 2001; Gutman and Nachliel, 1990) and the photosynthetic reaction center, as well as in C*c*O (Adelroth and Brzezinski, 2004). Surface exposed protonatable groups, e.g., carboxylate residues and histidines, which capture protons from the bulk solvent and transfer them along the surface of the protein by a process of release and recapture, effectively increasing the local proton concentration near the entry point of a pathway. The single turnover experiments show that the reprotonation rate of E286 from the bulk solvent, via D132 and the D-pathway water chain, is 1,000-fold greater than the bimolecular rate constant for the diffusion limited transfer of a buffer proton to D132 (Namslauer *et al.*, 2003). This is interpreted as evidence for a proton antenna for the D-pathway. Without subunit III, the number of antenna residues on the inner surface of C*c*O may fall below the threshold required for its operation (Georgievskii *et al.*, 2002)

In the reconstituted C*c*O, the rate of O_2 reduction is slow due to the inhibition of proton uptake against a high membrane potential. However, a slow rate of "controlled" turnover is maintained by proton backflow from the outer surface of the enzyme (Mills *et*

al., 2003) to the active site. The removal of subunit III inhibits this backflow of protons, as evidenced by a much slower rate of controlled turnover (Mills and Ferguson-Miller, 2003). The effect of inhibition by removing subunit III is similar, but additive, to the inhibition effect by zinc. It seems that subunit III facilitates both the uptake and exit of pump protons, suggesting that the backflow proton pathway operates via the reversal of the exit path. This is consistent with the long-known observation that the removal of subunit III decreases the efficiency of proton pumping to approximately half that of subunit III-containing C*c*O (Gregory and Ferguson-Miller, 1988; Wilson and Prochaska, 1990).

Particularly, subunit III-less CcO has been reported to exhibit suicide inactivation with a decreased catalytic life span, dependent on the number of turnovers. Multiple turnovers result in the irreversible loss of activity (Haltia *et al.*, 1991) apparently due to structural alteration of the Cu_B center during the catalytic cycle (Bratton et al., 1999; Hosler, 2004). Suicide inactivation is tightly linked to proton transfer (Mills and Hosler, 2005). Mutations that inhibit the D-pathway but not the K-pathway induce suicide inactivation. Likewise, the inhibited proton uptake at high membrane potential increases the possibility of suicide inactivation. It is argued that delay in proton transfer increases the life time of a reactive O_2 intermediate such as an oxoferryl form or a tyrosyl radical. The D132A/R481K double mutant increases the probability of suicide inactivation even with subunit III present because of simultaneous inhibition of proton uptake both from backflow and from inner surface. This result suggests a physiological role of proton backflow. Under conditions of a high membrane potential, where proton uptake by the

D-pathway is strongly inhibited, proton flow to the active site, via the backflow pathway, helps to prevent inactivation of C*c*O.

1.3. Proton Pumping Mechanism of Cytochrome *c* Oxidase

Protons are known to move rapidly through ordered chains of water, but how the rate and the direction of the proton movement are controlled, and how it is coupled to electron transfer, is controversial. Mechanistic questions also arise from the fact that protons are moved against an electrochemical gradient, requiring a gating process to prevent the backflow of protons.

Comprehensive knowledge of C*c*O structure, function, and kinetic /spectroscopic properties has allowed the creation of various models to explain how the proton pump functions. A cluster of heme propionates, two arginines, and an associated water network above the hemes is likely to be an acceptor site for protons, regardless of the mechanism of the pump. Proton transfer in C*c*O involves hydrogen-bonded water chains, but experimental results and computational analyses reveal complexities which are yet to be solved, such as the apparent discontinuities in the water chains in the hydrophobic regions.

1.3.1. Approaches to Understanding the Catalytic Mechanism

1.3.1.1. Electrometric Measurement

The electrometric technique may be used to monitor charge translocation due to both electron and proton transfer perpendicular to the membrane during different reaction steps in the catalytic cycle. Time-resolved potential measurements are a powerful method

to test whether catalytic steps are coupled to proton uptake and pumping (Wikstrom and Verkhovsky, 2002). Membrane potentials across the membrane can be generated by the fast injection of single electrons from laser-flash-excited, Ru^{II} (2,2'-bipyridyl)$_3^{2+}$ as a photo reductant (Ruitenberg *et al.*, 2000; Zaslavsky *et al.*, 1993; Zaslavsky *et al.*, 1995). Generation of membrane potential results mainly from three events: vectorial electron transfer into heme *a*, uptake of a charge compensating proton from the opposite side of the membrane, and pumping of protons across the membrane. Electrometric measurements that follow the movement of charge in the protein have been used to deduce the rate of proton transfer during the metal reduction phase (Ruitenberg *et al.*, 2002; Verkhovsky *et al.*, 1999; Wikstrom and Verkhovsky, 2002) and during the F to O transition (Konstantinov *et al.*, 1997; Siletsky *et al.*, 2004).

Proton pumping was thought to be linked exclusively to the oxidative phase when oxygen is reduced to water and the electrons used up are replaced (Wikstrom, 1989). However, it is argued that proton pumping also can occur during the reductive phase when electrons are supplied to the binuclear center before O_2 binding, with full efficiency but only when it is immediately preceded by an oxidative phase (Verkhovsky et al., 1999). Starting from the oxidized state, a first electron leads to pumping of one proton when there is a preceeding turnover. The energy required for pumping in the metal reduction phase may be conserved from the O_2 reduction phase by the retention of hydroxyl ligands with a high pKa or by a high redox potential for heme a_3/Cu_B during steady state turnover. The proton pathway may be partially different at each phase. The substrate protons

appear to be taken up by the K-pathway in the O→E and E →R transition (reductive phase), but substrate protons are taken up through the D-pathway in P → F and the F → O transition (oxidative phase). However, the D-pathway is required for proton pumping in both cases.

1.3.1.2. Electrostatic Calculations

Electrostatic calculations are important for estimating the pKa of important amino acid residues that may be dependent upon the redox states of heme *a*, a_3, and Cu_B, and thus aid in predictions of proton movement. Using a continuum dielectric model and Poisson-Boltzmann solution (Tiede *et al.*, 1993), a cluster of 18 residues in C*c*O were calculated to form an electrostatic network (Kannt *et al.*, 1998a). The effect of the redox status of the metal centers, in subunit I, on the pKa values of these residues was examined. In the K-pathway, the K362 did not alter its protonation state upon redox state changes, but E101 at the entrance to the K-pathway did, even though it is 25 Å away from the active site. The redox status of heme *a* was linked to changes in the arginine pair (R481/R482 in *R.sphaeroides* numbering) above the propionates of heme *a* and a_3 and was also linked with R52, which closely interacts with the formyl group of heme *a* (Kannt *et al.*, 1998a; Lancaster, 2003). The result was interesting because the salt bridges between the arginine pair and the D-propionates of the hemes were predicted to not be a part of the proton pump (Popovic and Stuchebrukhov, 2004). In this regard, there was a consensus among different analyses on different C*c*O structures. The mutagenesis (Branden *et al.*, 2005; Mills *et al.*, 2005), computational prediction (Seibold *et al.*, 2005),

and FTIR spectroscopy experiments (Behr *et al.*, 2000) implicate that the arginine/propionate cluster is part of the exit route for protons.

In the D-pathway, E286 remained protonated in all redox states. However, later electrostatic analysis of *P.denitrificans* C*c*O suggested that the protonation of E286 was sensitive to redox changes (Soares *et al.*, 2004). The quantum mechanical analysis by Olsson (Olsson *et al.*, 2005) proposed that there was a movement of a proton from the D-pathway to E286 in concert with the movement of a proton from E286 to an acceptor toward the outer surface. The protonation of the D-propionate of heme a_3 is followed by protonation of a hydroxyl bound at the heme a_3/Cu_B center. Neutralization of this hydroxyl may repulse the proton from the propionate to the outside and cause a high energy barrier for the backflow of protons.

1.3.1.3. Molecular Dynamics Simulations

The acquisition of high resolution crystal structures of C*c*O, along with increased computing power, has allowed the prediction of proton movement by computational methods (Cukier, 2004; Pomes *et al.*, 1998; Popovic and Stuchebrukhov, 2005; Xu and Voth, 2005). The movement of protein residues and the formation of water chains can be simulated by molecular dynamics methods, which along with electrostatic calculations suggest a new mechanistic view of C*c*O.

Although crystal structures can reveal information on side chain positions and stable waters in C*c*O, mobile residues and waters are not clearly observed in a crystal structure. For example, even with a high resolution crystal structure such as the recently

resolved two subunit *R.sphaeroides* C*c*O at 2.0 Å resolution (Qin *et al.*, 2006), fewer waters (178 waters) were observed than the calculated possible number. An important part of proton conduction in the C*c*O involves changes in the formation of water chains during the reaction cycle. The position of waters may aid in the understanding of proton transfer and the pumping mechanism. Therefore, prediction of the location of water and study of its mobility using computational methods is increasingly valuable for developing a mechanistic model. Programs such as DOWSER (Hofacker and Schulten, 1998; Zhang and Hermans, 1996) or GRID (Olkhova *et al.*, 2004) can be used to fill potential water sites in a structure with no *van der Waals* overlaps (Hosler *et al.*, 2006). For example, the DOWSER program places water molecules by searching for hydrophilic cavities, where hydrophilicity is measured as the interaction energy between a water molecule in the cavity and the surrounding protein. The number of waters that have been placed within the two-subunit structures of C*c*O varies from 130 to 755 depending upon selection criteria, such as interaction energies (Cukier, 2005; Hofacker and Schulten, 1998; Olkhova *et al.*, 2004; Zheng *et al.*, 2003).

Using MD simulations, methods have been developed to monitor the formation, nature, and persistence of hydrogen bonded water chains (Cukier, 2004, 2005; Seibold *et al.*, 2005). Seibold *et al.* shows regulation of formation of water chains by mutatgenesis (Seibold *et al.*, 2005). Usually MD simulations are carried out with varying restraints on protein movement; either by fixing the complete protein backbone, or fixing everything outside the area of interest. These constraints are needed to minimize the computational cost. In order to predict the movement of protons themselves through water chains,

quantum mechanical calculations have been combined with MD (Cukier, 2004; Olsson *et al.*, 2005; Xu and Voth, 2005). In this way, water chain formation can be observed in well solvated fully reduced wild type *R.sphaeroides* C*c*O, without any enzyme or water constraints. Waters were initially placed in the C*c*O by an algorithm designed to find possible stable water locations. The simulation results in numerous transient water chains in various region of the C*c*O. These water chains have a limited lifetime, but are constantly forming, breaking and re-forming quite persistently. For example, a snapshot from the MD simulation shows a continuous hydrogen-bonded network of 13 waters which spans the regions from E286 to Mg^{2+} where only one water molecule has been found in the X-ray structure (Qin *et al.*, 2006). Only two conserved waters have been found in the K-pathway in all of the C*c*O crystal structures. However, water chains can be formed during an MD simulation after the addition of extra waters (Cukier, 2005). An interesting finding was that the T359 side chain has to rotate for the formation of a hydrogen bonded water chain that spans from S299 to the hydroxyl of the heme a_3 farnesyl chain. Another water chain was formed from this farnesyl hydroxyl to the active site via Y288 in a hydrophobic region. When the heme *a* is reduced with oxidized heme a_3, a water chain was formed consisting of two waters extending from E286 to a nearby water molecule or to the D-propionate of heme a_3. In contrast, when the heme *a* was oxidized with a reduced heme a_3-Cu_B binuclear center, a water chain consisting of three waters, connected E286 to the hydroxyl group on Cu_B (Seibold *et al.*, 2005). MD showed no conformational change in K362, which has been suggested to undergo a conformational change (Adelroth *et al.*, 1998). This is not surprising because there are

limitations to this method: a MD simulation is normally performed up to 2 ns, whereas a full turnover occurs in the millisecond time scale.

MD simulations could possibly be applied to trace the exit pathway for pump protons. The continuous hydrogen-bonded water chain extending from E286 to the Mg^{2+} center is observed, but no dominant water chains are observed in the crystal structure to the outside although the region above the hemes shows a significant amount of H_2O. The R481K mutation causes a loop movement during the MD simulation containing the conserved residues W172 and Y175, leading to the collapse of a water chain (Seibold *et al.*, 2005), consistent with the observed phenotype of inhibited backflow in R481K (Mills *et al.*, 2005). This suggests that significant conformational changes may occur in response to a single mutation in an exit pathway residue.

It has been proposed that E286 may undergo some conformational change during the O_2 reduction phase, based on experimental, crystallographic, and computational methods (Cukier, 2004; Vakkasoglu *et al.*, 2006). Alternatively, W172 (Seibold *et al.*, 2005) may be a residue which undergoes conformational change as well as E286. A loop movement induced by the rotation of W172 could deliver a proton from E286 to the area above the hemes. This loop containing two highly conserved residues, W172 and Y175,has mostly hydrophobic residues (~70%) and makes hydrophobic contacts with helices II, VI, and VII of subunit I. During the MD simulation of both the wild type and the R481K mutant, this loop changes its conformation and shifts some of its amino acids and their hydrogen bonding away from the positions shown in the crystal structure.

1.3.1.4. Single-Turnover Experiments

It is not always possible to divide a catalytic cycle into partial reactions. If all substrates must be present before a reaction occurs, or if there is only one substrate, then isolated partial reactions are not possible. However, the kinetics of the system can be observed using a single-turnover of the fully reduced or mixed valence C*c*O. Methods used for studying C*c*O in order to understand each individual step during the catalytic turnover are described below.

Flow-Flash Technique

In order to try to understand the rapid movement of protons and electrons in C*c*O, various fast kinetic methods have been used that allow observation in the □ s time frame. One of these is the flow-flash technique which can give detailed information about the individual reaction steps that C*c*O undergoes under different conditions. C*c*O is initially reduced either in the two electron (mixed valence) or four electron (fully reduced) state in the presence of carbon monoxide (CO), which binds to the reduced heme a_3 /Cu_B site and blocks the site from binding O_2. The fully reduced C*c*O-CO complex is rapidly mixed with an O_2-containing solution and the reaction with O_2 is then initiated by a flash of light which induces the dissociation of the CO ligand from C*c*O. The rapid binding of O_2 is followed by O_2 reduction and bond-cleavage utilizing the electrons available at the a_3/Cu_B site. The flow-flash method can provide information on the timing and order of the proton and electron transfer reactions in a time-resolved manner (Salomonsson *et al.*,

2005) including proton uptake (Adelroth *et al.*, 1997; Oliveberg *et al.*, 1991) and proton pumping (Faxen *et al.*, 2005; Nilsson *et al.*, 1990) observed on the outside using pH sensitive dyes during the catalytic transitions in these single turnover experiments. In order to thoroughly study the proton pumping, the C*c*O is reconstituted into lipid vesicles to separate the interior from the exterior changes. The pH changes can be monitored using the pH indicator phenol red (Oliveberg *et al.*, 1991). After complete consumption of O_2, the CO re-binds to C*c*O providing ligand association kinetics. This method can also be used in the absence of oxygen, in which case the loss of CO in the 2-electron reduced enzyme is followed by flow of electrons from heme a_3 back to heme *a*.

Laser-Induced Electron Injection

A method for studying intracomplex electron transfer has been developed that utilizes a photoactive tris(bipyridine) ruthenium group [Ru(II)] which is covalently attached to the protein substrate cytochrome *c* (Durham *et al.*, 1989). Rapid electron transfer is initiated by a flash of light. Photoexcitation of Ru(II) to Ru(II*), which is a strong reducing agent, is followed by rapid electron transfer to the ferric heme group in cytochrome *c*. Subsequent electron transfer from photoreduced heme *c* to the redox centers in C*c*O occurs on a fast time scale of <50 ns (Millett and Durham, 2002). The Ru-39-C*c* derivative was designed to measure intracomplex electron transfer to the initial acceptor in C*c*O (Geren *et al.*, 1995) (Figure 1.9). These investigations determined what position could be modified on cytochrome *c* without interfering with its efficient binding to C*c*O. The electron transfer is initiated from Ru(II*) to heme *c* and continues to Cu_A

and heme *a* leading to the determination of the rate constants for each individual step in the reaction. Millett and colleagues have also developed very efficient ruthenium dimers that can react at the same site as cytochrome *c* and eliminate the sometimes rate-limiting cytochrome *c* to C*c*O reaction.

Possible intermediates associated with individual steps can be isolated and identified. For example, C*c*O was converted to state F by reaction with H_2O_2. When formed under alkaline conditions, the H_2O_2-generated F intermediate has a visible absorbance band at 580 nm (Junemann *et al.*, 2000). The sequence of the electron reductions and the rate constant for electron transfer between Cu_A and heme *a* were monitored at 830nm and 605nm (Zaslavsky *et al.*, 1998) and the reduction of the oxyferryl heme a_3 was followed at 580nm (Siletsky *et al.*, 2006). These intermediate states can be compared with the states observed in the fast electron transfer measurement.

Proton release and uptake events during a single electron transfer are monitored with pH sensitive dyes (Zaslavsky *et al.*, 2004) in order to observe the proton movements concurrently with the electron transfer. All of these reactions depend on an initial fast electron transfer from the photoreductant into Cu_A in C*c*O.

1.3.1.5. EPR Spectroscopy Analysis

The paramagnetic spin 5/2 of the high-spin heme a_3 and the spin 1/2 of Cu_B in the oxidized enzyme should make them ideal for study by EPR. However, a combination of

magnetic dipole and electronic exchange coupling between these two sites makes them both undetectable by EPR. The heme a_3 signal is EPR-visible when there is an addition of a single electron that can reduce Cu_B and this breaks the coupling between heme a_3 and Cu_B. This high-spin a_3 spectrum could be produced with high yield (nearly 100%) by adding high levels of reductant (Schmidt *et al.*, 2004).

Besides the redox-active metals, additional non-redox-active metal centers are present in C*c*O of different species (Espe *et al.*, 1995). Beef heart oxidase contains one zinc (Zn^{2+}) and one magnesium (Mg^{2+}) atom per monomer as well as Ca^{2+} or Na^{+}. *P.denitrificans* and *R.sphaeroides* C*c*O have magnesium (Mg^{2+}) and calcium (Ca^{2+}). The structural and functional roles of these metals are not clear. Even though the Mg^{2+} site is not conserved in all species, it is well conserved in all of the eukaryotic C*c*O and several bacterial C*c*O, suggesting an important role of this site.

Unlike Mg^{2+}, Mn^{2+} is visible by EPR spectroscopy. Mn^{2+} can be incorporated into the nonredox active Mg^{2+} site during growth without any changes in C*c*O activity (Hosler *et al.*, 1995) to provide a probe that can monitor the movement of water and protons close to the Mn^{2+} site. Mn^{2+} gives a strong EPR signal in the g=2.0 region of the EPR spectrum. EPR spectroscopy shows that the Mn^{2+} atom is tightly bound and the coordination geometry of the metal changes upon the reduction of the redox active metal centers. When Mg^{2+} is replaced with Mn^{2+} this creates a sensitive probe for water and proton movement above the hemes (Florens *et al.*, 2001; Schmidt *et al.*, 2004; Schmidt *et*

al., 2003). Mg^{2+} and Mn^{2+} have similar coordination so that the replacement of Mg^{2+} by Mn^{2+} results in a native proton structure. A rapid freeze-quench, electron spin echo envelop modulation (ESEEM) technique was applied to monitor water movement in the millisecond timescale using the magnetic interaction between the oxygen isotope ^{17}O and the Mn^{2+}. The ^{17}O was detected, in the form of isotopically labeled water, $H_2{}^{17}O$, at the Mg^{2+}/Mn^{2+} site with a significant line broadening of the Mn^{2+} EPR spectrum after a limited number of turnovers. In parallel experiments, D_2O was mixed with C*c*O on a fast time scale and the deuterium observed at the Mn site in <10 ms. The results suggest that the exchange of bulk water at the Mg^{2+}/Mn^{2+} site is on a catalytically relevant time scale both from the outside and from the active site. This EPR signal broadening with ^{17}O was no longer seen when the samples were allowed to turnover for 30sec, indicating that the product water at the active site had escaped when turnover was completed. A water exit pathway was proposed based on these results that reach the $Mg^{2+/}Mn^{2+}$ from the heme a_3-Cu_B site. However, the exact water pathway from the Mg^{2+}/Mn^{2+} site to the outside has not been defined. The water pathway may be involved in proton transfer as well. Moreover, the Mg^{2+}/Mn^{2+} site could provide a mechanism for preventing the backflow of protons by electrostatic repulsion, if the water exit/ backflow pathway shares the same water channel.

1.3.1.6. FTIR Spectroscopy Analysis

Fourier transform infrared (FTIR) spectroscopy has been used extensively to probe structural changes in the internal structure and amino acid protonation states of C*c*O (Iwaki *et al.*, 2003; Moody *et al.*, 1995; Nyquist *et al.*, 2003; Rich and Breton, 2001). It is a technique whereby spectra are collected based on IR using a time-domain measurement of the electromagnetic radiation. In order to understand protein dynamics, monitoring the minute changes in structure during catalytic turnover is useful in a large complex protein such as C*c*O. The identification of the important amino acids that can be protonated during the catalytic-cycle can show proton-accepting site changes during the catalytic cycle, as a first step to understand the pumping mechanism. FTIR spectroscopy can potentially resolve single proton transfer events between cofactors and amino acid side chains if the residues can be individually detected. FTIR techniques based on the vibrational differences between two samples can be used to analyze any changes in the catalytic intermediates of C*c*O. Drawbacks of the method include the large signal of water, so that C*c*O is needed to be prepared at a very high concentration as well as the difficulty of dealing with the very complex spectrum of a large protein.

The heme propionates are possible candidates for a protonation site upon reduction of C*c*O, as well as glutamate (E286) (Rich et al., 1998) and the "propionate/ arginine/ water cluster" site (Wikstrom et al., 2003). In the case of the propionates, different approaches are required in order to observe changes. The combination of isotopic labeling and redox-FTIR difference spectroscopy was applied to study the possible role of heme propionates in protonation/ deprotonation (Behr et al., 1998). The

carboxyl groups of the heme propionates were ^{13}C–labelled after supplementation with a ^{13}C labeled heme precursor, [1-^{13}C]-5-aminolevulinate. The reduced-minus-oxidized FTIR difference spectra of ^{13}C-labeled C*c*O was compared to those of unlabeled C*c*O, allowing the assignment of the signal to a C=O stretching mode of a carboxyl group ($^{13}COOH$) of at least one of the four heme propionates at 1538 cm^{-1}, which was shifted to 1500 cm^{-1} upon redox change, suggesting that it was undergoing a change in protonation or a conformational change.

Besides the carboxyl group of the heme propionate, FTIR spectroscopy can be applied to investigate protonation/ deprotonation state of carboxyl groups and has been extensively applied to the C*c*O (Okuno *et al.*, 2003; Puustinen *et al.*, 1997). The fully reduced-minus-oxidized difference spectrum in the carboxyl stretching region provided two negative bands at 1749 and 1737 cm^{-1}. These bands were assigned to E242 and D51, respectively, in bovine C*c*O. These results indicate that the orientation of the carboxyl side chains are different in the fully reduced and oxidized state, suggesting that these sites may play a key role in proton pumping through the H pathway (Yoshikawa *et al.*, 1998).

Comparison between specific ^{15}N labeled histidines and unlabeled C*c*O, showed that histidine ligands of hemes and Cu_B could be protonated upon C*c*O reduction (Schmidt *et al.*, 2004). A high degree of conservation and favorable pKa for protonation/deprotonation suggested that heme and copper-binding histidines are essential to the proton pumping mechanism (Wikstrom *et al.*, 1994). Moreover, histidine has been suggested to play an essential role in the proton antenna associated with D-

pathway proton uptake. Measuring histidine that has been specifically labeled with ^{15}N shows local changes within the C*c*O that depend on the redox state of the metals. This could be important in the proton pumping mechanism.

1.3.1.7. X-Ray Crystallography

The first atomic resolution crystal structures of mammalian (Tsukihara *et al.*, 1995) and bacterial C*c*O (Iwata *et al.*, 1995) immediately provided a better understanding of C*c*O function and its mechanism. But, defined water structures, which have an important role in proton movement, in the C*c*O can only be acquired in a very high resolution crystal.

Even with all the difficulties in making membrane protein crystals that diffract to high resolution, progress has been made to produce crystals of C*c*O under various conditions (Qin *et al.*, 2006; Qin *et al.*, 2007; Yoshikawa *et al.*, 1998). Many detergent/ lipid alkyl chains occupy essentially identical positions on the surface of C*c*O in the crystal structures of oxidases from *R.sphaeroides* and *P.denitrificans* and are also found in bovine heart C*c*O. These sites may have a critical role in structure and activity (Qin *et al.*, 2006). Conserved waters in C*c*O have helped identify two distinct proton uptake pathways on the basis of the X-ray crystallographic waters at high resolution (Figure 1.10). However, not all of the proton pathways are resolved within the crystal structures and there are still too few waters resolved to allow water chain formation. Flexible regions in the structures are also rarely resolved. Even with these limitations, various

forms of X-ray crystals (reduced/ oxidized/ with inhibitor/mutants) give information on the different forms of C*c*O, and are expected to provide important insights into structure and function, including specific association with lipids, detergents, steroids, metals and water.

Cadmium/zinc binding sites are identified at the crystallographic surface and at the entrance of the proton pathways either on the D- or K-pathways in the solubilized C*c*O (Muramoto *et al.*, 2007; Qin *et al.*, 2007). It is proposed that at least three inhibitory metal binding sites on C*c*O block the proton movement through these pathways. Only two have so far been identified by mutation and crystallography.

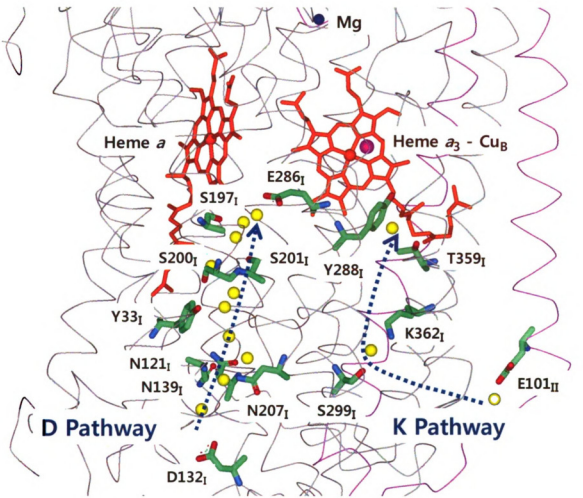

Figure 1. 10 The D and K proton uptake pathways in Cytochrome *c* Oxidase.
Two proton uptake pathways (blue arrow) are well defined in the X-ray crystal structure. These pathways are defined by water molecules (yellow ball) in subunit I from the structure of *R.sphaeroides* cytochrome *c* oxidase. Water chains are formed by a hydrogen bonding network with polar residues and water molecules. The important residues are labeled by residue number and showing the proton pumping paths. (The figure is from Dr. Ling Qin)

1.3.1.8. Amide H/D Exchange Mass Spectrometry

The transitions between catalytic intermediates in C*c*O are modulated by the opening and closing of specific proton pathways, providing alternating access for protons, and ultimately transporting protons across the membrane. It is by no means clear whether conformational changes occur that are significant in size, or only highly localized and small. The peptide backbones of C*c*O that could undergo redox dependent conformational changes were traced by H/D exchange kinetics combined with sequence based Mass spectrometry (Busenlehner and Armstrong, 2005; Busenlehner *et al.*, 2008). The chemical exchange reactions can be monitored with either continuous flow MS methods or chemical quenching followed by sample collection and direct flow injection into a mass spectrometer. The continuous flow method has been used to study H/D exchange in long-lived enzyme intermediates while chemical quenching is well-suited for the detection of short lived chemical species as in the case of C*c*O.

H/D exchange was performed on C*c*O for each intermediate state (O, R, P_M, and F) (Busenlehner *et al.*, 2006). The total percentage of deutrerium incorporated into the peptide backbone of those peptides that could be recovered, was measured as a function of time and fitted to exponential equations. For example, peptide residue numbers 352-366 contain residues involved in the K-pathway (*R.sphaeroides* numbering), while peptide 282-292 contains residues important in the D-pathway, including E286 and the Y288-H284 covalent cross-link. Peptide 123-135 contains D132 at the entrance of the D-pathway. Peptide 320-340 (subunit I) and 225-229 of subunit II were considered as being part of a possible proton exit pathway to gain information at the subunit I-II interface.

The results showed that there was a redox-dependent structural and dynamic perturbation in C*c*O. Amide H/D exchange kinetics suggested that the transition from O→R that controls proton uptake by the K-pathway is connected to structural changes that may block proton access through the D-pathway. Upon oxygen binding (R→P_M) the K-pathway peptide reporter was weakly labeled. The results were interpreted to indicate the spatial location of a gate, which controls the unidirectional proton flux through the enzyme, and to indicate that some conformational changes are likely to be involved in the pumping process.

.

1.3.1.9. Biomimetic Model Study

The biochemical characteristization of C*c*O and its various mutants has shown that proton movement is coupled to O_2 reduction at the active site and the electron transfer is coordinated with proton pumping activity. However, because of the inherent complexity of C*c*O, it is very difficult to manipulate the native enzyme. Site directed mutagenesis is a good molecular biological tool to understand the mechanism by studying the effects by making different mutations. However, it is not useful if the mutation severely inhibits the activity or causes inactivation of C*c*O (Pfitzner *et al.*, 1998). Another approach is to try to simplify the system by creating a model of the active site.

A recent model of C*c*O was established by using a mimetic system with similar structural coordination including Fe a_3, Cu_B and tyrosine designed on the basis of the native enzyme placed onto a self-assembeled monolayer of gold coated electrodes

(Collman *et al.*, 2007). In this model, the steady state catalytic reduction of O_2 was studied using this synthetic C*c*O with a mimicked structure of tyrosine 244, which delivers an electron to bound oxygen in the active site. The active site model supports the primary role of the redox center to provide four electrons rapidly to reduce dioxygen whilst preventing the release of toxic radical oxygen species (ROS). A kinetic study of the engineered active center may give information toward the understanding of the functional mechanism of native enzyme.

1.3.2. Study of Reconstituted Systems

Phospholipid vesicles can be formed to incorporate purified membrane proteins (proteoliposomes) and are a powerful tool for functional and structural studies of C*c*O. Reconstitution allows analysis of important properties of membrane proteins, such as lipid-protein and protein-protein interactions, topology of the constituent subunits and redox centers, and involvement of subunits in the energy transfer processes (Rigaud *et al.*, 1995). Particularly, the reconstitution in liposomes of energy transducing enzymes of oxidative phosphorylation has contributed evidence for the concept of chemiosmotic coupling between redox processes and ATP synthesis in mitochondrial as well as bacterial systems. In energy transducing enzymes such as C*c*O, reconstituted vesicles are an essential tool for understanding the proton translocation mechanism across the membrane. Usually membrane proteins can be isolated either in a mixed micelle with detergent, dissolved in an organic solvent, or in an aqueous environment as an aggregate or membrane fragment. After isolation and purification, membrane proteins can be reconstituted into liposomes following three main strategies: organic solvent mediated

reconstitution (reverse-phase evaporation, rehydration of lipid-protein films), mechanical means (sonication, French press, freeze-thaw), detergent-mediated reconstitutions (detergent removal, dilution or direct incorporation) (Figure 1.11). No single reconstitution procedure works for all membrane proteins. It has been possible to define a number of experimental variables that are critical to obtaining proper reconstitution systems for many proteins. In some cases, several methods are applied together.

Many of the studies on reconstituted systems have employed defined phospholipid mixtures or phospholipids extracted from soybeans, known as 'asolectin', which is a mixture dominated by phosphatidylcholine and is similar to that present in the inner mitochondrial membrane with regard to the kinds of phospholipids and unsaturated fatty acyl chains. Asolectin lipid (Avanti Polar Lipids, Inc.) contains phosphatidyl choline (45.7%), phosphatidyl ethanolamine (22.1%), phosphatidyl inositol (18.4%) and some phostatidic acid (6.9%) including some impurities (~6%).

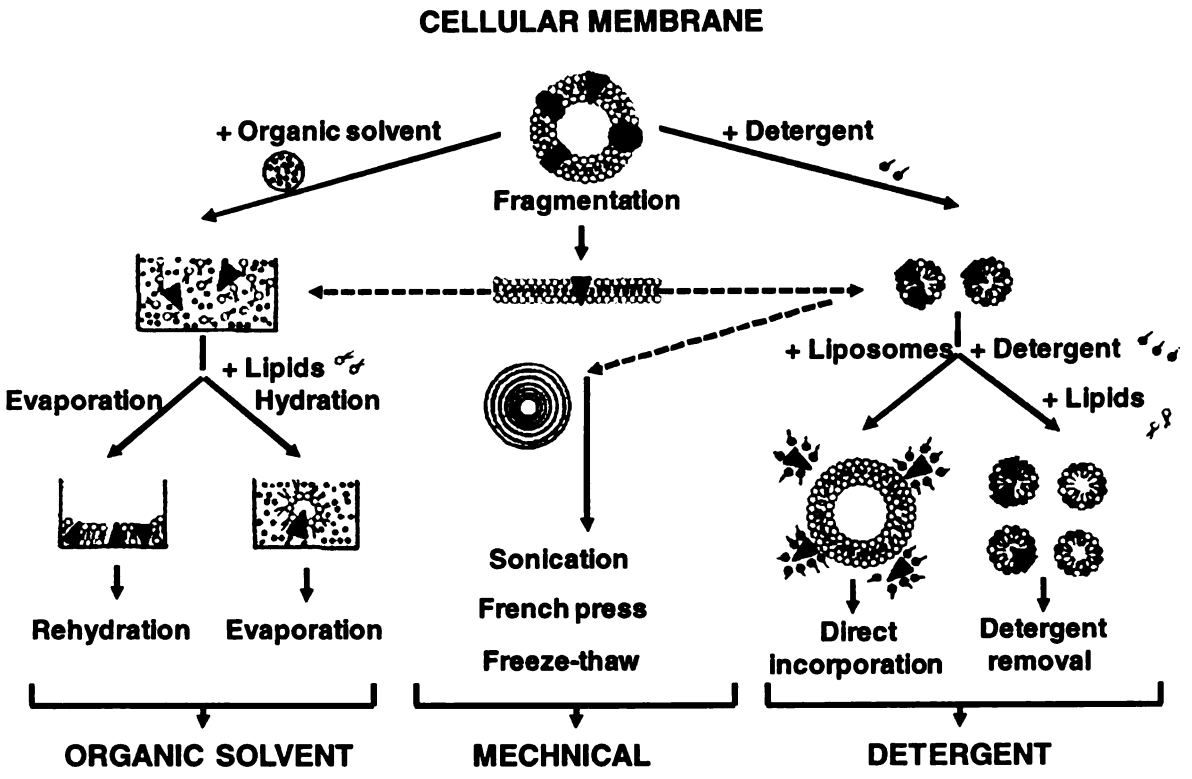

Figure 1.11 Schematic diagram for the functional reassembly of membrane protein into liposomes with different strategies.
Membrane proteins can be isolated, either in mixed micelles with detergent, by dissolving proteins in organic solvent, or in an aqueous environment as aggregates. Isolated protein can be reconstituted following three main strategies: organic solvent-mediated reconstitutions (reverse-phase evaporation, rehydration of lipid-protein films); mechanical means (sonication, French press, freeze-thaw); detergent-mediated reconstitution (detergent removal, dilution or direct incorporation). The figure is from Rigaud *et al.* (Rigaud *et al.*, 1995)

1.3.2.1. Organic solvent-mediated reconstitutions

Organic solvents have been widely used to prepare liposomes. Reconstituted vesicles which are prepared in this method have a large internal aqueous space and entrap dye efficiently. A range of buffer compositions with high ionic strength are prepared. Large liposomes of C*c*O could be formed by an evaporation procedure where a protein-lipid complex is dissolved in organic solvent followed by rehydration with aqueous buffer (Butko and Nicholls, 1993). However, this method produces a very heterogeneous population of proteoliposomes, with a large proportion of multilamellar vesicles, which have multi layers of the lipid bilayer.

The reverse phase evaporation method (Szoka and Papahadjopoulos, 1978) allowed efficient incorporation of rhodopsin (Darszon *et al.*, 1979) and bacteriorhodopsin (Rigaud *et al.*, 1983). Large unilamellar proteoliposomes (0.2 to 5μm) are formed from water-in-oil emulsion of phospholipid-protein-aqueous buffer in an excess of organic solvent, followed by removal of the organic phase under reduced pressure. Pentane, hexane, di-isopropyl ether and diethyl ether have been commonly used as organic solvents for these systems. However, organic solvents denature some amphiphilic membrane proteins. The organic solvent-mediated reconstitution method is precluded for functional studies of the reconstituted C*c*O.

1.3.2.2. Mechanical means

Dried phospholipid films, which are obtained by evaporation of solvent, are followed by a swelling procedure with an excess amount of aqueous buffer. Mulitlamellar lipid vesicles form spontaneouly. In order to produce large unilamellar

vesicles (LUV) or small unilamellar vesicles (SUV), which have higher free energies, some energy must be applied into the multilamellar system. The most commonly used technique to prepare SUV is the sonication of miltilamellar vesicles (MLV). French pressing (Barenholzt *et al.*, 1979) is also performed for the same reason, or for conversion of SUV into LUV in a reverse way, feeze-thawing (Pick, 1981) can be applied.

Sonication of a mixed suspension of lipid detergent and isolated proteins has been widely used when detergent dialysis was inefficient. The advantage of this sonication procedure is that it is rapid and requires no extra detergent, but major crucial drawbacks can be irreproducibility, inactivation of many proteins by long sonication, and the small size of the resulting proteoliposomes (20-40 nm). A major disadvantage is that it is difficult to reproduce the power output of the sonicator, particularly when small volumes are to be sonicated. Local heating is difficult to control with a probe-type sonicator. The length of time of sonication is, of course, the most critical feature and must be determined with each protein that is being reconstituted.

Freeze-thawing methods can be used, with or without sonication, to get better reconstitution (Kasahara and Hinkle, 1977). Sonication with freeze-thaw is followed by a mixing of sonicated SUV and protein with a rapid freeze technique in liquid nitrogen. This method was first used for the preparation of proteoliposomes with the glucose carrier from red blood cells (Kasahara and Hinkle, 1976). After thawing at room temperature, the mixture is exposed to brief periods of sonication (less than 2 min). This method is very suitable for proteins that are sensitive to sonication, such as cytochrome oxidase, without much loss of enzymatic activity. Very large proteoliposomes are

formed which can be broken by a short sonication leading to a preparation of unilamellar proteoliposomes with diameters ranging from 20-200 nm. The lipid bilayer is easily fractured and the exposed hydrophobic cores allow the formation of large liposomes by fusion during the slow thawing. This method is rapid and can be applied to proteins that are sensitive to detergent. However, proteoliposomes have a relatively wide range of size and have random orientation of the protein in the membrane. Possible aggregation is another limitation with this method.

Liposomes that contain phosphatidylethanolamine and about 30% of either phosphatidylserine or cardiolipin fuse rapidly on addition of Ca^{2+} or by manipulation of the pH of the mixture (Schneider *et al.*, 1980). Fusion can be measured kinetically by measuring the increase in respiration (loss of respiratory control) when ATPase is incorporated by fusion into the same vesicle that contains cytochrome oxidase. This method yields larger liposomes than the other reconstitution procedures.

1.3.2.3. Detergent-mediated reconstitutions

The most successful and frequently used strategy for the preparation of proteoliposomes for functional and mechanistical studies is a detergent-mediated reconstitution method, because most membrane proteins are isolated and purified in the presence of detergents. Proteins are first co-solubilized with phospholipids in the appropriate detergent in order to form an isotropic solution of lipid-protein-detergent and

lipid-detergent micelles. The detergent removal results in the formation of bilayer vesicles with incorporated protein.

There are various methods of detergent removal based on the physiochemical properties of detergents such as the critical micelle concentration (CMC). The 'CMC' is defined as the concentration at which the detergent monomers start forming micellar aggregates, which is related to the balance between hydrophobic and hydrophilic characteristics of the detergent. Cholate, deoxycholate, and octyl-glucoside, which exhibit a high CMC, are most suitable for a dialysis-based procedure (Allen *et al.*, 1980). The cholate-dialyis procedure was the first method used for the reconstitution of enzymes involved in oxidative phosphorylation (Kagawa and Racker, 1971). The basic procedure is to mix a suspension of phospholipids that were exposed to sonication in the presence of sodium cholate, with the isolated protein also at appropriate cholate concentrations. This is followed by the slow removal of the detergent by dialysis for about 20 hours. The cholate-dialysis method is simple and has been intensively used for a variety of membrane systems including cytochrome *c* oxidase (Brunori *et al.*, 1985). The respiratory control ratio was measured as a criterion of successful reconstitution, since it indicates a response of the enzyme to build up a membrane potential. Well reconstituted COVs allowed monitoring of the proton pumping of CcO in the vesicles by stopped flow techniques. The orientation of the protein in the liposomes is dependent of the method of reconstitution used. Vesicles prepared by the cholate dialysis method present over 80% of the reconstituted CcO oriented right-side-out (Casey *et al.*, 1984; Gregory and Ferguson-Miller, 1989). The cholate dialysis method combined with a his-tag

purification method using Ni-NTA resin that bound to a his-tagged C*c*O, improved the signal/ noise ratio by giving more homogeniously oriented COVs without background signal interference (Hiser *et al.*, 2001).

Gel filtration also can be applied to eliminate the detergent (Abeywardena *et al.*, 1983; Kagawa *et al.*, 1973). The reconstituted mixture of protein, detergent and lipid was applied to a gel-exclusion column. The protein integrated into the liposomes moves most rapidly through the column, while detergent micelles are included in the resin and eluted later. Depending upon the size of the micelles, different resin type/size can be selected for fractionization such as Sephadex G25/200 and Sepharose 4B (Wrigglesworth *et al.*, 1987). The most significant advantage of this technique is its rapidity, avoiding long periods of exposure to detergent which is common in dialysis. However, it turns into a disadvantage in terms of incomplete protein incorporation, and also in terms of a broader size distribution of proteoliposomes than found by dialysis (Abeywardena *et al.*, 1983). Too rapid a removal through a detergent free Sephadex column has yielded poor reconstitution.

Detergents with low CMC (e.g., Triton X-100) are poorly removed by gel chromatography, or by dialysis. Moreover, the dialysis requires a long time to reach an equilibrium condition. These detergents can be efficiently removed by the addition of detergent–absorbing hydrophobic polystyrene resins such as Bio-Beads SM-2 adsorbent (Bio-Rad laboratories) (Rigaud *et al.*, 1997). The hydrophobic absorption has been shown to be efficient for all kinds of detergents including those with a high CMC. The Bio-bead methods allow achievement of relatively large, more homogenous, and

impermeant proteoliposomes (Levy *et al.*, 1990; Richard *et al.*, 1995; Rigaud *et al.*, 1988). C*c*O can be successfully reconstituted in the vesicles using a Bio-Beads treatment, allowing the measurement of proton pumping (Han *et al.*, 2005) and measurement of the electrical membrane potential (Jasaitis *et al.*, 1999).

Another procedure for obtaining proteoliposomes from lipid-detergent-micellar solutions consists of diluting the reconstitution mixture (Racker *et al.*, 1979). Dilution lowers the detergent concentration to below its CMC and proteoliposomes are formed spontaneously (Dolder *et al.*, 1996). The simple dilution of a reconstitution mixture containing about 0.8% cholate lowered the concentration of the detergent sufficiently to allow the assay to be performed. The procedure is rapid since it usually requires only a short period of incubation (10-20 min) before dilution. Detergents with high CMCs such as cholate or octyl glucoside have been used. Generally, the dilution is followed by centrifugation of the diluted proteoliposomes to increase the concentration. Although employed with some success for reconstitution of different classes of proteins (e.g., ATPase complex of spinach chloroplast), the dilution techniques have failed in several systems that have been successfully reconstituted by the cholate-dialysis procedure (e.g., bacteriorhodopsin). This failure may be mainly related to incomplete removal of detergents.

1.3.3. Proton Pumping Mechanism

To better define the processes of proton exit and backflow, and to determine whether proton backflow can only supply the active site, or whether the proton can move all the way through the protein, it was important to quantify the amount of protons that are translocated through the membrane during the catalytic cycle. Measurement of protons both in the interior and the outside of C*c*O reconstituted into vesicles would be necessary to achieve this aim. There is little research on the accurate measurement of proton movement through C*c*O due to technical problems. The work reported in this thesis was directed at solving a number of these problems in order to better define the proton pumping/backflow reactions in cytochrome c oxidase.

1.3.3.1. Electroneutrality Model

The ability of C*c*O to pump protons was first established by Marten Wikstrom (Wikstrom, 1977). The mechanisms of redox-driven proton pumps has been discussed in detail and there is an extensive body of knowledge on the mechanism of C*c*O (Malmstrom, 1985; Popovic and Stuchebrukhov, 2004; Wikstrom *et al.*, 1981b). However, the molecular basis of coupling between electron transfer and proton translocation in C*c*O is not established.

One general concept is that preservation of electroneutrality is the major driving force for proton movement (Mitchell and Rich, 1994). Each electron that is transferred into the buried heme *a* and heme a_3/Cu_B sites should induce uptake of a compensating positively charged proton. The protons that are to be pumped are loaded to the vicinity of

the heme a_3 propionate (pump site), and moved toward the exterior by electrostatic repulsion due to the chemical proton uptake (Morgan *et al.*, 1994; Rich, 1995). The proton translocation, which occurs against a $\Delta\mu H^+$ and $\Delta\Psi$ in an endergonic process, requires that there be appropriate sites for loading the protons and gates to prevent their back leak.

1.3.3.2. Proton Pumping Element

The propionates of the hemes (Iwata *et al.*, 1995), the δ^- nitrogen of histidine 291 (bovine numbering) (Popovic and Stuchebrukhov, 2004), and the water cluster above the heme groups have all been proposed as possible pump sites.

The proton affinity induced by a pKa change of a proton pumping site may be modulated by changes that occur during reaction. The pumping element must be accessible to protons from the inner surface of the oxidase (N-side) and at a later point be accessible to the outer surface (P-side) to release the proton.

As discussed (Section 1.3.2.4), it has been suggested that a conformational change of E286 (*R.sphaeroides* numbering) may occur, dependent on its protonation state. The likely conformational change of E286 is supported by FTIR spectroscopy (Nyquist *et al.*, 2003), computational analysis (Cukier, 2004; Pomes *et al.*, 1998), and structural data (Svensson-Ek *et al.*, 2002).

1.3.3.3. Proton Pumping Mediated by Cu_A or Heme *a*

Initial models of proton pumping in C*c*O suggested a role for the dinuclear Cu_A in controlling proton movement (Blair *et al.*, 1986). A second proposal was based on the heme *a* redox center (Babcock and Callahan, 1983). There is evidence that the heme *a* redox potential does vary as the C*c*O is turning over (Wikstrom, 1981). The steady state reduction level of heme *a* is dependent on both the pH and the transmembrane potential. It was suggested that a redox-driven change of the hydrogen bond strength between the formyl substituent of the porphyrin ring of heme *a* could be used to translocate a proton (Babcock and Callahan, 1983). The formyl group is involved in a hydrogen bond with a nearby proton donor from the protein, and is observed to change its stretching frequency (measured by Raman spectroscopy) upon reduction of heme *a*. The hydrogen bond appears to be strengthened upon reduction by 2-2.5 kcal/mol (Babcock and Callahan, 1983). This energy may contribute to driving a proton against the electrochemical gradient across the inner mitochondrial membrane.

An alternate model was proposed based on an important role for Cu_A as the site of redox coupling to proton translocation. This model suggested ligand switching at the Cu_A site, driven by conformational changes in the coordination geometry of Cu_A upon reduction and reoxidation of the Cu_A (Chan and Li, 1990; Gelles *et al.*, 1986). Redox energy from the reduction of the Cu_A site is proposed to move the proton from the matrix side of the pump site to the cytosolic side through ligand exchange and proton transfer. Chemical modification of the Cu_A site inhibited proton pumping, supporting this idea.

However, these mechanisms lost support with the finding that the heme-Cu oxidase of *E.coli*, a bo_3 type quinol oxidase, pumps protons without the benefit of Cu_A or a formyl group on its low spin heme *a* (Puustinen *et al.*, 1989) and the finding that mutational modifications to the site did not inhibit proton pumping (Zhen *et al.*, 2002).

A more recently proposed mechanism, based on the high resolution crystal structures of bovine C*c*O (Tsukihara *et al.*, 1995), involves an aspartate residue (D51 in bovine numbering) near the outer surface of subunit I which changes its position based on a change in the redox state of heme a. In the X-ray structure of the oxidized state, the aspartate is buried in the hydrophobic environment with a high affinity for protons, and is proposed to be connected to a channel involving a water cluster and the formyl group of heme *a*. In the reduced form, the aspartate is exposed to the outer surface with a low affinity for protons and is disconnected from its proton source based on the altered water chain in the oxidized versus reduced enzyme structure.

1.3.3.4. Proton Pumping Mediated by the Heme a_3/ Cu_B Active Site

There is considerable controversy about the mechanism of how proton pumping is linked to the O_2 chemistry at the active site.

The histidine cycle is an example of a proton pump directly coupled to the redox chemistry at the active site (Morgan *et al.*, 1994). In this proposal, protons transferred from the negatively charged aqueous N-side of the membrane are moved to a pump site because of the negative charge in the buried heme center introduced by electron transfer.

A histidine ligand of Cu_B has been suggested as the proton loading/ pump site. In this mechanism, the histidine serves as the proton transfer vehicle by cycling between imidazolate (Im^-), imidazole (ImH), and imidazolium (ImH_2^+) states. This idea in its original form, involving the changes due to oxygen chemistry seemed less likely when kinetic data revealed that proton pumping occurred during the reductive phase of the catalytic cycle (Bloch *et al.*, 2004; Verkhovsky *et al.*, 1999) as well as oxidative steps.

The free energy available during the O_2 reduction phase is larger than that available during the initial metal reduction phase, due to highly exergonic nature of the oxygen reaction. However, the paradigm that all proton translocation by the C*c*O takes place during and after the breaking of the O-O bond has been challenged by recent time-resolved spectroscopy and also time-resolved electrometry, which detects charge movements within the dielectric of the enzyme after laser-activated electron injection. The data show that there is proton translocation during the reduction phase before oxygen binds (Verkhovsky *et al.*, 1999). Some evidence supports that the first electron reduction of the C*c*O does not lead to proton pumping unless a preceding oxidative phase (R→O) has just occurred. C*c*O may conserve part of the energy of the oxygen chemistry so that proton translocation is driven in the later reductive phase of the catalytic cycle (Verkhovsky *et al.*, 1999).

1.3.3.5. Conformational Changes in C*c*O

Various models of proton pumping in C*c*O have been proposed that suggest conformational changes of certain important amino acids due to their protonation states.

E286 is considered to be an important pumping element that is not a metal ligand but is close to the active site. It is proposed that E286 serves as a branch point that alternately directs protons to the pump site or to the active site.

A detailed mechanism, based on a conformational change of E286, and dependent on its protonation state, was postulated (Brzezinski and Larsson, 2003). The movement of E286 is supported by FTIR spectroscopy evidence (Lubben *et al.*, 1999; Nyquist *et al.*, 2003) and computational analyses (Cukier, 2004; Hofacker and Schulten, 1998; Pomes *et al.*, 1998) in addition to the structural data (Svensson-Ek *et al.*, 2002). A modified mechanism has been proposed (Branden *et al.*, 2006) where the pumped proton controls the electron transfer.

A conformational change of the D51 residue (bovine numbering) has been proposed (Yoshikawa *et al.*, 1998) as a key element in the H-pathway proposed for the bovine C*c*O (see Section 1.3.3.7. H-Pathway). Mutations of a histidine (H93 in *R.sphaeroides* numbering), which has the closest spatial alignment with D51 in bovine C*c*O, were made in order to probe the conformational movement in this region, because D51 is not conserved in bacterial C*c*O. A conformational change was observed upon binding of cytochrome *c* by using fluorescent labeling techniques with the H93C mutant C*c*O. Additionally, substantial movement of H93 was also observed in a molecular

dynamics study of the R481K mutation (Seibold *et al.*, 2005) along with the nearby E182 residue .

An MD simulation study also suggested a possible conformational change at a different loop area induced by mutation of R481 to K481 (*R.sphaeroides numbering*), resulted in blocking the water chain formation in C*c*O (Seibold *et al.*, 2005). In the R481K mutant, the W172 was shifted 4.4 Å away from the original position of the wild type C*c*O. A recent crystal structure of the reduced form of *R.sphaeroides* C*c*O (Qin *et al.* unpublished) shows a significant conformational change in the heme a_3 porphyrin ring and farnesyl tail, as well as residues in the K-pathway.

Several high resolution structures of bovine C*c*O (Yoshikawa *et al.*, 1998), have led to the proposal of a unique conformational change in subunit I that may be involved in proton pumping. A significant change in the pKa of an acidic group can be introduced by a very small conformational change in C*c*O. Careful comparisons of crystal structures in various oxidation states at high resolution suggest a redox driven change in the conformation of D51 (bovine numbering), proposed to release protons from the negative side surface to the mitochondrial exterior via the hydrogen-bond water network. (as discussed in 1.3.3.3)

1.3.4. Mutational Analysis of Proton Pathways

1.3.4.1. D-Pathway for Proton Uptake

The D-pathway is considered to start at an aspartate (D132 in the *Rhodobacter sphaeroides* oxidase) located at the negative side (N-side) and to continue to a glutamate (E286) about 25 Å distant from D132 and 12 Å from the hemes (low spin heme *a* and high spin heme a_3) via a hydrogen bonded network involving a chain of water molecules and protonatable residues (Figure 1.12). The D-pathway is likely to be involved in the major proton uptake of both substrate protons used at the active site for oxygen reduction to form water molecules, and of protons to be pumped across the lipid membrane (Adelroth *et al.*, 1997; Konstantinov *et al.*, 1997). It appears that all four pumped protons and two substrate protons consumed during the oxidative phase (P→F and F→O transition) are taken up via the D-pathway. There are twelve crystallographically resolved water molecules that form a pathway between D132 and E286 that facilitates rapid proton transfer from the bulk aqueous phase to the enzyme interior. However, no obvious proton connectivity is found beyond E286 in X-ray structures. The area between the E286 and the binuclear center / heme a_3 propionate group is predicted by statistical-mechanical calculations (Riistama *et al.*, 1997) to be involved in a water-mediated proton transfer through this hydrophobic cavity. The area must contain water during the catalytic reation in order to fulfill the complete proton transfer for oxygen reduction. A possible transient water pathway within this hydrophobic cavity was also predicted by other modeling approaches (Cukier, 2004; Tashiro and Stuchebrukhov, 2005; Wikstrom *et al.*, 2003). Movement of water molecules during the catalytic cycle could limit electron

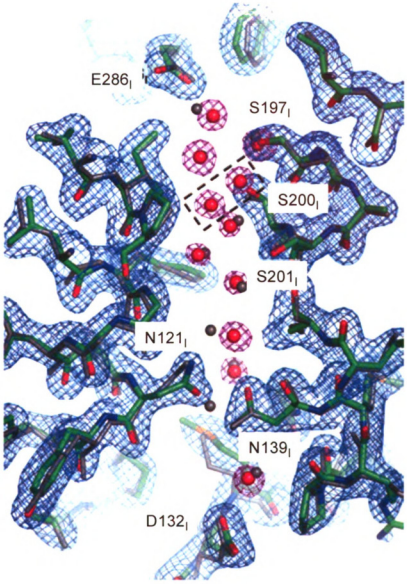

Figure 1.12 The resolved waters in the oxidase D-path structure.
The resolved waters in the D-pathway of proton uptake in the two-subunit crystal structures of *Rs* C*c*O (C,green; O,red; N,blue) from Qin *et al.* (Qin *et al.*, 2006). Four-subunit *Rs* C*c*O (1M56) is superimposed on the two-subunit crystal (gray color). The dotted black box indicates two additional waters which were resolved in the two-subunit *Rs*C*c*O. The $(2F_o\text{-}F_c)$ difference electron density map contoured at 1.0σ is shown in blue and magenta.

transfer (Kornblatt, 1998). Water molecules might provide proton conductivity from E286 to the propionate as well as the binuclear site via water dipole reorientation (Wikstrom *et al.*, 2003) in which the Grotthuss array (Wraight, 2006) for proton transfer switches as redox states of the metal centers (heme *a* or heme a_3/Cu_B) change.

One of the protonatable amino acid residues that has a central role in the D-pathway is E286 in subunit I of C*c*O. The role of E286 in regulating the proton transfer through the D-pathway has been extensively examined by mutagenesis (Aagaard *et al.*, 2000; Adelroth *et al.*, 2000; Namslauer *et al.*, 2003; Namslauer *et al.*, 2007). E286 has been proposed to be a part of the proton pumping pathway, based on the crystal structure of C*c*O from *Paracoccus denitrificans* (Iwata *et al.*, 1995). E286 is buried at the end of the D-pathway between the two hemes. It is probably a branching point from which protons may be transferred, either to the catalytic site or toward the heme propionates, depending on a redox-linked transient conformational change. E286 has been proposed to accept the pumped protons and shuttle these protons to an acceptor located further away (Nyquist *et al.*, 2003; Popovic and Stuchebrukhov, 2004). In the native state, E286 is postulated to be in its protonated form because of its proposed high pKa, which allows rapid reprotonation from the bulk solvent through D132 (Namslauer and Brzezinski, 2004). When it was mutated to a non-carboxylic amino acid (E286Q, *Rhodobacter* numbering), the mutant showed an overall turnover that was strongly inhibited (0.02% of wild type), but with the same rate and absorbance changes for the single electron transfer for the formation of the peroxy intermediate. However, electron transfer after formation of the peroxy intermediate (P) is impaired (0.2% of that of the wild type). Cu_A remains

reduced, and no protons are taken up from the medium during the reaction with oxygen (Adelroth *et al.*, 1997). This is different from the D132A mutant, which is at the beginning of the D path and is chemically rescued by arachidonic acid. Rescue by arachidonic acid is not observed for E286Q. When E286Q is reconstituted into vesicles, the very low activity is highest under the controlled condition, as observed with the D132A mutant. Protons from the external side of the membrane can supplement those from the impaired D pathway to stimulate the activity and allow some slow electron transfer to proceed.

Even the conservative mutation to an aspartate (E286D) results in decreased activity (50% of that of the wild type) as well as a lowered deuterium isotope effect (~2.5 as compared with ~7 in the wild type C*c*O) (Adelroth *et al.*, 2000). The smaller deuterium isotope effect in E286D indicates that proton transfer from E286 determines the rate. It was proposed that the proton transfer from E286 to the binuclear center determines the transition rate of of both $P_R \rightarrow F$ and $F \rightarrow O$ transitions (Mills *et al.*, 2000; Verkhovskaya *et al.*, 1997).

When the amino acid D132 is mutated to any non-carboxylate residue, the residual activity is only 5% of wild-type in the *R. sphaeroides* aa_3 oxidase (Fetter *et al.*, 1995; Mills *et al.*, 2000) and proton pumping is lost by blocking the entrance of the D-pathway. This result provided the first evidence for the critical role of the D-pathway in transferring the pumped protons. A similar mutation effect was found in an other type of enzymes such as the *E.coli* bo_3 oxidase (Thomas *et al.*, 1993). Blocking proton uptake

from the D-pathway in *E.coli* bo_3 oxidase by the equivalent mutation of D135 (in *E.coli* numbering) to asparagines, results in the decoupling of the proton pumping with diminished turnover activity. When the D132A is reconstituted into the lipid vesicles, protons from the outside, in the presence of a membrane potential, stimulated the activity, resulting in a reverse respiratory control (RCR<1). The result indicates that contribution of protons supplied from the outside can control the activity of CcO when it is inhibited from taking protons from the inside as well as inhibited by the presence of a membrane potential.

Even more clear evidence for the importance of the D-pathway was found when conserved aspargines in the D-pathway (Han *et al.*, 2006; Pawate *et al.*, 2002; Pfitzner *et al.*, 2000) were mutated to aspartate (N139D and N207D in *R.sphaeroides* numbering). These mutations lead to decoupling of the proton pump, either without altering the activity, or by increasing the activity. Several possible explanations were proposed. First, based on kinetic experiments, the reason for this short-circuit was attributed to an electrostatic effect which raised the pKa of E286 (Branden *et al.*, 2006). This could affect the proton movement in the pathway from E286 to the outside versus to the active site. The higher pKa of E286 could make it more difficult to protonate an external pump site, so the proton will go to the active site instead. Interestingly, replacement of the acidic residue, D132, by Asn in the N139D mutant giving the D132N/N139D double mutant, results in restoration of the E286 pKa to the original value and recoupling of the proton pump during steady state turnover (Branden *et al.*, 2006) even with a decreased turnover of about 20% of wild-type CcO.

The precise conserved location of the carboxyl residue at the 286 position seems to be somewhat flexible. The double mutant E286A/I112E, which has a glutamate relocated to the opposite side of the proton transfer pathway, showed higher turnover activity than the E286A single mutant and is still able to pump protons with about a 0.4 H^+/e^- stoichiometry (as compared to ~1 H^+/e^- for the wild type enzyme) (Aagaard *et al.*, 2000). The D132 mutant C*c*O activity (e.g. D132A or D132N) was rescued by the addition of long chain fatty acids (Fetter *et al.*, 1996). However, fatty acids do not restore the proton pumping, presumably because of competitive kinetics between the backward and forward directions of the protons in the pathway.

1.3.4.2. K-Pathway for Proton Uptake

The K-pathway appears to start with a glutamate residue (E101) and a histidine (H96) in subunit II on the cytoplasmic surface of the enzyme, based on mutagenesis results and X-ray structure analysis (Qin *et al.*, 2008; Qin *et al.*, 2007) (Figure 1.13). An important conserved amino acid, lysine 362, was mutated to methionine in the K-pathway, resulting in extremely low activity (less than 0.2% of wild type) and heme a_3 becoming very difficult to reduce, whereas heme *a* is readily reduced. Interestingly, the K362M is slow to reduce except in the first measurement of reduction, as it elutes from the column. However, the fully reduced K362M mutant becomes fully oxidized in about the same time period as the wild type and displayed similar proton uptake as the wild type (Adelroth *et al.*, 1998). It has been postulated that K362 could be required as a proton trap, rather than being used for proton uptake for neutralization of the charge at heme a_3

/Cu_B (Junemann *et al.*, 1997). However, this result indicates that the K362 is important in proton uptake during the reductive phase of the catalytic cycle. Unlike the initial proposal that the D- and K-pathways correspond to the uptake of pumped and substrate protons, respectively (Iwata *et al.*, 1995), it appears that all four pumped protons are taken up via the D-pathway and two substrate protons as well, taken up during the oxidative phase ($P_M \rightarrow F$ and $F \rightarrow O$ transition) via the D-pathway through E286 (Adelroth *et al.*, 1997). The K-pathway is not involved in proton uptake during oxidation of the enzyme by O_2 (oxidative phase). The K-pathway is exclusively used for proton uptake during the reductive phase (O to R transition)(Adelroth *et al.*, 1998; Branden *et al.*, 2001). Both of the substrate protons for heme a_3/Cu_B reduction are likely taken up by the K-pathway (Forte *et al.*, 2004; Vygodina *et al.*, 1998). It has been proposed that the first proton is taken up by the K-pathway and the second by the D-pathway (Ruitenberg *et al.*, 2000; Sharpe and Ferguson-Miller, 2008; Wikstrom *et al.*, 2000) or, that the K-pathway is used for proton uptake only immediately after oxidation of the fully reduced C*c*O (Branden *et al.*, 2001). The precise number and timing are still an issue.

The K-pathway appears to sequentially involve E101, S299, K362, T359, the hydroxyl farnesyl of heme a_3 and Y288 of subunit I. The T359 is suggested as a potential polar group for hydrogen bonding with water to aid in proton translocation. Y288, which is placed close to the binuclear center and forms a cross-link with H284 (Ostermeier *et al.*, 1997; Yoshikawa *et al.*, 1998), appears to play an important role in the catalysis of O-O

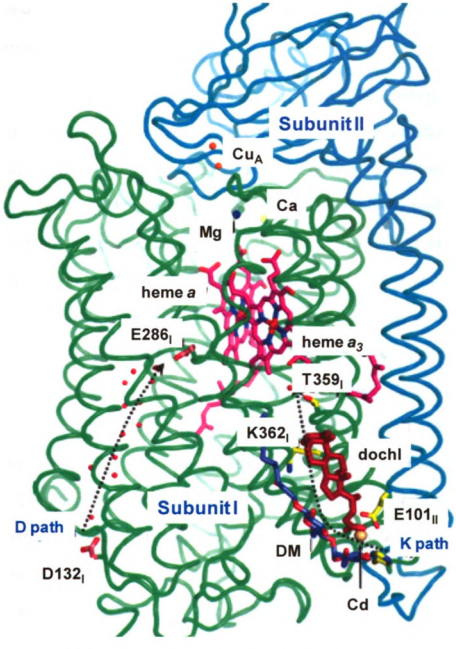

Figure 1. 13 The K-pathway and important residues.
The core subunit I (green) and II (cyan) is shown with deoxycholate (red sticks) resolved near the K path entrance in the structure of *Rs*C*c*O (Qin et al., 2008). Decyl maltoside (DM) is also resolved nearby. The metal centers are shown as spheres (Cu, orange; Fe, red; Mg,blue; Ca,yellow; Cd,wheat). The heme groups are colored by atom type. The black dotted lines indicate the proton uptake channel which is mediated by water molecules within the pathway, shown as red spheres.

breakage by donating both an electron and a proton (Gorbikova *et al.*, 2008; Sharpe and Ferguson-Miller, 2008).

Computational methods have been applied (Cukier, 2005) to study the formation and properties of water chains because there are only two crystallographically resolved water molecules in the K-pathway of C*c*O. The hydrogen bonded water chains are likely formed on the MD time (ns) scale. Water chains are readily formed in the region of the K-pathway suggesting the possibility of side-chain movements of the residues K362 (Branden *et al.*, 2001), T359 (Cukier, 2005), and Y288 (Sharpe *et al.*, 2005) which have been proposed. The results from molecular dynamics calculations suggest that a structural change of the K362 side chain, via the water rearrangement facilitates proton transfer to the catalytic site (Hofacker and Schulten, 1998). The K362 side chain may be flexible and shuttle protons from S299 to T359 (Cukier, 2005). According to electrostatic calculations, K362 is in a neutral state over a wide range of pH due to the lack of compensating dipolar or charge-charge interactions. More recent data indicate that the K362 is protonated at pH 7 and moves transiently to an upward position during formation of the P_R intermediate to compensate for the change in the charge state at the binuclear center (Branden *et al.*, 2001). Other analyses (Sharpe and Ferguson-Miller, 2008) suggest that K362 may be associated with a hydroxyl rather than a water, stabilizing its positively charged form.

Proton transfer via the K-pathway can be very fast (Belevich *et al.*, 2006) based on a kinetic study of reversal of electron flow from heme a_3 to a in the two electron reduced, mixed valence C*c*O. Fast (nanosecond to microsecond) electron transfer from

heme a_3 to heme *a* is followed by proton release from the C*c*O through the K-pathway to the bulk medium. Even though the fast rate of proton transfer in the reverse direction from the binuclear center to the inner, N-side of the membrane was measured (Belevich *et al.*, 2006), the rate of proton transfer in the forward direction may be much slower as it may be limited by the rate by which protons from the aqueous phase enter the pathway. Proton uptake may be strongly enhanced in the case of the D-pathway due to the proton collecting antenna groups around the entrance (Karpefors *et al.*, 1998). However, the proton uptake through the K-pathway might be much slower because there is no such antenna around its entry point.

The K-pathway appears not to be capable of transferring a proton to the proton loading site for the pump, whereas the D-pathway is capable of transferring both substrate and pump protons. Electron transfer from heme *a* to the binuclear site without a proton in the pump site may be very unfavorable energetically, and proton transfer to the binuclear site without an accompanying electron is also thermodynamically unfavorable. Therefore, if protonation of the pump site is impaired, turnover will be slow despite an active K-pathway. This is a plausible explanation for why the K-pathway cannot substitute for the D-pathway mutations (Mills and Ferguson-Miller, 1998; Wikstrom and Verkhovsky, 2007). However, a different explanation for the reciprocal case is needed: why the D-pathway cannot substitute for a blockage of the K-pathway. It is suggested that the binuclear site might have a discrete protonation state which shows different chemistry in the reductive phase (O→E→R), so as to prevent its protonation by E286 via the D-pathway. Such a preference could be achieved if Y288 is the proton acceptor and

is reprotonated only via the K-pathway during the reductive phase (O→R) but not the oxidative phase (P→F→O). In this condition, the substrate proton uptake via the D-pathway cannot substitute for the K-pathway mutations (Wikstrom and Verkhovsky, 2007). The reverse scenario has also been proposed (Sharpe and Ferguson-Miller, 2008): that the Cu_B-OH group is the proton acceptor from the K-pathway during the O →R (metal reduction) phase, whereas the His-Tyr group is the proton donor in the P→F→O phase, and can only be reprotonated by the D-pathway.

1.3.4.3. H-Pathway in Bovine Heart Mitochondrial Cytochrome *c* Oxidase

Redox-coupled conformational changes were observed in a segment from G49 to N55 in bovine heart mitochondrial C*c*O (bovine numbering) in the 2.3 Å resolution crystal structure of the reduced enzyme (2OCC) (Yoshikawa *et al.*, 1998). Based on this observation, the H-pathway has been proposed, in bovine C*c*O, to pump protons.

D51 in the oxidized state is completely buried inside the protein at the outer end of the proposed H-pathway (Yoshikawa *et al.*, 1998) and is connected with the matrix surface by a hydrogen-bonded network involving water and a peptide backbone. In this configuration, the residue D51 can only take up protons from the matrix side, and is inaccessible from the cytosolic side. Water channels on the bottom of the H-pathway are proposed to be capable of accessing water molecules in the matrix. This channel extends to the formyl group of heme *a*, connecting with D51 via the propionate of heme *a* (Yoshikawa *et al.*, 2006a). It is suggested that reduction followed by oxidation of the low

spin heme *a* drives the active proton transfer from the interior to D51 across the enzyme via a water channel and hydrogen-bonded network.

The mechanistic proposal suggests that upon reduction of the fully oxidized C*c*O, the hydrogen bond between the key peptide amide and a carboxyl group of D51 is broken. Consequently, D51 loses its accessibility to the matrix side and moves toward the cytosolic surface via a rearranged hydrogen-bonded network which now connects D51 to the outer surface to release protons to the mitochondrial exterior. A peptide bond in the hydrogen bonded network gives directionality, which inhibits reverse proton transfer. In addition, upon reduction, the pKa of the D51 carboxyl group is expected to be decreased by about 5 pH units, causing the carboxyl group to be deprotonated in the reduced state (Yoshikawa *et al.*, 2006b).

All of the amino acids in the network connected to D51 in bovine heart C*c*O are conserved in mammalian systems. However, the H-pathway proposal is not yet generally accepted because of the lack of conserved residues, including D51, in the bacterial enzyme (Lee *et al.*, 2000) and the lack of effect of mutations in that region.

Mutational evidence for the involvement of the key residue, D51, in proton pumping has been reported in studies with the mammalian enzyme. Asp51 of subunit I was replaced with Asn, a non protonatable and isosteric amino acid, by a hybrid enzyme formation method in which mutant bovine subunit I was introduced into HeLa cells and imported into the mitochondria to formed a hybrid enzyme with the remaining 12 human subunits (Tsukihara *et al.*, 2003). The D51N mutation abolished proton pumping activity

while maintaining full electron transfer activity (Shimokata *et al.*, 2007). Mutations which block either the water channel or proton transfer abolish the pumping activity as seen in the D51N mutant. These results significantly strengthen the proposal that the H-pathway is involved in proton pumping in the mammalian C*c*O.

1.3.4.4. Exit Pathways for Protons and Water

Although the two proton uptake pathways (D and K-pathway) are well studied by biochemical and crystallographic approaches, the pathway for protons beyond E286 is not resolved from structural or functional studies. It is proposed that protons are moved to protonation sites, in the vicinity of the heme propionates (heme *a* and a_3), through a water-mediated network that may involve specific amino acids and water chains (Behr *et al.*, 2000; Puustinen and Wikstrom, 1999a; Xu *et al.*, 2007).

Many waters forming a hydrogen-bonded network and connecting the propionates of the hemes to the outside are located at the interface between subunit I and II (Schmidt *et al.*, 2003). This network, containing the propionates, could be a part of an exit pathway. In all eukaryotic C*c*O, the region above the hemes contains a non-redox-active metal site containing a Mg^{2+}. The role of the metal site in the exit pathway is not clear. The Mg^{2+} can be replaced with an EPR active probe, Mn^{2+}, retaining full activity (Hosler *et al.*, 1995) and maintaining the structural character of this enzyme. Protons or water molecules that coordinate the metal can be exchanged with $^{2}H_2O$ on a catalytically relevant time scale. The deuterium exchange, using a combination of rapid freeze-quench and electron spin echo envelope modulation (ESEEM) analysis of Mn^{2+}

substituted CcO, showed that three inner sphere $^{2}H_2O$ exchanged per Mn^{2+}. It is prosposed that the Mg^{2+}/ Mn^{2+} could provide a mechanism for preventing back flow of protons by electrostatic repulsion, if the water/proton exit channel involves waters ligated to the metal (Schmidt *et al.*, 2003). (see Section1.3.2.5 for details)

In mechanistically simpler systems, such as bacteriorhodopsin, each proton pumping event is driven by a conformational change by photoisomerization of the retinal (Lanyi, 1997; Lanyi and Luecke, 2001). This process involves a shift of the proton paths so that one is closed and the other open. A conformational change of E286 is suggested as one possible way to transiently connect the D-pathway with the exit pathway. A side chain shift of E286 upon deprotonation to an "up"-position may result in a change in the water arrangement inside the hydrophobic cavity above it, thereby forming a proton transfer pathway. This is supported by experimental (Bailey *et al.*, 2002; Karpefors *et al.*, 2000a) and theoretical studies (Hofacker and Schulten, 1998; Seibold et al., 2005). The conforfmational changes are postulated to exist transiently only in specific steps of the catalytic cycle and therefore are not easy to capture in the static crystal structure. Since E286 has a high pKa, the deprotonated state of E286 is unfavorable; rapid relocation to a 'down' position would disrupt the water chain above it, preventing the backflow of protons from the exit pathway. The E286 is assumed to be reprotonated through the D-pathway after returning to its original conformation. The turnover activity and proton pumping efficiency of the E286A mutant CcO was restored by placing a Ser and a Tyr near the 286 position of the *P.denitrificans* CcO (E278A/G275S in the *Paracoccus* CcO) (Backgren *et al.*, 2000), which indicates that proton translocation can take place without

the conserved glutamic acid residue. This suggests that the effect of deprotonation of E286 on water chain formation is not direct, but rather involves modulation of the electrostatic field around this residue.

1.3.4.5. Proton Backflow Pathway

Understanding the proton back flow mechanism is important for studying the role of C*c*O in energy transduction efficiency. Proton back flow may be important physiologically and mechanistically in terms of regulation of the energy efficiency, heat versus ATP production. Proton backflow may also inhibit formation of ROS (reactive oxygen species) due to a lowering of the membrane potential by allowing electron transfer to the active site without proton pumping.

A mutant of *R.sphaeroides* C*c*O that blocks proton uptake from the D-pathway provided the first evidence of a proton backflow route. When D132 in *R.sphaeroides* C*c*O is mutated to any non-carboxyl residue, the residual activity is about 5% of wild-type (Fetter *et al.*, 1995; Mills *et al.*, 2000; Verkhovskaya *et al.*, 1997). With a compromised D-pathway, but with the presence of a membrane potential, the activity of the mutant was stimulated. This observation led to the suggestion that proton backflow could partially repair the blockage of the D-pathway and that this backflow could occur by reversal of the exit pathway. However, neither a proton exit, nor backflow pathways above the hemes have been identified in the crystal structures, suggesting that water chain

formation is transient, and that the crystal structures obtained so far are not in the correct state, with the exit path in an "open" state.

In order to study the possible involvement of the region above the hemes, the well conserved arginine (R481), which interacts with the heme propionates, has been mutated (Mills *et al.*, 2005; Puustinen and Wikstrom, 1999b; Qian *et al.*, 2004). Mutation of R481 suggests that even a conservative change, R481K, affects the proton movement above the hemes without perturbation of the hemes or the Cu_A spectrum. Oxygen consumption is most strongly inhibited in R481K C*c*O reconstituted into vesicles in the presence of a membrane potential and pH gradient, showing high RCR (respiratory control ratio). This suggests the involvement of the R481 residue in a backflow pathway for proton uptake from outside in the presence of membrane potential. However, this mutant shows normal proton pumping efficiency, suggesting that it does not prevent proton exit.

1.4. Statement of purpose

Tremendous efforts have been made using X-ray crystallography, kinetic, and spectroscopic studies in order to obtain a comprehensive knowledge of the structure, function and regulation of C*c*O. These techniques have provided the basis for rational models for mechanisms of proton pumping, which is coupled to electron transfer, reducing the oxygen into water, using protons from well defined proton uptake pathways. However, despite the remarkable achievement of high resolution crystals in different states and from different species, and various key mutants which have altered

biochemical properties and disturbed proton pumping, there are still unsolved questions. The proton release and proton backflow pathways are not yet defined. Moreover, control of oxidase activity and efficiency is not understood. The central issue of the mechanism of proton pumping in C*c*O is the question of how protons are moved against an electrochemical gradient and how this is tightly coupled to the electron transfer. Therefore, in order to understand the detailed mechanism, I have been trying to develop a sensitive method to observe proton movement both inside and outside of the reconstituted vesicles of *R.sphaeroides* C*c*O. In this thesis, I address the progress that has been made in terms of quantification of proton movement in the system. The measurement of size and internal capacity of the vesicles will be reported.

My goal was to entrap sufficient pH indicator on the inside to enable measurement of internal pH changes. This was achieved by using Bio-beads for removal of detergent, which are shown by electron microscopy to produce large vesicles. Although a complete quantitative understanding of proton/electron stoichiometry was not obtained, I will discuss the results with regard to the signal amplitudes and the rate of H^+/e^- consumption at standard conditions. I will report the efforts in further analysis of the resulting data conducted by global fitting of full spectra, in order to produce a kinetic model that provides better understanding and quantification of proton movements. Moreover, the regulation of oxidase activity will be discussed in terms of the role of exit/ backflow of protons in the presence/ absence of inhibitor zinc, using the wild-type enzyme. In addition to the wild-type C*c*O, I will discuss studies with a set of mutants of the residue

H93, which may have a role in proton pumping and proton backflow. These approaches add to our understanding of the mechanism and pathways for proton pumping in C*c*O.

Chapter 2 Optimization / Characterization of Proteoliposomes and pH Sensitive Dyes to Achieve Internal and External pH Measurement

2.1. Introduction

The coupling of protons and electrons in C*c*O was investigated in order to clarify the role of proton pathways and how proton movement is linked with electron transfer. A liposomal system has been used as a model for studying membrane proteins and their function. A number of techniques have been investigated for producing model membranes from lipids for this study. Limitations to mimicking the bilayer environment are caused by the presence of detergents used to solubilize and stabilize the membrane protein when it is purified. Purified integral proteins maintain a functional conformation when solubilized in detergents, but insertion of a purified membrane protein into a lipid model system is dependent on detergent removal steps. Reconstituted cytochorme *c* oxidase vesicles (COVs) exhibit respiratory control and proton pumping, similar to that observed in mitochondria (Wikstrom, 1977).

Small size vesicles with a diameter range of 20-30 nm, measured by EM, may have a limited use in model membrane studies. The aqueous volume enclosed in the vesicles is too small to monitor inside pH changes due to the small number of captured dye molecules. There is also the problem of a proton shortage for pumping, unless vesicles are prepared under conditions of high internal buffering. In this chapter, attempts to optimize the condition of vesicles are described, and are designed to maximize signal and reduce noise by increasing the size of the vesicles, or by purifying

the COVs to minimalize the contribution of background noise and buffering in the vesicles without C*c*O. Changes in buffer capacity and dye concentration on the inside of vesicles were also explored.

The new Bio-bead method developed (Figure 2.1) increased the size of the vesicles almost three-fold compared to the previous cholate-dialysis method. As a result of the increased size, the amount of dye was increased on the interior of the COVs, leading to an increase in the signal-to-noise ratio and allowing for the corresponding observation of pH changes as proton pumping occurs. The unilamellar system (single layer of lipid bilayer) with larger vesicle sizes was made by a Bio-bead method, which could better monitor the pH changes on the inside with a reduced buffering capacity, and maximize the ability to monitor the internal pH changes. The orientation of the C*c*O is found to be predominantly with the large soluble "head" region of subunit II pointing outside, and not randomly oriented in the COVs. However, mis-oriented C*c*O vesicles (COVs) can be removed by using a his-tagged C*c*O purification technique using a Ni-NTA resin and a his-tag on subunit II on the outside, so that only those vesicles containing a his-tag can be preferentially selected. Void vesicles, which do not have C*c*O, will also not be retained by a Ni-NTA column and can be separated, eliminating background noise. The use of Bio-bead COVs, combined with the purification step using his-tagged C*c*O results in relatively pure homogeneous outward facing COVs.

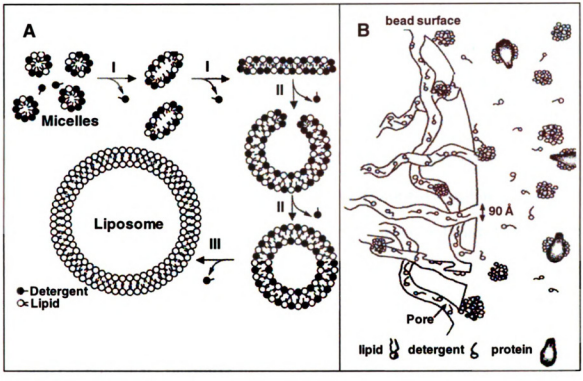

Figure 2.1 Model of liposome formation and reconstitution with membrane proteins. (A) Size transformation process during the removal of detergent. The curvature of the liposomes is dependent upon the level of residual detergent remaining in the detergent and lipid mixture. Micelles undergo a size transformation to larger vesicles through fusion and lipid exchange as the detergent concentration is decreased. Detergent removal from lipid-detergent micelles may cause the transformation of small micelles to larger ones (I), which bend upon further detergent removal to form curved mixed micelles. Subsequently, detergent-saturated vesicles should be formed (II) which undergo size growth through fusion and lipid exchange (III) to larger unilamellar liposomes. (B) Proposed mechanisms of detergent binding onto Bio-Beads. Adsorption of detergents, lipids, and proteins depend upon the accessibility through the pores of the beads. Hydrophobic detergent monomers and small micelles are included; larger mixed micelles, protein, and vesicles are excluded. Details of the protocol were introduced in Figure 2.3. Figures are obtained from Rigaud *et al.* (European Biophysics Journal 1998 27:305-309) with modification.

Too much buffering on the inside can result in small pH changes. However, without sufficient buffering on the inside of vesicles, measurement of pumping can also be difficult due to a lack of available protons. Various buffering conditions and different dye concentrations were used in order to get a better signal on both the inside and the outside of the COVS at the same time. The stopped-flow measurement of activity allows electron consumption, proton uptake, and proton release to be monitored in a millisecond time scale. Osmolarity was maintained with sucrose in order to prevent excessive swelling or shrinkage of the COVs.

2.2. Experimental Procedures

2.2.1. Production and Isolation of Cytochrome c Oxidase

Bacterial Growth

Rhodobacter (R.) sphaeroides strains were grown aerobically in the dark at 30°C in 2.8 L Fernbach flasks containing 600 mL of Sistrom's media (1962 Sistrom J.Gen.Microbial.28, 607) with 25μg/mL streptomycin, 25μg/mL spectinomycin and 1μg/mL tetracycline as described (Hiser *et al.*, 2001). The cells were harvested after 3 days at 30°C when the culture had attained an optical density at 600 nm of 1.5-1.8 and pH of 8.5-9.0, and cells were stored frozen at -70°C.

Preparation of Cytoplasmic Membranes

R.sphaeroides membranes were prepared as described (Zhen *et al.*, 1998) with some modifications. Frozen cells were resuspended using a large paintbrush into 150-

200 ml of 50 mM KH_2PO_4, pH6.5, 1mM EDTA, 50 μg/ml DNase I, RNAse (few grains) and were homogenized with a handheld glass homogenizer and Teflon pestle. The cells were broken by passing through a French Press at 20,000 psi. Whole cells and debris were removed by centrifugation at 31,000 x *g* for 30 minutes. The membranes were pelleted by centrifugation at 200,000 x *g* for 1.5 h and were resuspended in 10mM Tris-HCl pH8.0, 40mM KCl (200mM KCl for subunit II his-tagged C*c*O).

Purification of Cytochrome *c* Oxidase

Isolation and purification steps were done as described (Hosler *et al.*, 1992; Zhen *et al.*, 1998). The wild type and mutant oxidases were isolated using a histidine tag either on the C-terminal end of subunit I or C-terminal end of subunit II. C*c*O was solubilized from the membrane with a 10mM Tris-HCl pH8.0 containing 40mM KCl (200 mm KCl for subunit II his-tag), 3% lauryl maltoside (2% for his-tag II), and stirred in the cold room for 30 minutes. Sample volume at this point was 90-100 ml. Solubilized oxidase was centrifuged at 200,000 x *g* for 30 minutes to spin down unsolubilized material. The expression yield was calculated in a mixture of 200μl of solubilized oxidase in 800μl of buffer by measuring the reduced minus oxidized absorbance at 500-700nm and by using an extinction coefficient of 28,900 $M^{-1}cm^{-1}$. A volume of Qiagen Ni^{2+}-NTA resin was prepared (1 ml/mg aa_3) based on the spectral analysis. The supernatant was mixed with Qiagen Ni^{2+}-NTA resin and stirred in the cold room overnight. This solution was loaded onto a gravity column and washed first with one column volume of imidazole buffer, 10 mM Tris-HCl pH8.0 + 40mM KCl + 10mM imidazole + 0.1% lauryl maltoside (10 mM

Tris-HCl pH8.0 + 200 mM KCl + 10mM imidazole + 0.1% lauryl maltoside for his-tag II), then with two column volumes of the same buffer without imidazole. Tightly bound C*c*O was eluted with 80mM histidine + 10mM Tris-HCl pH8.0 + 40mM KCl (200mM KCl for his-tag II) + 0.1% lauryl maltoside and concentrated in a 100 K MW cut-off Millipore centrifugal filter to remove the histidine-Ni complex. The eluted C*c*O was washed with 10mM KH_2PO_4 (pH8.0),1mM EDTA, 0.2% lauryl maltoside and applied to a fast protein liquid chromatograpy system (FPLC, Amersham Bioscience,Inc., AKTA-519) with an anion exchange column (tandem DEAE-5PW,Tosoh-Haas), equilibrated with the same buffer (Hiser *et al.*, 2001). The sample was eluted using a linear gradient of KCl and concentrated by using an Amicon Ultra centrifugal filter device (Millipore).

2.2.2. Characterization of Cytochrome c Oxidase

UV-Visible Spectroscopy

UV-visible spectra were recorded on a Perkin-Elmer Lambda 40P spectrophotometer after appropriate dilution of C*c*O into 100 mM KH_2PO_4, 0.1% LM, pH7.2. The concentration of C*c*O was determined by measuring the dithionite-reduced, absolute spectrum at $A_{606-640}$ with an absorption coefficient of 37,000 $M^{-1}cm^{-1}$. The purity was determined from the A_{280}/A_{420} ratio, which was found to be about 1.9-2.0. Both heme groups make a major contribution in the Soret region, with heme *a* being dominant in the alpha (α) region around 605nm (bovine) (Vanneste, 1966; Wikstrom *et al.*, 1981a) and 606 nm (*Rs*) (Hosler *et al.*, 1992).

Steady State Activity Measurement by Oxygraph

Oxygen consumption activity of C*c*O was measured, either with the solubilized form of the enzyme, or in the reconstituted vesicles. The measurements were made in a Gilson Oxygraph with a closed thermostated chamber containing a Clark-type oxygen electrode (Ferguson-Miller *et al.*, 1976). The V_{max} in the steady-state turnover was measured in KH_2PO_4 at pH 6.5 with 10 pmoles of C*c*O, or in COVs. Horse heart cytochrome *c* (30μM), ascorbate (5.6mM) and TMPD (0.28mM) were added as electron donors with isolated enzyme (C*c*O) in the presence/absence of soybean phospholipids, asolectin (1mg/ml) at 25°C (Hosler *et al.*, 1992). A 30μM cytochrome *c* concentration was selected as a standard condition for steady-state measurement, based on a RCR calculation (RCR=uncontrolled state activity/ controlled state activity). The RCR was independent of cytochrome *c* concentration in the range of 3.5~56 μM (Figure 2.2).

Measurement of the activity of COVs were made in the controlled state (absence of ionophores), and with the addition of valinomycin, which dissipates the membrane potential by equilibrating K^+ across the membrane to remove the charge ($\Delta\Psi=0$). However, the proton gradient, ΔpH, will be maintained. The uncontrolled condition occurs with the addition of uncouplers, FCCP (or CCCP), which transfers protons across the membrane, and this causes the proton gradient to be dissipated ($\Delta pH=0$) showing the highest rate of activity.

Rapid Scanning Stopped-Flow

For stopped-flow, pre-steady-state measurements the electron donor, horse heart cytochrome *c*, was reduced by sodium dithonite followed by desalting and depolymerizing through a Sephadex G-75 (Amersham Biosciences, Inc.) gel filtration column into 0.5 mM HEPES-KOH pH7.4, 45mM KCl. Respiratory control and activity of C*c*O in the reconstituted vesicles was measured in 100mM HEPES-KOH pH7.4, 50mM KCl in the absence or presence of ionophores (valinomycin and FCCP). Stock solutions of 2mM valinomycin and 10mM FCCP (Sigma) were prepared in ethanol. The turnover numbers, in electrons consumed per second per C*c*O (e^-/sec/aa_3), were calculated from the oxygen consumption traces. The respiratory control ratio (RCR) was calculated from the uncontrolled state turnovers, where both valinomycin and FCCP are present, divided by the controlled turnovers where no ionophores are present. A controlled state without ionophores shows the slowest reaction due to the high membrane potential and pH gradient, which is built up across the membrane during the reaction.

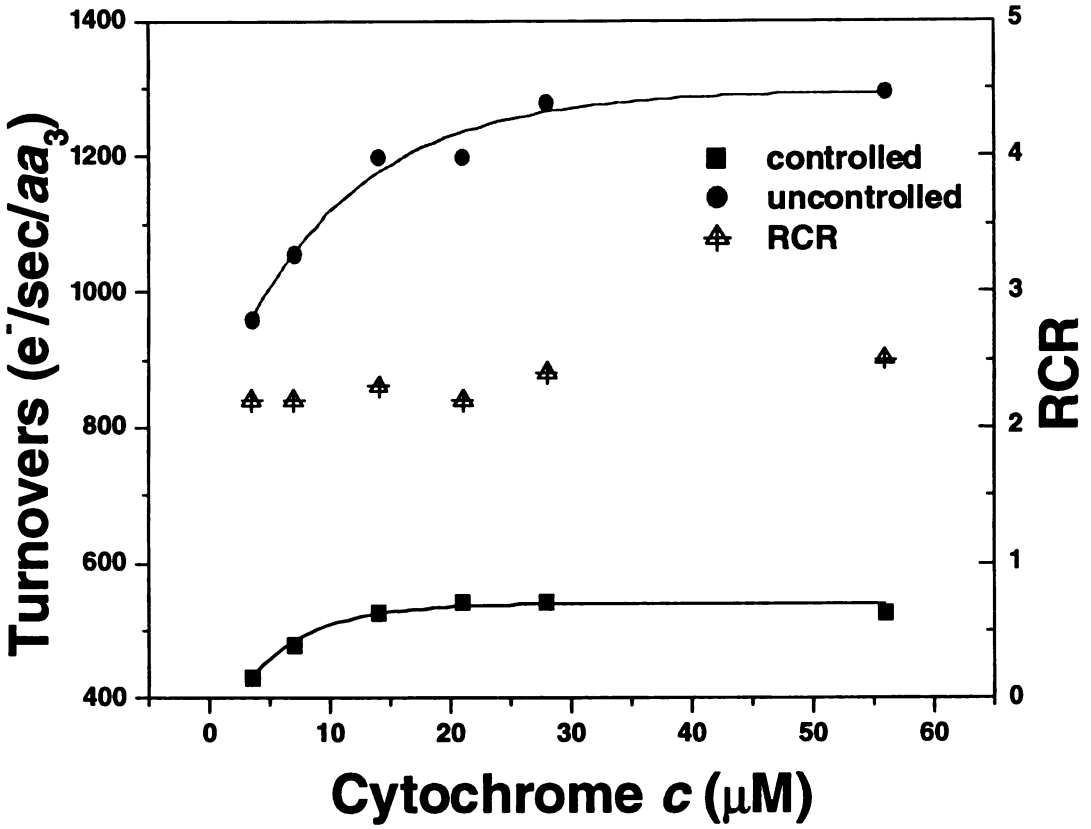

Figure 2.2 Cytochrome *c* dependence of activity and RCR (Respiratory Control Ratio) in the steady-state condition.

Steady-state measurements were made in the presence of ascorbate (5.6mM) and TMPD (0.28mM) and an increasing concentration of cytochrome *c* as electron donors to C*c*O, in 50mM HEPES-KOH pH7.4, 25mM KCl. The RCR was calculated from the uncontrolled activity divided by the controlled activity. Cytochrome *c* at 30μM was selected as a standard condition for the steady-state measurements.

Measurement of cytochrome c oxidation was made either with an Applied Photophysics SX.18MV-R Stopped-Flow reaction analyser (Applied Photophysics) or with a rapid scanning stopped-flow spectrophotometer Olis RSM system (Olis). The stopped-flow measurement allows a limited turnover number and was measured by using the concentration of pre-reduced horse heart cytochrome *c* for the calculated amount of electrons. This is not performed at saturating conditions, nor near the V_{max}, but it allows for comparable proton pumping measurements to be monitored in both the inside and outside of the vesicles. An equal volume of the two reactant solutions, one containing reduced cytochrome *c* (in one syringe), and the other containing a pH-sensitive dye and COVs (in the other syringe) were rapidly mixed ($\leq$ 2msec). Therefore the concentration in the observation cell after mixing is half of that in the syringes.

After mixing two samples, in either the absence or the presence of ionophores (valinomycin alone or valinomycin plus FCCP) which are pre-equilibrated with COVs in the syringe, data were collected and the rates were fit to the oxidation of cytochrome *c* at 550nm, using single exponential fitting to the kinetic traces with Microcal Orign Pro software. The concentration of valinomycin must be high enough to make the K^+ transport by valinomycin not rate limiting, but excessive valinomycin concentrations, which mediate H^+ transport, must be avoided. A suitable valinomycin concentration has to be determined. The enzyme turnover was calculated using the equation below, based on k_{obs} from the kinetic analysis:

Turnover (activity, e^-/sec/aa_3) = k_{obs} x [reduced cytochrome *c*] /[C*c*O]

Inside pH changes, which are probed by pyranine dye, were measured either in the fluorescence mode (Photophysics) or the absorbance mode (Olis) depending on the type of measurement. In the fluorescence mode, the emitted light is usually detected by a photomultiplier after it has passed through a suitable optical filter. The cut-off filter (490nm) was used to separate fluorescence emission from the excitation light, which may be scattered by the solution and maximizes the collection of emission signal at 510nm with an excitation λ at 465nm and a 10nm slit width. Otherwise, in order to restrict the range of the emission signal and to reject all other unwanted radiation, a bandpass filter FB500-40 (Central Wavelength 500nm, 40nm bandpass regions) from ThorLabs was applied instead of a cut-off filter.

For the absorbance measurement of pyranine, the isosbestic point of cytochrome *c*, where absorbance does not change upon a redox change of cytochrome *c* was selected at 435nm, in the absence of phenol red. The isosbestic points were measured by a wavelength scanning method using the Olis stopped flow instrument. External acidification of the COVs was measured by using a phenol red dye. Absorbance changes at 557 nm (another isosbestic point of cytochrome *c*) were monitored during the catalytic reaction in 50μM HEPES-KOH pH7.4, 45mM KCl and 100μM phenol red placed on the outside. Even though the sample contains pyranine already on the inside of the vesicles, the phenol red signal is not contaminated by the pyranine because their absorption ranges differ. Both inside and outside pH probes and cytochrome *c* oxidation were measured in the absorbance mode by rapid scanning (1ms) from 365 nm to 595 nm (Groove Density 400, Span 230nm, Resolution 1nm). These scans were collected by the computer which

was linked to the detector system. The kinetic traces for phenol red at 557nm, pyranine at 435nm and cytochrome *c* at 550nm were extracted from this data after averaging at least three sets of data. The cytochrome *c* concentration was calculated using an extinction coefficient of 17,000 $M^{-1}cm^{-1}$ (reduced-minus-oxidized) (Brunori *et al.*, 1985). Unlike the Applied phtophysics stopped-flow, which has only a single wavelength selection during the turnover, the Olis stopped-flow rapid scanning instrument allowed wavelength scanning across a wide region (365-590nm) and 1 ms/scan. Therefore, the complete spectrum of the reaction can be monitored over time, and isosbestic points can be chosen to monitor changes in the different probes, or the complete spectrum can be used for SVD (Singular Value Decomposition) or global analysis methods. The relationship of ΔpH to the absorbance changes in the dyes were estimated as described in results.

Membrane Potential Measurement in COVs

Positively charged cyanine dye,$DiSC_3(5)$(3',3'- dipropylthiadicarbocyanine iodide) is a fluorophore that responds to a membrane potential and is used to monitor changes in the membrane potential ($\Delta\Psi$) of COVs (Sims *et al.*, 1974; Singh *et al.*, 1985). The fluorescence quenching of the dye results from a potential-dependent stacking of the dye molecules in the polarized membranes of the vesicles (Singh and Nicholls, 1985a).

Bio-bead COVs (final 0.1μM aa_3 concentration) with an internal buffer of 20mM HEPES-KOH pH7.4 + 38.9mM KCl + 52mM sucrose are diluted into high salt buffer (50 mM HEPES-KOH pH7.4 + 25mM KCl + 20mM sucrose + 800 mM NaCl). The

membrane potential formed across the vesicles was observed by measuring fluorescence quenching (ex 625nm, em 680nm) with a FluoroMax-2 (HORIBA Jobin Yvon Inc) fluorometer. This illustrates the response of the dye to a membrane potential.

Under experimental conditions, the largest polarization of COV's that occurs during the turnover is ~140mV, interior negative. To measure the development of the membrane potential COVs were mixed with $DiSC_3(5)$ at 2.5μM final concentration, and equilibrated for about 5 minutes before measurement. A steady-state condition is prepared with the presence of ascorbate (12mM), TMPD (57μM) and horse heart cytochrome *c* (2μM) in 50mM HEPES-KOH pH7.4, 24mM KCl. The formation of membrane potential during steady-state turnover is measured with a QuantaMaster™ Luminescence instrument by Photon Technology International (PTI) and a Felix 32 analysis software module. Generation of turnovers by addition of ascorbate and TMPD with COVs, which were made by the Bio-bead method, causes the large decrease in fluorescence signal. Stacking of the probe in the vesicle membrane under the influence of the potential gradient may cause self quenching of the dye and decrease the intensity of the signal (Singh and Nicholls, 1985a). The nigericin releases the pH gradient. Then, the membrane potential is released by addition of valinomycin, causing the increase in fluorescent signal (Fetter *et al.*, 1996). Depolarization of the membrane potential produces an increase in the fluorescence signal by reducing dye accumulation in the membrane.

2.2.3. Reconstitution of Cytochrome *c* Oxidase

The soybean polar lipid extract, asolectin, used in C*c*O reconstitution, was obtained from Avanti Polar Lipid, Inc. (Cat No 541602). It is composed of phosphatidyl ethanolamine (22.1%), phosphatidyl inositol (18.4%), phosphatidyl choline (45.7%), phosphatidic acid (6.9%), and other components (6.9%). Polar lipid extract is the total lipid extract which is precipitated with acetone and then extracted with diethyl ether by Avanti Polar Lipids, Inc. Anagrade sodium cholic acid was obtained from Anatrace. All glassware was rinsed with ethanol and MilliQ water before use.

Cholate-Dialysis COVs

Various methods of reconstitution of C*c*O into COVs have been tried, to obtain a good signal-to-noise ratio and a good measurement of respiratory control. Two types of COVs were mainly prepared; either by using the cholate-dialysis method, or by the Bio-bead method in order to remove detergent.

Cholate, a detergent, is added to the enzyme to displace the dodecyl maltoside detergent from the enzyme. Cholate detergent is subsequently easily eliminated by dialysis due to its large CMC, critical micelle concentration, of 14 mM. As the detergent concentration is gradually decreased, in the presence of lipid a unilamellar vesicular structure is formed.

In a typical protocol, the lipid, asolectin, was suspended to 40mg/ml and sonicated at 0°C under argon gas using a microtip sonicator (Heat systems-Ultrasonics

sonicator Model W-225) with 2% cholate in 75mM HEPES-KOH pH7.4 with 14mM KCl until the solution reached clarity. The sonicated suspension was centrifuged for 15min at 12,000 x *g* to remove titanium particles. On the other hand, C*c*O was prepared at 4μM final concentration at pH 7.4 with 4% cholate in the same buffer condition (75mM HEPES-KOH pH7.4 + 14mM KCl), separately. The C*c*O solution was mixed (1:1 v/v) with the sonicated asolectin suspension to obtain a final concentration of 2μM oxidase and 20mg/ml lipids with 3% final cholate concentration. (Hiser *et al.*, 2001). The cholate was removed using five steps of dialysis with rapid stirring at 4°C in Spectrapor dialysis tubing (#25225/204, 12-14,000 Mr cut-off) to remove detergent and form the COVs. For example, 75mM HEPES-KOH buffered COVs were made by following a buffer exchange procedure which was: 1) 6h in a 100 volume of 75mM HEPES-KOH pH7.4, 14mM KCl with, and then 2) without 0.1% cholate respectively; 3) 12h in 100 volumes of 50mM HEPES-KOH pH7.4, 25mM KCl, 15mM sucrose; 4) +5) a 12h dialysis two times in a 500 volume of 50μM HEPES-KOH pH7.4, 45mM KCl, and 44 mM sucrose as previously described (Hosler *et al.*, 1992). Because of the lowered buffering condition on the outside of the formed COVs, sucrose was added to maintain a fairly constant osmotic condition. The steady state activities of a set of reconstituted COVs, with different internal buffering, were measured polarographically by the Gilson oxygraph using a Clark-type electrode, in order to verify the success of the COV reconstitution. After cholate dialysis, the vesicles were shown to have C*c*O in the predominantly mitochondrial configuration (Nicholls *et al.*, 1980) with the the cytochrome *c* binding site on the outside and to have a high respiratory control ratio.

The reconstitution of C*c*O into phospholipid vesicles (Brunori *et al.*, 1985), with various interior concentrations of HEPES-KOH buffer was performed using the cholate dialysis method (Hinkle *et al.*, 1972) to determine the best optimized buffer conditions for C*c*O activity. Internal buffer concentrations were varied between 5mM to 75mM HEPES-KOH, while the final external buffer was kept to a minimum at 50μM HEPES-KOH at pH7.4 in order to observe the external pH changes on the outside of the COVS.

Bio-Bead COVs purified by Ni^{2+}-NTA column

A method using Bio-Beads SM-2 (Bio-Rad Laboratories), which are neutral, porous styrene divinylbenzene beads to remove detergent, has been introduced as an alternative way to form larger unilamellar vesicles for proton pumping measurements, rather than using the dialysis-cholate method which results in relatively small COVs. The inside pH was adjusted to 20mM HEPES-KOH pH7.4 buffer as a final concentration, based on the preliminary oxygen consumption activity measurement in the oxygraph, in the steady-state condition, with the dialysis-cholate COVs.

Lipid mixture (2mL) was prepared in 20mM Hepes-KOH pH 7.4, 38.9mM KCl, 52mM sucrose, 1mM EDTA and 3% cholate (w/v) with 80mg/ml asolectin. The mixture was sonicated for 30 sec more than 3 times with internal pH probe pyranine (20mM) and centrifuged for 15min at 12,000 x *g* to remove titanium particles. FPLC purified C*c*O (4μM) which containing no cholate was diluted in the supernatant of sonicated lipids, which is prepared in previous step, at 4 °C in glass stirring beaker (20mL) for 2-3min.

Cholate detergent was efficiently removed with Bio-beads SM-2 by continuous addition for 7 hours (Jasaitis *et al.*, 1999) in a strring beaker (Table 2.1). The liposomes and the Bio-beads were separated by gentle centrifuge (~100 x g) with a filter column made of an inert stable polymer, polypropylene (Fisher Scientific #11-387-50) inside a Corning tube (15mL). Untrapped free pyranine and remaining cholate were removed from samples (~3mL) using a size exclusion sephadex G-25 gel-filtration using a 2 cm internal diameter, 45cm length column which is equilibrated with the same buffer as inside (20mM HEPES-KOH pH 7.4, 38.9mM KCl, 52mM sucrose, no EDTA).

The formation of COVs was followed by a Ni^{2+}-NTA binding step for further purification as previously described by Hiser *et al.* (Hiser *et al.*, 2001). All of the excluded, green fluorescent COV fractions (Figure 2.3) from the sephadex G-25 column filtration were pooled (10-12mL volume) and carefully adjusted to pH 8.0 with KOH and a final 200mM KCl concentration before addition to the Ni^{2+}-NTA agarose in order to maximize the specific binding. Additionally, Ni^{2+}-NTA resin also was washed with water and high salt buffer (200mM KCl) before use to increase the oxidase binding onto the Ni^{2+}-NTA. A high concentration of salts in the buffers was necessary for the metal affinity column to bind the histidine-tagged C*c*O, due to apparent lack of accessibility of the his-tag at the lower salt concentration. Increasing the salt concentration provided better screening of the charges, keeping the his-tag available for the interaction with the nickel on the resin rather than binding to the negatively charged carboxylates on subunit II. The samples and the prepared Ni-NTA resin were stirred for 20 minutes at 4°C. C*c*O

was artificially engineered to create a his-tag on subunit II to be outward-facing so that the COVs would have a his-tag accessible on the outside. This his-tag is able to bind to a Ni-NTA agarose column to allow the COVS, with the C*c*O correctly oriented, to have the his-tag on the outside, in order to separate the COVs with oxidase present. A sample was loaded onto the gravity column washed with two column volumes of high salt buffer (20mM HEPES-KOH pH8.0, 200mM KCl, with no imidazole) and eluted with histidine buffer (80mM histidine, 38mM sucrose, 20mM Hepes-KOH at pH7.4 with no imidazole). Resin bound COV fractions, which contain correctly oriented oxidase, were separated from the flow-through part, which is not tightly bound to the resin and includes the vesicles void of oxidase. The eluted COVs (~15mL) were then concentrated to 2mL final volume in a filtration system with a Centricon 100 (Amicon YM100) membrane under gentle pressure with stirring and dialyzed against 1000mL buffer (50μM Hepes-KOH pH7.4 with 45mM KCl and 44mM sucrose) for 12 hours to exchange the outside buffer. All flowthrough part (45-50mL) also was collected and followed the same step of concentration and dialysis. The final concentration of oxidase in the vesicles was estimated by measuring the V_{max} in the steady-state condition with uncoupling agents (valinomycin and FCCP), and the total volume of sample prepared. Some volume (100μl) of the sample was reserved for further use in transmission electron microscopy (TEM). The recovered yield of reconstituted COVs was about 25% from the Ni-NTA purified Bio-bead COV preparation.

Protocol for Detergent Removal		
Time(min)	**Amount of Biobeads added (mg/ml)**	**Temp.**
0	33.2	4 °C
30	33.2	4 °C
60	33.2	4 °C
90	33.2	4 °C
120	66.5	4 °C
180	66.5	4 °C
240	133	RT
270	133	RT
300	266 add 1mL of 20mM HEPES-KOH pH7.4	RT
360	266	RT
420	Ready	RT

Table 2.1 The protocol for detergent removal by Bio-beads.
Bio-beads are gradually added over time in 30 minute intervals at 4 °C for up to 2hrs and then at RT according to the table, into a 20mM HEPES-KOH pH7.4 + 38.9 KCl + 52mM sucrose buffer with stirring in a beaker (2ml of sonicated vesicles with 4μM aa_3) at room temperature (RT).

Figure 2. 3 A new method for reconstitution of *Cc*O into vesicles
*Cc*O was reconstituted into lipid vesicles using the Bio-bead method with pyranine inside (bright yellow) and an external his-tag on subunit II. Lipid Sonication mixture (A) was prepared in 80mg/ml Asolectin, 3% cholate (w/v), 20mM Hepes-KOH pH7.4, 38.09mM KCl, 52mM sucrose, 1mM EDTA, 20mM pyranine (0.01g/1ml). Supernatant (B) void of metal precipitant was set apart for mixing with *Cc*O (C). 4μM of FPLC purified *Cc*O (C) (no cholate, w/LM) was preincubated for 2-3min at 4°C and mixed with (B) in a glass beaker (20mL) with 1cm stirring bar. Continuous addition (Table 2.1) of Biobeads followed by centrifugal filtering step results in (D), 3mL COVs. Filter column used for Bio-beads separation using gentle centrifuge (~100 x *g*) inside a 15mL Corning plastic tube. Untrapped free pyranine on the outside of COVs and trace of cholate remainder were removed by Sephadex G-25 gel filtration (45cm length and 2cm internal diameter sized column) column which is equilibrated with the same buffer as inside of vesicles; 20mM Hepes-KOH pH7.4, 38.9mM KCl, 52mM Sucrose, no cholate. All excluded COVs (E, 10-12mL) which have fluorescent color and placed lower band of column were collected. Further purification of the COVs was achieved using a Ni-NTA resin, which bound to the his-tag on the COVs under high salt concentrations. Sample was adjusted to final pH 8.0 with 200mM KCl concentration at this step before binding with Ni-NTA resins. Ni-NTA resins were pre-washed with two column volume of water and high salt buffer (20mM Hepes-KOH, 200mM KCL at pH8.0), respectively. Prepared COVs from previous steps and pre washed Ni-NTA were mixed together for 20 min. The first flow-through (F,10-15mL) and the second flow-through (G,45-50mL, two column volume washing with 20mM Hepes-KOH pH8.0, 200mL KCl without imidazole) was combinded, concentrated, washed as with purified COVs (H, 15-20mL, elution with 80mM Histidine, 38mM sucrose, 20mM Hepes-KOH at pH7.4). All elutions(F+G & H) were separately concentrated with Centricon 100 (amicon YM100 membrane) under gentle pressure of N_2 (5 psi),washed (x 10 vol. of buffer; 20mM Hepes-KOH pH7.4, 38.9mM KCl, 52mM Sucrose) and re-concentrated to reach final volume (I, ~1.8-2.0mL). The external buffer was replaced using dialysis for 12 hours into 50μM Hepes-KOH pH7.4 (1:500 v/v), 45mM KCl, 44mM Sucrose. Finally, COVs samples (J) were prepared for stopped-flow measurement.

(A) Lipid Sonication mixture (total 2mL)

80mg/ml Asolectin
3% cholate(w/v)
20mM Hepes-KOH pH7.4
38.9mM KCl
52mM sucrose
1mM EDTA
20mM Pyranine (0.01g/1ml)

(B)
Liposome

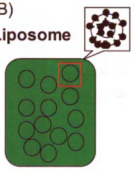

Sonication
for 30sec on/ 30sec off
more than 3 times

Centrifugation
Remove metal (12K, 15min)

(C)
His-tagged CcO

(B) Supernatant

(C) Add CcO

(**4uM**, FPLC purified, no cholate, w/ LM)
mix for 2-3min at 4°C in glass beaker (20mL)
w/ 1cm stirring bar

Biobead addition steps
7 hours continuous addition of Bio-beads SM-2 (Bio-rad)

Protocol for Detergent Removal		
Time (min)	Amount of Bio-beads added (mg/ml)	Temp.
0	33.2	4 °C
30	33.2	4 °C
60	33.2	4 °C
90	33.2	4 °C
120	66.5	4 °C
180	66.5	4 °C
240	133	RT
270	133	RT
300	266 add 1mL of 20mM HEP ES-KOH pH7.4	RT
360	266	RT
420	Ready	

Bio-beads

COVs

Filtering Separation of Biobeads by filter column by gentle centrifuge (~100xg) inside a 15mL Corning plastic tube

(Figure 2.3 continued)

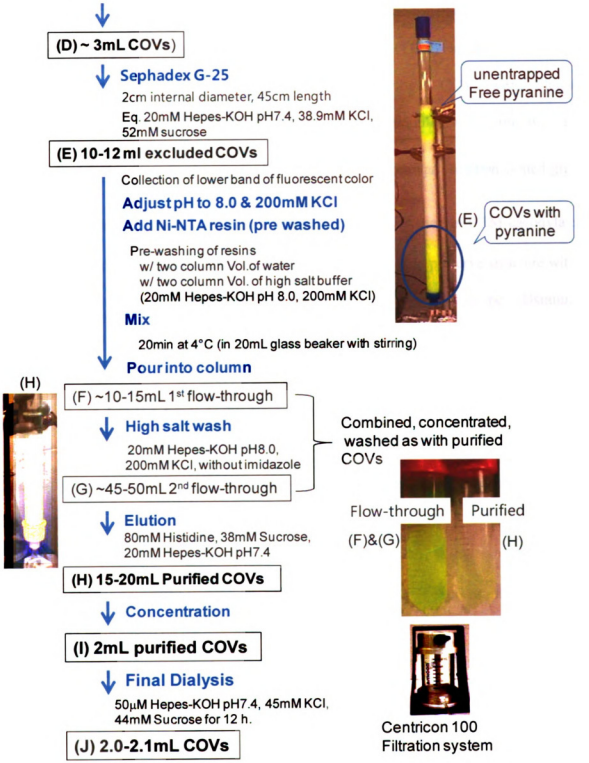

2.2.4. Measurement of COV Size by Electron Microscopy

In order to estimate the size of COVs made by different methods, their size was measured directly by transmission electron microscopy (TEM) at Michigan State University in the Center for Advanced Microscopy facility. COVs were diluted 200~2000 fold to get well separated samples of the vesicle population for counting. In order to fix COVs onto a fresh polyvinyl formal polymer, Formvar®-carbon coated grid support film, one volume of 2% osmium tetroxide (OsO_4) was used in 0.1M cacodylate buffer (pH7.4) at room temperature. The purpose of fixation is to preserve structure with minimal alteration during staining and viewing in the electron microscope. Osmium tetroxide acts as a fixative as well as an electron dense stain. In the reduced state, this fixative renders the sample black, permitting it to be more easily seen during processing. The pH of the fixative needs to be close to the sample pH (pH7.4) to be effective; otherwise, the structure and behavior of the proteins may be altered. The excess mixture was easily removed with a Whatman filter paper and dried at room temperature. The prepared specimen was stained with 1% uranyl acetate in distilled water for a few seconds for negative staining. COVs contained pyranine on the inside to increase the contrast for better observation of the COVs. Photographic images of an arbitrary number of the COVs were saved on the computer for size analysis.

2.3. Results

2.3.1. Dye Characterization

Two pH probes, pyranine (8-hydroxypyrene-1,3,6-trisulfonic acid) and phenol red, were used to monitor the proton movement on the inside and outside of COVs, respectively (Figure 2.4). Proton pumping (or proton release) was measured by using phenol red on the outside, because it is water soluble, has an amenable isosbestic point and shows absorbance changes in the required range, 344-750 nm. However, a very low external concentration of buffer was required in order to monitor the small changes in pH. Phenol red changes color from yellow to red over the pH range 6.6 to 8.0; its pKa is close to neutral pH (pKa ~7.5, Molecular Probes).

Pyranine is a water-soluble, membrane impermeable fluorescent dye with a high quantum yield, which is measured by either fluorescence or absorbance. Because of its polyanionic character, pyranine does not bind significantly to phospholipid vesicles, having a net anionic surface charge. COVs were prepared with entrapped pyranine, which does not readily leak out of the vesicles. It is observed that ionization of the 8-hydroxyl group of pyranine at alkaline pH is associated with a pronounced red shift in the fluorescence excitation maximum, from 400 (pH 4) to 450nm (pH 10), while the 510 nm emission maximum remained essentially unchanged. Therefore, at maximum excitation (465nm) at pH 7.4, the amplitude fluorescence emission at 510nm reflects the concentration of the unprotonated pyranine.

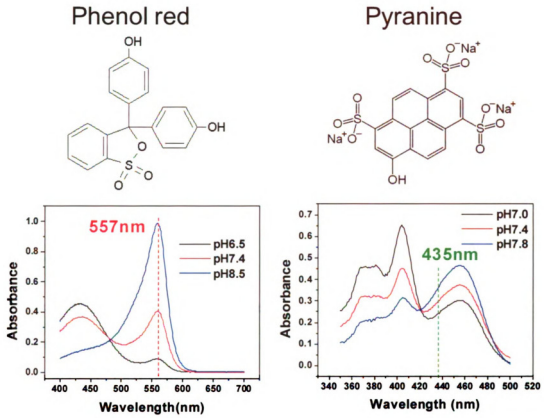

Figure 2. 4 Structures and absorption spectra of pH probes, phenol red and pyranine.

A hydrophilic pH-sensitive fluorescent dye, pyranine (trisodium 8- hydroxypyrene-1,2,6 trisulfonate), was entrapped inside cytochrome *c* oxidase vesicles (COVs) to monitor inside pH changes at 435nm during enzyme turnover. Another pH probe, phenol red (phenolsulfophthalein), was placed on the outside of the COVs to monitor proton pumping, measured at 557nm. The dotted lines indicate the absorption wavelength used to monitor the proton changes on the outside (left) and inside (right), separately.

Any trace amount of un-entrapped pyranine, which is associated possibly with outer surface lipid head groups, could be estimated by quenching with the addition of DPX [p-Xylene-bis(N-pyridinium bromide)], a water soluble collisional quencher of pyranine fluorescence which does not cross the membrane. No significant quenching effect was observed by addition of DPX to the purified Biobead COVs (Figure 2.5) suggesting the absence of remaining pyranine on the surface of COVs after the purification. This allows pyranine to be used as a reliable reporter of aqueous pH changes inside of the vesicles without DPX.

Both pyranine and phenol red were selected for the pH measurements because of their high absorption coefficients and because the pKas of both probes are very close to the initial pH conditions, which were selected in order to follow the pH changes during turnover. The pKas of the dyes are, 7.2 (pyranine) (Clement and Gould, 1981) and 7.5 (phenol red) (Faxen *et al.*, 2005). In order to eliminate the contamination of absorption signals from cytochrome *c* (the electron donor to C*c*O), an isosbestic point is used. This means that at the isosbestic point there are no changes in absorption of that spectral species during reduction of cytochrome *c*. In the absorbance mode, pyranine and phenol red signal changes were observed at 435nm and 557nm, respectively (Figure 2.6). The increase in pyranine absorbance at 435nm indicates alkalinization due to proton consumption on the inside (Figure 2.6,B). The absorbance change was measured at 557nm indicating outside pH changes with phenol red (Figure 2.6,C). Absorbance was decreased corresponding to the decrease in pH by pumped proton, whereas the absorbance was increased as protons move to inside of COVs due to the backflow. The

cytochrome *c* oxidation rate was calculated from a SVD (singular value decomposition) fitting method using the whole spectrum, or based on absorbance measured at 550nm (Figure 2.6,A) in the OLIS stopped-flow instrument (Figure 2.11).

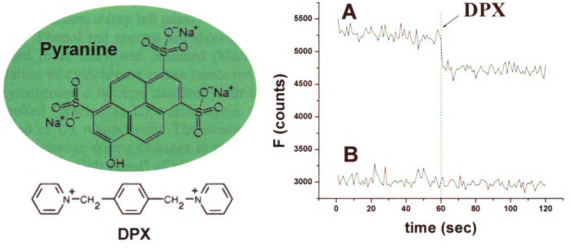

Figure 2. 5 Measurement of the residual pyranine on the outside surface of the COVs.

Structures of pyranine and DPX are shown on the left. The fluorescence emission (ex 465nm, em 510nm) of pyranine was quenched about 10% by addition of DPX in the aqueous buffer (20mM HEPES-KOH pH7.4 +38.9mM KCl + 52mM sucrose) (A) measured in a FluoroMax-2 fluorometer instrument. Pyranine fluorescence emission did not change with the addition of DPX in the purified COVs (B). This suggests that there is no significant amount of any residual external pyranine on the surface of the purified COVs.

Figure 2. 6 The use of pH probes and isosbestic points of cytochrome *c*.
The left panel shows: absorption spectra of reduced (blue line) and oxidized (black line) cytochrome *c* (top left panel) with pyranine absorbance spectra in green (top left panel). Phenol red spectra are shown in red (lower left panel) with cytochrome *c* reduced (blue line), and oxidized (black line). In the right top panel the rate of oxidation of cytochrome *c* was measured at 550nm. The absorbance was decreased as cytochrome *c* became oxidized with different rate at three different conditions, controlled (labeled as C), valinomycin (labeled as V) and uncontrolled condition (labeled as U), respectively. The isosbestic points, where cytochrome *c* absorbance does not change during changes in the reduction state, were selected for absorbance measurements (left panel) of pyranine, 435nm (B, top (left panel) and phenol red (C, lower left panel) at 557nm. The right panel shows the changes in absorbance over time during cytochrome *c* oxidation. The controlled state, C (black line), pumping state with valinomycin (blue line) and uncontrolled state (red line), are shown with (A) cytochrome *c* oxidation (B) pyranine absorbance changes on the inside of the COVs and (C) phenol red changes on the outside. The increase in pyranine absorbance at 435nm (B) indicates alkalinization due to proton consumption on the inside in all three conditions with different amplitude. The absorbance change was measured at 557nm indicating outside pH changes with phenol red (C). Absorbance in the controlled state was decreased for a short time and then increased. In the presence of valinomycin, the absorbance was decreased corresponding to the decrease in pH due to pumped protons, whereas absorbance was increased as protons move to the inside of COVs in the presence of both valinomycin and FCCP. Data fitting of the absorbance changes was performed using Microcal OriginPro computer software.

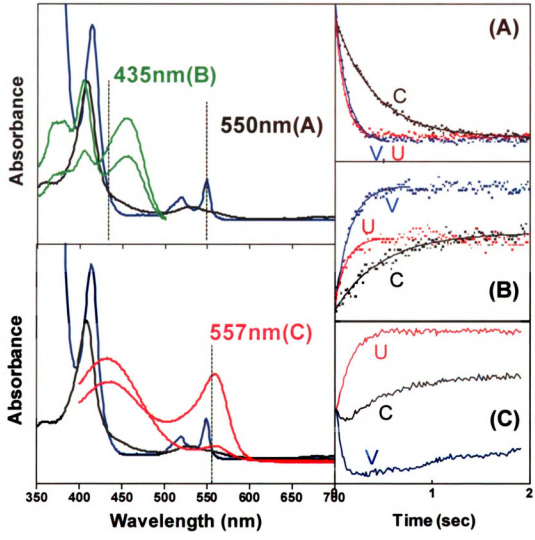
Absorbance
435nm(B)
550nm(A)
Absorbance
557nm(C)
350
400
450
500
550
600
650
700
Wavelength (nm)
(A)
C
V, U
V
U
C
(B)
U
C
(C)
V
1
2
Time (sec)

2.3.2. Initial Measurement of COVs with Fluorescence Mode

Membrane Potential Measurement of COVs

The fluorescence dye, $DiSC_3(5)$ was used to characterize the vesicles to determine whether a potential was properly established. The effect of membrane potential on changes in the fluorescent signal of $DiSC_3(5)$ can be quantified by measuring the diffusion potentials (Singh and Nicholls, 1985b), which are built up with a known amount of salt (K^+ and Na^+) on the outside in the presence of valinomycin. The created diffusion potential with valinomycin, which equilibrates $[K^+]$ across the membrane, can be calculated from a known amount of $[Na^+]$ by using the Nernst equation. When the membrane is in thermodynamic equilibrium, i.e. no net flux of ions, the membrane potential must be equal to the Nernst potential.

$$E = RT/zF \ln [\text{ion outside cell}] / [\text{ion inside cell}]$$

E, membrane potential; R, gas constant (8.31 $JK^{-1}mol^{-1}$); T, absolute temperature in kelvins; z, charge of a ion; F, Faraday constant (9.65×10^4 Coulomb mol^{-1})

During the proton pumping of COVs, due to the active transport of protons, a membrane potential is developed. It can be measured in the steady-state condition by addition of electron donors (horse heart cytochrome *c*, ascorbate, and TMPD) with $DiSC_3(5)$, carbocyanine fluorescence probes with a QuantaMaster™ Luminescence instrument by Photon Technology International (PTI) and a Felix 32 analysis software module (Figure 2.7).

As turnovers occur, the fluorescence was decreased, indicating the formation of a membrane potential due to catalytic reduction of O_2 to H_2O consuming the protons and electrons. Nigericin (1μM) was added to release the pH gradient, and all of the protonmotive force is now expressed in an increased membrane potential. Addition of valinomycin (2μM), which allows the electrogenic movement of K^+ to abolish the membrane potential, caused the fluorescence recovery (increase in fluorescence) (Figure 2.7). A larger size of vesicle is considered to form less membrane potential than a smaller vesicle. However, the flow-through vesicles (larger size) that do not tightly bind to the Ni^{2+}-NTA resin showed the same fluorescence signal as the purified vesicles using Ni-NTA resin. The increased buffering of flow-through vesicles containing many empty vesicles (no oxidase) may cause the observed difference in amplitude for fluorescence recovery. The results indicate that both vesicle populations are performing a good turnover, as expected, with a properly oriented C*c*O in the membrane. The electron donor, cytochrome *c*, can properly bind to the oxidase which is reconstituted in the vesicles. Although the potential was not calibrated for these vesicles a membrane potential of 140-160mV during turnover has been measured with similar vesicles (Singh and Nicholls, 1985a).

PROTON MOVEMENT IN CYTOCHROME *C* OXIDASE OF *RHODOBACTER SPHAEROIDES*

VOLUME II

By

NAMJOON KIM

A DISSERTATION

Submitted to
Michigan State University
in partial fulfillment of the requirements
for the degree of

DOCTOR OF PHILOSOPHY

Biochemistry & Molecular Biology

2009

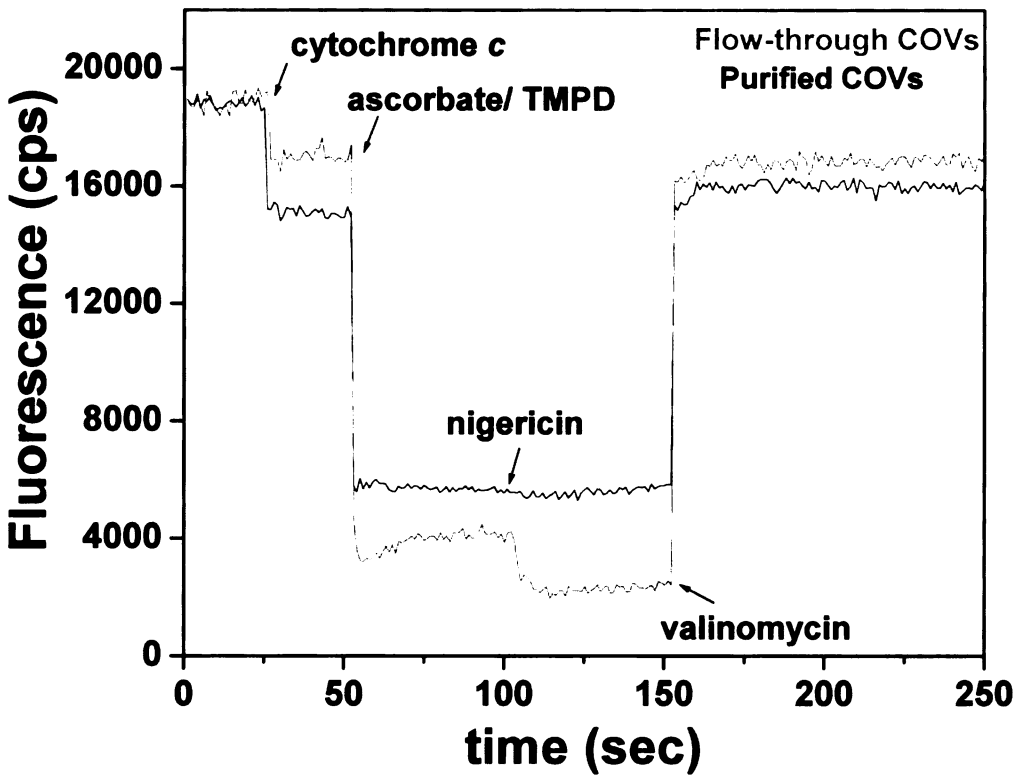

Figure 2. 7 Membrane potential measurements with the wild type COVs

COVs were made by the Bio-bead method using a $DiSC_3(5)$ fluorescence probe as a monitor of electrochemical potential during turnovers with a QuantaMaster™ Luminescence instrument by Photon Technology International (PTI) equipped with a Felix 32 analysis software module. The steady-state condition was prepared in the presence of ascorbate (12mM), TMPD (57μM) and horse heart cytochrome *c* (2.1μM) in 50mM Hepes-KOH pH7.4, 24mM KCl. 200μl of purified COVs or 100 μl of flow-through vesicles (0.2μM final aa_3 concentration) were added into a 2ml volume of sample cell with 2.58μM of $DiSC_3(5)$ which is pre-equilibrated with vesicles for 4min before measurement. The addition of cytochrome *c* is required as an electron donor; however, it quenches the fluorescence signal to some extent. Major quenching of the fluorescence signal was observed during the turnovers, which build up a membrane potential. Addition of nigericin (1μM) releases the pH gradient, and the addition of valinomycin (2μM), removes the membrane potential and allows K^+ equilibrium,

(Figure 2.7 continued)

recovering the fluorescence signal to its original level. Both purified (tightly bound to Ni-NTA resin) and flow-through COVs (less tightly bound) show good development of a membrane potential, indicating a proper orientation of C*c*O in the membrane. Both fluorescence signals were normalized at the same starting point. The increased buffering of the flow-through vesicles, which contain many empty vesicles with no C*c*O, may cause the different response to $DiSC_3(5)$ fluorescence changes in the presence of nigericin, resulting in an apparent increase in the membrane potential.

$DiSC_3(5)$, carbocyanine, fluorescence changes were also measured in the stopped-flow system and to measure the membrane potential build up versus time by rapid mixing. However, this was not successful in a fast-time scale in a pre-steady state rapid-mixing condition with the Applied Photophysics stopped-flow instrument, possibly because the response of $DiSC_3(5)$ is slower than the pH dye responses.

Fluorescence Monitoring of pH changes on the inside of COVs

In order to look at internal pH changes, a number of studies have been performed using phenol red, which is entrapped on the inside of COVs (Faxen and Brzezinski, 2007; Faxen et al., 2005). However, the absorbance of phenol red did not give a good signal to noise level because its pKa appears to shift to a significantly higher value when incorporated into the vesicles. We therefore chose pyranine for monitoring pH changes on the inside of COVs because of its better sensitivity to pH and the fact that it can be measured by absorption or fluorescence. The pyranine emission signal is observed only at 510nm no matter what excitation wavelength is applied. The signal increases in fluorescence intensity at high pH. Pyranine in the vesicles exhibits similar fluorescent properties as in solution, with a very slight alkaline shift in the pKa, possibly resulting from the proximity of negatively charged phospholipids on the inner surface of the bilayer (Clement and Gould, 1981). These unique characteristics of pyranine made it more useful as a monitor of inside pH changes in the fluorescence or absorption mode than phenol red.

Data collection was performed initially with the Applied Photophysics stopped-flow instrument (Figure 2.8) in which the solutions are rapidly mixed in a millisecond time scale. The outside pH change could be easily measured with phenol red which would not interfere with the internal pH probe. The oxidation rate of cytochrome *c* and the phenol red absorbance changes on the outside during turnover were measured in the absorbance mode, while inside pH changes of the pyranine dye were measured in the fluorescence mode using the Applied Photophysics stopped-flow instrument with a cut-off filter (Figure 2.9). Each reaction is repeated at least three times and averaged for single exponential fitting.

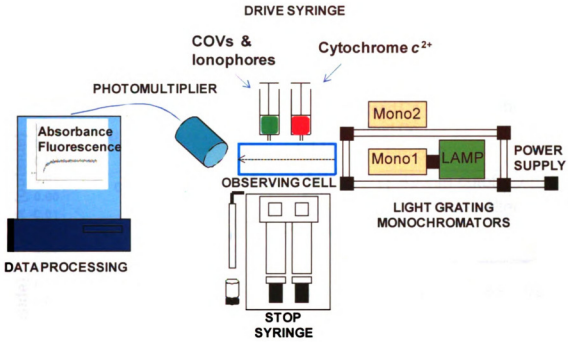

Figure 2. 8 Scheme of Applied Photophysics stopped-flow instrument.
A single wavelength was used for absorbance or fluorescence. The emission wavelength was selected from the light source, which is grated by monochromators. Samples are rapidly mixed in the observation cell and changes are monitored in the millisecond to second time scale, either in a fluorescence or absorbance mode. Fluorescence signals were filtered by using a cut-off filter (490nm) before collection of the signals at the photomultiplier, and were transferred to the computer and analyzed.

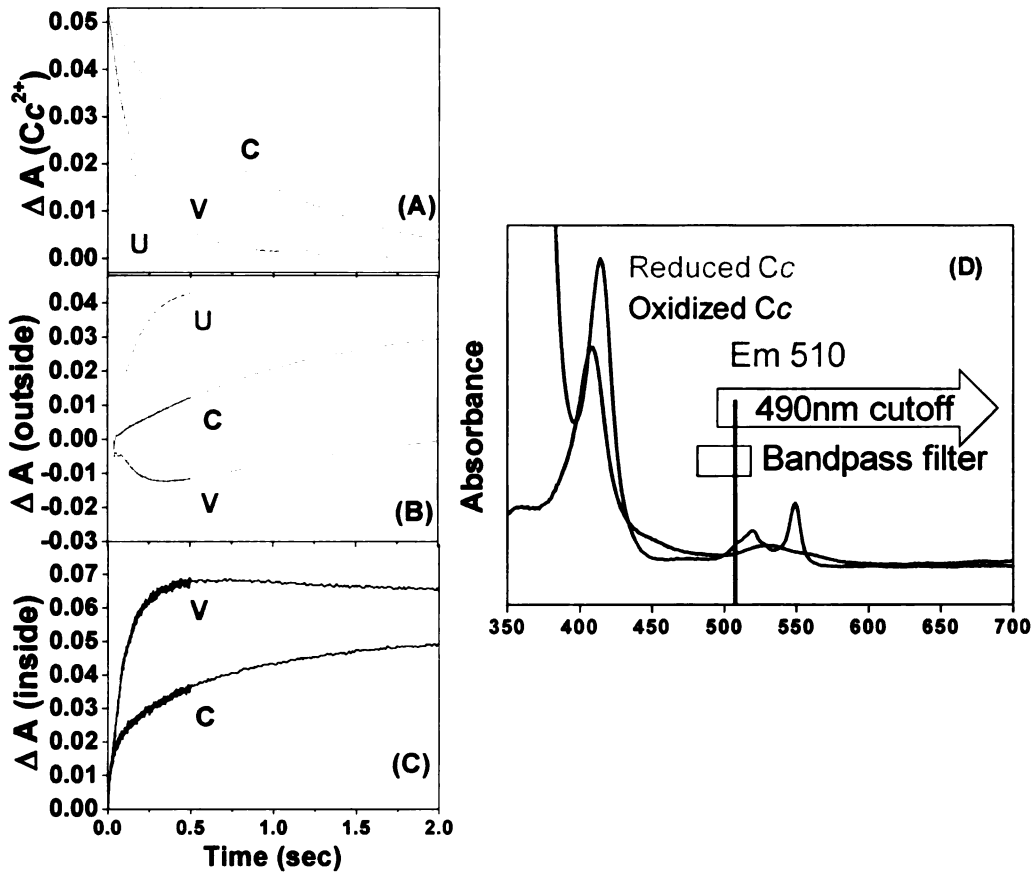

Figure 2. 9 Initial measurements of COVs made using the cholate-dialysis method. The fluorescence mode was used in an Applied Photophysics stopped-flow instrument for measuring internal pH. Each reaction was repeated at least three times and averaged for single exponential fitting. (A) Cytochrome *c* oxidation in the controlled, C, condition, V, valinomycin; and U, uncontrolled states (B) proton pumping was measured externally using an absorbance signal of phenol red. (C) Internal pH changes were monitored by using pyranine dye entrapped inside the COVs with the fluorescence emission detector with a cut-off filter measured in separate experiments from (A) and (B). The machine configuration has to be changed in order to change the detection mode from absorbance to fluorescence. Even with strong fluorescence emission signals, it was hard to determine the initial starting point and end point of the reaction. Using an extrapolation of the data, the starting and end point of the reaction was determined. However, the emission signal was severely contaminated by the cytochrome *c* itself either with cut-off or bandpass filters because cytochrome *c* absorbed emission siganal and worked like an inner-filter in the system (D), resulting in differential fluorescence quenching as turnover occurs.

Even though the fluorescence mode enabled the measurement of inside pH changes with a strong signal-to-noise ratio (Figure 2.9 C), some limitations were found in this measurement. The quantification of protons was a major problem because cytochrome *c* had an internal quenching effect on the emission of pyranine since it absorbs strongly and variably in the 500-550 region. The variable reduction state of cytochrome *c* gave a variable re-absorption of the emitted light which is called an "inner-filter effect". Initially, a cut-off fitler that allowed transmission of all fluorescence signals over 490nm was used, but in order to reduce the quenching effect, another band-pass filter (480-520nm) was introduced. However, under these conditions the fluorescence emission was too small to measure accurately.

Another difficulty in the fluorescence measurement was determining the initial zero time point, as it shifted greatly between samples. In addition, the detector configuration had to be changed in order to change the detection mode from absorbance to fluorescence, so we could not get the two measurements (absorbance and fluorescence) at once on the same sample. These technical and systematic limitations to the use of the fluorescence as a tool, resulted in a change to use absorbance measurements for the inside pH determination, with the Olis rapid scanning stopped-flow.

2.3.3. Initial Measurement of COVs with Absorbance Mode

Pyranine is a particularily valuable probe because it has high sensitivity in both the absorption and fluorescence modes, making different measurement methods possible. Internal and external proton movements in vesicles can be measured in an absorbance

mode at the same time as cytochrome *c* oxidation, with COVs containing pyranine inside and phenol red on the outside, by using a rapid scanning Olis stopped-flow instrument (Figure 2.10).

The signal from the pH probe pyranine, in the interior of the COVs, was weak under the conditions examined initially (Figure 2.11 C), compared to the outside proton changes, which are probed by phenol red. The only viable isosbestic point of cytochrome *c* for pyranine measurement was 435nm where relatively small changes are monitored in this region during turnover (Figure 2.4 and 2.6). A major problem was identified as being the small volume of the vesicle interior, giving low dye entrapment. The volume of the vesicle can be calculated based on the known width of the bilayer and the diameter of the COVs (Figure 2.12). In addition to the concentration of the entrapped dye, another problem was considered, that proton pumping might be inhibited by the lack of sufficient proton supply from the inside due to the low buffering and the small capacity of the vesicle interior. Therefore, it seemed important to increase the internal volume capacity of the COVs and to optimize internal buffering conditions.

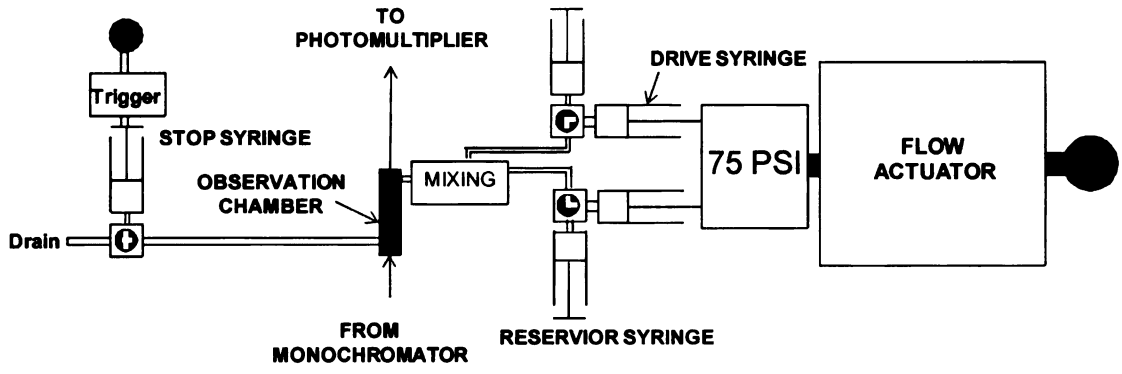

Figure 2. 10 Scheme of Olis stopped-flow instrument.
The basic setup is similar to that of the Applied Photophysics stopped-flow except that this instrument has the ability to scan multiple wavelengths over time monitoring light absorption. Data is collected over a set wavelength range in 1 millisecond. This is feasible because of the use of a patented "DeSa" subtractive double grating monochromator with a moving intermediate slit. Kinetic analysis of cytochrome *c* oxidation was performed either by a SVD (singular value deconvolution) method or by Microcal OriginPro software.

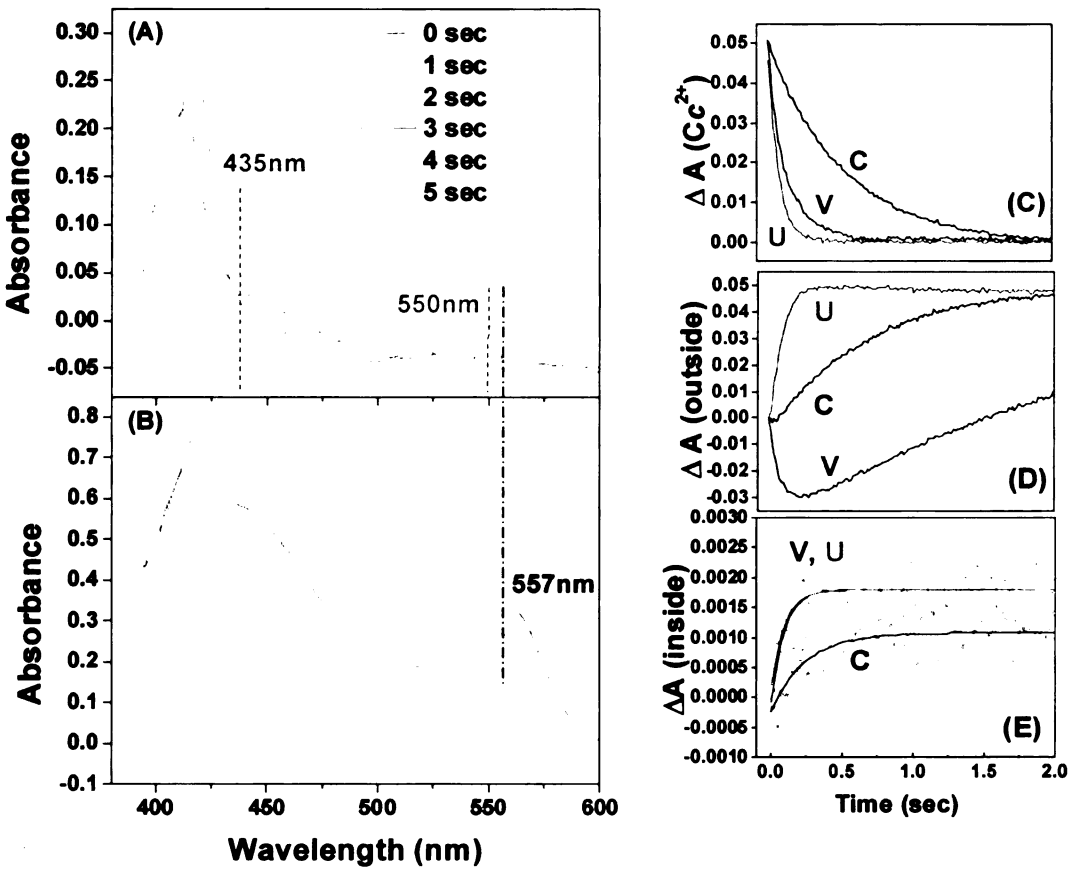

Figure 2. 11 Initial measurements of COVs made with the cholate-dialysis method in the absorbance mode of the Olis stopped-flow instrument.
All probes were monitored using the isosbestic wavelength of cytochrome *c*. The right panel shows cytochrome *c* oxidation in C, controlled; V, valinomycin; U, uncontrolled states (C), proton pumping probed with phenol red (D), and internal pH changes probed with pyranine (E) entrapped inside the COVs. Measurements were made over the wavelength range (right panel) as in (A)&(B) every 1msec. A typical wavelength scan of cytochrome *c* oxidation over 5 seconds in the presence of pyranine inside the COVs is shown in (A) at 550nm. An increase in pyranine absorption is observed, due to proton consumption on the inside, during turnover at the 435nm isosbestic point. The sensitivity of changes in the pyranine absorbance was limited. Phenol red absorption changes were monitored in the presence of both pyranine and cytochrome *c* at the 557nm isosbestic point of cytochrome *c* (B). Pyranine does not contaminate the phenol red absorption signal in the wavelength range observed.

Figure 2. 12 Size estimation of COVs.

The total Internal volume of the COVs was calculated (A) based on the measured mean diameter of COVs by EM and an estimate of the total number of vesicles based on the C*c*O concentration assuming, minimally, 1 C*c*O/vesicle (B). The equation for a sphere volume calculation ($V=4/3\ \pi r^3$) was applied with a 5nm estimated bilayer width. The amount of entrapped pyranine was calculated based on an estimate of the volume of the vesicles assuming an internal 20mM final pyranine concentration in 20mM HEPES-KOH pH7.4 (with 38.9mM KCl+52mM sucrose). As the mean diameter increased from 20nm to 75nm, the internal volume increased to a large extent, entrapping a lot more pyranine molecules inside of a single vesicle from 6 to 1,730 molecules as shown in red. The total internal volume in the 80μl cell in the Olis stopped-flow instrument was calculated based on a varied mean diameter (MD) (C). e.g. 0.69 μl of total internal volume is calculated with a 75nm mean diameter. Another way of calculation was made for internal volume estimation. Direct absorbance of pyranine measured from the stopped-flow could be used to calculate the pyranine concentration and the total internal volume (D) with a 0.4cm bandpath and 7.1 $mM^{-1}cm^{-1}$ as an absorption coefficient measured from a standard curve at 435nm. There was a 7-fold difference between the calculated (75nm mean diameter, 0.69μl), and measured total internal volume (0.1μl) using the absorbance of pyranine in the cell.

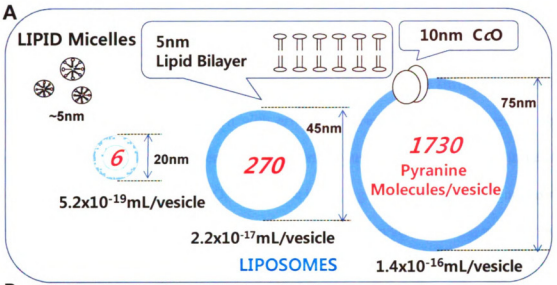

B

80µl Cell (Olis stopped-flow)

MD

20mM
Pyranine

Total # of vesicles
= total # of CcO
assuming
1 CcO/vesicle

Internal volume
$= 4/3\ \pi r^3$

$$\text{radius} = \frac{[\text{MD} - (2\text{x Bilayer width})]}{2}$$

C

Calculated Total Internal Volume
using a mean diameter
measured by electron microscopy

MD (Mean Diameter, nm)	Total Volume (µl/ 80µl cell)
75	0.69
60	0.32
53	0.20
50	0.16
40	0.07

D

Pyranine
Absorbance
of stopped-flow

$A = \varepsilon bc$

$\varepsilon_{435nm} = 7.1\ mM^{-1}\ cm^{-1}$

$b = 0.4\ cm$

[Pyranine] x 80µl
= 20mM x total internal
volume
of COVs
Measured Total Internal
Volume = 0.1 (±0.01) µl

2.3.4. Modification of preparation method and Characterization of COVs

Bio-beads COVs with purification steps by Ni-NTA and his-tagged C*c*O

The small capacity of the interior of the COVs did not give sufficient signal for good absorbance measurements even with efficient probes, such as pyranine. A new method to make vesicles was attempted with further purification steps with Bio-beads, Ni-NTA and a histidine-tagged C*c*O, to obtain a better signal to noise ratio by increasing the size of COVs and by eliminating background signals from void vesicles, which do not contain C*c*O.

Bio-beads have been introduced as a simple alternative to other conventional detergent removal strategies such as dialysis, gel chromatography and dilution. A mechanism using the adsorption of detergent onto polystyrene beads, allowing the more rapid formation of liposomes has been proposed by Rigaud *et al.* (Rigaud *et al.*, 1998)(Figure 2.1). The use of Bio-beads has been shown to be a reproducible method to prepare unilamellar and homogeneous preparations of bovine cytochrome *c* oxidase proteoliposomes from micellar mixtures (Jasaitis *et al.*, 1999). This method was adopted for producing vesicles of *Rs*C*c*O as described in experimental procedure (Section 2.2) and in Figure 2.3. A batch procedure, with successive additions of beads, allows control of the detergent removal rate, which is essential to prevent a heterogeneous preparation, in terms of size and multilamellarity. In the early steps of reconstitution, a low bead to detergent ratio was applied to promote the micellar to lamellar (bilayer) transition. After such a transition, the bead concentration was increased up to the adsorptive capacity in order to remove residual detergent from COVs. Untrapped pyranine was removed

successfully by sephadex G-25 gel filtration where good separation between the vesicles and the dye was achieved (Figure 2.3, Sephadex G-25 column). The Ni^{2+}-NTA purification with subunit II his-tagged C*c*O, allowed correctly (outward facing) oriented COVs to be isolated with 25% recovery yield, and eliminating background mainly attributed to empty vesicles lacking in C*c*O.

Size Measurement by Transmission Electron Microscopy

The size of COVs reconstituted by detergent removal with Bio-beads under different vesicle preparation conditions was analyzed in detail by transmission electron microscopy (TEM) by negative staining after fixation. Images from many different vesicles preparation (13 different COV sets) were examined. It was difficult to get the right concentration of sample to get a good visualization of the vesicles. The best conditions were obtained with a 500 fold dilution (using 20mM HEPES-KOH, 38.9mM KCl, 52mM sucrose buffer) and showed reproducible differences between COVs prepared by different methods.

Cholate-dialysis COVs were found to have a mean diameter about 25~30 nm (Figure 2.15 A, B) with or without C*c*O (Figure 2.13). Cholate-dialysis COVs, combined with purification by Ni^{2+}-NTA were compared in size, and showed similar morphology (sphere) and homogeneity in size distribution. Unlike cholate-dialysis COVs, Bio-beads COVs (Figure 2.14) showed almost three times larger average size (70~80nm in mean diameter) (Figure 2.15 C,D).

Total internal volume of the COVs, which corresponds to $1.4x10^{-16}$ mL per liposome (with mean diameter of 75nm) was calculated based on an estimated total number of vesicles assuming, minimally, one oxidase per vesicle after the Ni^{2+}-NTA column purification (Figure 2.12). The amount of entrapped pyranine was also calculated based on an estimated volume of vesicles assuming the 20mM internal pyranine concentration. As the mean diameter increased, the volume contribution was greatly increased as well as the amount of pyranine dye entrapment. This is a really important fact, because low pyranine entrapment inside of COVs was a major limiting factor in measuring the pH changes in the absorbance mode.

Direct absorbance of the sample was also applied to calculate the total internal volume of COVs. The baseline scattering was corrected by subtracting the end scan absorbance point in the Olis-stopped flow scan. A known value of bandpath (0.4cm) and measured absorption coefficient (7.1 $mM^{-1}cm^{-1}$) from a standard curve was used to calculate pyranine concentration at 435nm. The total internal volume was calculated from this measured pyranine concentration using the known observing cell volume. There was an almost 7-fold difference between the calculated (based on EM mean diameter) and measured (based on absorbance) total internal volume. It is possible that we might have many uncounted small vesicles, which contribute to the reduction of the real mean

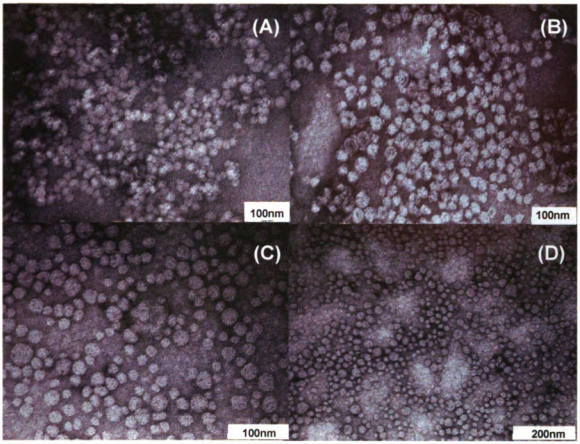

Figure 2. 13 Transmission electron microscopy (TEM) of reconstituted cytochrome *c* oxidase vesicles (COVs) by a cholate-dialysis method.
(A) Cholate-dialysis COVs whole mixture with empty vesicles (B) Ni-NTA purified COVs from a cholate-dialysis method; (C)&(D) Protein-free vesicles made by the same cholate-dialysis method. Vesicles were fixed with 2% osmium tetroxide in 0.1M cacodylate buffer pH7.4, and stained with 1% uranyl acetate for negative staining. The size bars represent 100nm (A,B,C) and 200nm (D) in the micrograph.

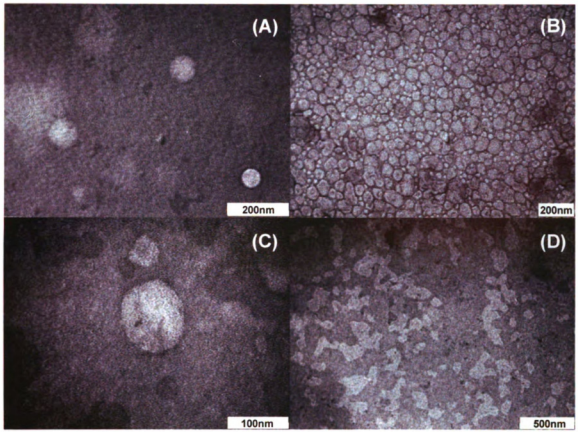

Figure 2. 14 TEM of reconstituted cytochrome *c* oxidase vesicles (COVs) by the Bio-bead method.

(A) Bio-bead COVs purified by Ni-NTA; (B) Bio-beads from the flow-through from a Ni-NTA column; (C) A single COV made by the Bio-bead method with Ni-NTA purification; (D) Disrupted vesicles in the presence of detergent (2% lauryl maltoside). Vesicles were fixed with 2% osmium tetroxide in 0.1M cacodylate buffer pH7.4 and stained with 1% uranyl acetate for negative staining. The size bars represent 100nm (C), 200nm (A,B) and 500nm (D) in the micrograph, respectively.

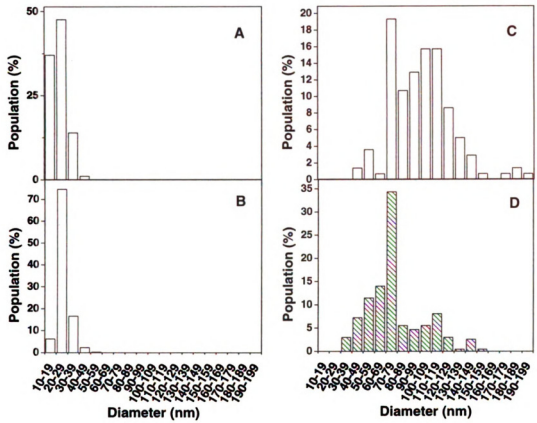

Figure 2. 15 Size distribution histogram obtained from TEM of COVs.
Size distribution histogram obtained from TEM of COVs. Size population (%) of total counted COVs is shown with the measured mean diameter size (nm). (A) Void vesicles (free of CcO) made by the cholate-dialysis method. (B) Cholate dialysis COVs followed by a Ni-NTA purification step. (C) Bio-bead COVs which flow-through and do not bind to the Ni-NTA column. (D) Purified Bio-bead COVs using Ni-NTA column.

diameter of COVs. Alternatively, the final concentration of pyranine entrapped inside the vesicles might be lower because of its binding onto the Bio-bead surface, or due to the exclusion of dye from the small internal volume. If the vesicle average diameter is assumed to be 53 nm, or if the actual internal dye concentration is assumed to be 10 mM, then the two estimates would be a close match (0.2µl/80µl cell, Figure 2.12).

An attempt to measure vesicle size using a dynamic light scattering method was not successful because of the heterogeneous character of prepared vesicles in our method.

The number of oxidase molecules per unit vesicle could not be measured by the TEM technique; however, freeze fracture electron microscopy has reported that 1 or 2 C*c*O molecules could be embedded in reconstituted vesicles of this size range (60-70nm) similar to our COVs (Madden *et al.*, 1984) (Figure 2.16).

Permeability of COVs and Calibration of Absorbance Change

The permeability of the COVs was measured by using a pH gradient in the Olis stopped-flow instrument. This was produced by mixing vesicles at pH 7.4 (20mM HEPES-KOH) with a buffer (20mM MES-KOH) at pH 6.3. Void vesicles, without C*c*O, were made by the same procedure as used for Bio-bead COVs, and were compared as a control. Both types of vesicles exhibited similar changes in internal pH indicating low permeability to protons under a pH gradient

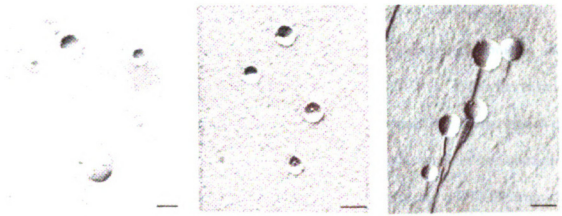

Figure 2. 16 Freeze-fracture electron micrographs of reconstituted cytochrome oxidase vesicles which are made by the cholate dialysis method.
The bars on the bottom represent 100nm in each micrograph. The freeze fracture micrograph shows 1-2 C*c*O molecules (60~70nm diameter size) that could be embedded in the reconstituted vesicles. Electron micrograph was obtained from Madden *et al.* (Madden *et al.*, 1984).

without turnovers. Pyranine absorbance was measured at the isosbestic point of cytochrome *c* (435nm) and did not change much, unless the uncoupling chemicals, such as valinomycin and FCCP were added to the system (Figure 2.17 A). When the vesicles were fully equilibrated, the pH was measured as pH 6.31, showing little change due to the much greater external volume. The pH change on the inside was obtained by subtracting the final pH (pH6.31) in the presence of ionophores (valinomycin + FCCP) from the initial starting pH (pH7.40). A 1.09 pH unit change corresponds to Δ ABS = 0.10 in the Olis stopped-flow absorbance measurement at 435nm (Figure 2.17 A). We normally observed ~0.008 unit absorbance changes during the pumping measured at 435nm by the same stopped-flow machine (Figure 2.19, B:blue trace). The proton concentration calculated near pH 7.4 (Figure 2.17,B inset) showed an almost linear relationship with the absorbance changes observed at 435nm in the Perkin-Elmer spectrophotometer. Therefore, we estimated that the 0.008 absorbance change corresponds to about 0.1 pH unit change (pH 7.4 → pH 7.5) during the pumping measurement, on the inside of the COVs, a reasonable number according to known estimates. In order to get the actual H^+/e^- pumping stoichiometry, the amplitude of the absorbance signal was used to estimate how many protons are consumed from inside, with an internal standard assuming that $1H^+/e^-$ is consumed under uncontrolled condition.

Figure 2. 17 A measurement of the permeability of COVs and calibration of absorbance changes.

Vesicles without C*c*O were prepared as a control and compared with wild type COVs made by the Bio-bead method in 20mM HEPES-KOH pH7.4. (A) The permeability of the COVs was measured by using a pH jump, where an acidic 20mM MES-KOH buffer (pH6.3) was placed on the outside while pH 7.4 maintained on the inside of the COVs. Both types of vesicles showed poor proton permeability under a pH gradient (20mM MES buffer, pH6.3 outside) unless ionophores were added. Full equilibration was only achieved in the uncoupled condition with both valinomycin (V) and CCCP (C). (B) pH dependent absorbance changes of aqueous pyranine were measured in the Perkin-Elmer spectrophotometer in 50mM HEPES-KOH, 50mM MES-KOH and 50mM CHES buffer. Pyranine absorbance at the isosbestic point (435nm) of cytochrome *c* showed an almost linear relationship with a pKa near 7.4. Approximately 0.1 pH unit changes are expected during the pumping reaction in the normal condition with valinomycin in the COVs. The proton concentration in this region showed a linear relationship with absorbance signal, as observed (inset).

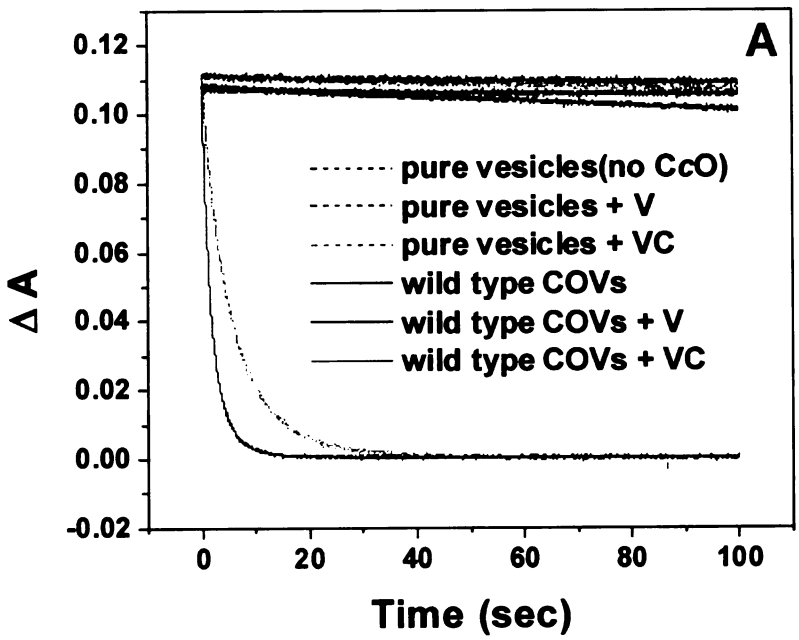
A
0.12
0.10
0.08
0.06
0.04
0.02
0.00
-0.02
Δ A
pure vesicles(no CcO)
pure vesicles + V
pure vesicles + VC
wild type COVs
wild type COVs + V
wild type COVs + VC
0
20
40
60
80
100
Time (sec)

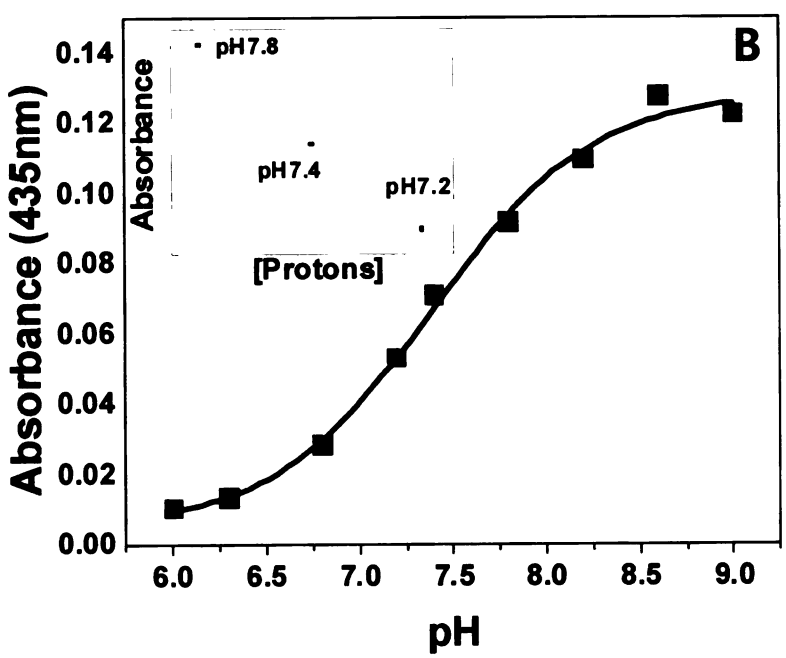
B
Absorbance (435nm)
0.14
0.12
0.10
0.08
0.06
0.04
0.02
0.00
Absorbance
pH7.8
pH7.4
pH7.2
[Protons]
6.0
6.5
7.0
7.5
8.0
8.5
9.0
pH

2.3.5. Optimizing Conditions for Analysis of the Activity and Function of COVs

Internal Buffer Selection

Variously buffered COVs were prepared with different concentrations of HEPES-KOH pH 7.4, in order to determine the optimal buffering on the inside (Table 2.2). The respiratory control ratio (RCR), in which the activity with uncouplers (valinomycin and FCCP) is divided by the controlled activity containing no ionophores, was used to verify the condition of the vesicles. The osmolarity of COVs was adjusted to 135mOSM with sucrose. The changes in RCR, under the same osmolarity and ionic strength, could be attributed to the effect of buffer changes on the inside. The measured RCR was variable, from 6.5 to 2.0, as the buffer changed from higher to lower concentration, in the steady-state condition, with the same ionic strength. When the ionic strength was lowered to10 mM K^+, the RCR was lowered to 2-4, even with the same osmolarity, which was adjusted by using a high sucrose concentration. The yield of proton release to the outside, measured by phenol red, was increased as the inside buffer concentration increased in the pre-steady state stopped-flow condition (Figure 2.18).

In order to measure the inside pH changes of COVs with a pH probe, lowered interior buffering would be expected to increase changes in the dye signal; however, COVs with lowered buffering did not support a good RCR value, probably because of a shortage of sufficient protons to maintain enough turnovers during activity, which uses protons for the reduction of oxygen to water, as well as being pumped to the outside. The

buffer condition, with 20mM HEPES-KOH pH7.4, 45mM [K^+] on the inside of the COVs was selected in order to supply sufficient protons, with reduced buffering on the inside, in order to study proton movement by monitoring the dye absorbance changes from the inside and outside together during the turnover, in the millisecond time scale with stopped-flow techniques.

INSIDE [Hepes-KOH]	75mM	50mM	25mM	15mM	5mM	25mM	25mM
[K+]	45mM	45mM	45mM	45mM	45mM	10mM	10mM
[Sucrose]	None	None	20mM	30mM	40mM	None	90mM
Controlled (e^-/sec/aa_3)	119±20	177±18	212±4	109±32	95±12	121±1.4	205±73
Uncontrolled (e^-/sec/aa_3)	763±110	975±75	1101±180	470±270	274±37	514±80	407±86
RCR	**6.5**±0.9	**5.8**±0.6	**5.2**±0.6	**4.3**±1.3	**2.7**±0.4	**4.2**±0.6	**2.0**±0.7

Table 2. 2 Varying the internal conditions to optimize the COVs.
COVs were prepared with different inside buffering capacities using HEPES-KOH pH7.4 (outside, 50mM HEPES-KOH pH7.4 45mM [K^+]). The RCR (respiratory control ratio=uncontrolled activity/ controlled activity) was calculated and used as an indicator for testing the "leakiness" of the vesicles. Ionic strength was adjusted by addition of KCl, 45 mM or 10 mM. Osmolarity was controlled by varying the concentration of sucrose.

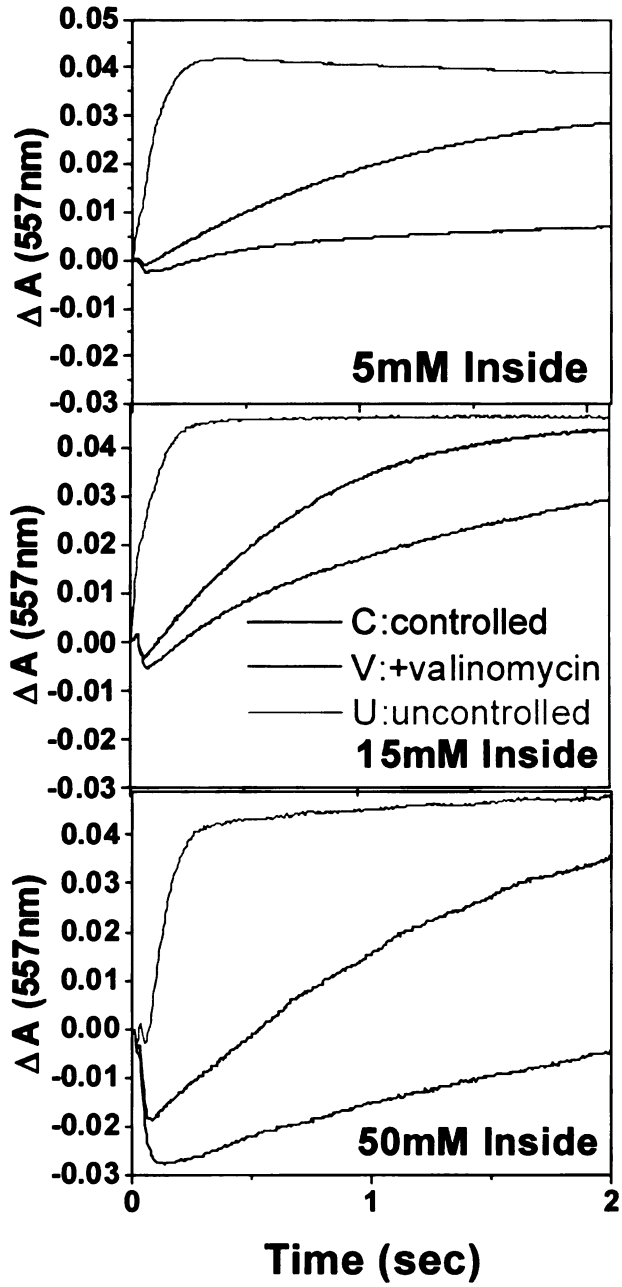

Figure 2. 18 Proton pumping on the outside of COVs.
Proton pumping on the outside of COVs measured by phenol red absorbance changes with increasing interior buffer concentrations of HEPES-KOH pH7.4. The proton pumping (blue line) shows a large decrease in absorbance almost equal to the increase in absorbance in the uncontrolled state with 50 mM buffering inside, showing that the stoichiometry of pumping is increased with an increase in the buffer strength under a pre-steady state condition. Measurements were made with the Applied Photophysics stopped-flow in the absorbance mode at 557nm, the isosbestic point of cytochrome *c*.

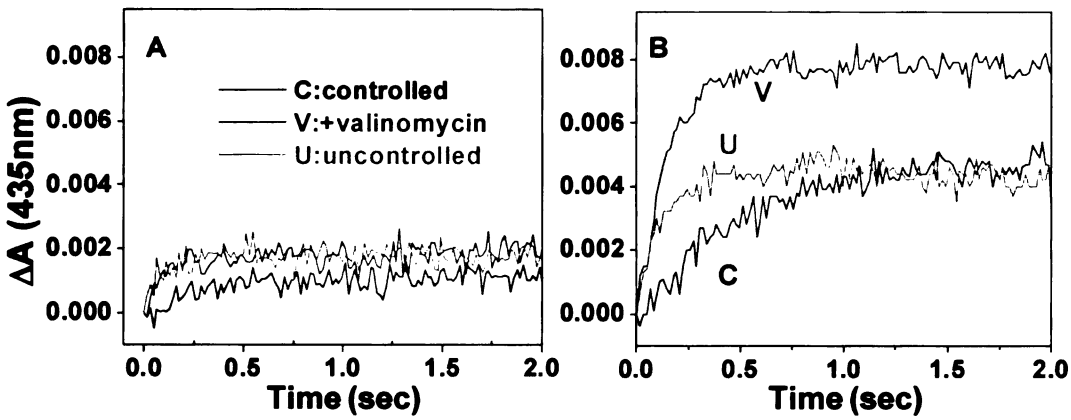

Figure 2. 19 A comparison of proton uptake in COVs either made by the cholate-dialysis method (A), or by the Bio-bead method, (B).
The COVs which were made with the Bio-bead method showed an increase in size, and also an increased pyranine absorbance. All three conditions: controlled (black), with valinomycin (blue) and uncontrolled, with both valinomycin and FCCP (red), show significant signal changes, with the greatest increase in absorbance with valinomycin added, due to the increase in proton uptake for both proton pumping and for protons required at the active site for chemistry.

Monitoring inside pH changes with various conditions

Larger COVs prepared by the Bio-bead method allowed the use of absorbance signals to monitor inside pH changes instead of using fluorescence, which has limitations due to a lack of quantification and the inner-filter effects of cytochrome *c*. Compared to the relatively small COVs made by the cholate-dialysis method (Figure 2.19 A), COVs made with Bio-beads gave a better signal to noise ratio (Figure 2.19 B). The amplitude of the proton pumping signal was almost twice as large as that of the controlled state, as expected, since during proton pumping twice the amount of protons will be consumed from the inside. Analysis of absorbance changes of internal pyranine indicated a maximal response at 20mM pyranine (Figure 2.20). However, the signal observed during the turnovers in the stopped-flow was still not as strong as expected. This may be due to the buffering on the interior, or a self-quenching of pyranine at a higher internal concentration, or exclusion of dye due to the still small internal volume (Figure 2.12).

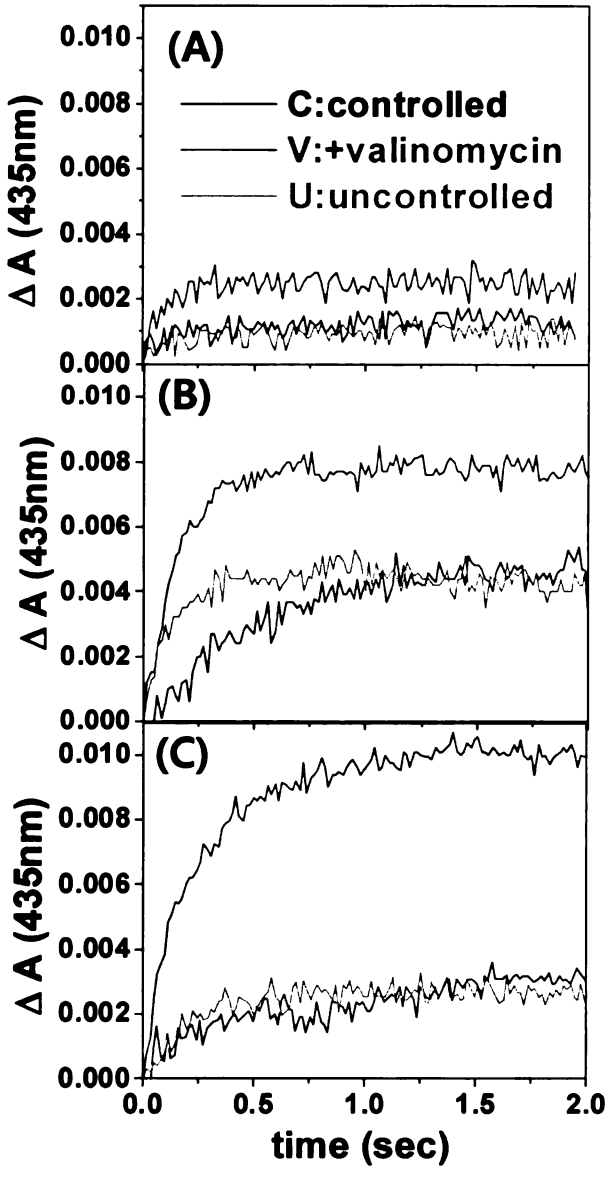

Figure 2. 20 Concentration dependent absorbance changes of pyranine measured from the inside of Bio-bead COVs with entrapped pyranine.
(A) 10mM, (B) 20mM, (C) 40mM pyranine. The Olis stopped-flow was used to monitor changes in pyranine at 435nm, the isosbestic point of cytochrome *c*. Bio-beads were added slowly over 7 hours. Increases in the pyranine concentration caused an increase in the signal, mostly under the pumping condition with valinomycin. The controlled and uncontrolled conditions showed the least change in absorbance. Pyranine may contribute to the buffering capacity on the inside when it is at a high concentration.

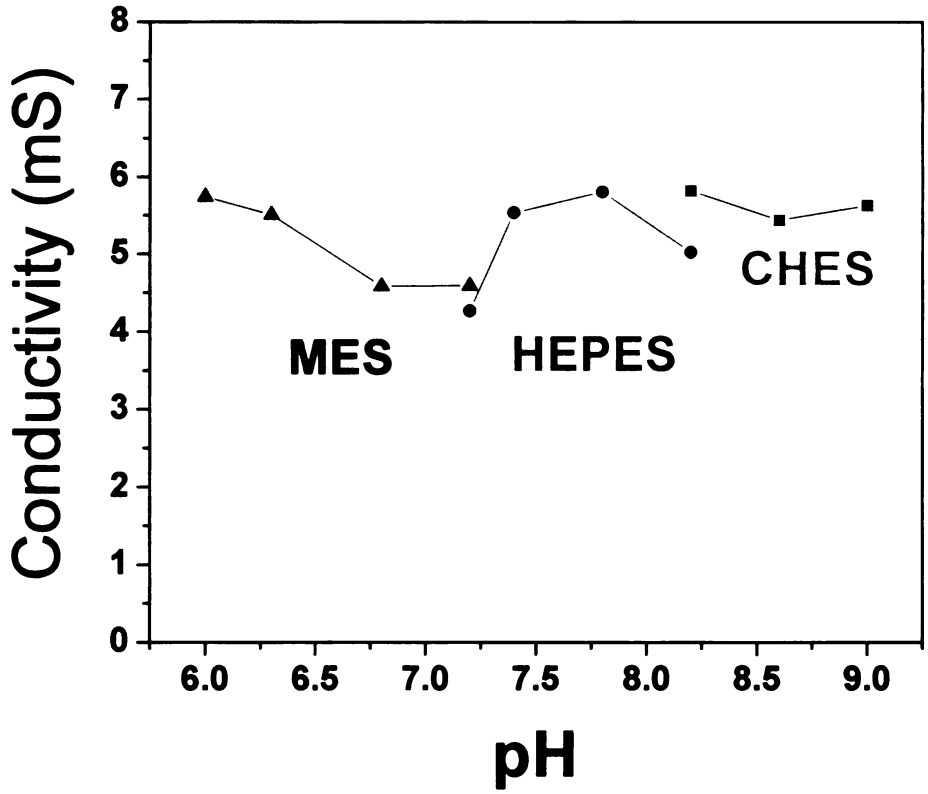

Figure 2. 21 Conductivity measurements with a three-buffer system; MES, HEPES and CHES buffer for use with COVs over a range of pH.

The ionic strength of the different buffer solutions was measured from the total of all the ions present in the solution. A conductivity meter (Accumet) was used to measure the ionic strength of each buffer. Three different buffer systems, which have similar osmolarities, were used. Conductivity was expressed in millisiemens per centimeter (mS/cm). The prepared buffers were designed to have a similar ionic strength. Over most ranges, the amount of measured conductivity is directly proportional to the amount of salts (ionic strength) in the buffer solution.

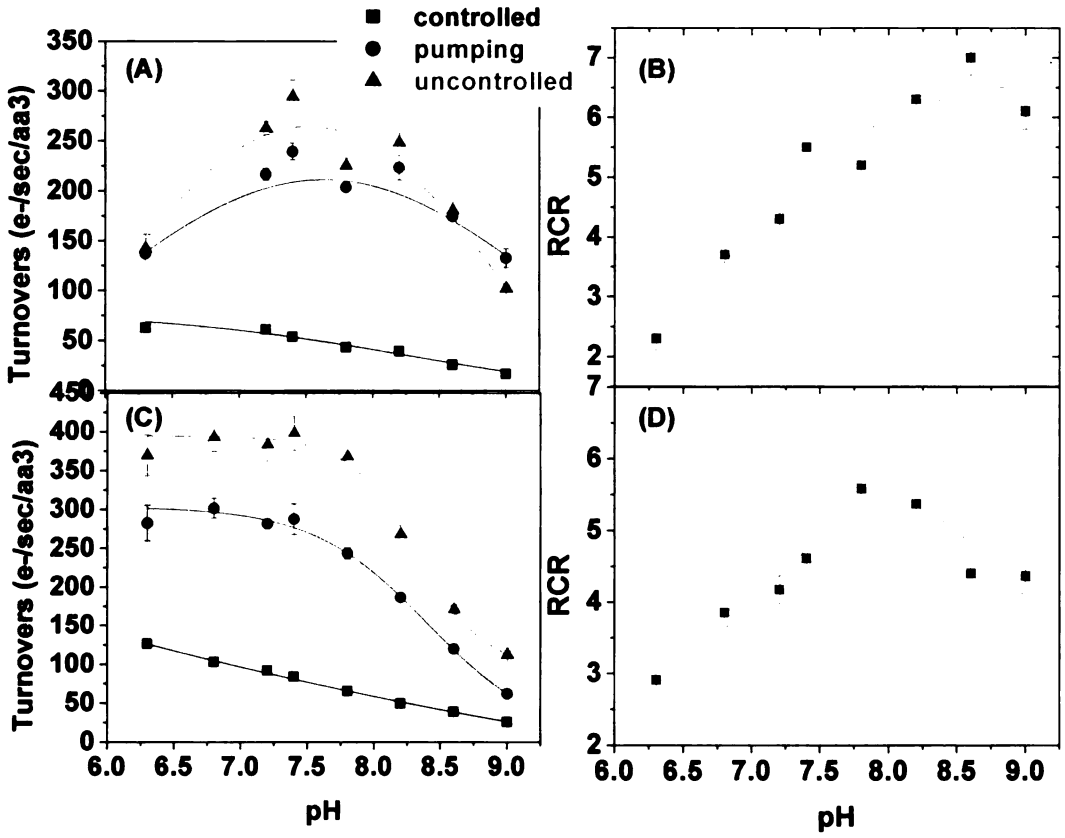

Figure 2. 22 pH dependent activity and measurement of the RCR with Biobead COVs (A,B) or cholate-dialysis COVs (C,D).
The size of the COVs in the Bio-bead method was almost three times bigger than the cholate-dialysis COVs. However, there was little difference between the small and large sized COVs in the stopped flow measurements, except at the high pH range.

The effect of pH on activity of COVs prepared by different methods

Three different buffer systems (MES, HEPES, and CHES) were prepared for measuring the activity of COVs under different pH conditions (Figure 2.21). The pH dependent activity and RCR of the Bio-bead COVs (Figure 2.22 A,B) was compared with that of the cholate-dialysis COVs (Figure 2.22 C,D) with these buffers. It has been reported that COVs made by the Bio-bead method have lowered RCRs (about 3~4) when they are measured with the Gilson Oxygraph under steady-state conditions. However, there was little difference between the small vesicles (cholate-dialysis COVs) and the large vesicles (Bio-beads COVs) in stopped-flow measurements, except at the high pH range.

2.4. Discussion

Difficulties in pH measurement on the inside of COVs

High buffering of vesicles on the inside makes it difficult to observe pH changes; however, it can be problematical to have very low buffering on the inside of reconstituted vesicles since protons must be available to be pumped. Further, it has been found that the apparent pKa of a pH sensitive dye can be shifted inside the vesicles. For example, phenol red has a pKa of 7.5 in solution, however, when loaded into liposomes the pKa appears to increase by approximately 1 pH unit (Faxen and Brzezinski, 2007). The concentration of a pH probe entrapped in the vesicles is usually very small due to the small volume. Moreover, the probe can be diluted during the preparation, especially with several steps of dialysis. This will give weak absorbance signals upon pH changes during the reaction. A new vesicle preparation was used to increase the signal to noise level of

COVs by increasing the vesicle size and volume by using Bio-beads. The larger volume of the COVs made from using Bio-beads increased the concentration of the entrapped dye. Purification steps with Ni^{2+}-NTA resin, using a subunit II histidine-tagged C*c*O, reduced the population of mis-oriented COVs in which the cytochrome *c* binding site faces the inward direction. Furthermore, it reduces the number of void vesicles, which do not contain oxidase. These vesicles otherwise interfere with the accurate measurements, contributing to a background signal because of the light scattering and artifactual pH changes and buffering

Internal Volume Estimation of COVs

A previous study of Ni-NTA purified, cholate-dialysis vesicles (Hiser *et al.*, 2001) showed up to 50% recovery of oxidase, but a 10-fold decrease in oxidase to lipid ratio, suggesting a 10-fold decrease in the proportion of empty vesicles and therefore resulting in the background effect. Bio-beads increase the vesicle diameter by about three fold. Purified vesicles by Ni-NTA showed a 25% recovery yield of the oxidase containing C*O*Vs, which is measured by the V_{max} of both purified and flow-through vesicles, with expected reduction in empty vesicles. From the TEM (transmisstion electron microscopy) measurements, a 75nm average diameter of the vesicles was determined. The internal volume of a single vesicle made by the Bio-bead method was estimated at 1.4×10^{-16} mL, which can hold 1,730 molecules of pyranine dye (assuming 20mM final concentration) (Figure 2.12). The total number of vesicles in cell (80µl, Olis stopped-flow) was estimated from the concentration of C*c*O in the membrane, because each

vesicle may contain 1 or 2 CcO when it is purified by Ni-NTA. Freeze fracture electron microscopy shows a reasonably comparable diameter size to our COVs and supports this estimation (Madden et al., 1984).

The use of pH probe, pyranine, and its advantages in absorbance measurement over fluorescence

Using absorbance as an assay method has the advantage of easier quantitation than fluorescence. Pyranine has a high molar extinction coefficient and the change in absorbance can be predicted from Beer's Law, which is independent of the spectrometer on which the measurement is made. However, fluorescence has the advantage of much greater sensitivity, although quantitation of the signal is much more difficult. The limitation to using fluorescence under our conditions is attributed to complications of cytochrome *c* absorbance interfering with the fluorescence signal in a non-linear way. Pyranine, as a pH probe, has the advantage of high polarity due to three sulfonate groups, which makes it suitable for entrapment in lipid vesicles. The use of pyranine in the study of kinetics and the stoichiometry of protons/electron has been investigated for light-induced proton release and uptake of the bacteriorhodopsin (Grzesiek 1986 FEBS letters). The absorption changes of pyranine have also been used for proton kinetics in bacteriorhodopsin (Dioumaev et al., 1998). The studies reported in this chapter showed some success in the utilizing pyranine for internal pH measurements in cytochrome oxidase vesicles. Nevertheless, the results of these studies, aimed at optimizing conditions for its use in cytochrome oxidase pumping measurements, raised many issues

regarding the challenge for the achievement of high signal to noise which will be explored further in Chapter 3.

Chapter 3 Application and Analysis of Internal and External pH Changes in Reconstituted *Cc*O Vesicles to Understand Proton Pathways

3.1. Introduction

To understand the role of proton pathways during turnover, proton movement from both the inside and the outside has to be measured and quantified in order to calculate the rate and extent of proton translocation. Previous attempts to quantify internal and external proton movements have been made under single turnover conditions (Faxen and Brzezinski, 2007; Faxen *et al.*, 2005). However, a more physiological condition involves many turnovers ($\geq$ 10 TN), where there is the build up of a membrane potential, which is one of the controlling factors of *Cc*O activity, as is observed in mitochondria.

No research has yet been done to measure proton movement, from the inside and the outside, and electron transfer at the same time with multiple turnovers, due to technical difficulties, such as shifts in the pKa of entrapped dyes, or scattering caused by the small vesicles. The single turnover experiments performed on COVs with phenol red entrapped inside by Faxen *et al.* (Faxen and Brzezinski, 2007) gave some interesting data, but different COVs had to be prepared to measure outside pH changes. In this chapter, I describe the results of using the two dye method with vesicles of a larger size prepared by the Bio-bead procedure, followed by a purification step using a Ni^{2+}-NTA column. By improving the vesicle preparation conditions, we obtained larger vesicles, allowing more of the pH dye to be trapped on the inside, reducing the background noise and the

scattering effects, which may be a key limitation of obtaining good signal-to-noise ratios. While some technical problems remain, the results provide new insight concerning proton pumping and its regulation.

3.2. Results

3.2.1. Raw Data Analysis of The Wild Type COV Measurements

The stopped-flow technique allows catalytic turnover (cytochrome *c* oxidation), proton uptake, and proton release to be measured in a millisecond time scale on both the inside and outside of COVs, with different optical signals for each. Under the conditions used, full oxidation of cytochrome *c* was accomplished in a few seconds. In the stopped-flow, the full spectrum of absorbance changes over 365nm to 595nm are recorded in 1 ms, which includes the signals from pyranine, phenol red and cytochrome *c*. These are stored digitally, and processed, in order to get precise starting points of the reactions which can be obscured by mixing artifacts. Cytochrome *c* can be monitored at its maximum absorbance at 550nm, showing a decrease in absorbance over time as it becomes oxidized. The Olis stopped-flow is used to measure turnover in milliseconds to seconds. This data can be easily converted to electrons consumed per C*c*O/sec. The absorption coefficient of 17,000 $M^{-1}cm^{-1}$ at 550nm was used for C*c* with a band path of 0.4 cm for the OLIS-rsm, and a 1cm band path for the Applied Photophysics stopped-flow cell. The absorption signal changes that occur during the first few millisecond of mixing, but do not correspond to actual electron transfer from cytochrome *c*, are considered to be mixing

artifacts (Figure 3.1 A,B,C). To find the starting point of zero time absorption for each of the dyes the signals of either cytochrome *c* and pyranine, or cytochrome *c* and phenol red were plotted against each other and then fitted by a linear regression method in the OriginPro data processing program (Figure 3.1 D,E,F,G,H,and I). Isosbestic points were selected for each dye to eliminate interference by cytochrome *c* during the catalytic cycle. The wavelengths of 435nm, for the pyranine signal, 557nm for the phenol red changes, and 550nm for the cytochrome *c* are used. The data was aligned after processing the artifacts of the zero time signal by this method (Figure 3.2). The conditions for measurement of activity of COVs were previously described (Section 2.2.2)(Figure 2.6 in Chapter 2). The data shown in Figure 3.2 A,B,C supports the idea that proton backflow through the C*c*O is a large contributor to the controlled activity as well as proton uptake from the inside, as indicated by the increased absorbance at 557nm (alkalinization on the outside, Figure 3.2 B) and increased absorbance at 435nm (alkalinization on the inside, Figure 3.2 C).

Zinc is an inhibitor of C*c*O, both in the purified enzyme and the reconstituted COVs (Figure 3.2 D,E,F), and especially in the controlled state, where both a high membrane potential and proton gradient are maintained. Zinc inhibited the rates of proton backflow (alkalinization on the outside, Figure 3.2 E) as well as uptake from the inside (Figure 3.2 F) as expected for the inhibition of cytochrome *c* oxidation (Table 3.1), particularly in the controlled state. We will discuss the possible role of zinc in terms of its affect on the backflow of protons in COVs, in Section 3.2.3.

Figure 3.1 Data processing for zero time staring absorbance points
To obtain a more reliable zero time absorbance point, original data sets, for cytochrome *c* oxidation (A), and phenol red (B) or pyranine (C) from the Olis stopped-flow measurements, were processed by using a correlation curve fitting method which plots the absorbance changes of cytochrome *c* against pyranine (D,E&F) or phenol red (G,H&I) over the same reaction period. The absorption signals, which did not correlate with the electron consumption measured at 550nm, were considered to be mixing artifacts. Correlation curves were fitted by OriginPro, using a linear regression method. The isosbestic wavelength of cytochrome *c* at 435nm was selected in order to monitor changes in pyranine absorbance on the inside of the COVs. A wavelength of 557nm, isosbestic for cytochrome *c*, was selected for phenol red absorbance changes on the outside.

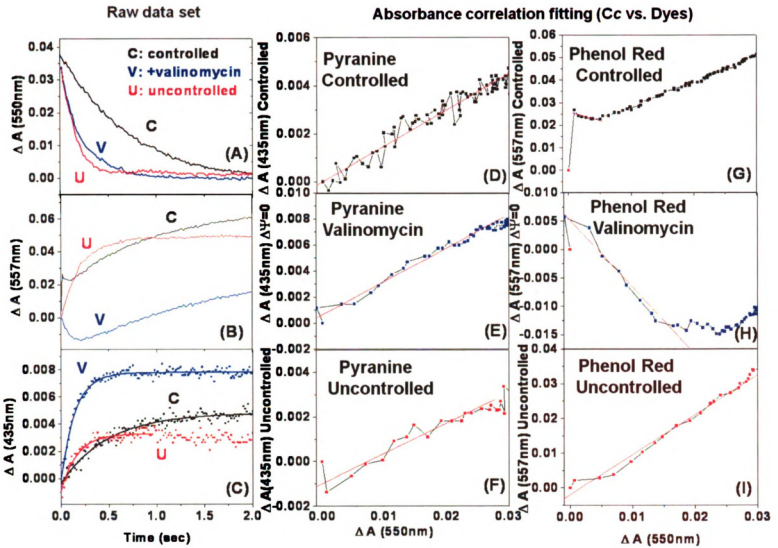
Raw data set
Absorbance correlation fitting (Cc vs. Dyes)
C: controlled
V: +valinomycin
U: uncontrolled
Δ A (550nm)
Δ A (557nm)
Δ A (435nm)
Time (sec)
(A)
(B)
(C)
Pyranine Controlled
Pyranine Valinomycin
Pyranine Uncontrolled
Phenol Red Controlled
Phenol Red Valinomycin
Phenol Red Uncontrolled
Δ A (435nm) Controlled
Δ A (435nm) ΔΨ=0
Δ A(435nm) Uncontrolled
Δ A (557nm) Controlled
Δ A (557nm) ΔΨ=0
Δ A (557nm) Uncontrolled
Δ A (550nm)
(D)
(E)
(F)
(G)
(H)
(I)

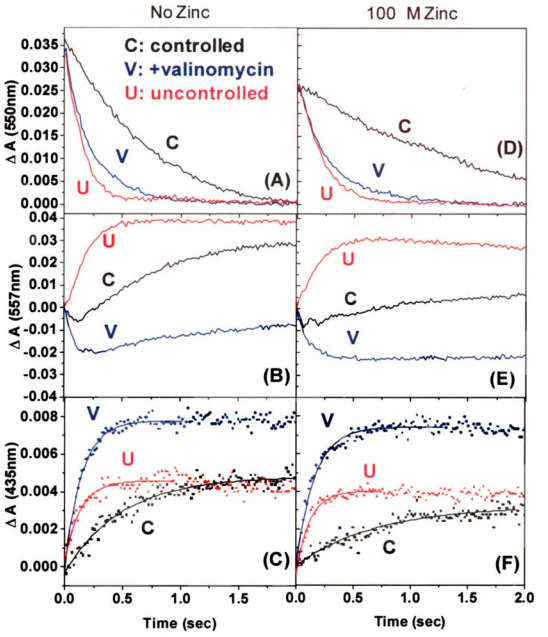

Figure 3.2 A processed data set with the artifacts eliminated from the signals by using a correlation plot.

Controlled state (black line), pumping state with 2μM valinomycin (blue), and uncontrolled state with valinomycin + 1μM FCCP (red) (A,B&C) were compared to the normal condition without zinc on the outside. The inhibition of COV activity was observed in the presence of 100μM zinc (D,E&F).

	Controlled	≡valinomycin	Uncontrolled	RCR
WT	76±0.4	217±2.8	313±5.5	4.1
WT+Zinc	39±0.4	166±2.2	238±2.9	6.1

Table 3.1 Measurement of CcO activity in COVs prepared by the Bio-bead method. Measurement of C*c*O activity in COVs prepared by the Bio-bead method in 20mM HEPES-KOH + 39mM KCl +52mM sucrose, pH7.4 on the inside. COVs (0.1 μM aa_3 final concentration) were mixed in the Olis-rsm stopped-flow instrument with 5μM cytochrome c^{2+} in 50μM HEPES-KOH + 45mM KCl, pH7.4 in the absence and presence of 100μM zinc with wild type COVs. Rates of oxidation were calculated from the kinetic traces at 550nm with an average of three data sets for each condition (Figure 3.2).

3.2.2. Quantitative Analysis of Data from Stopped-Flow

Proton pumping efficiency (H^+_{pumped} /e^-) can be calculated from the turnover ***rate***, which is measured by the cytochrome *c* oxidation rate (electron consumption rate) and the ***rate*** of proton release on the outside (pumped protons) in order to obtain the stoichiometry, or by the ***amount*** of protons released compared to the amount of electrons consumed. The rate or amount of proton release to the outside is measured at an absorbance of 557nm with the phenol red dye on the outside. At this isosbestic wavelength, the absorbance of cytochrome *c* does not change during the catalytic reaction. In order to calculate the H^+/e^- stoichiometry using phenol red as the pH probe, the amplitude of acidification of phenol red on the outside with valinomycin added, is divided by the amplitude of the alkalinization observed at the same wavelength when FCCP (carbonyl cyanide 4-(trifluoromethoxy) phenlyhydrazine) is added. FCCP allows the protons to equilibrate across the membrane so that no pumping is observed, only the net consumption of protons, seen as an alkalinization of the outside. The number of protons consumed on the inside for the oxygen chemistry corresponds to a $1H^+/e^-$ stoichiometry, providing an internal standard. The phenol red absorbance amplitudes with wild-type C*c*O often show 1, or less than 1 H^+/e^-, during proton pumping (Figure 3.2 B / Table 3.2 Top). However, when the rates of pumping, instead of amplitudes, are analyzed during the time- frame of the electron consumption (Figure 3.3 and Table 3.2 bottom) a 1:1 stoichiometry (H^+/e^-) of pumping is observed.

Quantification of the amount of protons taken up from the inside of the vesicles during the catalytic reaction was attempted, using the same internal standard conditions as were used with phenol red. In the uncontrolled condition, with both FCCP and valinomycin present, there is complete equilibrium of the proton concentration between the inside and the outside. Assuming a $1H^+/e^-$ stoichiometry under these conditions, the internal proton changes can be quantified based on their absorption amplitude change (Figure 3.3). In this way, the semi-quantitative analysis of coupling between proton movement and electron consumption was obtained (Table 3.2 top). The calculated values were reasonable except the controlled state, where the sum of the protons consumed on both sides of the membrane is apparently much greater than the expected 1 H^+/e^-, as if the two compartments were in equilibrium (see Discussion).

An alternative method of quantification has been developed in order to obtain a more accurate estimation of the relationship of the initial proton and electron coupling during the catalytic reaction, by comparing ***rates*** of electron consumption (cytochrome *c* oxidation) with ***rates*** of proton-linked absorbance changes on both the inside and outside of COVs (Figure 3.3 D, E and F). The rate of electron consumption during the reaction (e^-/sec, from the absorbance changes of cytochrome *c* measured at 550nm) was plotted against the rate of proton consumption (H^+/sec) as measured by absorbance changes calibrated to the uncontrolled condition as described above. The slope of the plotted graph gives the stoichiometry between protons and electrons (H^+/e^-) consumed during catalytic turnovers (Figure 3.3 D,E,F /Table 3.2).

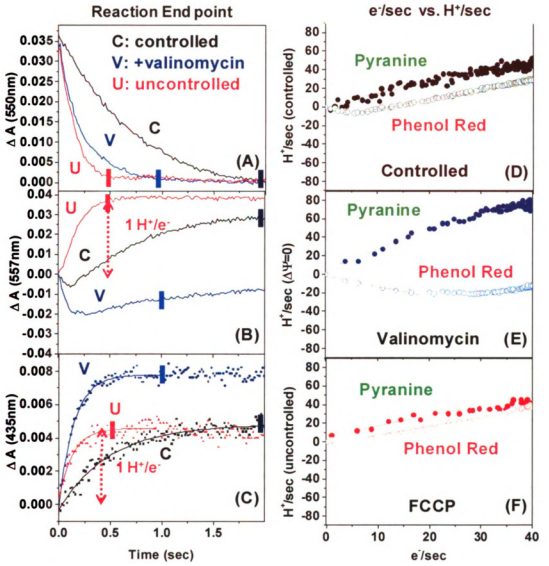

Figure 3.3 Semi-quantitative analyses of data from the Olis-rsm stopped-flow measurements.

The stoichiometry (H^+/e^-) is a measure of the efficiency of reconstituted C*c*O in the vesicles and was obtained from the internal standard condition, the uncontrolled state. The endpoint of the reaction in each state was set to 40 electrons consumed as determined from the cytochrome *c* complete oxidation. That endpoint in the uncontrolled reaction, gives the absolute change in pyranine and phenol red that represents $1H^+/e^-$ consumed. The rate of electron consumption (e^-/sec) can be measured from the 550nm absorbance and used as alternative way of quantification, by plotting this against H^+/sec, measured by absorbance changes of the pH sensitive dyes. The slopes from the correlation plots were used to obtain the stoichiometry, which shows the initial reaction during the catalytic turnover.

End point of reaction (A,B and C of Figure3.3)			
	INSIDE (Pyranine)	OUTSIDE (Phenol Red)	
	uptake	pumping	backflow
Controlled	-1.0	+0.2	-1.0
Controlled + zinc	-0.9	+0.2	-0.4
+Valinomycin	-2.0	+0.5	-0.2
+ Valinomycin + zinc	-2.0	+0.7	0
Uncontrolled (w/ or w/o zinc)	-1.0	N/D	-1.0
e^-/sec vs. H^+/sec (D, E and F of Figure 3.3)			
Controlled	-1.1±0.1	N/D	-1.1±0.1
Controlled + zinc	-1.2±0.1	N/D	-0.5±0.1
+Valinomycin	-2.2±0.2	+1.0±0.1	N/D
+ Valinomycin + zinc	-2.5±0.2	+1.1±0.1	N/D
Uncontrolled	-0.86±0.1	N/D	-0.8±0.1
Uncontrolled + zinc	-1.5±0.1	N/D	-1.1±0.1

Table 3.2 The stoichiometry table of H^+/e^- during turnover showing proton uptake, proton backflow and proton pumping with or without zinc.
First, the amplitude at the endpoint of the fitted reaction in the uncontrolled state (Figure 3.3 B & C) was used as a standard ($1H^+/e^-$) for comparison with the other fitted conditions, controlled and + valinomycin. Alternatively, the direct electron consumption rate (e^-/sec) was used with the corresponding proton consumption rate (H^+/sec). The slopes of the correlation plots (Figure 3.3 D,E & F) were obtained and produced the reaction stoichiometry (H^+/e^-) during turnover. Red color indicates the loss of protons either on the inside or the outside. Blue color indicates the gain of protons on the outside. N/D = not determined

The linear fitting range was restricted to the first 5 turnovers, in order to prevent a limitation due to possible insufficient proton supply from the vesicle interior. For example, in the pumping condition with valinomycin ($\Delta\Psi$=0), the stoichiometry (H^+/e^-), which was obtained from the slope in the data analysis, was no longer linear after 5 turnovers (half of the reaction). Under active pumping, twice the amount of protons was taken up from the interior, for oxygen reduction and for proton pumping. The one:one relationship of H^+/e^- was restored by addition of FCCP, allowing the protons to be fully equilibrated across the membrane.

Interestingly, it was observed that there was both a biphasic fast and slow proton consumption rate in the controlled condition during the initial part of the reaction (Figure 3.3 B and D). This transition point corresponded to the first turnover in the reaction (4 electrons, 4 protons and one molecule of O_2 were consumed per C*c*O). This suggests that protons could be pumped to the outside in the initial phase of the controlled state before a membrane potential was established during a single turnover (Figure 3.4). Therefore, the stoichiometry of H^+/e^- in the controlled state (with a membrane potential) was calculated from the data fitting after 1 full turnover.

A significant amount of backflow of protons from the outside to the inside, observed as alkalinization on the outside, was measured in the semi-quantitative analyses in the controlled state (Table 3.2). This proton backflow was inhibited by the addition of zinc on the outside of COVs, especially in the controlled condition, in the absence of ionophores. This result was consistent with a previous report indicating the existence of proton backflow under a high membrane potential and proton gradient (Mills et al., 2002)

which resulted in ~50% inhibition of activity in the presence of zinc. The proton backflow on the outside, during proton pumping, is difficult to measure because the proton backflow competes with the proton pumping (proton release on the outside) during turnover. The stoichiometry of proton pumping was variable, from 0.5 H^+/e^- to $1H^+/e^-$. In the presence of zinc, the proton pumping stoichiometry seemed to increase (from 0.5 to 0.7 or from 1.0 to 1.1), possibly because the binding of zinc inhibits the backflow pathway leading to an apparent increase in net pumping.

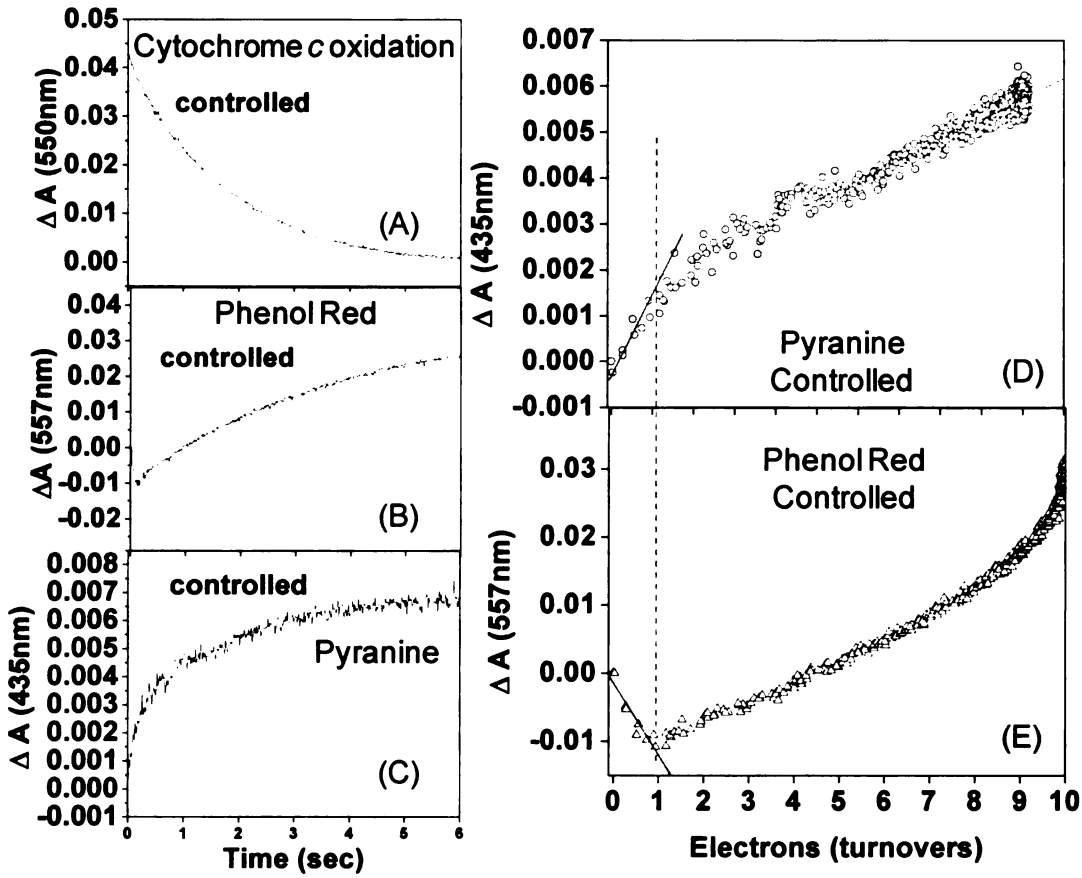

Figure 3. 4 Correlation of the controlled state proton movements from the inside and outside of COVs with pyranine (top panel) or phenol red (bottom panel). The biphasic fast and slow proton consumption rates were observed from the inside after 1 turnover (A) blue dashed line. Proton pumping was observed until the reaction reached 1 turnover before the membrane potential was built up at ~ 1 turnover (B). This graph was obtained from a different set of results which shows a slower oxidation rate of cytochrome *c*. As the reaction slowed, the rate of the transition due to the membrane potential was shown more clearly.

3.2.3. Exit/ Backflow Study of *Cc*O with Zinc

Cytochrome *c* oxidase (C*c*O) transfers protons from the inner surface of the enzyme to the O_2 reduction site through two different proton pathways, the K and D paths. These pathways can be inhibited by metals such as zinc, cadmium, or nickel. Recent studies on purified *Rhodobacter sphaeroides* C*c*O show both high and low affinity binding sites for Zn^{2+} (Aagaard and Brzezinski, 2001), which result in inhibition of intermediate reaction steps in cytochrome *c* oxidase that are associated with proton pumping, suggesting that the zinc inhibits proton uptake through the D-pathway where several carboxylates and histidine residues are found that may co-ordinate Zn^{2+}.

Recently, a high resolution structure of C*c*O, with cadmium added, revealed metal binding sites on proton donor/acceptors at the entrance of the K-pathway (Qin *et al.*, 2007). A mutant of C*c*O that lacks glutamate (E101) and histidine (H96) eliminated metal binding at this site. An additional zinc inhibition site is observed in the reconstituted C*c*O vesicles, in which addition of zinc to the outside surface causes inhibition with high affinity (KI $\leq$ 5μM) in the presence of a membrane potential (Mills *et al.*, 2002). Finding the location of potential metal binding sites is difficult because it appears that two of the metal coordinating ligands, such as histidine or carboxyl residues, must both be eliminated to prevent zinc binding. The subunit III-depleted double mutant, H96A/E101A in the K-pathway, which has altered both D (by subunit III removal) and K pathways, is not inhibited by zinc when added to the purified enzyme, but it is still inhibited by the addition of zinc to the outside of theCOVs (Figure 3.5). This result

substantiates the conclusion that there is a zinc-binding site on the external surface (P side) of the oxidase that is strongly inhibitory in the presence of a membrane potential ($\Delta\Psi$, negative inside) and a pH gradient.

When micromolar concentrations of zinc inhibit the enzyme activity in reconstituted vesicles, a dramatic increase in the respiratory control ratio (RCR) is often observed due to differential inhibition of the controlled state. The fact that a low concentration of zinc inhibits the controlled rate of COVs under a high membrane potential gradient provides evidence for a specific proton backflow pathway leading to the active site from the outer surface (Mills and Ferguson-Miller, 2002a). It may be that this zinc-inhibited backflow of protons occurs by reversal of the normal exit pathway for the proton pump, or by an independent pathway. The results shown here with the wild-type enzyme (Figure 3.2) are a good example of the zinc inhibition effect. Zinc binding efficiently inhibited the rate of proton backflow, seen as a slower rate of alkalinization on the outside (Figure 3.2E, controlled) along with the inhibited rate of proton uptake from the inside (Figure 3.2 F, controlled). The binding of zinc to the outside showed a significant inhibition of activity, but only in the controlled state, supporting the role of zinc as an inhibitor of the backflow pathway.

Other mutants (E101A, R481K, R481K/D132A) with the ability to affect the proton backflow pathway were studied by reconstitution of C*c*O into COVs by the Biobead method and with further purification. However, none of these were able to produce adequate data in the stopped flow pH analysis. The reason for this is uncertain, but may be due to the low activity of most of the mutant COVs used.

Figure 3. 5 The effect of zinc binding on the outside of COVs.

Measurement of COV activity prepared by the cholate dialysis method in 50mM HEPES-KOH + 24mM KCl, pH7.4. COVs (0.1 μM aa_3 final concentration) were mixed in the Olis-rsm stopped-flow instrument with 5 μM cytochrome c^{2+} in 50μM HEPES-KOH + 45mM KCl, pH7.4 in the absence and presence of 100μM zinc with wild type COVs and H96A/E101A sub III (-) COVs. The internal zinc binding site was eliminated by a double mutation in the absence of subunit III. When the mutant was reconstituted, zinc inhibition was observed by the binding of zinc on the surface of COVs, especially under a high membrane potential (controlled state shown, black line).

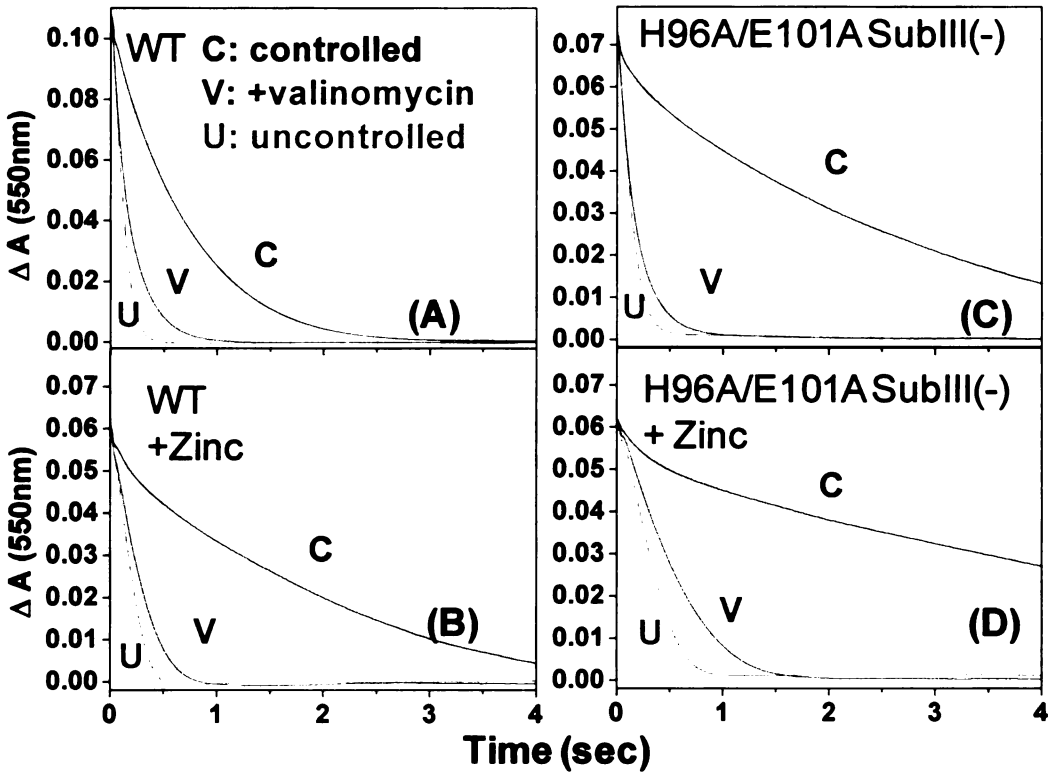

	Activity(e^-/sec/aa_3)		
	Controlled	uncontrolled	RCR
Wild Type	93.8 (±0.3)	428.9 (±4.7)	4.6
WT + Zinc	16.3 (±0.1)	246.7 (±2.3)	15.1
H96A/E101A SubIII (-)	18.3 (±0.1)	111.2 (±1.7)	6.1
H96A/E101A SubIII (-) + Zinc	4.4 (±0.01)	74.1 (±1.8)	16.8

Figure 3. 6 The inhibition of proton uptake by the D132A mutation allows the backflow of protons to contribute significantly to the observed rate under controlled conditions.

COVs (0.1 μM aa_3 final concentration) were rapidly mixed in the Olis-rsm stopped-flow instrument with 4 μM cytochrome c^{2+} in 50μM HEPES-KOH + 45mM KCl, pH7.4 (A) Under the conditions where there is a high membrane potential across the membrane, the controlled state oxidation rate gave the fastest reaction. (B) Protons were supplied from the outside, (8.4 ± 0.1 e^-/sec/aa_3) showing a rapid alkalinization, which corresponded to the increased activity in the controlled state. (C) COVs reconstituted by the Bio-bead method did not give a strong signal-to-noise ratio on the inside with pyranine when the reaction was very slow, due to the D132A mutation in the proton uptake pathway. When further inhibited by 100μM zinc (D), (E), (F), the controlled rate was slowed significantly, and there was some slight evidence of proton pumping, indicating competition between backflow and pumping.

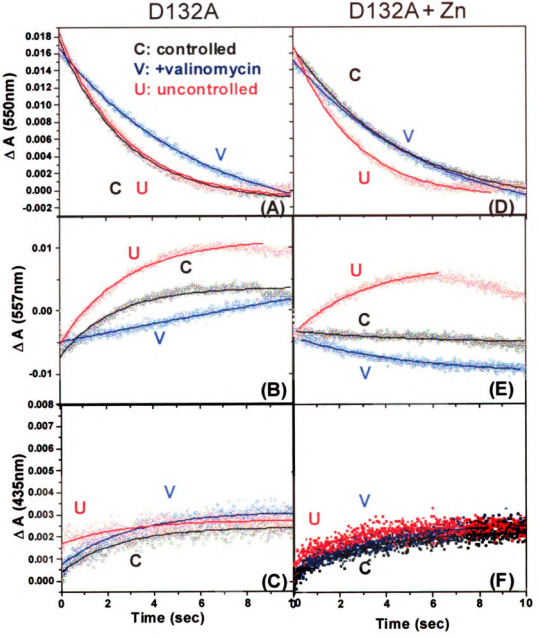
D132A
D132A+Zn
C: controlled
V: +valinomycin
U: uncontrolled
ΔA (550nm)
ΔA (557nm)
ΔA (435nm)
(A)
(B)
(C)
(D)
(E)
(F)
Time (sec)
Time (sec)

3.2.4. Further Study of Backflow with D132A Mutant.

The hydrogen-bonded water chain of the D-pathway begins at D132 on the inner surface of C*c*O. Site directed mutants of D132 in C*c*O that remove a carboxylate residue from this position strongly inhibit activity (<2% of WT) and proton pumping (Fetter *et al.*, 1995). The existence of proton backflow from the outer surface was initially postulated on the basis of studies on the D132A mutant (Fetter *et al.*, 1996), because the O_2 reduction activity of this mutant is accelerated, rather than inhibited, by a membrane potential. In the wild-type enzyme, where there is rapid uptake of protons via the D-path from the inside, a positive-outside membrane potential inhibits the reaction. However, in the D132 mutant where the D-path is blocked, proton backflow supports the reaction and is driven by the potential gradient (positive outside) across the membrane (Mills and Ferguson-Miller, 1998; Zhen *et al.*, 1999b). Proton backflow was confirmed by measurement of alkalinization on the outside of D132A vesicles upon initiation of turnover (Figure 3.6). It appears that when proton uptake from the inside is compromised, protons taken up from the outside become important to maintain the very slow activity, especially under the conditions of a high membrane potential. The controlled state oxidation rate (8.4 ±0.1 e^-/sec/aa_3) was faster than the rate in the presence of valinomycin, where the driving force was removed. Similar proton uptake from the outside is seen to occur in wild type C*c*O reconstituted into vesicles under a high membrane potential ($\Delta\Psi$), where the uptake from the inside is inhibited by the potential gradient, resulting in no net proton pumping in the controlled state (Figure 3.2 black trace in B). In the presence of zinc, D132A showed decreased activity as observed for wild type, due to the blockage of

backflow from the outer surface of C*c*O. We do not completely understand how these proton pathways, including the uptake, exit and backflow proton pathway, are connected during the turnover and how many protons are used from each pathway during the reaction. We hoped to better understand the role of these pathways by using site-directed mutants of C*c*O, like D132A and by being able to quantify both inside and outside pH changes. However, the inside signal changes of pyranine absorbance were very noisy, preventing the accurate quantification of the proton uptake on the inside.

Another interesting feature of the D132A mutant is the ability of micromolar concentrations of arachidonic acid (Aa) to rescue the mutant's activity, presumably by supplying a carboxylate group in the vicinity of the D-pathway (Fetter *et al.*, 1996). In the reconstituted enzyme both BSA and arachidonic acid need to be added to prevent excess fatty acid from making the vesicles leaky. These conditions restore even more activity (Mills *et al.*, 2003), but proton pumping was not observed in the previous analysis. However, when the COVs were made by the Bio-bead method, proton pumping was observed in the presence of BSA/Arachidonic acid (Figure 3.7). This is an interesting observation that is not completely unexpected. Proton pumping could be expected when a proton supply from the inside has been repaired by an alternative proton donor (Aa). The D132 mutation is located where arachidonic acid may replace the impaired residue.

Figure 3. 7 The rescued activity of D132A by addition of arachidonic acid.
The slow rate of activity, monitored by cytochrome *c* oxidation of D132A, was rescued by addition of the arachidonic acid (Aa) in the presence of bovine serum albumin (BSA) which acted as a buffer for the Aa to prevent it from making the membrane leaky. A 600μM BSA stock was prepared in water and a 250mM Aa stock was prepared in ethanol. The stopped-flow measurements were the same as in Figure 3.6. Controlled state, $\Delta\Psi=0$ in the presence of valinomycin and uncontrolled state with FCCP was shown in black, blue and red, respectively. The controlled activity (A) was increased from 8.4±0.1 e^-/sec/aa_3 to 17±0.3 e^-/sec/aa_3 in the presence of 6μM of BSA and 140μM of Aa. (B) Phenol red absorbance shows a lack of significant proton pumping for D132A (C). Pyranine on the inside showed some alkalinization for all 3 states. In the presence of BSA/ Aa (D) normal RCR was observed, with the controlled rate being the slowest and the uncontrolled state was the fastest. (E) A normal proton pumping (~$1H^+/e^-$) was observed. (F) Pyranine on the inside showed alkalinization as expected if protons are taken up from the inside for pumping and oxygen chemistry.

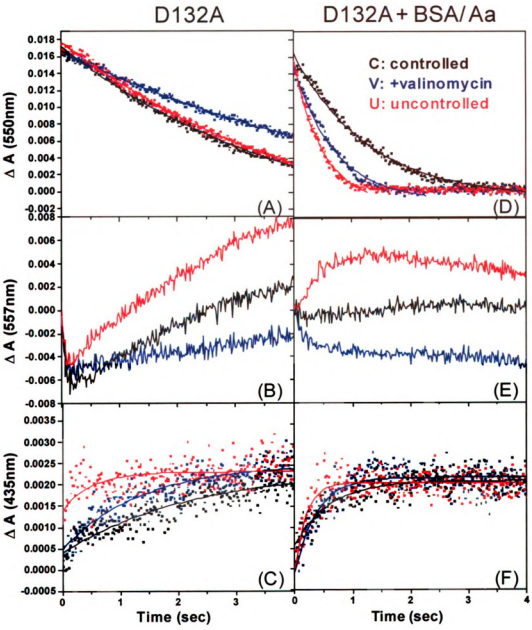
D132A
D132A + BSA/Aa
C: controlled
V: +valinomycin
U: uncontrolled
Δ A (550nm)
Δ A (557nm)
Δ A (435nm)
(A)
(B)
(C)
(D)
(E)
(F)
Time (sec)
Time (sec)

3.3. Discussion

3.3.1. Problems in Current Analysis

The aim of these studies was to measure changes in internal and external pH that could be quantified and correlated with the electron consumption in reconstituted vesicles of C*c*O. This aim was not completely achieved, mainly because of the low signal-to-noise and other apparent artifacts associated with measuring pH change on the interior of these small vesicles.

A buffering system with 20mM HEPES buffer at pH 7.4 was needed to supply enough protons to maintain proton pumping. However, the internal buffering conditions may also lead to low signal. The proton pumping stoichiometry appeared to be more accurately measured by using the rate of electron consumption (e^-/sec) compared to the corresponding rates of proton change (H^+/sec). Since it was hard to estimate the correct zero point of the reaction and to know what artifacts might affect the internal dye, the amplitudes of the absorbance changes appeared less accurate. One of the more puzzling observations that was reproducible, was that the total number of proton consumed from both the inside and outside of COVs in the controlled state, greatly exceeded (2x) the total expected number. This result implied that under the conditions of a high membrane potential, the pyranine dye behaves in an anomalous way.

Some interesting observations have been made, however, even if they are only qualitative. The inhibitor, zinc, clearly inhibited proton backflow under a variety of

conditions. Also, the D132A mutant, in the presence of arachidonic acid and BSA, restored proton pumping, which was not previously observed.

3.3.2. Further Analysis of Possibilities by Global Fitting and Model Studies

Our previous method of analysis, using a single wavelength selected from a complete spectrum range, was limited due to the small changes in absorbance at the appropriate isosobestic points and the problem of high buffering and light-scattering from the small lipid vesicles. However, the data collected in these experiments contains much more information. A complete spectra from 365 to 595nm at a resolution of 1nm with 1ms scan rate was made, so that the data can be used by applying global analysis and modeling approaches. The general principles of the global analysis and simulation study are illustrated in Figure 3.8. The iterative fitting and modification of a simplified model of the reaction kinetics of cytochrome oxidase is used to analyze the data (Figure 3.9). This model allows for the quantitative estimate of the rate constants for uptake and release of protons, as well as proton backflow. This analysis is being carried out in collaboration with Dr. Denis Proshlyakov and Dr. Martyn Sharpe. The global fitting analysis and modeling efforts will allow a more meaningful interpretation of the data sets which is currently available, and produce a testable model for further analysis.

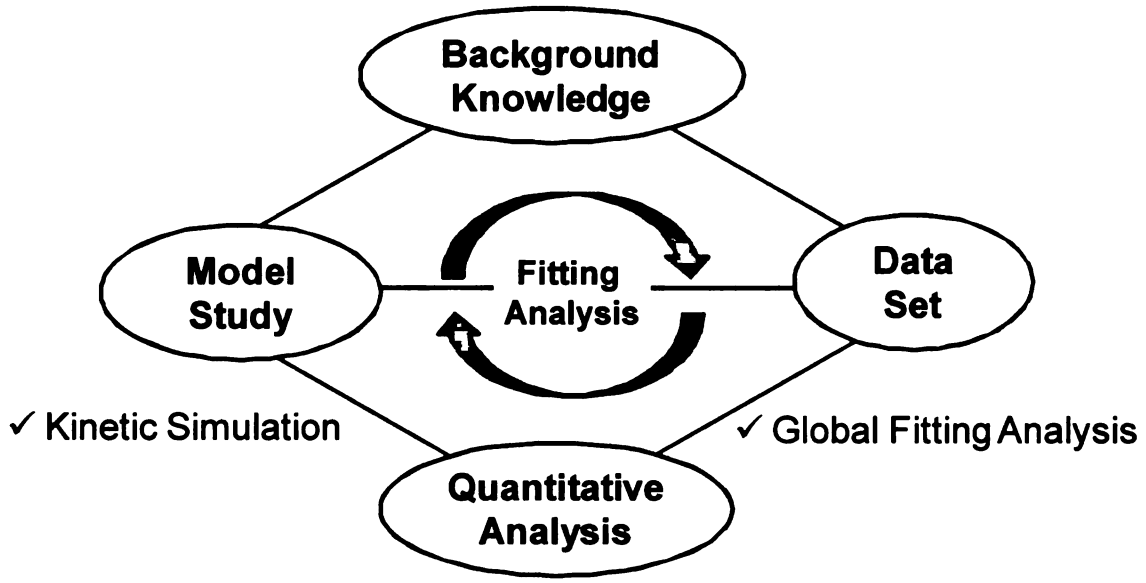

Figure 3. 8 Quantification process
A scheme for verification of the data from the proton pumping measurements. A raw data set is obtained from the kinetic analysis of stopped-flow measurements, including all wavelengths and over time. From this, a quantitative global analysis using IGOR data processing software can be used. A model was proposed from the kinetic simulation of proton movements with the COVs and will be compared to the new data set originally fitted from a raw data set. A new model will be established after modification of the proton pumping mechanism based on the amino acid mutations and zinc inhibition observed in the stopped-flow measurements. This process will be repeated until there is a good agreement between the model and the original measurements.

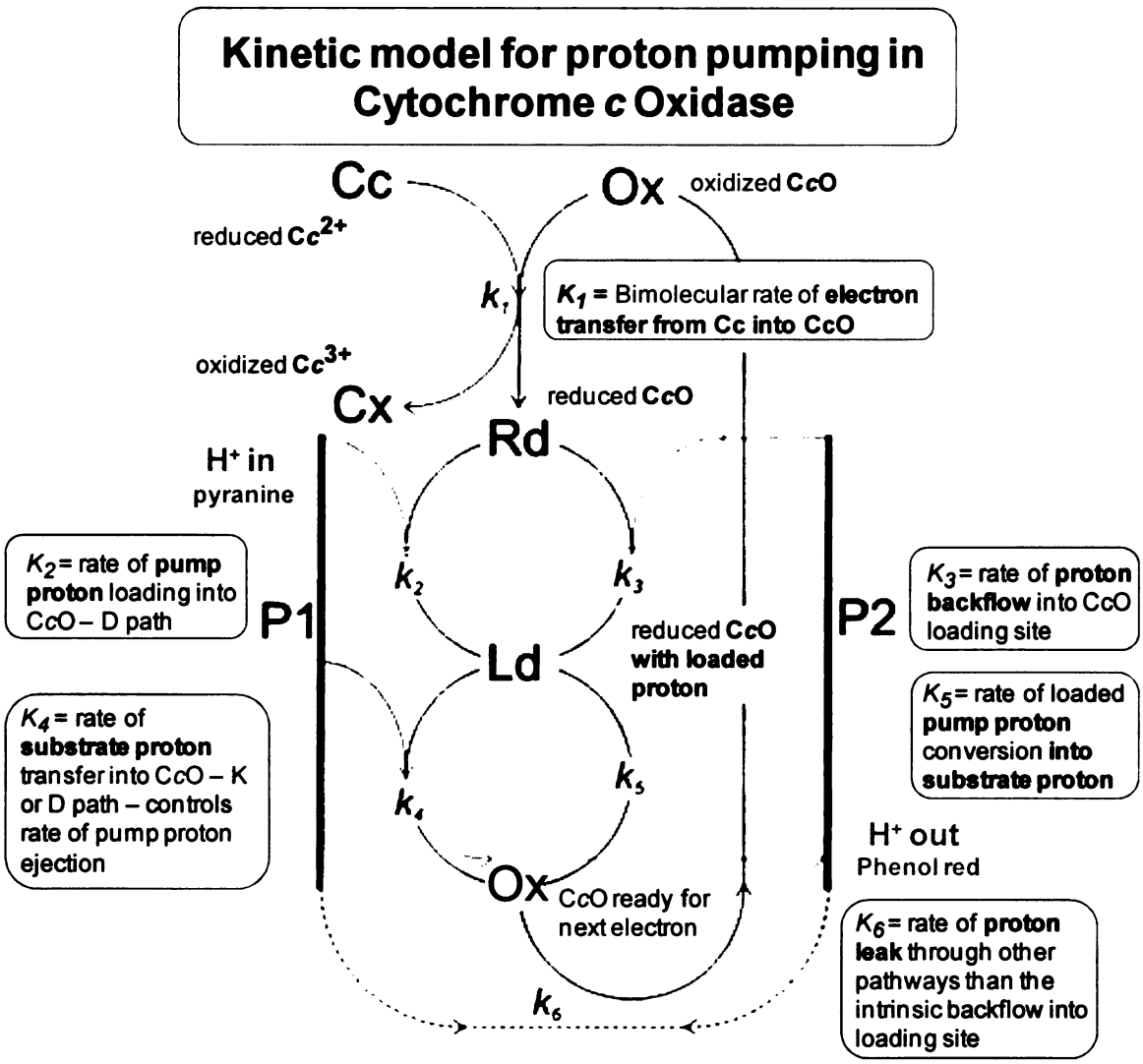

Figure 3. 9 Kinetic model for proton pumping in Cytochrome *c* Oxidase.
A conceptual, mathematical model to understand the proton pumping mechanism has been proposed using a global fitting analysis (IGOR) using multi-wavelengths from OLIS-rsm stopped-flow data. Catalytic turnovers were performed in the presence of 2 different pH probes, both inside and outside of COVs. Cc=reduced cytochrome *c*. Cx=oxidized cytochrome *c*. Ox=oxidized C*c*O. Rd=reduced C*c*O. Ld=reduced C*c*O with loaded proton. P1=Inside of vesicles measured with pyranine. P2=Outside of vesicles measured with phenol red. k_1=bimolecular rate of electron transfer from C*c* into C*c*O. k_2=rate of pump proton loading into C*c*O through the D-pathway. k_3=rate of proton backflow into C*c*O to the loading site. k_4=rate of substrate proton transfer into C*c*O through K or D-pathway, which controls the rate of pumping protons. k_5= rate of loaded pump proton conversion into substrate proton. k_6=rate of proton leak through other pathways than the intrinsic backflow into the loading site. Red traces indicate the proton movements.

Chapter 4 H93 Mutation and Its Putative Role in Proton Backflow Study

4.1. Introduction

In order to understand the control of protons for both pumping, and backflow under a membrane potential, it is important to find where the protons move through the protein. It is thought that the backflow of protons is important in regulation, providing a mechanism to control the proton pumping efficiency in C*c*O. A search for proton exit or backflow routes has utilized EPR techniques (Schmidt *et al.*, 2003) as well as mutation and proton measurements. It is proposed that water molecules produced at the active site move outwards towards the non-redox Mg metal site in subunit I, close to the subunit I/II/III interface. However, the actual path for water, and its relationship to paths for protons, has not been verified due to the difficulty in studying site-directed mutations of key residues in this area, as they are important in maintaining stability of the subunit I-II interface.

Another tool to study proton pathways is the metal ion, zinc. Addition of zinc in micromolar concentrations to the outside of COVs inhibits oxidase activity (Mills *et al.*, 2002), although the actual site of zinc binding remains unknown. The zinc appears to block a proton pathway that may be important in the regulation of proton backfow under conditions of a high membrane potential, allowing O_2 reduction activity to proceed without proton pumping.

In this thesis, a method has been described for measuring pH changes on the inside as well as the outside of reconstituted C*c*O vesicles (COVs). The measurements

are made with a rapid scanning stopped-flow spectrophotometer, which is capable of rapidly (1 scan/msec) recording spectral changes over time and over a large wavelength range. Sensitive pH dyes are used to measure the rates of absorbance (pH) changes during turnover. Considerable efforts were made to establish conditions for measuring internal pH with pyranine at the same time as monitoring phenol red on the outside. The results show that a membrane potential ($\Delta\Psi$) is rapidly built up in the controlled condition, in the absence of ionophores. It is observed that this condition is accompanied by proton back-flow from the outside of COVs, which appears to be used in the oxygen chemistry. Additionally, when proton uptake is inhibited by a mutation in the D-pathway (e.g. D132A), or under a high membrane potential, the remaining low activity is supported by the backflow protons. Nevertheless, few mutants that inhibit the backflow path have been described.

In the bovine C*c*O X-ray crystal structure, it was noticed that there was a structural change in the oxidized compared to the reduced C*c*O involving D51 (bovine numbering) on the outside of subunit I (Shimokata *et al.*, 2007; Yoshikawa *et al.*, 1998). A proton channel called the H-pathway was proposed based on this observation (see Section 1.3.3.3. for details). Although many of the residues that are proposed in the H-channel are not conserved in the bacterial C*c*O (Figure 4.1), D51 has been considered as a possible key exit residue in the proton pumping path of mitochondrial C*c*O, supported by a mutational study of bovine C*c*O. A D51N mutation engineered into Hela cells abolished proton pumping activity while maintaining full electron transfer activity (Shimokata *et al.*, 2007).

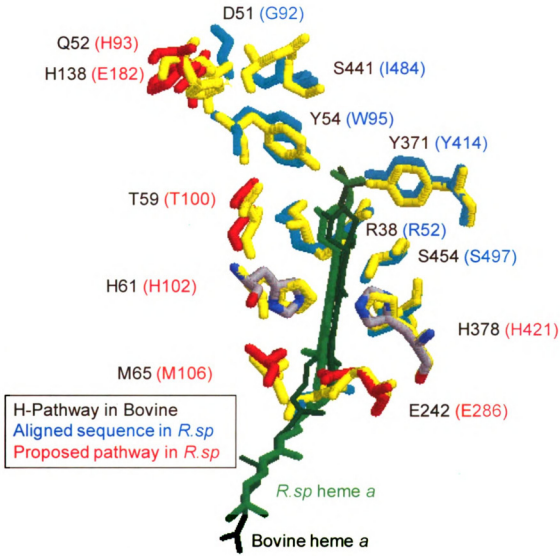

Figure 4. 1. Comparison between the proposed H-pathway residues close to heme *a* in the mammalian C*c*O, versus *Rs*C*c*O.

Comparison between the proposed H-pathway for proton pumping in bovine heart C*c*O(Tsukihara *et al.*, 1996) and a putative comparable proton pathway in *R.sphaeroides* C*c*O(Lee *et al.*, 2000). All bovine resicues are shown in yellow, while aligned residues in *R.sphaeroides* are shown in cyan. Residues of a proposed proton pathway in R.sphaeroides are shown in red.

Mutations of a non-conserved histidine (H93 in *R.sphaeroides* numbering) were made based on the observation that this histidine was the closest spatially aligned residue, with proton uptake capacity to D51 in the bovine C*c*O. Interestingly, helix II of subunit I contains several important residues such as T100, H102 and D132 (Figure 4.2). Mutation of T100 into lysine (T100L) resulted in strong inhibition and an altered redox potential of heme *a* (Schmidt, 2003). H102 is one of the ligands of heme *a* and D132 is in the helix II/III loop, and is the entry site for proton uptake into the D-pathway. Several mutations of H93 were prepared to test whether it was functionally related to D51 in bovine C*c*O and may have a role in the bacterial oxidase *Rs*C*c*O in controlling proton movement (Lee *et al.*, 2000). The possiblility was considered that this region may be involved in proton backflow. This could be examined by using stopped-flow techniques as described above.

In a previous study, a site-directed mutant, H93C, was made in order to look at the effects of adding a fluorescent label, fluorescein maleimide, to C*c*O. If the cysteine is exposed to solvent, fluorescein maleimide has the possibility of binding to the cysteine. If, however, the cysteine is buried in the interior of C*c*O, fluorescein may not react with it, as monitored by the absence of a fluorescent band on an SDS PAGE gel. Preliminary results showed that H93C was labeled only when cytochrome *c* was bound (Schmidt, 2003), suggesting that there is a conformational change upon cytochrome *c* binding in the region of H93 (Figure 4.3). However, mutation of H93 did not alter the steady-state affinity for cytochrome *c*.

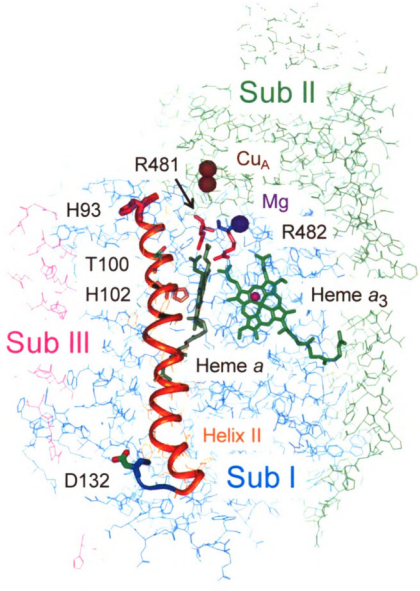

Figure 4. 2. Location of H93 and its neighbor residues.
The proximity of the residue H93 to subunit II (dark green) places it close to the cytochrome *c* binding site where electrons are delivered from a soluble cytochrome *c* (not shown) to Cu_A (brown spheres) and heme *a* (dark green stick) and finally to heme a_3 (green stick) and Cu_B (magenta sphere) at the active site in subunit I with the important residues R481 and R482, which interact with the heme propionates. H93 is approximately <9Å away from cytochrome *c*, based on a docking study (Roberts and Pique, 1999). Helix II of subunit I contains H93, T100, H102 and D132. The loop (blue ribbon) at the end of helix II contains D132, at the entrance of the D pathway for proton uptake.

Computational studies also support a significant movement in this external region, emphasizing the need of further crystallographic data as well as mutation studies. A substantial movement of H93 was observed in a molecular dynamics study of the R481K mutant (Seibold *et al.*, 2005). It is proposed that the R481K mutation may lead to a constriction of a water path above the hemes due to the movement of a loop between helix III/IV in subunit I. H93 of helix II is 6Å from a glutamate (E182), on a loop between helix III/IV in subunit I. This region has flexibility and may be involved in conformational changes that could regulate proton movement through the backflow pathway.

4.2. Methods of Site-Directed Mutagenesis of *Rs*C*c*O to Produce H93K

The central Nco1 fragment of the *R.sphaeroides* cox I gene was subcloned into pUC119. A PCR-based mutagenesis method (QuikChange Mutagenesis Kit, Stratagene) was used to replace H93 with lysine. Other mutants, such as H93N, H93C, and H93N/E182A were made by Dr. Carrie Hiser in our laboratory. The mutagenic primers were synthesized by the Macromolecular Structure, Sequencing and Synthesis Facility in the Michigan State University. After sequencing, the cox I fragment was ligated back into the rest of the genes and then cloned into the Hind III site in the expression vector, pRK415 (Figure 4.4). The operon which carries the his-tagged subunit II and subunit III was then added into a Pst I site. The expression plasmid was transformed into *E.coli* S17-1 cells and then transferred into the *R.sphaeroides* strain □ 123 cell line by biparental conjugation (Hiser *et al.*, 2001).

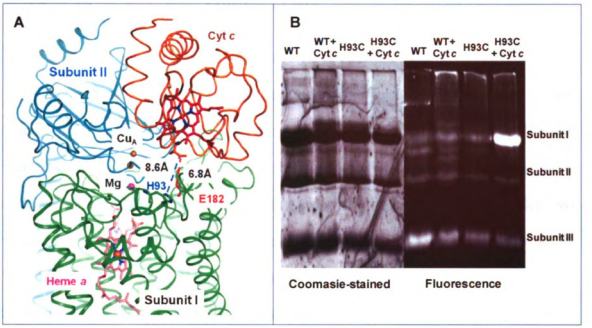

Figure 4. 3. The binding effect of C*c* onto the C*c*O.
(A) Predicted docking model between C*c* and C*c*O. The H93 residue is fairly close to the predicted C*c*(shown as a orange ribbon) docking site based on a docking simulation study (Roberts and Pique, 1999). The distance between H93 (δ1 nitrogen) and the closest C*c* residue (Ile 81 γ1 carbon) is about 8.6 Å. E182 (one carboxyl oxygen) is placed even closer to Ile 81(γ1 carbon) in 6.8 Å. (B) A conformational change is probed by a cystein specific FM (fluorescein maleimide) fluorescent label. Gel electrophoresis with wild-type and H93C was performed in the presence or absence of cytochrome *c*. The left panel shows the coomassie-stained subunits, I, II and III of C*c*O. The right panel shows fluorescent bands due to FM (fluorescein maleimide) binding in the absence of staining. A strongly fluorescent band was only observed in subunit I for the condition where H93C and cytochrome *c* were present. There was some background fluorescence, which was due to the cysteines of subunit III. The results suggest that there was a conformational change which allowed H93C to be exposed to the outside and to be lableled with FM, but only when cytochrome *c* was bound. An 18% acrylamide cross-linked gel was loaded with C*c*O containing H93C with a running buffer at pH7.9 to resolve the protein bands in SDS-PAGE. In resting oxidized H93C, no fluorescent labeling was observed. Wild-type C*c*O gave the same result with or without cytochrome *c*. The fluorescent labeling data presented here is courtesy of Dr. Bryan Schmidt.

4.3. Characterization of H93K mutants

4.3.1. Subunit Analysis by SDS-PAGE of Purified *Cc*O

The subunit composition of the purified H93 mutants was evaluated by sodium dodecyl sulfate-polyacrylamide gel electrophoresis (SDS-PAGE) (Figure 4.5). The site-directed mutants showed no changes in subunit stoichiometry or protein degradation, as evidenced from the Coomassie gel showing the presence of all four subunits, which have measured molecular mass of 74, 47, 35, and 8 kDa (predicted molecular masses is 63, 29, 30 and 0.5 kDa from the DNA-derived amino acid sequences) for subunits I, II, III, and IV, respectively. Polypeptide size was estimated from using a low molecular weight range marker from Bio-Rad Laboratories although the behavior of membrane proteins in SDS-gels is usually anomalous. Some polymerization of the subunits was observed (higher molecular weight bands > 90K). The purity of the isolated enzyme was also determined by UV-visible spectroscopy.

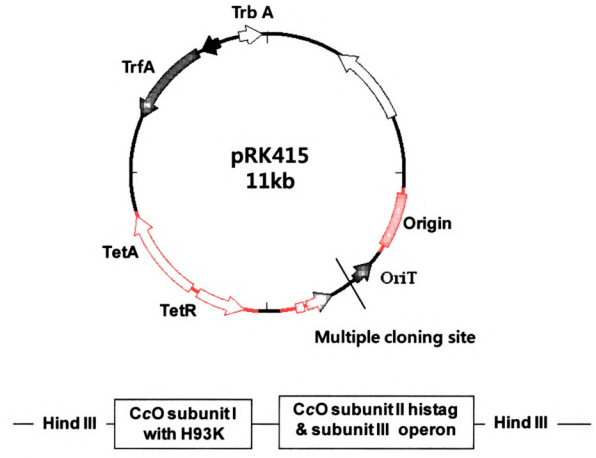

Figure 4. 4. Construction of expression plasmid of H93K.
This plasmid contains a broad host range origin of replication and origin of transfer (OriT). It also contains the tetracycline resistance gene (TetA,TetR), which can be used to screen the clones. The cox I gene with H93 mutation, and the his-tagged subunit II and subunit III, are inserted at multiple cloning sites.

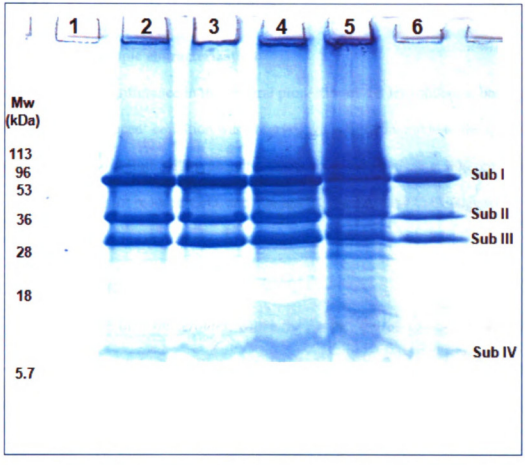

Figure 4. 5. An SDS-PAGE gel of all of the subunits of C*c*O.
The retention of all subunits of C*c*O, including subunit I, II, III and IV, was resovled by SDS-PAGE. SDS-PAGE urea gels were run as described (Peiffer *et al.*, 1990) and run at room temperature. A quick staining method was applied to the C*c*O. The gel was stained with Coomassie blue for 2 min in the microwave until it began to boil and was then put on a shaker for 5min. The gel was de-stained with acetic acid (7.5%) in a microwave for 2min for 3 or 4 times until clear blue bands were observed. Label indicates: 1; molecular weight markers from Bio-Rad laboratories, 2; Wild-type C*c*O, 3;H93K, 4;H93N/E182A, 5;H93C, 6;H93N. The resolving gel contains 18% acrylamide in Tris-HCl, pH8.8, 36% Urea, 0.1% SDS, AMPS and TEMED. The stacking gel contains 8% acrylamide in Tris-HCl pH6.8, 0.1% SDS, AMPS and TEMED. All 4 subunits were found in both wild type and mutant C*c*Os.

4.3.2. Spectroscopic characterization

UV-Visible spectroscopic characterization

No substantial difference in the spectral properties of the H93 mutants, both in 'as prepared' and the 'reduced' condition was observed and was comparable to the spectra of wild type (Figure 4.6). Both wild type and mutants show the □ -peak at 606 nm and the Soret peak at 445 nm for reduced C*c*O, and 424 nm for the oxidized C*c*O, suggesting that the mutations caused no major changes in the overall properties of the hemes.

EPR spectra of H93K

The active site of *R.sphaeroides*, where the oxygen chemistry occurs, contains 1 Cu (Cu_B) and 1 Fe(a_3). It is generally accepted that Cu_B is antiferromagnetically coupled to heme a_3, so that its reduction state is not easily detected. There is an EPR-detectable copper site, a dinuclear Cu_A, in subunit II, as well as heme *a*. It has been observed that a mutation in H93 (H93N) causes a change of about 40mV in the redox potential difference between heme *a* and Cu_A (Frank Millett unpublished data). However, no significant changes were detected in the EPR detectable Cu_A and heme *a* regions (Figure 4.7). Similarily, the H93K mutant is not expected to disrupt the metal centers, as observed in the normal EPR spectrum of H93K with heme *a* *g* value of g_x=2.82, g_x=2.31, and g_y=1.63 as described (Mills *et al.*, 2008). The difference in Cu_A signal between H93K and wild-type is very small and no increase in high spin heme a_3 is observed.

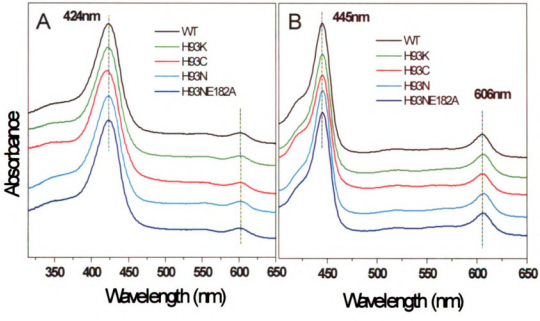

Figure 4. 6. UV-Visible spectra of wild type and H93K.
UV-Visible spectra of 'as prepared (A)' and 'reduced (B)' of wild type and H93K, H93C, H93C, H93N/E182A mutants. H93 mutants show no deviations from the wild type *Cc*O spectra in both the -peaks at 606nm (reduced) and the Soret peak at 424nm (oxidized) and 445nm (reduced). The measurements were taken in buffer containing 100 mM HEPES-KOH pH7.4 and 0.1% lauryl maltoside with sodium dithionite as a reductant in (B).

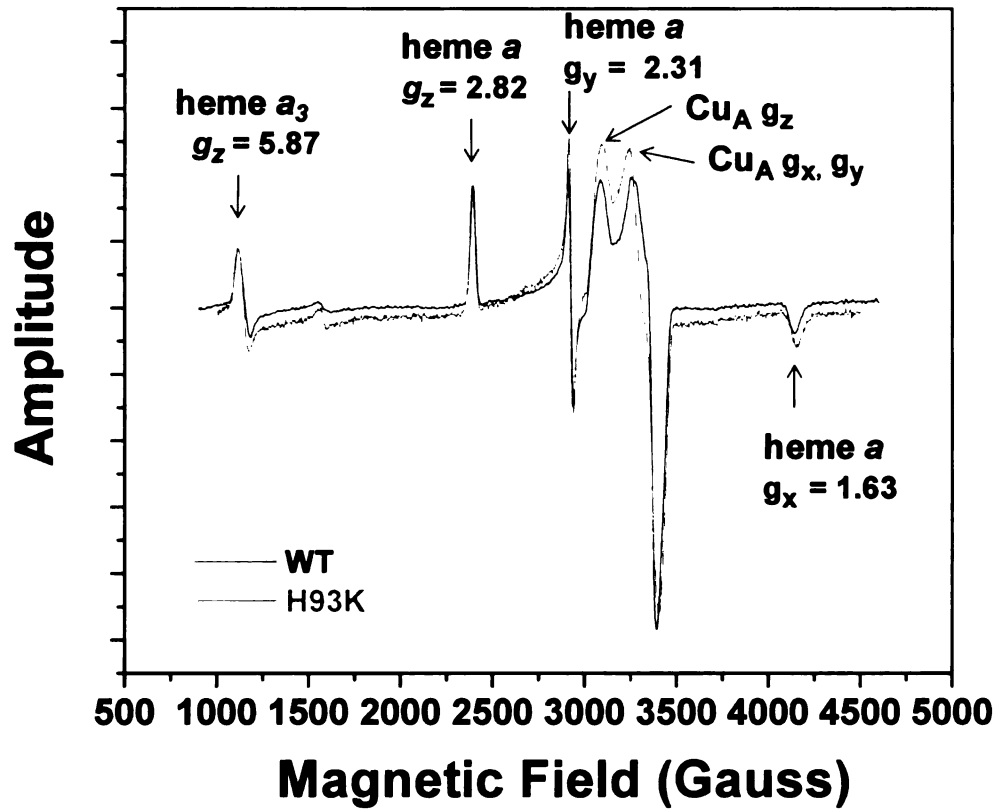

Figure 4. 7. EPR spectra of purified wild type (black line), and H93K (red line) *R.sphaeroides* C*c*O.

The *g* values were determined from direct measurements of the magnetic field strength and microwave frequency. Relevant *g* values are indicated by the arrows. The g_Z, g_X and g_Y values for heme *a* are 2.82, 2.31, and 1.63, respectively. Samples were made in a buffer of 20mM HEPES-KOH pH8.0, 14mM KCl, and 0.1% lauryl maltoside with a final concentration of 80 μM (wild type) and 60 μM (H93K) C*c*O. EPR experimental conditions: microwave frequency, 9.458 GHz; microwave power, 50uW; modulation frequency, 100 kHz; modulation amplitude, 20.0G; conversion time, 327 ms; temperature, 4.2K. (Measurements were made by Shujuan Xu).

4.3.3. pH and Lipid Dependence of Mutants

The effect of pH on the steady-state activity of the purified H93 mutants and wild type C*c*O was measured using a Gilson oxgygraph with cytochrome *c* in excess. C*c*O activity in the wild type increases as the pH is lowered; the activity of H93C, H93N and H93N/E182A show a slight decrease in activity below pH 7.0, giving a local maximum activity around pH 6.8, except for the H93K (Figure 4.8). Most of the mutants show a decrease in activity of about 30-40% compared to that of wild type, but not for H93N. Observed changes in the redox potential (~40mV lower) of heme *a* may be a factor in the decrease in the steady-state activity of the H93 mutants. Almost the same redox potential changes (~40mV) were observed upon the depletion of Ca^{2+} binding in the bovine oxidase structure. It is a yet untested possibility that the histidine mutations destabilized the position of the Ca^{2+} in *R.sphaeroides* C*c*O. The electron transfer from Cu_A to heme *a* can be a rate-limiting step when the redox potential of heme *a* is lowered. Since it has been observed that the D132A mutant can recover its activity with the addition of arachidonic acid, which supplies a carboxylic acid as a protonatable site for the D pathway, this fatty acid and other lipids were tested on the H93 mutants. However, the decreased activity of the H93 mutants was not rescued upon addition of extra lipids, including Cholate and arachidonic acid. Even the activity of a double mutant (H93N/E182A) was not increased greatly by the addition of extra lipid.

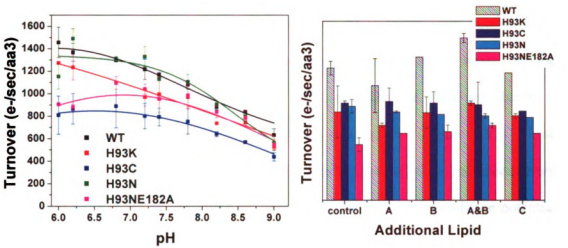

Figure 4. 8. Effect of pH and lipid addition on the catalytic activity of the free enzyme.

The activity of wild type and mutant of H93 residues of C*c*O increases as the pH of the buffer is decreased (left panel). The steady-state activity (e^-/sec/aa_3) of H93K,H93C,H93N,H93N/E182A and wild type *R.sphaerodies* C*c*O was measured by Oxygraph with a Clark electrode and compared over the pH range of 6-9, with error bars. The MES-KOH, HEPES-KOH, and CHES-KOH buffers were used at 50mM with appropriate amounts of KCl to give an approximate ionic strength of 45mM with respect to potassium, and with lauryl maltoside at 0.1% as prepared. H93N and H93K show similar activity to wild type. H93C and H93N/E182A double mutant shows an overall lower activity. Below pH 7.0, the H93 mutants show an increased inhibition of activity compared to wild-type, except for H93K. These data are for an average of 3 datasets. The addition of lipids (right panel) did not change the activity of H93 mutants; the effect of cholate (A), asolectin from Avanti (B), and arachinonic acid from Cayman Chemical Co.(C) are shown in a bar graph.

When the H93 mutants were reconstituted into lipid vesicles, larger differences were observed in comparison with wild type. The RCR (respiratory control ratio, uncontrolled rate/controlled rate) could be measured in this system as well. All the mutants showed higher RCR than wild type CcO, especially at high pH, due to a proportionately greater inhibition of the controlled sate activity (Figure 4.9). These results support the proposal that H93 may inhibit the proton backflow movement from the outside of C*c*O in the reconstituted vesicles in the presence of a membrane potential and proton gradient. The backflow of protons in the mutated H93 may not be as prominent as in the wild-type, and may not support a wild-type level of activity under membrane potential in the COVs.

H93N shows almost the same activity as wild type in the steady-state condition with free enzyme but only 50% the activity in the reconstituted controlled state. This result suggests that there may be a conformational change in C*c*O when the enzyme is under the condition of a high membrane potential. Previous fluorescence labeling data show a conformational change in the H93C mutant, when cytochrome *c* is bound (Schmidt, 2003).

4.3.4. Cytochrome *c* Binding Study

A cluster of conserved lysine residues in the backbone of cytochrome *c* (C*c*) interact with carboxyl residues in subunit II of C*c*O (Figure 4.10) with high affinity (Roberts and Pique, 1999). There is an ionic strength dependent interaction between C*c* and C*c*O (Wang *et al.*, 1999). At low ionic strength, wild type C*c*O is electrostatically stabilized and is at the optimal orientation for rapid electron transfer.

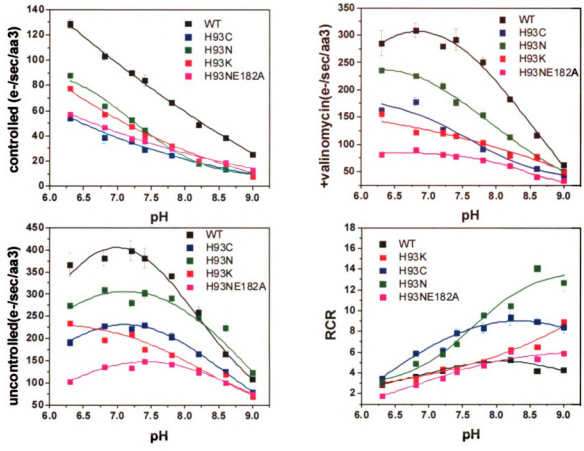

Figure 4. 9. Effect of pH on oxygen consumption activity and RCR of CcO, reconstituted in the vesicles under various conditions.

The catalytic activity was measured in the Olism stopped-flow rapid scanning spectrophotometer with a defined amount of cytochrome c in order to have ~10 turnovers. The lowest rate of activity is in the controlled state due to the presence of a $\Delta\Psi$ and ΔpH (top left panel). Addition of the ionophore, valinomycin (top right panel), removes the $\Delta\Psi$ and increases activity (this is the state in which proton pumping is observed). Addition of the proton uncoupler, FCCP, to the pumping state (lower left panel) results in the fastest activity due to the lack of restraints (no $\Delta\Psi$ or ΔpH). The RCR (respiratory controlled ratio, is determined by dividing the uncontrolled rate by the controlled rate) is shown over the pH region 6.25-9.0 (lower right panel). All mutant forms show ~50% inhibition when they are reconstituted into vesicles. A jump in the RCR was observed at the higher pH range, particularly with the H93N mutant.

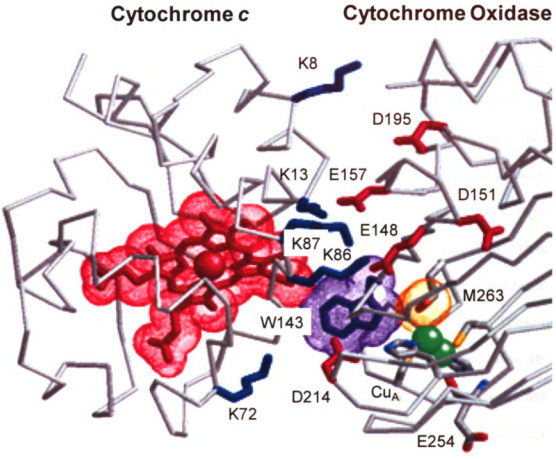

Figure 4. 10. Model for the high affinity complex between horse heart cytochrome *c* and bovine CcO.

The conserved lysine residues in the Cc backbone interact with the acidic carboxyl residues in subunit II of CcO with high affinity. This interaction is ionic strength dependent. This figure was obtained from Wang *et al.* (Wang *et al.*, 1999)

The H93 residue is very close to the predicted cytochrome *c* docking site, lying in the surface region of subunit I, below C*c*. The proximity of H93 to cytochrome *c* (<9Å away) and to subunit II of C*c*O suggests a potential interaction with the cytochrome *c* docking site. The equilibrium dissociation constants between horse heart cytochrome *c* and *R.sphaeroides* C*c*O were measured by analytical ultracentrifugation (Figure 4.11). The analytical ultracentrifuge instrument is fitted with optical systems designed to record the concentration or a concentration gradient of the sedimenting molecules as a function of their position in the double sector center piece cell. C*c*, C*c*O and C*c*/C*c*O complex, which initially were distributed uniformly through the cell, were sedimented at different rates towards the bottom of the cell under a high centrifugal force. During centrifugation, the concentration in the plateau region decreases, due to radial dilution. Thus, the binding affinity of mixed samples of C*c* and C*c*O can be directly measured after 1h at 48,000 rpm. The complex of C*c*O and C*c*, with a larger molecular weight, moves much faster than free C*c*. Free C*c* sedimented at a sedimentation velocity of 1.74 S, while C*c*O sedimented at 9.7 S.

The equilibrium dissociation constant (K_D) was measured for several mutants of H93 and wild type C*c*O under different ionic strengths as described by Wang *et al.* (Wang *et al.*, 1999). The absorbance at 410nm was measured during ultracentrifugation because this wavelength is at the Soret peak of oxidized C*c*O and the wavelength maximum of oxidized cytochrome *c* (C*c*). The measured absorbance is proportional to the heme concentration (amount of C*c*) and gives a large signal compared to that at 606nm.

Figure 4. 11. Analitical Ultracentrifugation measurements of the binding affinity of horse heart cytochrome *c* binding to wild type C*c*O.
The upper panel shows a scheme for the analytical ultracentrifuge instrument and the comparison between wild-type with a his-tag on subunit I and subunit II. The H93C, H93K and H93N/E182A mutant data were shown in the lower panels. Analytical ultracentrifuge was used in the sedimentation velocity mode at a speed of 48,000 rpm. A scanning UV/Vis detection system is used to measure the absorbance at 410nm and the scans recorded every 5 min through the sample cell (maximum volume of 0.45mL, 12mm bandpath) during the high speed centrifugation after 1hr in order to calculate the dissociation constant of free cytochrome *c*. K_D values were calculated from the difference between total C*c* and free C*c* after 1 hr with 0-250 mM KCl by a Beckman Coulter Optima XL-1 analytical ultracentrifuge with an AN60Ti rotor in sedimentation velocity mode. The sample solution contained: 6 μM C*c* and 6.6 μM C*c*O in 5mM Tris-HCl at pH8.0, 0.1% lauryl maltoside; and 0, 20, 40, 60, 80, 100, and 250 mM NaCl (from bottom to top). The sharp spike is the sample meniscus (Wang *et al.*, 1999).

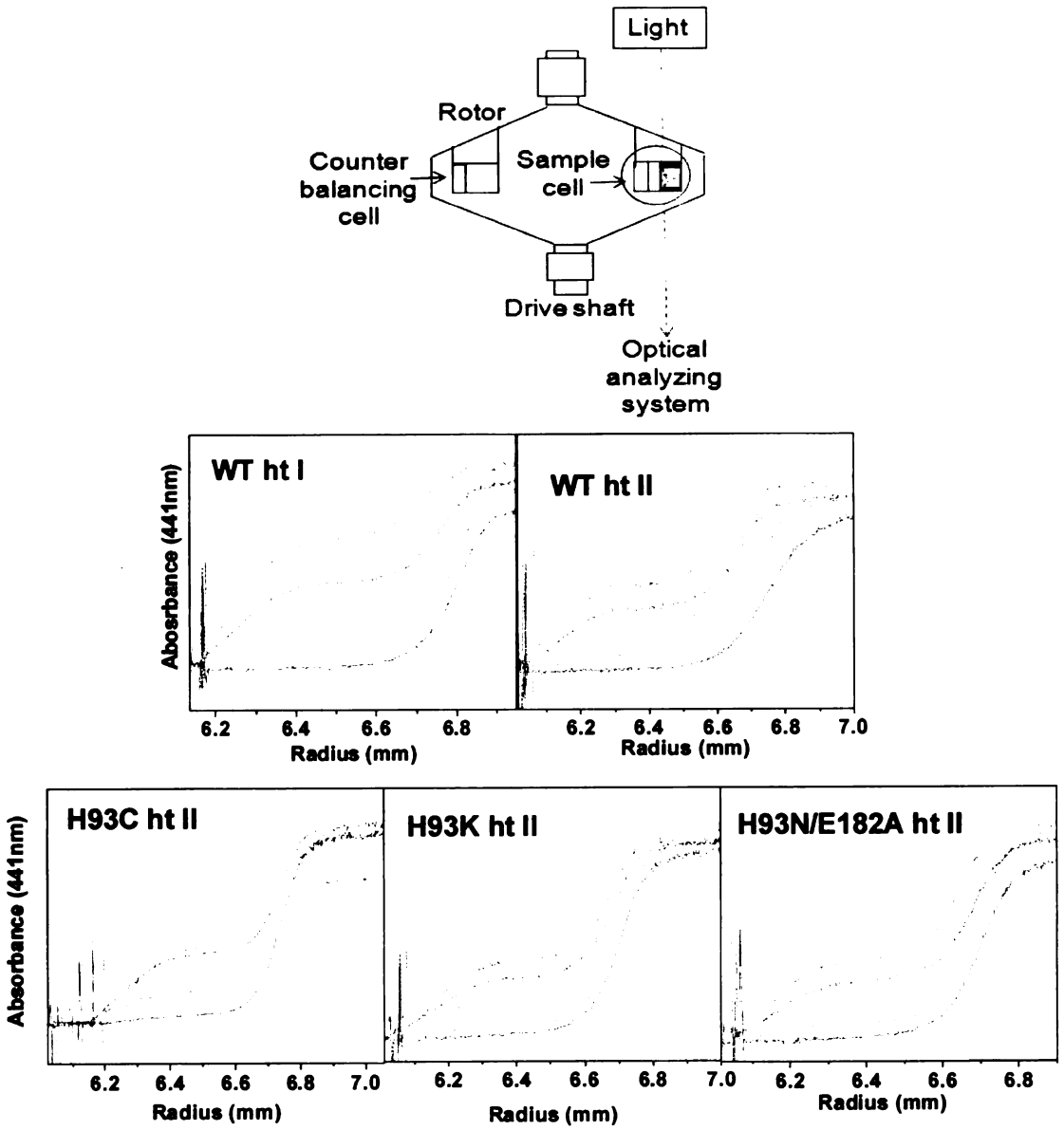
Light
Rotor
Counter balancing cell
Sample cell
Drive shaft
Optical analyzing system
WT ht I
WT ht II
Aborbance (441nm)
6.2
6.4
6.6
6.8
7.0
Radius (mm)
H93C ht II
H93K ht II
H93N/E182A ht II
Absorbance (441nm)

The 1:1 ratio of horse *Cc* and *CcO* was prepared in 5mM Tris-HCl, pH 8.0, 0.1% LM, 0~250 mM NaCl. *Cc* will occupy the high affinity site on *CcO* first in this condition. Thus, this condition allows measurement of the K_D for binding of horse *Cc* to the high affinity site on *R.sphaeroides* *CcO* (Zhen *et al.*, 1999a). The change in the electrostatic potential of the surface of *CcO*, due to the mutation or ionic strength will affect the interaction between *Cc* and *CcO*, and alter the electron transfer (Zhen *et al.*, 1999a). At 0 mM NaCl, all of *Cc* was complexed to *CcO* showing a single band of 11.4 S (Svedberg) (Figure 4.11). As the ionic strength was increased, a second band which has a plateau region appears with a sedimentation velocity of 1.74 S, which is due to uncomplexed *Cc*, indicating a significant amount of dissociated *Cc*. The concentration of uncomplexed *Cc* was directly quantified from the 410nm absorbance at the plateau of the *Cc*, as described by Cann (Cann, 1970). The concentration of uncomplexed *Cc* increased as the ionic strength was increased, until it reached the total concentration of *Cc* in the cell at 250 mM NaCl. The equilibrium dissociation constant of the complex was calculated from Equation 1.

$$K_D = [Cc][CcO]/[Cc \cdot CcO] \qquad \text{(Eq.1)}$$

This equation assumes the formation of a 1:1 complex between *Cc* and *CcO*.

The position of the histidine-tag, used for purification of *CcO*, may cause a change in the interaction between *Cc* and *CcO* because the histidine-tag was engineered onto the C-terminal end of *R.sphaeroides* *CcO* subunit II, close to the *Cc* binding region. However, there was no major change in binding behavior between subunit I and II his-tag

wild type C*c*O on K_D (Table 4.1). The calculated K_D of the mutants (H93K and H93N/E182A) was similar to wild type suggesting that the mutants do not alter the affinity between C*c* and C*c*O. The greatest effect (higher than the WT and other H93 mutant, e.g. 4-5 fold larger in 0-20mM range) among the H93 mutants was that the dissociation constant was altered in the H93C mutant. The results obtained for wild type were in good agreement with those of Wang *et al.* (Wang *et al.*, 1999) showing a K_D of <0.2 at 0-30mM, 1.0 at 40mM, 5.6 at 60mM, 18 at 80mM, and 35 at 100mM NaCl.

4.3.5. Proton pumping in COVs

The H93 mutants and wild type C*c*O were reconstituted into lipid vesicles by a Bio-bead method (see Chapter 2 for details) in order to analyze their activity and proton pumping (Figure 4.12). All mutants of H93 show a proton pumping efficiency of ~ $1H^+/e^-$ as calculated by the quantification method introduced in Chapter 3 supporting the idea that the use of the H-channel in proton pumping in *R.sphaeroides* is unlikely. However, a conformational change around H93 is predicted, based on the binding of fluorescein to H93C when C*c* is present, but not in its absence. Since the binding site of cytochrome *c* is in the vicinity, it may be that a conformational change occurs in this region that might alter proton backflow but not affect the proton pumping.

CcO	K_D					
	0mM NaCl	20mM	40mM	60mM	80mM	100mM
WT ht I	0.01	0.5	3.8	12.4	34.5	N/D
WT htII	0.01	0.6	4.9	13	31.4	76
H93K htII	0.06	0.4	5.6	18.1	40.5	112.4
H93N/E182A htII	0.05	0.6	6.6	13.5	28	76.9
H93C htII	0.24	2.6	8.2	70.3	374.5	N/D

Table 4. 1 Equilibrium dissociation constants, K_D, for the binding of horse C*c* to the high affinity site on *R.sphaeroides* cytochrome *c* oxidase.

K_D (in μM) was measured using the analytical ultracentrifuge in the sedimentation velocity mode for 1 h at 48,000 rpm. Experimental conditions are the same as Figure 4.11.

Figure 4. 12 The catalytic activity and proton pumping of COVs of wild type and H93 mutants.

Cytochrome *c* oxidation is measured at 550nm (top panel) under controlled conditions (black line), with valinomycin (blue line), and under uncontrolled conditions (red line) for 5 seconds. Measurement of proton movements (uptake & release) in COVs was obtained by using the externally added pH-sensitive dye, phenol red, on the outside of vesicles with final 100 μM concentration in 50μM HEPES-KOH at pH7.4 and was monitored at 557 nm (lower panel), at an isosbestic point for cytochrome *c*. A final concentration of ~0.1 μM aa_3 was mixed with a defined amount of C*c* to give 10 turnovers. The controlled state (black trace) shows an increased absorbance indicating alkalinization on the outside of the COVs as a result of proton backflow under a high membrane potential and proton gradient. Addition of valinomycin shows a decrease in absorbance due to the pumping of protons to the outside, which decreases the pH and leads to a decrease in absorbance (lower, blue trace) by eliminating the membrane potential. The addition of FCCP and valinomycin relieves both the $\Delta\Psi$ and ΔpH and the protons equilibrate across the membrane, causing an alkalinization on the outside, which is the uncontrolled state (lower, red trace).

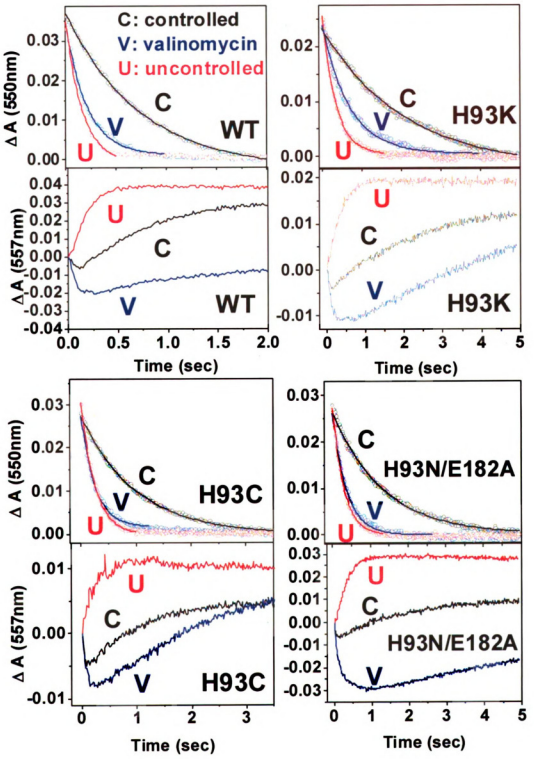
C: controlled
V: valinomycin
U: uncontrolled
ΔA (550nm)
ΔA (557nm)
Time (sec)
WT
H93K
H93C
H93N/E182A
C
V
U

4.3.6. Zinc Inhibition Study in Putative Backflow Pathway

Since H93 is one of the few histidine residues on the external surface of C*c*O, it is a potential target for zinc binding. The H93K and H93N/E182A mutant COVs were prepared in order to test their ability to bind zinc. Zinc can only bind to the outside surface exposed residues of C*c*O when it is embedded in vesicles. Zinc binding is expected to be located at the entry point of a proton channel, where several carboxylates and/or histidine residues are clustered to favor high affinity zinc binding. It is observed that zinc binding on the outside reduces activity in wild-type (Chapter 3. Figure 3.2) and the H93 mutants (Figure 4.13 and 4.14).

The H93K mutation was designed in order to maintain the positive charge, but would be expected to reduce the affinity of binding to Zn^{2+}. The double mutant H93N/E182A may give further reduced zinc binding efficiency by eliminating the nearby carboxyl group, which has the possibility of interacting with H93. However, mutation of H93 does not alter zinc inhibition. Inhibition by zinc was observed in both H93K and H93N/E182A COVs to the same extent as wild type COVs, even though the effect on proton pumping seems significantly different, Zn showing much greater inhibition of pumping in the mutants (Figure 4.13 and 4.14). These results suggest that zinc binding still occurs in the mutants and this is confirmed by the fact that H93C shows a similar inhibition with zinc as observed with wild type COVs (Table 4.2). The source of the different effects of Zn is still being investigated.

Figure 4. 13 Monitoring the proton movement in H93K COVs.
The movement of protons from the outside and inside of H93K COVs in the absence(A,B &C) and presence of zinc (D,E &F), and the movement of protons monitored by phenol red absorbance changes (B,E) and pyranine absorption changes(C,F) on the inside. Cytochrome *c* oxidation at 550 nm is measured over 5 seconds in the controlled state (A, black line), but this is slowed with the addition of zinc (100 μM) (D, black line). Zinc shows little inhibition of C*c*O when valinomycin is added (D, blue line) and no inhibition by zinc under the uncontrolled state, with valinomycin and FCCP (D, red line). Proton backflow was observed by monitoring outside pH changes with phenol red in the controlled (B, black line) and with zinc (E), with the addition of valinomycin (B, blue line), which has a high proton gradient. The uncontrolled state COVs rapidly equilibrate the protons across the membranes and cause alkalinization on the outside (B, red line). Zinc did not contribute to blocking the backflow to any real extent in the uncontrolled state (E, red). Pyranine (20mM) was added to the inside of COVs as a monitor of internal proton changes seen in (C) and with added zinc (F) at 435nm under different condition.

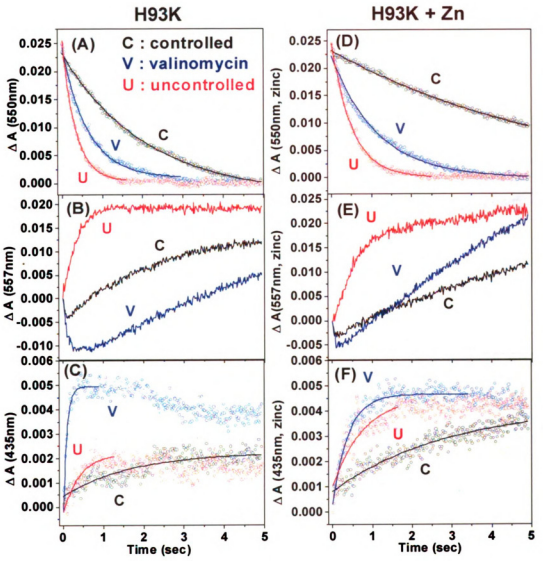
H93K
H93K + Zn
(A)
C : controlled
V : valinomycin
U : uncontrolled
(B)
(C)
(D)
(E)
(F)
Δ A (550nm)
Δ A (557nm)
Δ A (435nm)
Δ A (550nm, zinc)
Δ A (557nm, zinc)
Δ A (435nm, zinc)
Time (sec)

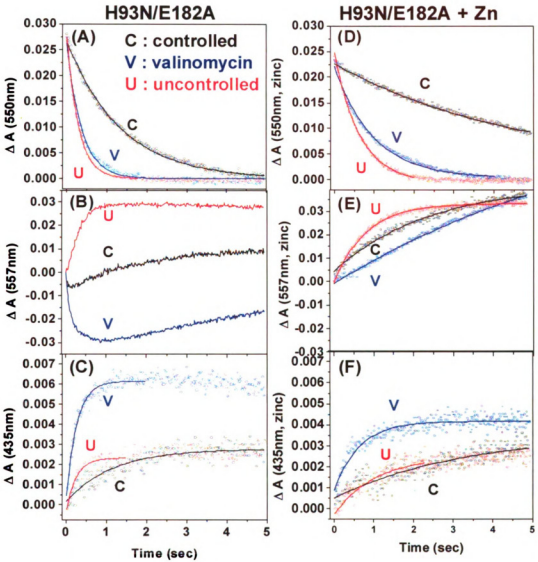

Figure 4. 14 Monitoring the proton movement in H93N/ E182A COVs.
The movement of protons from the outside and inside of H93N/E182A COVs in the absence (A, B, and C) and in the presence (D, E, and F) of zinc. (see Figure 4.13.). Strong inhibition is observed in the presence of zinc (100 M). The proton backflow was observed by monitoring outside pH changes with phenol red in the controlled state (B, black), which has a high membrane potential and proton gradient with reconstituted COVs in the absence of ionophores. Proton pumping was not observed in the presence of zinc with valinomycin (E, blue line), and cytochrome *c* oxidation was very slow with the addition of zinc (D).

COVs	Turnover rate (e^-/sec/aa_3)			RCR
	Controlled	Pumping	Uncontrolled	
WT	76±0.4	217±2.8	313±5.5	4.1
WT + Zinc	39±0.4	166±2.2	238±2.9	6.1
H93K	30±0.1	67±0.6	142±1.2	4.7
H93K + Zinc	5.7± 0.2	32±0.3	67±0.5	11.8
H93C	45±0.2	172±2.0	177±2.0	3.9
H93C + Zinc	7.9±0.1	50±0.2	119±1.0	15.1
H93N/E182A	37±0.2	135±1.5	172±1.4	4.6
H93N/E182A + Zinc	7.3±0.3	33.2±0.2	58.4±0.3	8

Table 4. 2 Effect of zinc on the turnover activity of COVs prepared by the Bio-bead method.

The buffer conditions were; 20mM HEPES-KOH, 39mM KCl, 52mM sucrose, pH7.4 on the inside and 50μM HEPES-KOH, 45mM KCl on the outside. Measurements were made in the Olis-rsm stopped-flow instrument. Cytochrome *c* oxidation rates were calculated from the kinetic traces at 550nm by multiplying the kinetic rate (e^-/sec) x [C*c*] μM / [aa_3] μM. RCR (Respiratory Control Ratio was calculated from uncontrolled rate /controlled rate. Experimental Conditions were as in Figure4.12. Final 100 μM $ZnSO_4$ was added for the zinc inhibition measurements.

4.4. Discussion

The H-channel appears a likely proton channel in bovine C*c*O as it spans the protein and is close to heme *a*, which has been suggested as a site for coupling of electron transfer to proton pumping (Capitanio *et al.*, 1996). It is also the only area of the protein that differs in conformation between the oxidized and reduced crystal structures of bovine C*c*O. Mutation studies support the existence and important role of D51, even though there is a lack of conservation of the residues reported in bacterial *Rs* C*c*O (Lee *et al.*, 2000). The spacially closest, proton-accepting residue, H93, in *R.sphaeroides* was selected to test the hypothesis of the H-pathway in bacterial C*c*O. The fluorescein-binding data suggests that there is a conformational change at the position of H93 upon binding of C*c* in the bacterial enzyme although no change in structure is seen between oxidized and reduced forms of RsC*c*O ((Qin, 2008; Qin *et al.*, 2006) unpublished). However, various H93 mutants show close to normal proton pumping (~$1H^+/e^-$ stoichiometry). The results suggest that this residue is not important in proton pumping of *R.sphaeroides* C*c*O.

The mutation of H93 to a cysteine altered the redox potential of heme *a* as measured by fast electron transfer (Millett & Schmidt unpublished data). H93 is on helix II as is the heme a ligand H102. A conformational change at H93 may alter the ligand binding to heme *a* which could alter the redox potential. Also, the nearby residue T100 was mutated to a lysine with similar reduction of the heme a redox potential. Results indicate that other mutations of H93 may change ~~in~~ the redox potential of heme *a* ((Millett *et al.*) unpublished).

Closeness of H93 to E182 and the flexibility of both suggest this could be a zinc binding site. However, zinc inhibition is also observed in both single mutants of H93 (H93C, H93K) and double mutations (H93N/E182A). The results rule out an essential role of H93 in zinc binding. However, several unique characteristics have been noted for this mutant.

A normal efficiency of proton pumping ($1H^+/e^-$) suggests that H93 is not essential for proton release to the outside; however, it is still possible that the H93 residue may exert control on proton backflow. In the wild type C*c*O, activity is increased as the pH is lowered due to the increased concentration of protons, one of the substrates of the reaction mechanism for oxygen consumption activity. The activity of the purified H93 mutants (Figure 4.8) showed much less increase in activity at low pH, below 7.0, suggesting that something other than protons had become rate limiting at lower pH. The lowered activity (below that of wild type) at low pH for the H93 mutants might suggest that the protonation state of H93 is important, possibly contributing to a conformational gate. The increased RCR observed at high pH for all the H93 mutants is similar to that of the R481K mutant (Qian *et al.*, 2004). Under the controlled state, proton supply from the outside is important, and at high pH it may be rate limiting in H93 mutants. One interpretation of these results is that H93 is a part of a proton backflow path (that also involves R481) which is separate from the proton exit path and involves partners we have not yet identified. Further mutagenesis studies and X-ray crystal structures will be required to define this pathway.

The location of H93 on the outside surface of C*c*O raises the possibility that the effects observed are due to changes in the binding of C*c* to C*c*O. Any changes in the on and off rates of C*c* binding can change the electron transfer rate and efficiency. Indeed, the proposed docking site of cytochrome *c* (Roberts and Pique, 1999) is less than 9 Å from H93. However, no significant changes were observed in the dissociation constant (K_D), measured in the analytical ultracentrifuge for the H93K and double mutants. However, H93C shows a significantly increased K_D across a range of ionic strengths. This mutant, which is likely to move to an interior position, may be giving important information.

A possible interaction of C*c*O with VDAC (voltage-dependent anion channel) was recently proposed (Roman *et al.*, 2005). VDAC, a mitochondrial outer membrane channel, is involved in the control of the apoptotic process. The binding region to C*c*O identified by phage display and direct measurements is on the outer surface of subunit I of human C*c*O. This binding region corresponds to the region containing the E182 in *R.sphaeroides*, which interacts with the H93 residue nearby. This idea gives a novel, and potentially important, regulation possibly involving H93.

Chapter 5 Summary and Perspectives

The importance of regulation of Cytochrome c Oxidase and energy metabolism

Strict regulation of energy metabolism is essential for the survival of a living cell. However, this is a complex process, involving many levels of hormonal, neuronal, and metabolic control, including regulation at the most fundamental level, the mitochondrial electron transport chain. It is important to fully understand the mechanisms involved in oxidative phosphorylation in order to probe the reasons for defective energy regulation, which is the cause of many human diseases. Mitochondria use oxidative phosphorylation to convert dietary food sources (proteins, carbohydrates and fats) into energy and heat through a process that is dependent on a sequential drop in potential energy, and by the energy released from the reduction of oxygen at the active site of C*c*O. The energy released by the flow of electrons through the electron transport chain (ETC) is used to pump protons out of the mitochondrial inner membrane, or the bacterial membrane, to the intermembrane space through complexes I, III, and IV. The potential energy stored in the electrochemical gradient that is produced by the movement of protons and electrons is coupled to ATP synthesis in complex V. Meanwhile, reactive oxygen species (ROS) can be generated as a toxic by-product. Inhibition of the electron transport chain may generate ROS that can damage the cell. It has been proposed that mitochondrial dysfunction plays a central role in a wide range of diseases, such as Alzheimers and age-related diseases (Wallace, 2005), since the mitochondrial DNA encodes essential genes for energy production (Schon and Manfredi, 2003) (Figure 5.1).

The efficiency of energy conversion from dietary food sources, NADH and succinate to ATP, is determined by the coupling efficiency. The highly efficient mitochondria have a minimal leakiness for protons in the inner membrane, allowing efficient generation of ATP per electron consumed. This is a tightly "coupled" condition. By contrast, if the proton pumping efficiency is reduced by any uncoupling reaction (increased proton leak), less ATP will be generated while producing more heat (Figure 5.2). This is called the "uncoupled" condition. In an endothermic animal, the coupling efficiency determines the ratio of calories to the amount of work, versus the need to maintain temperature through uncoupling processes. The amount of leakiness in the electron transfer chain is dependent on the ability of the proteins to move protons across the membrane rather than having the protons move through the membrane. This would result in loss of a pH gradient and uncoupling the electron transport from ATP synthesis, and producing heat. Our data suggests that C*c*O itself has an important role in regulating efficiency (H^+/e^-) in an intrinsic manner, allowing the backflow of protons through the protein under conditions of a high membrane potential ($\Delta\Psi$) and proton gradient (Δ pH) (Mills and Ferguson-Miller, 2002b).

ROS are generated as a toxic by-product during respiration, especially when electron transfer is slowed down. The ETC continues to transfer electrons and pump protons until the electrostatic potential gradient builds up and inhibits further electron transfer and proton pumping. At this point, the ETC stalls and the electron carriers become maximaly occupied with electrons (reduced).

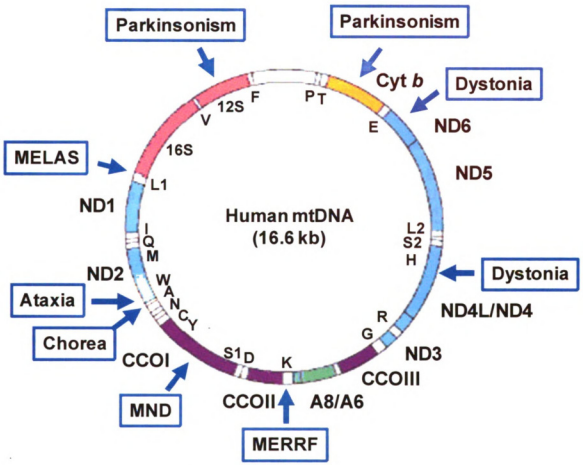

Figure 5. 1 Map of the human mitochondrial genome.
Polypeptide-coding genes, which are in boldface and outside of the circle, specifying seven subunits of NADH hydrogenase-coenzyme Q oxidoreductase (ND), one subunit of coenzyme Q-cytochrome *c* oxidoreductase (cyt *b*), three subunits of cytochrome *c* oxidase (CCO), and two subunits of ATP synthase (A). Protein synthesis genes (12S and 16S rRNAs , and 22 tRNAs) are inside the circle. Mutations in mtDNA associated with MELAS and MERRF, and mutations with features of neurodegenerative disorders, such as ataxia, chorea, dystonia, motor neuron disease (MND), and parkinsonism, are boxed. The figure is obtained from (Schon and Manfredi, 2003).

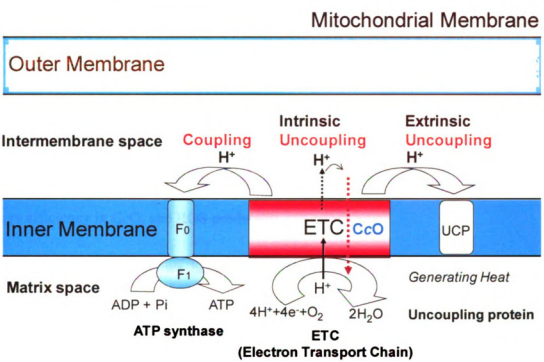

Figure 5. 2 Electron transport chain complex, and proton coupling and uncoupling. Electrons are generated from dietary food sources, and are transferred to the final electron acceptor, O_2, which is reduced to form water. Complex I, III, and IV transport protons into the intermembrane space and form the electrochemcial potential gradient produced by the electrons and protons. The build up of a proton gradient, ΔpH, is used to produce ATP from ADP and phosphate in the ATP synthase. The uncoupling protein (UCP) causes the dissipation of a proton gradient, and this results in the production of energy in the form of heat. *Cc*O itself can act as an intrinsic uncoupling protein in the ETC, in order to dissipate the high membrane potential by allowing protons to move through a backflow pathway, which may prevent the production of ROS during turnover.

These electrons can then be transferred to O_2 via flavin and quinone moieties to generate various forms of oxygen radicals ($O_2^{\cdot}$, H_2O_2, $OH^{\cdot}$). An active, but partially uncoupled, C*c*O can help reduce the formation of a high membrane potential, by the rapid reduction of oxygen at the active site of C*c*O, preventing the build up of electrons upstream and limiting ROS production. The question of how partial uncoupling of C*c*O is achieved and under what conditions is a major issue in understanding the physiological function of C*c*O. The hypothesis is that proton backflow is an important biological valve to control energy efficiency in C*c*O, and ROS production.

In this dissertation, we have studied the presence of proton backflow and its regulation in C*c*O, as an intrinsic uncoupling mechanism, by the mutation of important residues, and by examining the effect of zinc binding. Zinc is an inhibitor of the controlled state, under the condition of a high $\Delta\Psi$ and ΔpH. The binding of zinc on the outside of reconstituted C*c*O in phospholipid vesicles appears to inhibit proton back-leak (Mills *et al.*, 2002). Proton backflow in C*c*O was initially recognized in a D132A mutant, where the proton uptake through the D pathway is greatly slowed. Our effort to look at pH changes, both inside and outside of COVs, under the same conditions, is aimed at increasing our understanding of energy regulation in C*c*O during turnover. However, these measurements are technically very difficult. An attempt was made to correlate

the inside signal changes to the outside signal changes using different pH probes, with multiple turnovers of C*c*O, and with a good signal-to-noise ratio, by increasing the internal volume, and the concentration of dye entrapped in the COVs (Chapter 2). However, the results were not as definitive as hoped, due to continued technical difficulties in assessing the internal pH. Further, we still do not know the location of the proton backflow pathway. We also do not fully comprehend how the coupling of proton movement is linked to the electron movement. The proton path above the hemes for proton pumping in C*c*O is not resolved. Water is resolved in the D and K proton uptake pathways, which, along with mutagenesis, helped to define the route for protons (Qin *et al.*, 2006; Svensson-Ek *et al.*, 2002). Water is not usually observed except with highly resolving crystals < 2.5 Å. By obtaining higher X-ray crystal diffraction structures, and using site-directed mutagenesis, it is hoped that the exit path for protons, and the proton backflow path, as well as the zinc binding site, will be determined (Chapter 3).

Various H93 mutants, were intensively studied in order to determine whether H93 is an important residue in controlling proton backflow in bacterial (*R.sphaerodies*) oxidase (Chapter 4). This residue was selected because of its proximity to D51 in bovine oxidase that is proposed to be at an outlet of the exit path for protons. The H93 mutants showed a heightened inhibition by high pH when reconstituted into vesicles, suggesting a possible role in proton movement. Additionally, a high RCR was observed, due to a low controlled rate, suggesting that proton backflow was limited. Another possible role of H93 has been proposed in relation to VDAC (voltage-dependent anion channel), which is

involved in the control of apoptosis and has an interaction with C*c*O in the area of H93 (Roman *et al.*, 2005).

Further studies on the control of C*c*O activity, and the role of proton backflow, will be clarified by developing a kinetic model capable of describing the rates of proton uptake, backflow, and electron transfer under different conditions, to allow more incisive testing of the structural basis of these processes (Chapter 3).

Bibliography

Aagaard, A., and Brzezinski, P. (2001). Zinc ions inhibit oxidation of cytochrome *c* oxidase by oxygen. FEBS Letters *494*, 157-160.

Aagaard, A., Gilderson, G., Mills, D.A., Ferguson-Miller, S., and Brzezinski, P. (2000). Redesign of the proton-pumping machinery of cytochrome c oxidase: proton pumping does not require Glu(I-286). Biochemistry *39*, 15847-15850.

Aagaard, A., Namslauer, A., and Brzezinski, P. (2002). Inhibition of proton transfer in cytochrome c oxidase by zinc ions: delayed proton uptake during oxygen reduction. Biochim Biophys Acta *1555*, 133-139.

Abeywardena, M.Y., Allen, T.M., and Charnock, J.S. (1983). Lipid-protein interactions of reconstituted membrane-associated adenosinetriphosphatases. Use of a gel-filtration procedure to examine phospholipid-activity relationships. Biochim Biophys Acta *729*, 62-74.

Adelroth, P., and Brzezinski, P. (2004). Surface-mediated proton-transfer reactions in membrane-bound proteins. Biochim Biophys Acta *1655*, 102-115.

Adelroth, P., Ek, M.S., Mitchell, D.M., Gennis, R.B., and Brzezinski, P. (1997). Glutamate 286 in cytochrome aa3 from Rhodobacter sphaeroides is involved in proton uptake during the reaction of the fully-reduced enzyme with dioxygen. Biochemistry *36*, 13824-13829.

Adelroth, P., Gennis, R.B., and Brzezinski, P. (1998). Role of the pathway through K(I-362) in proton transfer in cytochrome c oxidase from R. sphaeroides. Biochemistry *37*, 2470-2476.

Adelroth, P., Karpefors, M., Gilderson, G., Tomson, F.L., Gennis, R., and Brzezinski, P. (2000). Proton transfer from glutamate 286 determines the transition rates between oxygen intermediates in cytochrome *c* oxidase. Biochimica et Biophysica Acta *1459*, 533-539.

Agmon, N. (1995). The Grotthuss mechanism. Chem Phys Lett *244*, 456-462.

Allen, T.M., Romans, A.Y., Kercret, H., and Segrest, J.P. (1980). Detergent removal during membrane reconstitution. Biochim Biophys Acta *601*, 328-342.

Antonini, E., Brunori, M., Colosimo, A., Greenwood, C., and Wilson, M.T. (1977). Oxygen "pulsed" cytochrome c oxidase: functional properties and catalytic relevance. Proc Natl Acad Sci U S A *74*, 3128-3132.

Babcock, G.T., and Callahan, P.M. (1983). Redox-Linked Hydrogen Bond Strength Changes in Cytochrome *a*: Implications for a Cytochrome Oxidase Proton Pump. Biochemistry *22*, 2314-2319.

Babcock, G.T., and Wikstrom, M. (1992). Oxygen activation and the conservation of energy in cell respiration. Nature *356*, 301-309.

Backgren, C., Hummer, G., Wikstrom, M., and Puustinen, A. (2000). Proton translocation by cytochrome *c* oxidase can take place without the conserved glutamic acid in subunit I. Biochemistry *39*, 7863-7867.

Bailey, J.A., Tomson, F.L., Mecklenburg, S.L., MacDonald, G.M., Katsonouri, A., Puustinen, A., Gennis, R.B., Woodruff, W.H., and Dyer, R.B. (2002). Time-resolved step-scan Fourier transform infrared spectroscopy of the CO adducts of bovine cytochrome c oxidase and of cytochrome bo(3) from Escherichia coli. Biochemistry *41*, 2675-2683.

Barenholzt, Y., Amselem, S., and Lichtenberg, D. (1979). A new method for preparation of phospholipid vesicles (liposomes) - French press. FEBS Lett *99*, 210-214.

Behr, J., Hellwig, P., Mantele, W., and Michel, H. (1998). Redox dependent changes at the heme propionates in cytochrome c oxidase from Paracoccus denitrificans: direct evidence from FTIR difference spectroscopy in combination with heme propionate 13C labeling. Biochemistry *37*, 7400-7406.

Behr, J., Michel, H., Mantele, W., and Hellwig, P. (2000). Functional properties of the heme propionates in cytochrome *c* oxidase from *Paracoccus denitrificans*. Evidence from FTIR difference spectroscopy and site-directed mutagenesis. Biochemistry *39*, 1356-1363.

Belevich, I., Tuukkanen, A., Wikstrom, M., and Verkhovsky, M.I. (2006). Proton-coupled electron equilibrium in soluble and membrane-bound cytochrome c oxidase from Paracoccus denitrificans. Biochemistry *45*, 4000-4006.

Blair, D.F., Gelles, J., and Chan, S.I. (1986). Redox-linked proton translocation in cytochrome oxidase: the importance of gating electron flow. The effects of slip in a model transducer. Biophysical journal *50*, 713-733.

Bloch, D., Belevich, I., Jasaitis, A., Ribacka, C., Puustinen, A., Verkhovsky, M.I., and Wikstrom, M. (2004). The catalytic cycle of cytochrome c oxidase is not the sum of its two halves. Proc Natl Acad Sci U S A *101*, 529-533.

Brand, M.D., Buckingham, J.A., Esteves, T.C., Green, K., Lambert, A.J., Miwa, S., Murphy, M.P., Pakay, J.L., Talbot, D.A., and Echtay, K.S. (2004). Mitochondrial

superoxide and aging: uncoupling-protein activity and superoxide production. Biochem Soc Symp, 203-213.

Branden, G., Branden, M., Schmidt, B., Mills, D.A., Ferguson-Miller, S., and Brzezinski, P. (2005). The protonation state of a heme propionate controls electron transfer in cytochrome c oxidase. Biochemistry *44*, 10466-10474.

Branden, G., Pawate, A.S., Gennis, R.B., and Brzezinski, P. (2006). Controlled uncoupling and recoupling of proton pumping in cytochrome c oxidase. Proc Natl Acad Sci U S A *103*, 317-322.

Branden, M., Sigurdson, H., Namslauer, A., Gennis, R.B., Adelroth, P., and Brzezinski, P. (2001). On the role of the K-proton transfer pathway in cytochrome c oxidase. Proc Natl Acad Sci U S A *98*, 5013-5018.

Branden, M., Tomson, F., Gennis, R.B., and Brzezinski, P. (2002). The entry point of the K-proton-transfer pathway in cytochrome c oxidase. Biochemistry *41*, 10794-10798.

Bratton, M., Pressler, M., and Hosler, J. (1999). Suicide inactivation of cytochrome c oxidase: Catalytic turnover in the absence of subunit III alters the active site. Biochemistry *38*, 16236-16245.

Brown, G.C., and Brand, M.D. (1991). On the nature of the mitochondrial proton leak. Biochim Biophys Acta *1059*, 55-62.

Brunori, M., Giuffre, A., and Sarti, P. (2005). Cytochrome c oxidase, ligands and electrons. Journal of inorganic biochemistry *99*, 324-336.

Brunori, M., Sarti, P., Colosimo, A., Antonini, G., Malatesta, F., Jones, M.G., and Wilson, M.T. (1985). Mechanism of control of cytochrome oxidase activity by the electrochemical-potential gradient. Embo J *4*, 2365-2368.

Brzezinski, P., and Adelroth, P. (1998). Pathways of proton transfer in cytochrome c oxidase. Journal of bioenergetics and biomembranes *30*, 99-107.

Brzezinski, P., and Larsson, G. (2003). Redox-driven proton pumping by heme-copper oxidases. Biochim Biophys Acta *1605*, 1-13.

Buse, G., Soulimane, T., Dewor, M., Meyer, H.E., and Bluggel, M. (1999). Evidence for a Copper-Coordinated Histidine-tyrosine Cross-link in the Active Site of Cytochrome c Oxidase. Protein Science *8*, 985-990.

Busenlehner, L.S., and Armstrong, R.N. (2005). Insights into enzyme structure and dynamics elucidated by amide H/D exchange mass spectrometry. Archives of biochemistry and biophysics *433*, 34-46.

Busenlehner, L.S., Branden, G., Namslauer, I., Brzezinski, P., and Armstrong, R.N. (2008). Structural elements involved in proton translocation by cytochrome c oxidase as revealed by backbone amide hydrogen-deuterium exchange of the E286H mutant. Biochemistry *47*, 73-83.

Busenlehner, L.S., Salomonsson, L., Brzezinski, P., and Armstrong, R.N. (2006). Mapping protein dynamics in catalytic intermediates of the redox-driven proton pump cytochrome c oxidase. Proc Natl Acad Sci U S A *103*, 15398-15403.

Butko, P., and Nicholls, P. (1993). Protons, Pumps, and Potentials: Control of Cytochrome Oxidase. Journal of bioenergetics and biomembranes *25*, 137.

Cann, J.R. (1970). Interacting Macromolecules: The theory and Practice of Their Electrophoresis, Ultracentrifugation, and Chromatograhy (New York and London, Academic Press).

Capitanio, N., Capitanio, G., Demarinis, D.A., De Nitto, E., Massari, S., and Papa, S. (1996). Factors affecting the H+/e- stoichiometry in mitochondrial cytochrome c oxidase: influence of the rate of electron flow and transmembrane delta pH. Biochemistry *35*, 10800-10806.

Casey, R.P., O'Shea, P.S., Chappell, J.B., and Azzi, A. (1984). A Quantitative Characterization of H^+ Translocation by Cytochrome *c* Oxidase Vesicles. Biochim Biophys Acta *765*, 30-37.

Chan, S.I., and Li, P.M. (1990). Cytochrome *c* Oxidase: Understanding Nature's Design of a Proton Pump. Biochemistry *29*, 1-12.

Checover, S., Marantz, Y., Nachliel, E., Gutman, M., Pfeiffer, M., Tittor, J., Oesterhelt, D., and Dencher, N.A. (2001). Dynamics of the proton transfer reaction on the cytoplasmic surface of bacteriorhodopsin. Biochemistry *40*, 4281-4292.

Cherny, V., and DeCoursey, T. (1999). pH-dependent inhibition of voltage-gated H+ currents in rat alveolar epithelial cells by Zn^{2+} and other divalent cations. J Gen Physiol *114*, 819-838.

Clement, N.R., and Gould, J.M. (1981). Pyranine (8-hydroxy-1,3,6-pyrenetrisulfonate) as a probe of internal aqueous hydrogen ion concentration in phospholipid vesicles. Biochemistry *20*, 1534-1538.

Collman, J.P., Devaraj, N.K., Decreau, R.A., Yang, Y., Yan, Y.L., Ebina, W., Eberspacher, T.A., and Chidsey, C.E. (2007). A cytochrome C oxidase model catalyzes oxygen to water reduction under rate-limiting electron flux. Science *315*, 1565-1568.

Cukier, R.I. (2004). Quantum molecular dynamics simulation of proton transfer in cytochrome *c* oxidase. Biochim Biophys Acta *1656*, 189-202.

Cukier, R.I. (2005). A molecular dynamics study of water chain formation in the proton conduction K channel of cytochrome *c* oxidase. Biochim Biophys Acta *1706*, 134-146.

Darszon, A., Vandenberg, C.A., Ellisman, M.H., and Montal, M. (1979). Incorporation of membrane proteins into large single bilayer vesicles. Application to rhodopsin. The Journal of cell biology *81*, 446-452.

Davis, R.E., Miller, S., Herrnstadt, C., Ghosh, S.S., Fahy, E., Shinobu, L.A., Galasko, D., Thal, L.J., Beal, M.F., Howell, N., *et al.* (1997). Mutations in mitochondrial cytochrome c oxidase genes segregate with late-onset Alzheimer disease. Proc Natl Acad Sci U S A *94*, 4526-4531.

de Grotthuss, C.J.T. (1806). Sur la decomposition de l'eau et des corps qu'elle tient en dissolution a l'aide de l'electricite galvanique. Annales de Chimie (Paris) *LVIII*, 54-74.

DeCoursey, T. (2003). Voltage-gated channels and and other proton transfer pathways. Physiol Rev *83*, 475-579.

Dellago, C., Naor, M.M., and Hummer, G. (2003). Proton transport through water-filled carbon nanotubes. Phys Rev Lett *90*, 105902.

Dioumaev, A.K., Richter, H.T., Brown, L.S., Tanio, M., Tuzi, S., Saito, H., Kimura, Y., Needleman, R., and Lanyi, J.K. (1998). Existence of a proton transfer chain in bacteriorhodopsin: participation of Glu-194 in the release of protons to the extracellular surface. Biochemistry *37*, 2496-2506.

Dolder, M., Engel, A., and Zulauf, M. (1996). The micelle to vesicle transition of lipids and detergents in the presence of a membrane protein: towards a rationale for 2D crystallization. FEBS Lett *382*, 203-208.

Durham, B., Pan, L.P., Long, J.E., and Millett, F. (1989). Photoinduced electron-transfer kinetics of singly labeled ruthenium bis(bipyridine) dicarboxybipyridine cytochrome c derivatives. Biochemistry *28*, 8659-8665.

Errede, B., and Kamen, M.D. (1978). Comparative kinetic studies of cytochromes c in reactions with mitochondrial cytochrome c oxidase and reductase. Biochemistry *17*, 1015-1027.

Espe, M.P., Hosler, J.P., Ferguson-Miller, S., Babcock, G.T., and McCracken, J. (1995). A Continuous Wave and Pulsed EPR Characterization of the Mn^{2+} Binding Site in *Rhodobacter sphaeroides* Cytochrome *c* Oxidase. Biochemistry *34*, 7593-7602.

Fabian, M., Wong, W.W., Gennis, R.B., and Palmer, G. (1999). Mass spectrometric determination of dioxygen bond splitting in the "peroxy" intermediate of cytochrome c oxidase. Proc Natl Acad Sci U S A *96*, 13114-13117.

Faxen, K., and Brzezinski, P. (2007). The inside pH determines rates of electron and proton transfer in vesicle-reconstituted cytochrome c oxidase. Biochim Biophys Acta *1767*, 381-386.

Faxen, K., Gilderson, G., Adelroth, P., and Brzezinski, P. (2005). A mechanistic principle for proton pumping by cytochrome c oxidase. Nature *437*, 286-289.

Ferguson-Miller, S., and Babcock, G. (1996). Heme/copper terminal oxidases. Chemical Reviews *96*, 2889-2907.

Ferguson-Miller, S., Brautigan, D., and Margoliash, E. (1976). Correlation of the Kinetics of Electron Transfer Activity of Various Eukaryotic Cytochrome c with Binding to Mitochondrial Cytochrome c Oxidase. J Biol Chem *251*, 1104-1115.

Ferguson-Miller, S., Brautigan, D.L., and Margoliash, E. (1978). Definition of Cytochrome c Binding Domains by Chemical Modification. J Biol Chem *253*, 149-159.

Fetter, J., Sharpe, M., Qian, J., Mills, D., Ferguson-Miller, S., and Nicholls, P. (1996). Fatty acids stimulate activity and restore respiratory control in a proton channel mutant of cytochrome c oxidase. FEBS Lett *393*, 155-160.

Fetter, J.R., Qian, J., Shapleigh, J., Thomas, J.W., Garcia-Horsman, A., Schmidt, E., Hosler, J., Babcock, G.T., Gennis, R.B., and Ferguson-Miller, S. (1995). Possible proton relay pathways in cytochrome c oxidase. Proc Natl Acad Sci U S A *92*, 1604-1608.

Florens, L., Schmidt, B., McCracken, J., and Ferguson-Miller, S. (2001). Fast deuterium access to the buried magnesium/manganese site in cytochrome c oxidase. Biochemistry *40*, 7491-7497.

Forte, E., Scandurra, F., Richter, O.-M.H., D'Itri, E., Sarti, P., Brunori, M., Ludwig, B., and Giuffre, A. (2004). Proton uptake upon anaerobic reduction of *Paracoccus denitrificans* cytochrome *c* oxidase: A kinetic investigation of the K354M and D124N mutants. Biochemistry *43*, 2957-2963.

Francia, F., Giachini, L., Boscherini, F., Venturoli, G., Capitanio, G., Martino, P.L., and Papa, S. (2007). The inhibitory binding site(s) of Zn2+ in cytochrome c oxidase. FEBS Lett *581*, 611-616.

García-Horsman, J., Barquera, B., Rumbley, J., Ma, J., and Gennis, R.B. (1994). The Superfamily of Heme-Copper Respiratory Oxidases. J Bacteriol *176*, 5587-5600.

Gelles, J., Blair, D.F., and Chan, S.I. (1986). The proton-pumping site of cytochrome c oxidase: a model of its structure and mechanism. Biochim Biophys Acta *853*, 205-236.

Gennis, R., and Ferguson-Miller, S. (1995). Structure of Cytochrome *c* Oxidase, Energy Generator of Aerobic Life. Science *269*, 1063-1064.

Gennis, R.B. (1998). Cytochrome oxidase:one proton, two mechanism? Science *280*, 1712-1713.

Georgievskii, Y., Medvedev, E.S., and Stuchebrukhov, A.A. (2002). Proton transport via the membrane surface. Biophysical journal *82*, 2833-2846.

Geren, L.M., Beasley, J.R., Fine, B.R., Saunders, A.J., Hibdon, S., Pielak, G.J., Durham, B., and Millett, F. (1995). Design of a ruthenium-cytochrome *c* derivative to measure electron transfer to the initial acceptor in cytochrome *c* oxidase. J Biol Chem *270*, 2466 - 2662.

Gilderson, G., Salomonsson, L., Aagaard, A., Gray, J., Brzezinski, P., and Hosler, J. (2003). Subunit III of cytochrome c oxidase of Rhodobacter sphaeroides is required to maintain rapid proton uptake through the D pathway at physiologic pH. Biochemistry *42*, 7400-7409.

Gorbikova, E.A., Belevich, I., Wikstrom, M., and Verkhovsky, M.I. (2008). The proton donor for O-O bond scission by cytochrome c oxidase. Proc Natl Acad Sci U S A *105*, 10733-10737.

Gregory, L., and Ferguson-Miller, S. (1989). Independent control of respiration in cytochrome *c* oxidase vesicles by pH and electrical gradients. Biochemistry *28*, 2655-2662.

Gregory, L.C., and Ferguson-Miller, S. (1988). Effect of Subunit III Removal on Control of Cytochrome *c* Oxidase Activity by pH. Biochemistry *27*, 6307-6314.

Gutman, M., and Nachliel, E. (1990). The dynamic aspects of proton transfer processes. Biochem Biophys Acta *1015*, 391-414.

Haltia, T., Finel, M., Harms, N., Nakari, T., Raitio, M., Wikstrom, M., and Saraste, M. (1989). Deletion of the gene for subunit III leads to defective assembly of bacterial cytochrome oxidase. Embo J *8*, 3571-3579.

Haltia, T., Saraste, M., and Wikstrom, M. (1991). Subunit III of cytochrome c oxidase is not involved in proton translocation: a site-directed mutagenesis study. Embo J *10*, 2015-2021.

Han, D., Morgan, J.E., and Gennis, R.B. (2005). G204D, a mutation that blocks the proton-conducting D-channel of the aa3-type cytochrome c oxidase from Rhodobacter sphaeroides. Biochemistry *44*, 12767-12774.

Han, D., Namslauer, A., Pawate, A., Morgan, J.E., Nagy, S., Vakkasoglu, A.S., Brzezinski, P., and Gennis, R.B. (2006). Replacing Asn207 by aspartate at the neck of the D channel in the aa3-type cytochrome c oxidase from Rhodobacter sphaeroides results in decoupling the proton pump. Biochemistry *45*, 14064-14074.

Han, S.H., Ching, Y.C., and Rousseau, D.L. (1990). Cytochrome c oxidase: decay of the primary oxygen intermediate involves direct electron transfer from cytochrome a. Proc Natl Acad Sci U S A *87*, 8408-8412.

Harrenga, A., and Michel, H. (1999). The cytochrome c oxidase from Paracoccus denitrificans does not change the metal center ligation upon reduction. J Biol Chem *274*, 33296-33299.

Hinkle, P.C., Kim, J.J., and Racker, E. (1972). Ion Transport and Respiratory Control in Vesicles Formed From Cytochrome Oxidase and Phospholipids. J Biol Chem *247*, 1338-1339.

Hiser, C., Mills, D.A., Schall, M., and Ferguson-Miller, S. (2001). C-terminal truncation and histidine-tagging of cytochrome *c* oxidase subunit II reveals the native processing site, shows involvement of the C-terminus in cytochrome *c* binding, and improves the assay for proton pumping. Biochemistry *40*, 1606-1615.

Hofacker, I., and Schulten, K. (1998). Oxygen and proton pathways in cytochrome c oxidase. Proteins *30*, 100-107.

Hosler, J.P. (2004). The influence of subunit III of cytochrome c oxidase on the D pathway, the proton exit pathway and mechanism-based inactivation in subunit I. Biochim Biophys Acta *1655*, 332-339.

Hosler, J.P., Espe, M.P., Zhen, Y., Babcock, G.T., and Ferguson-Miller, S. (1995). Analysis of site-directed mutants locates a non-redox-active metal near the active site of cytochrome *c* oxidase of *Rhodobacter sphaeroides*. Biochemistry *34*, 7586-7592.

Hosler, J.P., Ferguson-Miller, S., Calhoun, M.W., Thomas, J.W., Hill, J., Lemieux, L., Ma, J., Georgiou, C., Fetter, J., Shapleigh, J., *et al.* (1993). Insight into the active-site structure and function of cytochrome oxidase by analysis of site-directed mutants of bacterial cytochrome aa3 and cytochrome bo. Journal of bioenergetics and biomembranes *25*, 121-136.

Hosler, J.P., Ferguson-Miller, S., and Mills, D.A. (2006). Energy Transduction: Proton Transfer Through the Respiratory Complexes. Annu Rev Biochem.

Hosler, J.P., Fetter, J., Tecklenburg, M.M., Espe, M., Lerma, C., and Ferguson-Miller, S. (1992). Cytochrome aa3 of Rhodobacter sphaeroides as a model for mitochondrial cytochrome c oxidase. Purification, kinetics, proton pumping, and spectral analysis. J Biol Chem *267*, 24264-24272.

Iwaki, M., Puustinen, A., Wikstrom, M., and Rich, P.R. (2003). ATR-FTIR Spectroscopy of the P(M) and F Intermediates of Bovine and Paracoccus denitrificans Cytochrome c Oxidase. Biochemistry *42*, 8809-8817.

Iwata, S., Ostermeier, C., Ludwig, B., and Michel, H. (1995). Structure at 2.8 A resolution of cytochrome c oxidase from Paracoccus denitrificans. Nature *376*, 660-669.

Jasaitis, A., Verkhovsky, M.I., Morgan, J.E., Verkhovskaya, M.L., and Wikstrom, M. (1999). Assignment and charge translocation stoichiometries of the major electrogenic phases in the reaction of cytochrome c oxidase with dioxygen. Biochemistry *38*, 2697-2706.

Junemann, S., Heathcote, P., and Rich, P.R. (2000). The reactions of hydrogen peroxide with bovine cytochrome c oxidase. Biochim Biophys Acta *1456*, 56-66.

Junemann, S., Meunier, B., Gennis, R.B., and Rich, P.R. (1997). Effects of Mutation of the Conserved Lysine-362 in Cytochrome c Oxidase from Rhodobacter sphaeroides. Biochemistry *36*, 14456-14464.

Kadenbach, B. (2003). Intrinsic and extrinsic uncoupling of oxidative phosphorylation. Biochim Biophys Acta *1604*, 77-94.

Kadenbach, B., Kuhn-Nentwig, L., and Buge, U. (1987). Curr Topics Bioenergetics *15*, 113 -161.

Kagawa, Y., Kandrach, A., and Racker, E. (1973). Partial resolution of the enzymes catalyzing oxidative phosphorylation. XXVI. Specificity of phospholipids required for energy transfer reactions. J Biol Chem *248*, 676-684.

Kagawa, Y., and Racker, E. (1971). Partial Resolution of the Enzymes Catalyzing Oxidative Phosphorylation: XXV Reconstitution of Vesicles Catalyzing $^{32}P_i$-Adenosine Triphosphate Exchange. J Biol Chem *246*, 5477-5487.

Kannt, A., Lancaster, C.R., and Michel, H. (1998a). The coupling of electron transfer and proton translocation: electrostatic calculations on *Paracoccus denitrificans* cytochrome *c* oxidase. Biophysical journal *74*, 708-721.

Kannt, A., Soulimane, T., Buse, G., Becker, A., Bamberg, E., and Michel, H. (1998b). Electrical current generation and proton pumping catalyzed by the ba_3- type cytochrome *c* oxidase from Thermus thermophilus. FEBS Lett *434*, 17-22.

Karpefors, M., Adelroth, P., and Brzezinski, P. (2000a). Localized control of proton transfer through the D-pathway in cytochrome *c* oxidase: Application of the proton inventory technique. Biochemistry *39*, 6850-6856.

Karpefors, M., Adelroth, P., Namslauer, A., Zhen, Y., and Brzezinski, P. (2000b). Formation of the "peroxy" intermediate in cytochrome c oxidase is associated with internal proton/hydrogen transfer. Biochemistry *39*, 14664-14669.

Karpefors, M., Adelroth, P., Zhen, Y., Ferguson-Miller, S., and Brzezinski, P. (1998). Proton uptake controls electron transfer in cytochrome *c* oxidase. Proc Natl Acad Sci USA *95*, 13606-13611.

Kasahara, M., and Hinkle, P.C. (1976). Reconstitution of D-glucose transport catalyzed by a protein fraction from human erythrocytes in sonicated liposomes. Proc Natl Acad Sci U S A *73*, 396-400.

Kasahara, M., and Hinkle, P.C. (1977). Reconstitution and purification of the D-glucose transporter from human erythrocytes. J Biol Chem *252*, 7384-7390.

Kell, D.B., John, P., and Ferguson, S.J. (1978). On the current-voltage relationships of energy-transducing membranes: phosphorylating membrane vesicles from Paracoccus denitrificans [proceedings]. Biochemical Society transactions *6*, 1292-1295.

Kirichenko, A., Vygodina, T., Mkrtchyan, H.M., and Konstantinov, A. (1998). Specific cation binding site in mammalian cytochrome c oxidase. FEBS Lett *423*, 329-333.

Kitagawa, T., and Ogura, T. (1998). Time-resolved resonance Raman investigation of oxygen reduction mechanism of bovine cytochrome c oxidase. Journal of bioenergetics and biomembranes *30*, 71-79.

Konstantinov, A.A., Siletsky, S., Mitchell, D., Kaulen, A., and Gennis, R.B. (1997). The roles of the two proton input channels in cytochrome c oxidase from Rhodobacter sphaeroides probed by the effects of site-directed mutations on time-resolved electrogenic intraprotein proton transfer. Proc Natl Acad Sci U S A *94*, 9085-9090.

Kornblatt, J.A. (1998). The water channel of cytochrome c oxidase: inferences from inhibitor studies. Biophysical journal *75*, 3127-3134.

Krishnamoorthy, G., and Hinkle, P.C. (1984). Non-ohmic proton conductance of mitochondria and liposomes. Biochemistry *23*, 1640-1645.

Lam, E., and Tu, S.I. (1980). Effects of monovalent cations on the activities associated with coupling site III of rat liver mitochondria. Biochemical and biophysical research communications *96*, 196-202.

Lancaster, C.R.D. (2003). The role of electrostatics in proton-conducting membrane protein complexes. FEBS Lett *545*, 52-60.

Lanyi, J.K. (1997). Mechanism of ion transport across membranes. Bacteriorhodopsin as a prototype for proton pumps. J Biol Chem *272*, 31209-31212.

Lanyi, J.K., and Luecke, H. (2001). Bacteriorhodopsin. Current opinion in structural biology *11*, 415-419.

Lee, A., Kirichenko, A., Vygodina, T., Siletsky, S.A., Das, T.K., Rousseau, D.L., Gennis, R., and Konstantinov, A.A. (2002). Ca(2+)-binding site in Rhodobacter sphaeroides cytochrome C oxidase. Biochemistry *41*, 8886-8898.

Lee, H.-M., Das, T., Rousseau, D., Mills, D., Ferguson-Miller, S., and Gennis, R. (2000). Mutations in the putative H-channel in the cytochrome *c* Oxidase from *Rhodobacter sphaeroides* show that this channel is not important for proton conduction but reveal modulation of the properties of heme *a*. Biochemistry *39*, 2989-2996.

Levy, D., Bluzat, A., Seigneuret, M., and Rigaud, J.L. (1990). A systematic study of liposome and proteoliposome reconstitution involving Bio-Bead-mediated Triton X-100 removal. Biochim Biophys Acta *1025*, 179-190.

Lubben, M., Prutsch, A., Mamat, B., and Gerwert, K. (1999). Electron Transfer Induces Side-Chain Changes of Glutamate-286 from Cytochrome bo_3. Biochemistry *38*, 2048-2056.

Ludwig, B., Bender, E., Arnold, S., Huttemann, M., Lee, I., and Kadenbach, B. (2001). Cytochrome *c* oxidase and the regulation of oxidative phosphorylation. Chembiochem *2*, 392-403.

MacMillan, F., Budiman, K., Angerer, H., and Michel, H. (2006). The role of tryptophan 272 in the Paracoccus denitrificans cytochrome c oxidase. FEBS Lett *580*, 1345-1349.

Madden, T.D., Hope, M.J., and Cullis, P.R. (1984). Influence of vesicle size and oxidase content on respiratory control in reconstituted cytochrome oxidase vesicles. Biochemistry *23*, 1413-1418.

Malmstrom, B.G. (1985). Cytochrome c oxidase as a proton pump: A transition-state mechanism. Biochim Biophys Acta *811*, 1-12.

Marantz, Y., Einarsdottir, O.O., Nachliel, E., and Gutman, M. (2001). Proton-collecting properties of bovine heart cytochrome C oxidase: kinetic and electrostatic analysis. Biochemistry *40*, 15086-15097.

Marantz, Y., Nachliel, E., Aagaard, A., Brzezinski, P., and Gutman, M. (1998). The Proton Collecting Function of the Inner Surface of Cytochrome *c* Oxidase from *Rhodobacter sphaeroides*. Proc Natl Acad Sci USA *95*, 8590-8595.

Millett, F., de Jong, C., Paulson, L., and Capaldi, R.A. (1983). Identification of Specific Carboxylate Groups on Cytochrome *c* Oxidase That are Involved in Binding Cytochrome *c*. Biochemistry *22*, 546-552.

Millett, F., and Durham, B. (2002). Design of photoactive ruthenium complexes to study interprotein electron transfer. Biochemistry *41*, 11315-11324.

Millett, F., Schmidt, B., Durham, B., Geren, L., and Ferguson-Miller, S. Unpublished.

Mills, D.A., and Ferguson-Miller, S. (1998). Proton uptake and release in cytochrome c oxidase:seperate pathways in time and space? Biochimica et Biophysica Acta *1365*, 46-52.

Mills, D.A., and Ferguson-Miller, S. (2002). Influence of structure, pH and membrane potential on proton movement in cytochrome *c* oxidase. Biochim Biophys Acta *1555*, 96-100.

Mills, D.A., and Ferguson-Miller, S. (2003). Understanding the mechanism of proton movement linked to oxygen reduction in cytochrome *c* oxidase: Lessons from other proteins. FEBS Lett *545*, 47-51.

Mills, D.A., Florens, L., Hiser, C., Qian, J., and Ferguson-Miller, S. (2000). Where is 'outside' in cytochrome c oxidase and how and when do protons get there? Biochim Biophys Acta *1458*, 180-187.

Mills, D.A., Geren, L., Hiser, C., Schmidt, B., Durham, B., Millett, F., and Ferguson-Miller, S. (2005). An arginine to lysine mutation in the vicinity of the heme propionates affects the redox potentials of the hemes and associated electron and proton transfer in cytochrome *c* oxidase. Biochemistry *44*, 10457-10465.

Mills, D.A., and Hosler, J.P. (2005). Slow proton transfer through the pathways for pumped protons in cytochrome *c* oxidase induces suicide inactivation of the enzyme. Biochemistry *44*, 4656-4666.

Mills, D.A., Schmidt, B., Hiser, C., Westley, E., and Ferguson-Miller, S. (2002). Membrane potential-controlled inhibition of cytochrome *c* oxidase by zinc. J Biol Chem *277*, 14894-14901.

Mills, D.A., Tan, Z., Ferguson-Miller, S., and Hosler, J. (2003). A role for subunit III in proton uptake into the D pathway and a possible proton exit pathway in Rhodobacter sphaeroides cytochrome c oxidase. Biochemistry *42*, 7410-7417.

Mills, D.A., Xu, S., Geren, L., Hiser, C., Qin, L., Sharpe, M.A., McCracken, J., Durham, B., Millett, F., and Ferguson-Miller, S. (2008). Proton-dependent electron transfer from CuA to heme a and altered EPR spectra in mutants close to heme a of cytochrome oxidase. Biochemistry *47*, 11499-11509.

Mitchell, R., and Rich, P.R. (1994). Proton uptake by cytochrome c oxidase on reduction and on ligand binding. Biochim Biophys Acta *1186*, 19-26.

Moody, A.J., von Germar, F., Mantele, W., and Rich, P.R. (1995). Rapid-scan FTIR spectroscopic studies on the photolysis and recombination of the cyanide adduct of fully reduced bovine cytochrome c oxidase. Biochemical Society transactions *23*, 521S.

Morgan, J.E., Verkhovsky, M.I., Palmer, G., and Wikstrom, M. (2001). Role of the PR intermediate in the reaction of cytochrome c oxidase with O2. Biochemistry *40*, 6882-6892.

Morgan, J.E., Verkhovsky, M.I., and Wikstrom, M. (1994). The histidine cycle: a new model for proton translocation in the respiratory heme-copper oxidases. Journal of bioenergetics and biomembranes *26*, 599-608.

Moroney, P.M., Scholes, T.A., and Hinkle, P.C. (1984). Effect of membrane potential and pH gradient on electron transfer in cytochrome oxidase. Biochemistry *23*, 4991-4997.

Moser, C.C., Farid, T.A., Chobot, S.E., and Dutton, P.L. (2006). Electron tunneling chains of mitochondria. Biochim Biophys Acta *1757*, 1096-1109.

Muramoto, K., Hirata, K., Shinzawa-Itoh, K., Yoko-o, S., Yamashita, E., Aoyama, H., Tsukihara, T., and Yoshikawa, S. (2007). A histidine residue acting as a controlling site for dioxygen reduction and proton pumping by cytochrome c oxidase. Proc Natl Acad Sci U S A *104*, 7881-7886.

Murphy, M.P. (1989). Slip and leak in mitochondrial oxidative phosphorylation. Biochim Biophys Acta *977*, 123-141.

Murphy, M.P., and Brand, M.D. (1987). Variable stoichiometry of proton pumping by the mitochondrial respiratory chain. Nature *329*, 170-172.

Namslauer, A., Aagaard, A., Katsonouri, A., and Brzezinski, P. (2003). Intramolecular proton-transfer reactions in a membrane-bound proton pump: the effect of pH on the peroxy to ferryl transition in cytochrome c oxidase. Biochemistry *42*, 1488-1498.

Namslauer, A., Branden, M., and Brzezinski, P. (2002). The rate of internal heme-heme electron transfer in cytochrome C oxidase. Biochemistry *41*, 10369-10374.

Namslauer, A., and Brzezinski, P. (2004). Structural elements involved in electron-coupled proton transfer in cytochrome c oxidase. FEBS Lett *567*, 103-110.

Namslauer, A., Lepp, H., Branden, M., Jasaitis, A., Verkhovsky, M.I., and Brzezinski, P. (2007). Plasticity of proton pathway structure and water coordination in cytochrome c oxidase. J Biol Chem *282*, 15148-15158.

Nicholls, D.G. (1974). The influence of respiration and ATP hydrolysis on the proton-electrochemical gradient across the inner membrane of rat-liver mitochondria as determined by ion distribution. European journal of biochemistry / FEBS *50*, 305-315.

Nicholls, P. (1975). The effect of sulphide on cytochrome aa3. Isosteric and allosteric shifts of the reduced alpha-peak. Biochim Biophys Acta *396*, 24-35.

Nicholls, P., Hildebrandt, V., and Wrigglesworth, J. (1980). Orientation and reactivity of cytochrome aa_3 heme groups in proteoliposomes. Arch Biochem Biophys *204*, 533-543.

Nilsson, T., Hallen, S., and Oliveberg, M. (1990). Rapid Proton Release During Flash-induced Oxidation of Cytochrome *c* Oxidase. FEBS Lett *260*, 45-47.

Nyquist, R.M., Heitbrink, D., Bolwien, C., Gennis, R.B., and Heberle, J. (2003). Direct observation of protonation reactions during the catalytic cycle of cytochrome c oxidase. Proc Natl Acad Sci U S A *100*, 8715-8720.

Okuno, D., Iwase, T., Shinzawa-Itoh, K., Yoshikawa, S., and Kitagawa, T. (2003). FTIR detection of protonation/deprotonation of key carboxyl side chains caused by redox change of the Cu(A)-heme a moiety and ligand dissociation from the heme a3-Cu(B) center of bovine heart cytochrome c oxidase. J Am Chem Soc *125*, 7209-7218.

Oliveberg, M., Brzezinski, P., and Malmstrom, B.G. (1989). The effect of pH and temperature on the reaction of fully reduced and mixed-valence cytochrome c oxidase with dioxygen. Biochim Biophys Acta *977*, 322-328.

Oliveberg, M., Hallen, S., and Nilsson, T. (1991). Uptake and Release of Protons During the Reaction Between Cytochrome *c* Oxidase and Molecular Oxygen: A Flow-Flash Investigation. Biochemistry *30*, 436-440.

Olkhova, E., Hutter, M.C., Lill, M.A., Helms, V., and Michel, H. (2004). Dynamic water networks in cytochrome C oxidase from Paracoccus denitrificans investigated by molecular dynamics simulations. Biophysical journal *86*, 1873-1889.

Olsson, M.H., Sharma, P.K., and Warshel, A. (2005). Simulating redox coupled proton transfer in cytochrome c oxidase: looking for the proton bottleneck. FEBS Lett *579*, 2026-2034.

Ostermeier, C., Harrenga, A., Ermler, U., and Michel, H. (1997). Structure at 2.7 A resolution of the Paracoccus denitrificans two-subunit cytochrome c oxidase complexed with an antibody FV fragment. Proc Natl Acad Sci U S A *94*, 10547-10553.

Paradies, G., Ruggiero, F.M., Petrosillo, G., and Quagliariello, E. (1997). Age-dependent decline in the cytochrome c oxidase activity in rat heart mitochondria: role of cardiolipin. FEBS Lett *406*, 136-138.

Pawate, A.S., Morgan, J., Namslauer, A., Mills, D., Brzezinski, P., Ferguson-Miller, S., and Gennis, R.B. (2002). A mutation in subunit I of cytochrome oxidase from *Rhodobacter sphaeroides* results in an increase in steady-state activity but completely eliminates proton pumping. Biochemistry *41*, 13417-13423.

Peiffer, W.E., Ingle, R.T., and Ferguson-Miller, S. (1990). Structurally unique plant cytochrome c oxidase isolated from wheat germ, a rich source of plant mitochondrial enzymes. Biochemistry *29*, 8696-8701.

Pfitzner, U., Hoffmeier, K., Harrenga, A., Kannt, A., Michel, H., Bamberg, E., Richter, O.M., and Ludwig, B. (2000). Tracing the D-pathway in reconstituted site-directed mutants of cytochrome *c* oxidase from *Paracoccus denitrificans*. Biochemistry *39*, 6756-6762.

Pfitzner, U., Odenwald, A., Ostermann, T., Weingard, L., Ludwig, B., and Richter, O.M. (1998). Cytochrome c oxidase (heme aa3) from Paracoccus denitrificans: analysis of mutations in putative proton channels of subunit I. Journal of bioenergetics and biomembranes *30*, 89-97.

Pick, U. (1981). Liposomes with a large trapping capacity prepared by freezing and thawing of sonicated phospholipid mixtures. Archives of biochemistry and biophysics *212*, 186-194.

Pomes, R., Hummer, G., and M, W. (1998). Structure and dynamics of a proton shuttle in cytochrome *c* oxidase. Biochim Biophys Acta *1365*, 255-260.

Popovic, D.M., and Stuchebrukhov, A.A. (2004). Proton pumping mechanism and catalytic cycle of cytochrome c oxidase: Coulomb pump model with kinetic gating. FEBS Lett *566*, 126-130.

Popovic, D.M., and Stuchebrukhov, A.A. (2005). Proton exit channels in bovine cytochrome *c* oxidase. JPhysChem B *109*, 1999-2006.

Prochaska, L.J., and Fink, P.S. (1987). On the role of Subunit III in proton translocation in cytochrome *c* oxidase. J Bioenerg Biomem *19*, 143-164.

Proshlyakov, D.A., Pressler, M.A., DeMaso, C., Leykam, J.F., DeWitt, D.L., and Babcock, G.T. (2000). Oxygen activation and reduction in respiration: involvement of redox-active tyrosine 244. Science *290*, 1588-1591.

Puustinen, A., Bailey, J.A., Dyer, R.B., Mecklenburg, S.L., Wikstrom, M., and Woodruff, W.H. (1997). Fourier transform infrared evidence for connectivity between Cu_B and glutamic acid 286 in cytochrome bo_3 from *Escherichia coli*. Biochemistry *36*, 13195-13200.

Puustinen, A., Finel, M., Virkki, M., and Wikstr?, M. (1989). Cytochrome *o(bo)* is a Proton Pump in *Paracoccus denitrificans* and *Escherichia coli*. FEBS Letters *249*, 163-167.

Puustinen, A., and Wikstrom, M. (1999a). Proton exit from the heme-copper oxidase of *Escherichia coli*. Proc Natl Acad Sci U S A *96*, 35-37.

Puustinen, A., and Wikstrom, M. (1999b). Proton Exit from the Heme-Copper Oxidase of Escherichia Coli. Proc Natl Acad Sci USA *96*, 35-37.

Qian, J., Mills, D.A., Geren, L., Wang, K., Hoganson, C.W., Schmidt, B., Hiser, C., Babcock, G.T., Durham, B., Millett, F., *et al.* (2004). Role of the conserved arginine pair in proton and electron transfer in cytochrome *c* oxidase. Biochemistry *43*, 5748-5756.

Qin, L. (2008). Unpublished.

Qin, L., Hiser, C., Mulichak, A., Garavito, R.M., and Ferguson-Miller, S. (2006). Identification of conserved lipid/detergent-binding sites in a high-resolution structure of the membrane protein cytochrome c oxidase. Proc Natl Acad Sci U S A *103*, 16117-16122.

Qin, L., Mills, D.A., Buhrow, L., Hiser, C., and Ferguson-Miller, S. (2008). A conserved steroid binding site in cytochrome C oxidase. Biochemistry *47*, 9931-9933.

Qin, L., Mills, D.A., Hiser, C., Murphree, A., Garavito, R.M., Ferguson-Miller, S., and Hosler, J. (2007). Crystallographic location and mutational analysis of Zn and Cd inhibitory sites and role of lipidic carboxylates in rescuing proton path mutants in cytochrome c oxidase. Biochemistry *46*, 6239-6248.

Racker, E., Violand, B., O'Neal, S., Alfonzo, M., and Telford, J. (1979). Reconstitution, a way of biochemical research; some new approaches to membrane-bound enzymes. Archives of biochemistry and biophysics *198*, 470-477.

Rich, P.R. (1995). Toward under standing the chemistry of oxygen reduction and proton translocation in iron - copper respiratory oxidases. Aust J Plant Physiol *22*, 479 - 484.

Rich, P.R., and Breton, J. (2001). FTIR studies of the CO and cyanide adducts of fully reduced bovine cytochrome c oxidase. Biochemistry *40*, 6441-6449.

Rich, P.R., Junemann, S., and Meunier, B. (1998). Protonmotive mechanism of heme-copper oxidases. J Bioenerg Biomemb *30*, 131-138.

Richard, P., Pitard, B., and Rigaud, J.L. (1995). ATP synthesis by the F0F1-ATPase from the thermophilic Bacillus PS3 co-reconstituted with bacteriorhodopsin into liposomes. Evidence for stimulation of ATP synthesis by ATP bound to a noncatalytic binding site. J Biol Chem *270*, 21571-21578.

Rigaud, J.L., Bluzat, A., and Buschlen, S. (1983). Incorporation of bacteriorhodopsin into large unilamellar liposomes by reverse phase evaporation. Biochemical and biophysical research communications *111*, 373-382.

Rigaud, J.L., Levy, D., Mosser, G., and Lambert, O. (1998). Detergent removal by non-polar polystyrene beads Eur Biophys J *27*, 305-319.

Rigaud, J.L., Mosser, G., Lacapere, J.J., Olofsson, A., Levy, D., and Ranck, J.L. (1997). Bio-Beads: an efficient strategy for two-dimensional crystallization of membrane proteins. Journal of structural biology *118*, 226-235.

Rigaud, J.L., Paternostre, M.T., and Bluzat, A. (1988). Mechanisms of membrane protein insertion into liposomes during reconstitution procedures involving the use of detergents. 2. Incorporation of the light-driven proton pump bacteriorhodopsin. Biochemistry *27*, 2677-2688.
Rigaud, J.L., Pitard, B., and Levy, D. (1995). Reconstitution of membrane proteins into liposomes: application to energy-transducing membrane proteins. Biochim Biophys Acta *1231*, 223-246.

Riistama, S., Hummer, G., Puustinen, A., Dyer, R.B., Woodruff, W.H., and Wikstrom, M. (1997). Bound water in the proton translocation mechanism of the haem-copper oxidases. FEBS Lett *414*, 275-280.

Riistama, S., Puustinen, A., Garcia-Horsman, A., Iwata, S., Michel, H., and Wikstrom, M. (1996). Channelling of Dioxygen into the Respiratory Enzyme. Biochim et Biophys Acta *1275*, 1-4.

Riistama, S., Puustinen, A., Verkhovsky, M.I., Morgan, J.E., and Wikstrom, M. (2000). Binding of O(2) and its reduction are both retarded by replacement of valine 279 by isoleucine in cytochrome c oxidase from Paracoccus denitrificans. Biochemistry *39*, 6365-6372.

Roberts, V.A., and Pique, M.E. (1999). Definition of the interaction domain for cytochrome c on cytochrome c oxidase. III. Prediction of the docked complex by a complete, systematic search. J Biol Chem *274*, 38051-38060.

Roman, I., Figys, J., Steurs, G., and Zizi, M. (2005). In vitro interactions between the two mitochondrial membrane proteins VDAC and cytochrome c oxidase. Biochemistry *44*, 13192-13201.

Ruitenberg, M., Kannt, A., Bamberg, E., Fendler, K., and Michel, H. (2002). Reduction of cytochrome *c* oxidase by a second electron leads to proton translocation. Nature *417*.

Ruitenberg, M., Kannt, A., Bamberg, E., Ludwig, B., Michel, H., and Fendler, K. (2000). Single-electron reduction of the oxidized state is coupled to proton uptake via the K pathway in *Paracoccus denitrificans* cytochrome *c* oxidase. Proc Natl Acad Sci U S A *97*, 4632-4636.

Saari, H., Penttila, T., and Wikstrom, M. (1980). Interactions of Ca2+ and H+ with heme A in cytochrome oxidase. Journal of bioenergetics and biomembranes *12*, 325-338.

Salomonsson, L., Faxen, K., Adelroth, P., and Brzezinski, P. (2005). The timing of proton migration in membrane-reconstituted cytochrome c oxidase. Proc Natl Acad Sci U S A *102*, 17624-17629.

Sarti, P., Jones, M.G., Antonini, G., Malatesta, F., Colosimo, A., Wilson, M.T., and Brunori, M. (1985). Kinetics of Redox-Linked Proton Pumping Activity of Native and Subunit III-Depleted Cytochrome *c* Oxidase: A Stopped-Flow Investigation. Proc Natl Acad Sci USA *82*, 4876-4880.

Schmidt, B. (2003). Proton and water exit in cytochrome c oxidase. Ph.D. Thesis (Michigan State Univ. East Lansing. MI. USA).

Schmidt, B., Hillier, W., McCracken, J., and Ferguson-Miller, S. (2004). The use of stable isotopes and spectroscopy to investigate the energy transducing function of cytochrome c oxidase. Biochim Biophys Acta *1655*, 248-255.

Schmidt, B., McCracken, J., and Ferguson-Miller, S. (2003). A discrete water exit pathway in the membrane protein cytochrome c oxidase. Proc Natl Acad Sci U S A *100*, 15539-15542.

Schneider, H., Lemasters, J.J., Hochli, M., and Hackenbrock, C.R. (1980). Fusion of liposomes with mitochondrial inner membranes. Proc Natl Acad Sci U S A *77*, 442-446.

Schon, E.A., and Manfredi, G. (2003). Neuronal degeneration and mitochondrial dysfunction. The Journal of clinical investigation *111*, 303-312.

Schonfeld, M., and Neumann, J. (1977). Proton conductance of the thylakoid membrane: modulation by light. FEBS Lett *73*, 51-54.

Seibold, S.A., Mills, D.A., Ferguson-Miller, S., and Cukier, R.I. (2005). Water chain formation and possible proton pumping routes in *Rhodobacter sphaeroides* cytochrome *c* oxidase: A molecular dynamics comparison of the wildtype and R481K mutant. Biochemistry *44*, 10475-10485.

Sharpe, M.A., and Ferguson-Miller, S. (2008). A chemically explicit model for the mechanism of proton pumping in heme-copper oxidases. Journal of bioenergetics and biomembranes.

Sharpe, M.A., Qin, L., and Ferguson-Miller, S. (2005). Biophysical and Structural Aspects of Bioenergetics,. In, M. Wikstrom, ed. (Cambridge, Royal Society of Chemistry).

Sharpe, M.A., Wrigglesworth, J.M., Loewen, J., and Nicholls, P. (1995). Small pH Gradients Inhibit Cytochrome *c* Oxidase: Implications for H^+ Entry to the Binuclear Center. Biochem Biophys Res Commun *216*, 931-938.

Shimokata, K., Katayama, Y., Murayama, H., Suematsu, M., Tsukihara, T., Muramoto, K., Aoyama, H., Yoshikawa, S., and Shimada, H. (2007). The proton pumping pathway of bovine heart cytochrome c oxidase. Proc Natl Acad Sci U S A *104*, 4200-4205.

Shinzawa-Itoh, K., Aoyama, H., Muramoto, K., Terada, H., Kurauchi, T., Tadehara, Y., Yamasaki, A., Sugimura, T., Kurono, S., Tsujimoto, K., *et al.* (2007). Structures and physiological roles of 13 integral lipids of bovine heart cytochrome c oxidase. Embo J. Sigel, E., and Carafoli, E. (1978). The proton pump of cytochrome c oxidase and its stoichiometry. European journal of biochemistry / FEBS *89*, 119-123.

Siletsky, S.A., Han, D., Brand, S., Morgan, J.E., Fabian, M., Geren, L., Millett, F., Durham, B., Konstantinov, A.A., and Gennis, R.B. (2006). Single-electron photoreduction of the P(M) intermediate of cytochrome c oxidase. Biochim Biophys Acta *1757*, 1122-1132.

Siletsky, S.A., Pawate, A.S., Weiss, K., Gennis, R.B., and Konstantinov, A.A. (2004). Transmembrane charge separation during the ferryl-oxo -> oxidized transition in a nonpumping mutant of cytochrome c oxidase. J Biol Chem *279*, 52558-52565.

Sims, P.J., Waggoner, A.S., Wang, C.H., and Hoffman, J.F. (1974). Studies on the mechanism by which cyanine dyes measure membrane potential in red blood cells and phosphatidylcholine vesicles. Biochemistry *13*, 3315-3330.

Singh, A.P., Chanady, G.A., and Nicholls, P. (1985). Interactions involving the cyanine dye, diS-C3-(5), cytochrome c and liposomes and their implications for estimations of delta psi in cytochrome c oxidase-reconstituted proteoliposomes. J Membr Biol *84*, 183-190.

Singh, A.P., and Nicholls, P. (1985a). Cyanine and safranine dyes as membrane potential probes in cytochrome c oxidase reconstituted proteoliposomes. Journal of biochemical and biophysical methods *11*, 95-108.

Singh, A.P., and Nicholls, P. (1985b). Cyanine and Safranine Dyes as Membrane Potential Probes in Cytochrome *c* Oxidase Reconstituted Proteoliposomes. J Biochem Biophys Meth *11*, 95-108.

Soares, C.M., Baptista, A.M., Pereira, M.M., and Teixeira, M. (2004). Investigation of protonatable residues in Rhodothermus marinus caa3 haem-copper oxygen reductase: comparison with Paracoccus denitrificans aa3 haem-copper oxygen reductase. J Biol Inorg Chem *9*, 124-134.

Soulimane, T., Buse, G., Bourenkov, G.P., Bartunik, H.D., Huber, R., and Than, M.E. (2000). Structure and mechanism of the aberrant ba(3)-cytochrome c oxidase from thermus thermophilus. EMBO Journal *19*, 1766-1776.

Steverding, D., Kohnke, D., Ludwig, B., and Kadenbach, B. (1993). Proton slippage in cytochrome c oxidase of Paracoccus denitrificans. Membrane-potential measurements with the two-subunit and three-subunit enzyme. European journal of biochemistry / FEBS *212*, 827-831.

Svensson-Ek, M., Abramson, J., Larsson, G., Tornroth, S., Brzezinski, P., and Iwata, S. (2002). The X-ray crystal structures of wild-type and EQ(I-286) mutant cytochrome c oxidases from Rhodobacter sphaeroides. Journal of molecular biology *321*, 329-339.

Szoka, F., Jr., and Papahadjopoulos, D. (1978). Procedure for preparation of liposomes with large internal aqueous space and high capture by reverse-phase evaporation. Proc Natl Acad Sci U S A *75*, 4194-4198.

Tashiro, M., and Stuchebrukhov, A.A. (2005). Thermodynamic properties of internal water molecules in the hydrophobic cavity around the catalytic center of cytochrome c oxidase. J Phys Chem B Condens Matter Mater Surf Interfaces Biophys *109*, 1015-1022.

Thomas, J.W., Puustinen, A., Alben, J.O., Gennis, R.B., and Wikstrom, M. (1993). Substitution of Asparagine for Aspartate-135 in Subunit I of the Cytochrome bo Ubiquinol Oxidase of *Escherichia coli* Eliminates Proton-Pumping Activity. Biochemistry *32*, 10923-10928.

Thompson, D.A., Gregory, L., and Ferguson-Miller, S. (1985). Cytochrome *c* Oxidase Depleted of Subunit III: Proton-Pumping, Respiratory Control, and pH Dependence of the Midpoint Potential of Cytochrome *a*. J Inorg Biochem *23*, 357-364.

Thornstrom, P.E., Brzezinski, P., Fredriksson, P.O., and Malmstrom, B.G. (1988). Cytochrome c oxidase as an electron-transport-driven proton pump: pH dependence of the reduction levels of the redox centers during turnover. Biochemistry *27*, 5441-5447.

Tiede, D.M., Vashishta, A.-C., and Gunner, M.R. (1993). Electron-transfer kinetics and electrostatic properties of the *Rhodobacter sphaeroides* reaction center and soluble c-cytochrome. Biochemistry *32*, 4515-4531.

Tsukihara, T., Aoyama, H., Yamashita, E., Tomizaki, T., Yamaguchi, H., Shinzawa-itoh, K., Nakashima, R., Yaono, R., and Yoshikawa, S. (1995). Structure of metal sites of oxidized bovine heart cytochrome *c* oxidase at 2.8 Science *269*, 1069-1074.

Tsukihara, T., Aoyama, H., Yamashita, E., Tomizaki, T., Yamaguchi, H., Shinzawa-Itoh, K., Nakashima, R., Yaono, R., and Yoshikawa, S. (1996). The whole structure of the 13-subunit oxidized cytochrome c oxidase at 2.8 A. Science *272*, 1136-1144.

Tsukihara, T., Shimokata, K., Katayama, Y., Shimada, H., Muramoto, K., Aoyama, H., Mochizuki, M., Shinzawa-Itoh, K., Yamashita, E., Yao, M., *et al.* (2003). The low-spin heme of cytochrome *c* oxidase as the driving element of the proton pumping process. Proc Nat Acad Sci (U SA) *100*, 15304-15309.

Vakkasoglu, A.S., Morgan, J.E., Han, D., Pawate, A.S., and Gennis, R.B. (2006). Mutations which decouple the proton pump of the cytochrome c oxidase from Rhodobacter sphaeroides perturb the environment of glutamate 286. FEBS Lett *580*, 4613-4617.

Vanneste, W.H. (1966). The stoichiometry and absorption spectra of components a and a-3 in cytochrome c oxidase. Biochemistry *5*, 838-848.

Verkhovskaya, M.L., Garcia-Horsman, A., Puustinen, A., Rigaud, J.L., Morgan, J.E., Verkhovsky, M.I., and Wikstrom, M. (1997). Glutamic acid 286 in subunit I of cytochrome bo_3 is involved in proton translocation. Proc Natl Acad Sci U S A *94*, 10128-10131.

Verkhovsky, M.I., Jasaitis, A., Verkhovskaya, M.L., Morgan, J.E., and Wikstrom, M. (1999). Proton translocation by cytochrome *c* oxidase. Nature *400*, 480-483.

Verkhovsky, M.I., Morgan, J.E., and Wikstrom, M. (1992). Intramolecular electron transfer in cytochrome *c* oxidase: a cascade of equilibria. Biochemistry *31*, 11860-11863.

Verkhovsky, M.I., Morgan, J.E., and Wikstrom, M. (1994). Oxygen binding and activation: early steps in the reaction of oxygen with cytochrome *c* oxidase. Biochemistry *33*, 3079-3086.

Vygodina, T.V., Pecoraro, C., Mitchell, D., Gennis, R., and Konstantinov, A.A. (1998). Mechanism of inhibition of electron transfer by amino acid replacement K362M in a proton channel of Rhodobacter sphaeroides cytochrome c oxidase. Biochemistry *37*, 3053-3061.

Wallace, D.C. (2005). A mitochondrial paradigm of metabolic and degenerative diseases, aging, and cancer: a dawn for evolutionary medicine. Annual review of genetics *39*, 359-407.

Wang, K., Zhen, Y., Sadoski, R., Grinnell, S., Geren, L., Ferguson-Miller, S., Durham, B., and Millett, F. (1999). Definition of the interaction domain for cytochrome c on cytochrome c oxidase. II. Rapid kinetic analysis of electron transfer from cytochrome c to Rhodobacter sphaeroides cytochrome oxidase surface mutants. J Biol Chem *274*, 38042-38050.

Wiertz, F.G., Richter, O.M., Cherepanov, A.V., MacMillan, F., Ludwig, B., and de Vries, S. (2004). An oxo-ferryl tryptophan radical catalytic intermediate in cytochrome c and quinol oxidases trapped by microsecond freeze-hyperquenching (MHQ). FEBS Lett *575*, 127-130.

Wikstrom, M. (1981). Energy-dependent reversal of the cytochrome oxidase reaction. Proc Natl Acad Sci U S A *78*, 4051-4054.
Wikstrom, M. (1989). Identification of the electron transfers in cytochrome oxidase that are coupled to proton-pumping. Nature *338*, 776-778.

Wikstrom, M., Bogachev, A., Finel, M., Morgan, J.E., Puustinen, A., Raitio, M., Verkhovskaya, M., and Verkhovsky, M.I. (1994). Mechanism of proton translocation by the respiratory oxidases. The histidine cycle. Biochim Biophys Acta *1187*, 106-111.

Wikstrom, M., Jasaitis, A., Backgren, C., Puustinen, A., and Verkhovsky, M.I. (2000). The role of the D- and K-pathways of proton transfer in the function of the haem-copper oxidases. Biochim Biophys Acta *1459*, 514-520.

Wikstrom, M., Krab, K., and Saraste, M. (1981a). Cytochrome Oxidase - A Synthesis (New York, Academic Press).

Wikstrom, M., Krab, K., and Saraste, M. (1981b). Proton-translocating cytochrome complexes. Annu Rev Biochem *50*, 623-655.

Wikstrom, M., and Saari, H. (1975). A spectral shift in cytochrome a induced by calcium ions. Biochim Biophys Acta *408*, 170-179.

Wikstrom, M., and Verkhovsky, M.I. (2002). Proton translocation by cytochrome c oxidase in different phases of the catalytic cycle. Biochim Biophys Acta *1555*, 128-132.

Wikstrom, M., and Verkhovsky, M.I. (2007). Mechanism and energetics of proton translocation by the respiratory heme-copper oxidases. Biochim Biophys Acta *1767*, 1200-1214.

Wikstrom, M., Verkhovsky, M.I., and Hummer, G. (2003). Water-gated mechanism of proton translocation by cytochrome c oxidase. Biochim Biophys Acta *1604*, 61-65.

Wikstrom, M.K. (1977). Proton pump coupled to cytochrome c oxidase in mitochondria. Nature *266*, 271-273.

Wilson, D.F., Erecinska, M., and Owen, C.S. (1976). Some properties of the redox components of cytochrome c oxidase and their interactions. Archives of biochemistry and biophysics *175*, 160-172.

Wilson, K.S., and Prochaska, L.J. (1990). Phospholipid Vesicles Containing Bovine Heart Mitochondrial Cytochrome *c* Oxidase and Subunit III-Deficient Enzyme: Analysis of Respiratory Control and Proton Translocating Activities. Arch Biochem Biophys *282*, 413-420.

Wraight, C.A. (2006). Chance and design--proton transfer in water, channels and bioenergetic proteins. Biochim Biophys Acta *1757*, 886-912.
Wrigglesworth, J.M., Wooster, M.S., Elsden, J., and Danneel, H.J. (1987). Dynamics of proteoliposome formation. Intermediate states during detergent dialysis. The Biochemical journal *246*, 737-744.

Wu, Y., and Voth, G.A. (2003). A computer simulation study of the hydrated proton in a synthetic proton channel. Biophysical journal *85*, 864-875.

Xu, J., Sharpe, M.A., Qin, L., Ferguson-Miller, S., and Voth, G.A. (2007). Storage of an Excess Proton in the Hydrogen-Bonded Network of the D-Pathway of Cytochrome c Oxidase: Identification of a Protonated Water Cluster. J Am Chem Soc.

Xu, J., and Voth, G.A. (2005). Computer simulation of explicit proton translocation in cytochrome c oxidase: the D-pathway. Proc Natl Acad Sci U S A *102*, 6795-6800.

Yoshikawa, S., Muramoto, K., Shinzawa-Itoh, K., Aoyama, H., Tsukihara, T., Ogura, T., Shimokata, K., Katayama, Y., and Shimada, H. (2006a). Reaction mechanism of bovine heart cytochrome c oxidase. Biochim Biophys Acta *1757*, 395-400.

Yoshikawa, S., Muramoto, K., Shinzawa-Itoh, K., Aoyama, H., Tsukihara, T., Shimokata, K., Katayama, Y., and Shimada, H. (2006b). Proton pumping mechanism of bovine heart cytochrome c oxidase. Biochim Biophys Acta *1757*, 1110-1116.

Yoshikawa, S., Shinzawa-Itoh, K., Nakashima, R., Yaono, R., Yamashita, E., Inoue, N., Yao, M., Fei, M.J., Libeu, C.P., Mizushima, T., *et al.* (1998). Redox-coupled crystal structural changes in bovine heart cytochrome c oxidase. Science *280*, 1723-1729.

Yoshikawa, S., Shinzawa-Itoh, K., and Tsukihara, T. (2000). X-ray structure and the reaction mechanism of bovine heart cytochrome *c* oxidase. Journal of inorganic biochemistry *82*, 1-7.

Zaslavsky, D., Kaulen, A.D., Smirnova, I.A., Vygodina, T., and Konstantinov, A.A. (1993). Flash-induced membrane potential generation by cytochrome c oxidase. FEBS Lett *336*, 389-393.

Zaslavsky, D., Sadoski, R.C., Rajagukguk, S., Geren, L., Millett, F., Durham, B., and Gennis, R.B. (2004). Direct measurement of proton release by cytochrome c oxidase in solution during the F-->O transition. Proc Natl Acad Sci U S A *101*, 10544-10547.

Zaslavsky, D., Sadoski, R.C., Wang, K., Durham, B., Gennis, R.B., and Millett, F. (1998). Single electron reduction of cytochrome *c* oxidase compound F: resolution of partial steps by transient spectroscopy. Biochemistry *37*, 14910-14916.

Zaslavsky, D.L., Smirnova, I.A., Siletsky, S.A., Kaulen, A.D., Millett, F., and Konstantinov, A.A. (1995). Rapid kinetics of membrane potential generation by cytochrome c oxidase with the photoactive Ru(II)-tris-bipyridyl derivative of cytochrome c as electron donor. FEBS Lett *359*, 27-30.

Zhang, L., and Hermans, J. (1996). Hydrophilicity of cavities in proteins. Proteins:Structure, Function and Genetics *24*, 433-438.

Zhen, Y., Hoganson, C.W., Babcock, G.T., and Ferguson-Miller, S. (1999a). Definition of the interaction domain for cytochrome c on cytochrome c oxidase. I. Biochemical, spectral, and kinetic characterization of surface mutants in subunit ii of Rhodobacter sphaeroides cytochrome aa(3). J Biol Chem *274*, 38032-38041.

Zhen, Y., Mills, D., Hoganson, C.W., Lucas, R.L., Shi, W., Babcock, G., and Ferguson-Miller, S. (1999b). Electron and proton transfer in heme-copper oxidases. In Frontiers of Cellular Bioenergetics: Molecular Biology, Biochemistry and Physiopathology, S. Papa, F. Guerrieri, and J.M. Tager, eds. (New York, Kluwer Academic/Plenum Press), pp. 157-178.

Zhen, Y., Qian, J., Follmann, K., Hosler, J., Hayward, T., Nilsson, T., and Ferguson-Miller, S. (1998). Overexpression and purification of cytochrome *c* oxidase from *Rhodobacter sphaeroides*. Protein Expression Purif *13*, 326-336.

Zhen, Y., Schmidt, B., Kang, U.G., Antholine, W., and Ferguson-Miller, S. (2002). Mutants of the Cu_A site in cytochrome *c* oxidase of *Rhodobacter sphaeroides*: I. Spectral and functional properties. Biochemistry *41*, 2288-2297.

Zheng, X., Medvedev, D.M., Swanson, J., and Stuchebrukhov, A.A. (2003). Computer simulation of water in cytochrome *c* oxidase. Biochim Biophys Acta *1557*, 99-107.

Zhu, Z., Yao, J., Johns, T., Fu, K., De Bie, I., Macmillan, C., Cuthbert, A.P., Newbold, R.F., Wang, J., Chevrette, M., *et al.* (1998). SURF1, encoding a factor involved in the biogenesis of cytochrome c oxidase, is mutated in Leigh syndrome. Nature genetics *20*, 337-343.